An investigation into the effect of surface waves on time reversed signals in a shallow-water waveguide and the use of chaotic signals for acoustic detection

Adamson, James

Award date:
2007

Awarding institution:
University of Bath

Table of contents

List of acronyms used in this thesis

DORT	Décomposition de l'Opérateur de Retournement Temporel (French acronym for "time reversal operator decomposition")
TRC	Time reversal cavity
TRM	Time reversal mirror
NDE	Non-destructive evaluation (also called NDT, for non-destructive testing)
A/D	Analogue/Digital
PRF	Pulse repetition frequency
MLOs	Mine-Like Objects

Chapter 1.

Thesis overview

1.1 Thesis outline

The object of this thesis is to investigate experimentally the effects of surface waves on time reversal in a shallow-water waveguide and to use chaotic signals to detect resonant objects. These two areas of research are separate but complementary. Chapters 2 to 4 will explain the background of acoustic time reversal techniques, and the associated experiments performed during this thesis. Chapters 5 and 6 will then focus on chaotic signals, and how they can be used to detect resonant objects underwater. The synergy of these two separate approaches is explored in Chapter 7, which summarises the findings for both areas of research and makes recommendations for further work in these areas.

1.2 Overview of research into the effects of waves on time reversed signals.

Time reversal is a powerful self-adapting technique capable of focusing (or refocusing) energy in media. The strength of time reversal is that it is an adaptive technique that can compensate for errors caused by both geometric distortions within an array of sensors (hydrophones in this case), and wave field distortion caused by inhomogeneities within a media *without any prior knowledge of either the array or the medium.* This ability makes time reversal a very attractive technique for focusing energy in areas such as waveguides, where the performance of conventional methods (such as beamforming) will be significantly reduced by multiple reflections, signal scattering etc. In the field of underwater acoustics, this can be applied to communications in complex environments and to mine hunting, especially in areas where other techniques may fail such as shallow water channels and littoral zones.

One of the assumptions of time reversal is that the medium can be considered invariant over the time of the process. In shallow-water channels and littoral zones, water depth fluctuations due to surface waves can become a significant proportion of the total water depth, and in these conditions the assumption of a static medium breaks down.

My research is to determine what effect surface waves have in shallow water waveguides, so that it might be used to determine the feasibility of using time reversal for mine-hunting and/or communication in these conditions.

1.3 Overview of research into the use of chaotic pulses for acoustic detection.

This research was carried out in collaboration with (and with partial funding from) QinetiQ. Dr. Alan Fenwick (QinetiQ) and his team had carried out simulations of chaotic (acoustic) pulses and their use in detecting resonant objects. The research presented in this thesis aimed at providing experimental validation of these simulations. As with the research into surface waves on time reversal, this area of research has applications in the field of mine hunting.

In conditions of harmonic resonance, chaotic signals produce sporadic higher-amplitude responses (called “bursts”) from a target. The present research aimed at using this characteristic to produce a method assisting in the detection of resonant objects.

My research provided the necessary experimental validation and research was then taken further to design a method of detection.

1.4 Brief Description of Thesis Chapters

Chapter 2: An Introduction to Time Reversal

This chapter discusses the theoretical and practical results of time reversal, and their applications, including how inhomogeneities and/or multiple scattering within a medium will act to increase the performance of the technique relative to its performance in free space. (This is counter to many conventional techniques, where inhomogeneities/multiple scattering will reduce a technique's performance).

This main asset of time reversal will be explored through a discussion of theoretical and practical results of time reversal in an underwater setting. Here it is found that (as with other instances) the technique shows an improvement in performance over other techniques (and over itself in free space) due to the effect of multiple images (reflections).

However, due to the assumption of time invariance, it was found that if the time reversal process were

slow with respect to surface wave motion, then the signal levels would be reduced. The purpose of my research into time reversal is to take a more detailed look at the performance of time reversal in relation to surface wave properties. This is outlined in Chapter 3.

Chapter 3: Description of Time reversal experiments

This chapter outlines the set-up (electrical/physical/acoustic) and the early experiments used to validate the technique with this set-up. Chapter 2 showed that many time reversal experiments are achieved with dedicated electronics consisting of a receiver amplifier, analogue-to-digital converter, storage memory, and a

programmable transmitter. However, due to initial uncertainty over the frequency ranges, and budget limitations, it was decided to use 'off the shelf' components and bespoke software to perform the time reversal. (This is analogous to many of the initial time reversal experiments and has the advantage of bringing time reversal to a wider range of experimentalists). Finally, changes to the experiment to incorporate the controlled production of surface waves are discussed. The optimised set-up is then used in our own series of experiments presented in Chapter 4.

Chapter 4: Results of surface wave experiments.

This chapter contains the results from the experiments investigating the effects of wave motion on time reversed signals. These results represent the bulk of the experiments carried out for this thesis.

The research into wave motion (produced by a paddle wavemaker) was split into 3 experimental variables:

1) The frequency of the waves
2) The stroke length of the wavemaker (linked to the height of the waves it produces)
3) The angle between the directions of propagation of the signal and the surface waves.

These experiments revealed the limits of the underlying assumptions of the wavemaker theory, and that the frequency and stroke length were both linked to wave height. A further set of measurements was taken to accurately measure the wave heights for the wavemaker settings used in these experiments; they are presented in this chapter.

The results are presented in two sections, the first comparing frequency (and wave height) to time reversed voltage output, and the second comparing the angle between the directions of propagation for the waves and signal.

The general trend is that increasing the height of surface waves will reduce the mean voltage and increase the standard deviation (variability) of the time reversed signals, except in a few particular instances. In addition it was shown that this trend generally holds regardless of the height of the waves present when the signal was time reversed. This is discussed in greater depth at the end of this chapter, along with possible explanations to this behaviour. One of the motivations behind this work was its potential use in mine hunting in shallow and littoral waters, and before moving on to the second part of the thesis work (and experiments), it was thought necessary to include a brief introduction to mine warfare and countermeasures. This is the object of Chapter 5.

Chapter 5: Introduction to naval mine warfare and countermeasures.

This chapter provides a broad introduction to naval mine warfare and countermeasures. It discusses the strategic and economic advantages of naval mines, and also their disadvantages. It broadly explains the types of mines and their triggers. It goes on to discuss the two methods of neutralising mines, sweeping and hunting with their relative merits. This indicates the continued importance of mine hunting, and demonstrates the importance of developing new methods to detect mines. This chapter helps at understanding the advantages of the time reversal techniques (and experiments) presented in the earlier chapters. It also shows another aspect of mine hunting that warrants further research, namely the detection of acoustic resonance through the innovative use of chaotic signals. This is the object of Chapter 6.

Chapter 6: The use of chaotic pulses for acoustic detection

This chapter begins by detailing the initial theoretical results produced by Dr A. J. Fenwick (QinetiQ) regarding the interactions of chaotic pulses with targets and possible acoustic resonances. It shows the general results produced by simulations, and their potential for the use in the field of acoustic detection.

My role in this collaboration was to provide the experimental validation of these theoretical results, and this chapter shows the experimental design and results. It goes on to show how we are able to take advantage of certain properties of chaotic signals to get a method of detecting acoustically resonant objects. This chapter combines results from laboratory experiments and also from a large-scale trial, demonstrating the effectiveness of the technique over a wide bandwidth.

Chapter 7: Results and conclusions of research.

This chapter merges the conclusions and discussions presented in previous chapters. It begins by discussing the conclusions of the time reversal experiments, (wave height and wave angle) separately, and then the overall conclusions of the time reversal experiments. Then, the conclusions and discussion of the chaotic signals work are presented. Finally, the possibility of using the two techniques (time reversal and chaotic signals) in unison is presented, along with avenues for further research.

Chapter 2.

An introduction to time reversal

2.1 Overview

Time reversal is a technique that takes advantage of the time invariant properties of transducers and many propagating media, and allows refocusing of a signal that has originated from an acoustic source and travelled through an inhomogeneous media. Time invariant properties have no dependence on time (although they may depend on derivatives of time). If we were to notionally reverse the direction of time, we would find no change in the physical laws. One common example is light travelling through a converging lens. Rays of light travelling through a lens will converge at the focal point. Sending the rays back, light would travel *backwards along the paths previously travelled*.

Time reversal also allows focusing of energy on reflective targets within such a medium, provided that they behave like an acoustic source when insonified, i.e. these scatterers are pseudo-sources. The time reversal process lets us convert a set of waves diverging from the source into a set of waves converging on the source.

The strength of time reversal is that it is an adaptive technique that can compensate for errors caused by both geometric distortions within an array, and wavefield distortion caused by inhomogeneities within a media *without any prior knowledge of either the array or the medium*. Time reversal has a wide range of applications including acoustic communication, non-destructive testing, and lithotripsy[1] (which was the driving force behind early experiments). It can also be

[1] Lithotripsy is the use of high-energy shock waves to fragment and disintegrate kidney stones (http://www.surgeryencyclopedia.com/index.html).

used in an iterative mode where we find that the time reversal technique can be used to selectively focus on a single scatterer (the most reflective in the region of interest). Furthermore, an additional technique called DORT (the French acronym for 'Décomposition de l'Opérateur de Retournement Temporel', "time reversal operator decomposition") allows us to decompose the time reversal operator and selectively focus on any of the scatterers within the region of interest.

2.2 Basic principles of time reversal

The basic principles of time reversal can be found in [1], and are summarised here. Consider the equation for the propagation of acoustic pressure, valid in a lossless medium with compressibility $\kappa(\mathbf{r})$ and density $\rho(\mathbf{r})$ varying with space. Introducing the local sound velocity as

$$C(\mathbf{r}) = (\rho(\mathbf{r}).\kappa(\mathbf{r}))^{-½} \tag{2.1}$$

We then obtain the propagation of the acoustic pressure field $p(\mathbf{r},t)$ in the transient regime (when considering short pulses) [1] as

$$\vec{\nabla}.\left(\frac{\vec{\nabla}p}{\rho}\right) - \frac{1}{\rho c^2}\frac{\partial^2 p}{\partial t^2} = 0 \tag{2.2}$$

We note that equation 2.2 has only second-order time-derivative operators, so if $p(\mathbf{r},t)$ is a solution to 2.2, then $p(\mathbf{r},-t)$ is also a valid solution. This property is specific to the time invariance of the time reversal operator.

Note that this equation is only valid for a lossless propagating medium. If there were any frequency-dependent attenuation coefficients, then these would introduce first-order terms into equation (2.2), and the time invariance property would

be lost. However, if (as in many media of interest) the attenuation coefficient is small enough in the range of frequencies used within an experiment, then the time reversal invariance remains (approximately) valid [1].

2.2.1 The time reversal Cavity

In any propagation experiment, the initial conditions (e.g. the acoustic source(s) and the boundary conditions) produce a unique solution to the wave equation. The aim of the time reversal process is to alter the initial conditions of the propagation to produce the (equally valid) solution p(**r**,-t). Due to causality requirements, it is not possible to produce p(**r**,-t), however we can produce p(**r**,T-t) where T is an arbitrary time interval.

The ideal method of achieving a time reversal cavity (TRC) would be to sample a three dimensional volume entirely enclosing the region of interest. We then sample the wavefield at this area for a time T, where T is large enough that all the acoustic energy produced by the source has completely left the region of interest, or has become too attenuated to be measured. This gives us the signal of p(**r**,t) over the entire 3-D sample volume. We then re-transmit the signal in the opposite direction (i.e. changing the outgoing diverging wavefield into an inward bound converging wavefield). This is shown in Fig 2.1

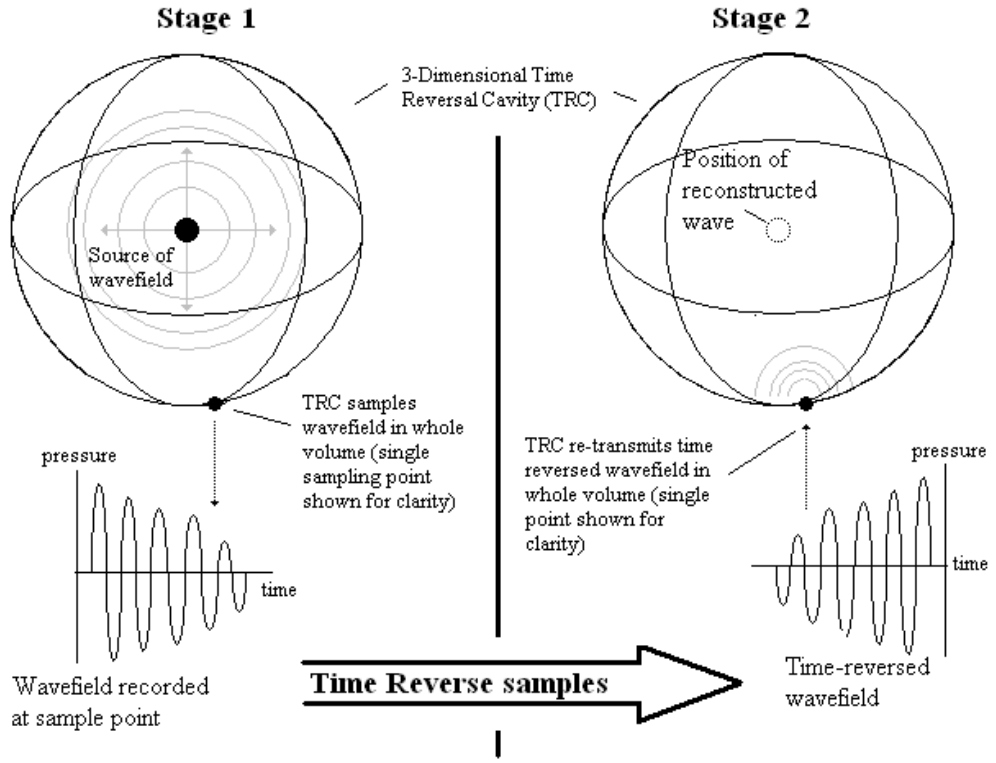

Fig. 2.1: Summary of time reversal process

This solution requires to fully sample an entire 3-D region with probes, re-emitting the signal from the same probes. This is impractical to achieve experimentally. We find a more practical solution by using the Huygens principle [e.g 2]; the wavefield in any point of a volume can be predicted by the knowledge of the field and its normal derivative on a closed surface surrounding the volume. This allows us to replace the fully 3-D TRC with a TRC consisting of a 2-D shell surrounding the region. Now if we are able to measure the pressure field produced by any sources in the region and their normal derivative, we can then calculate the solution and back-propagate the wavefield, focusing on the original sources.

Another method of focusing is adaptive time-delay focusing [3]. Time-delay focusing uses cross correlation to calculate its time delays, and it assumes that all the effects of the inhomogeneity on the spherical wavefront sum up as a simple distortion of the of the wavefront shape, i.e. the aberrator only modifies the propagation delay

between source and receivers. This only holds when the aberrator is thin, and located close to the array. This method is capable of out-performing adaptive time-delay focusing techniques [4] because it does not rely on the assumptions that:

1) Any inhomogeneities are located only in the area of the transducer array
2) Any inhomogeneities reduce to a simple time delay that varies across the transducers

Due to the finite bandwidth of ultrasonic signals, the time reversed solution $p(\mathbf{r},T-t)$ is not perfect across the whole volume, as any spatial inhomogeneities that are smaller in scale than the smallest wavelength of the source will be blurred. The maximum available resolution for focusing with a closed cavity is $\lambda/2$ where λ is the wavelength of the pulse [5]. Typically a time reversal cavity will take the form of a two dimensional surface with probes placed at regular intervals sampling the wavefield.

Experiments with a time reversal cavity

Initial time reversal experiments were performed with a time reversal cavity (TRC) [6] and from these early experiments it was learned that:

1) It can be proven that it is not necessary to measure and time-reverse both the pressure field and its normal derivative on the cavity surface. Measuring the pressure field and re-emitting the time reversed field in the backward direction yields the same results, provided that the evanescent parts of the acoustic wavefields have vanished (i.e. the field has travelled several wavelengths). This is because transducers receive in one direction, and transmit in the opposite direction. This change replaces the measurement and time reversal of the field-normal derivative.
2) Experimentally, it is not possible to measure and re-emit the pressure field at any point on a two dimensional surface. Experiments use transducer arrays

that spatially sample the surface. The spatial sampling must be less than $\frac{\lambda_{min}}{2}$ where λ_{min} is the minimum wavelength of the sampled signal to avoid grating lobes[2].

3) Temporal sampling must be at least $\frac{T_{min}}{8}$ to avoid secondary lobes, where T_{min} is the minimum period of the wavefield.
4) It is generally difficult to produce a TRC, so it is usually replaced with a time reversal mirror (TRM) of finite angular aperture. However, the propagating medium can often act to increase the apparent size of the aperture and result in a focal spot smaller than predicted by classical formulae (see later results in sections 2.2.2. and 2.2.3 for details).

Draeger *et al*. [6] performed an experiment involving a TRC in 1997. This experiment was notable in that it demonstrated the feasibility of reconstructing a point source using acoustic time reversal from a single transmitter/receiver. A two-dimensional silica cavity with chaotic ray dynamics (the cavity was shaped in such a way that any ray would never travel along the same path twice) and negligible absorption was used as the propagating medium. A short duration (~1μs) pulse was injected and allowed to travel through the silica. A receiver was placed at another point on the silica and was used to record the received signal. This received signal was over 10ms long (10,000 times the duration of the original signal), and contained waves that had reflected off the silica's boundary many times. This signal was time reversed and re-transmitted, and it was shown that it was capable of refocusing at the source location. This experiment demonstrated that multiple reflections can act to increase the apparent

[2] A grating lobe is any (usually undesired) maximum equal to the maximum of the main lobe in an array's beam pattern. Grating lobes are formed in arrays when the spacing between the elements is too large [2, 3].

aperture size of the receiver(s) in this case to 360^o, effectively sampling the entire wavefield from a single point in the TRC. This increased the apparent aperture, thus reducing the focal spot. It also demonstrated that it is possible to perform time reversal with a small number of transmitter/receivers.

2.2.2 The time reversal Mirror

The TRC is an idealised method of performing time reversal, and in many applications it is not practical or feasible to realise experimentally. For example, in many medical applications or in non-destructive evaluation (NDE) (also called NDT, for non-destructive testing), the transducers are typically positioned in a small physical area on one side of the region of interest. The probes are operated in pulse-echo mode, which allows focusing from a transducer array. In these cases, we are replacing the TRC with a time Reversal Mirror (TRM), which can be one or two dimensional, and can be plane or pre-focused[3]. Its ability to focus through an inhomogeneous (or otherwise aberrating) medium is comparable to the TRC [1]. Using a TRM does involve further limitations on its ability to focus, similar to those experienced by classical focusing using delay lines (cf. previous section): spatial sampling must be less than $\frac{\lambda_{\min}}{2}$, temporal sampling must be at least $\frac{T_{\min}}{8}$ etc.)

Experiments with a time reversal mirror (TRM)

The basic stages involved in performing time reversal with a TRM (or TRC: time reversal cavity) can be summed up as:

1) A wavefront is transmitted through the inhomogeneous medium to the target.
2) Target generates a scattered pressure field that is distorted by the medium

[3] A pre-focused array is designed so that a pulse applied across all elements will converge to a pre-determined focal spot.

3) The array records the signal received from the target.
4) The TRM creates and re-transmits the time reversed wavefield, which propagates through the inhomogeneous medium and focuses on the target.

Early time reversal experiments were performed using the prototype TRM outlined below [1].

The prototype was made of 64 programmable transmitters, each driven by a 4-kilobyte buffer memory, through a D/A converter operating with a 25 MHz sampling rate. This allowed a maximum storage interval of 160μs.

In transmit mode, the transmitters worked simultaneously, and were connected to a 64-element array. Each transmitter was capable of delivering a 175V peak-to-peak voltage to a 50Ω transducer impedance, with a 6 bit dynamic range. In receive mode, a single A/D converter was used with a multiplexer. This meant that in order to record on all 64 channels, 64 separate transmissions had to be made. This made full real time operation impossible. The recorded data was digitised using a sampling rate of 100 MHz, with an 8-bit dynamic range. The signals were then transferred to a computer that time reversed the signals, and transferred them back to each channel's transmitter memory. All 64 elements were then simultaneously fired.

Several experiments were performed with this array, in order to evaluate the experimental ability of a TRM to focus on a point source or point target. It was found that time reversal using a TRM was capable of compensating for:

1) Geometrical distortions in the time reversal mirror
2) Focusing through a random aberrating layer.
3) Focusing through a deflective prism (of less practical use, but used to demonstrate the robustness of the technique)

The performance of a TRM was compared to a delay-line focusing approach. Time delay focusing assumes that all the effects of the inhomogeneity on the spherical wavefront sum up as a simple distortion of the of the wavefront shape. This only holds when the aberrator is thin, and located close to the array. In experiments when this was the case, the performance of time reversal and time-delay approaches were similar. However, when these assumptions were not true, the time-delay approach no longer worked, whereas the time reversal approach remained valid. These experiments demonstrate the robustness of the time reversal technique.

Derode *et al.* [7] performed the first experimental demonstration of the reversibility of a multiply scattered wavefield using a time reversal mirror. In this experiment, a short pulse was transmit from a point (A) through a multiply scattering medium, with the TRM (B) was placed on the other side. The scattering medium consisted of hundreds of randomly distributed parallel steel rods ~0.8mm in diameter. The scattering medium was 15mm thick, and the average distance between rods was ~2.3mm. A 2.5 cycle 3.5M hz signal (1μs) was transmitted from the point source. This is shown in Fig.2.2.

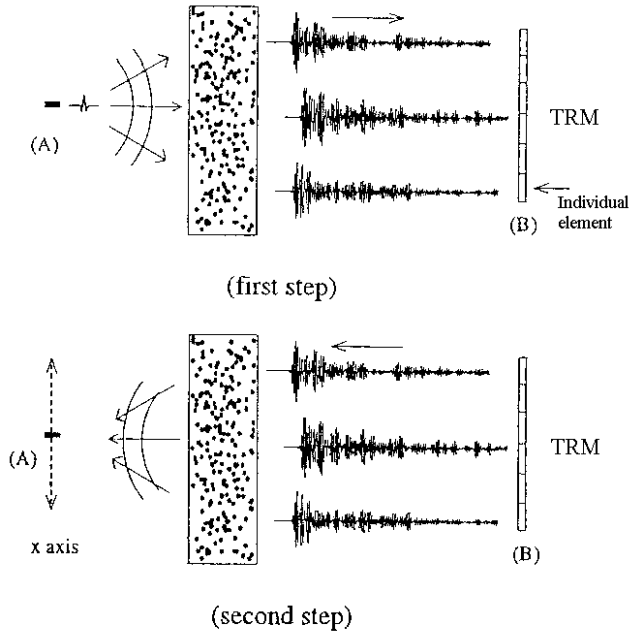

Fig 2.2: Schematic of experiment performed by Derode et al 2000 [7] (from [8]). The three traces show the signal received at that element. The first step displays a signal transmitted from the source probe, propagating through the bars and the signals received by the individual elements of the TRM. The second step displays the time reversed signal being transmitted by each element of the TRM, propagating back through the bars, and summing at the origin. A source probe is then used to measure the spatial resolution of the pulse in the x direction.

The signals received on each channel of the TRM corresponded to a high-amplitude initial arrival followed by an incoherent wave train, resulting from the multiply-scattered contribution. This signal corresponds to all the possible paths through the scattering medium to the receiver. Typically the signal received on each element was ~80μs long, i.e. ~100 times the original pulse duration. This is shown in more details in Fig. 2.3.

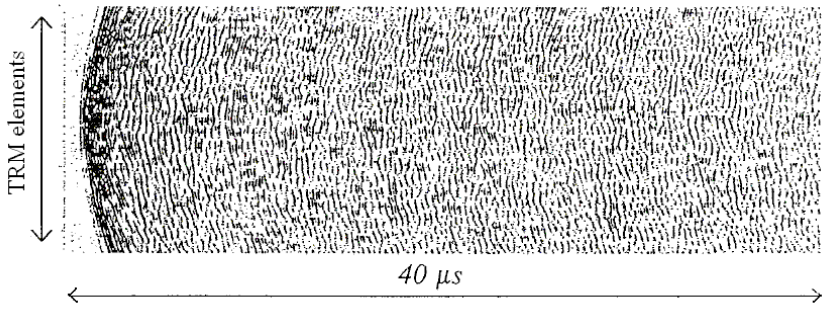

Fig 2.3 Signal received on a TRM after transmission through metal bars (from [8]) The x-axis represents a 40μs time window. The y-axis represents different elements of the TRM. (The plot is in effect made up of a series of horizontal strips). The black points represent pressure peaks, and the white parts pressure troughs.

The signal was then time reversed and re-transmitted. It was found that there was no degradation in the temporal compression of the signal (the re-focused signal had a duration of ~1μs). When the spatial resolution of the signal was evaluated it was found that there was no increase in focal spot size. In fact, the size of the focal spot was found to be ~6 times smaller than predicted by the classical diffraction limit. In effect, the multiply-scattering medium had acted to increase the apparent aperture size of the array. This demonstrates that this technique has performed better in a heterogeneous medium than a homogeneous medium.

The directivity patterns produced with and without the steel rods are shown in Fig 2.4. Note that the horizontal axis of the plot measures the position on the x-axis (as shown in Fig.2.2) rather than angle. This is because the way time reversal technique acts to focus energy on particular points within the medium has no angular dependence like we would expect for beamforming techniques (e.g. [3]).

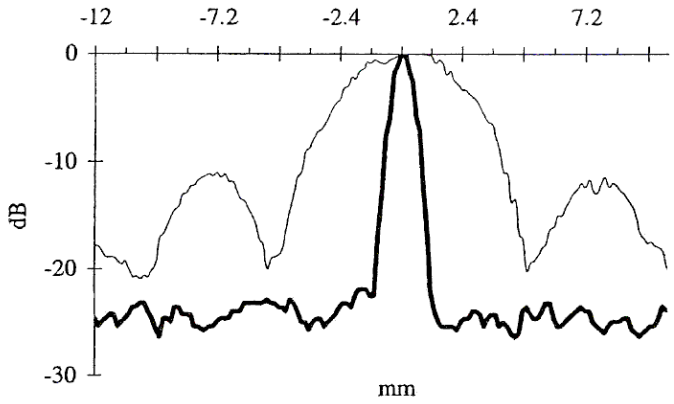

Fig 2.4. Directivity patterns of the TRM produced with the rods (thick line) and without the steel rods (thin line). From [8].

In effect, the TRM is acting like a temporal and spatial correlator, and investigations into its performance have shown it to be remarkably robust [8].

2.2.3 Time reversal in waveguides

When we consider a TRC like the one described in section 2.2.1, and particularly the experiment performed by Draeger *et al.* [6], we have seen how the large number of paths in the scattered signal widened the effective aperture of the TRM. The same effect occurs in waves propagating in a waveguide. This is because in effect the boundaries of the waveguide reflect parts of the wavefield that would not otherwise interact with the time reversal mirror into its path [8].

This increase in the amount of the wavefield captured acts to increase the apparent aperture size of the TRM with respect to its aperture size in free space. In order to fully take advantage of this effect, it is important to have a time window long enough to capture the multiply scattered part of the wavefield that arrives at the time reversal mirror some time later than the direct arrival (it is these later arrivals from multiple reflections that act to increase the aperture size).

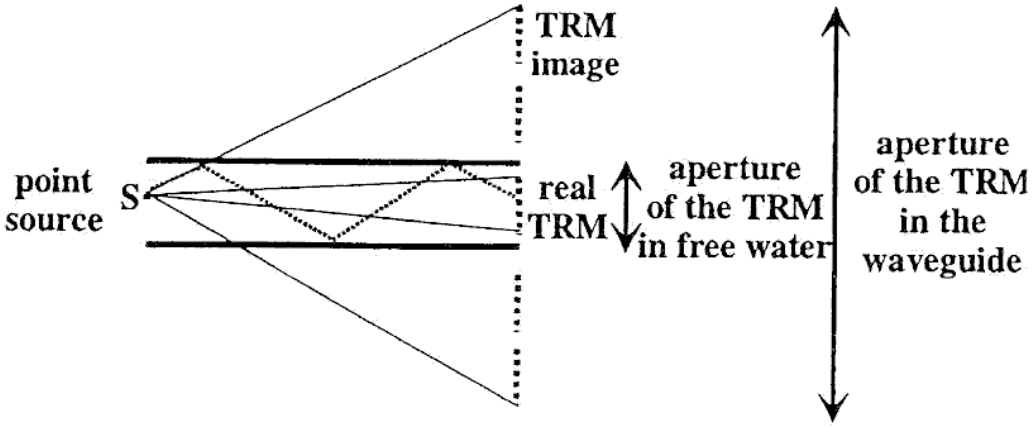

Fig 2.5: Multiple reflections increase the apparent size of the TRM, producing a smaller focal spot. From [8]

Experiments with time reversal in a waveguide.

Roux *et al*. [9] performed an experiment measuring the temporal and spatial resolution of focusing in a waveguide. In this experiment, the waveguide had two parallel plane boundaries, one between air and water and the other between water and steel. The depth of the guide was ~40mm and its length 800mm. As in the case for a multiply-scattering medium, a 2.5-cycle 3.5M hz signal (1μs) was used as the initial pulse. This experiment demonstrated that:

1) The temporal resolution of the signal was the same as that of a signal time reversed in free space.
2) The spatial resolution of the signal was improved by up to a factor of 9, because of the increase in the apparent aperture. The increase in spatial resolution increases with the number of boundary reflections, showing that the apparent aperture is linked to the size of the time window of the time reversal process. (The longer the signal used, the more reflections are included.)

This improvement in spatial resolution, as more and more of the multiple reflections are included in the time reversal, is shown in Fig 2.6.

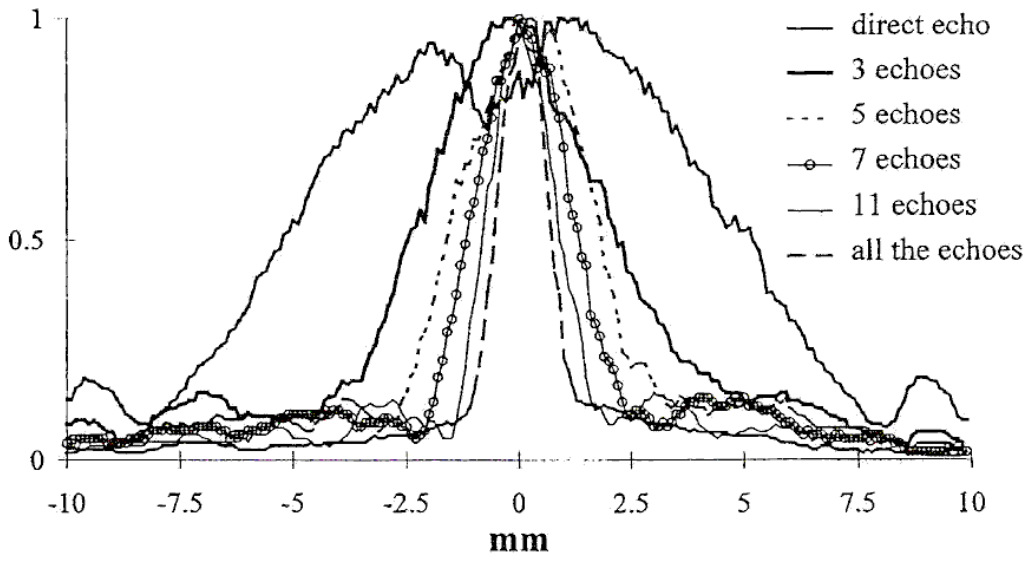

Fig 2.6. Improvement in spatial resolution in a waveguide (from [8]). The x-axis shows the position on the y-axis away from the origin.

2.2.4 Iterative time reversal

In addition to performing time reversal, we can also use a time reversal array in iterative mode. In that case, we are interested in focusing energy on targets within a medium. We perform iterative time reversal by using the signal scattered from the objects in our region of interest from one time reversal operation as the input for a subsequent time reversal. Not only does the process compensate for the inhomogeneities in the medium, but it also acts to automatically focus on the brightest scatterer in the region of interest.

This can be explained if we were to consider a medium containing two scatterers with different reflectivities. If we were to send a signal into the medium, then the signal we would measure would contain wavefields scattered from each of the two scatterers. If we were to time reverse this received signal, then we would refocus energy back at the positions of both of the scatterers, and the amplitude of the two reconstructed signals would be related to the two reflectivities of the two

scatterers (i.e. more energy will be focused at the strongest scatterer). After the first iteration of the time reversal process, more energy is focused on the stronger target than the weaker target. The signal received from the two scatterers will now contain even less of a contribution from the weaker target than for the previous iteration, so will focus even less energy after the second iteration.

We find that as we iterate the process, more and more of the energy of the TRM is being focused on the strongest scatterer until the contribution from the other scatterer is negligible. So in effect, *iterative time reversal acts to automatically focus energy at the brightest target within the region of interest.*

This result assumes that there is no multiple scattering between the targets. This can be experimentally achieved by time-windowing the received signal to exclude the multiply-scattered part of the signal.

Experiments using iterative time reversal

Several iterative time reversal experiments [10-12] have been performed demonstrating the effectiveness of the method. Wu *et al.* [10] used two different wires (a 1.5mm copper wire, and a 0.7mm brass wire) as their scatterers and a 1-D plane array as their TRM the centre frequency of the array was 3.5 MHz

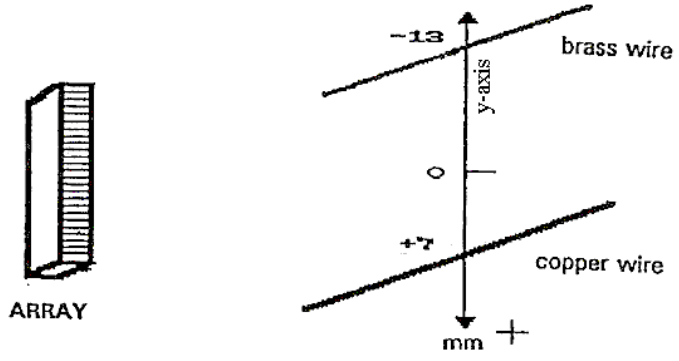

Fig 2.7. Experimental set-up for experiment performed by Wu et al (from [8]) The copper wire is placed at +7mm on the y-axis, and the brass wire at –13mm.

They illuminated an area containing the two wires, time reversed the received signals and then retransmitted them. Figure 2.8 shows the pressure field and echoes measured at each receiver after the first illumination and then after 1, 2 and 3 iterations. After the third iteration, only the (acoustically brighter) copper wire was illuminated. This clearly demonstrates the possibility to automatically focus on the brightest scatterer.

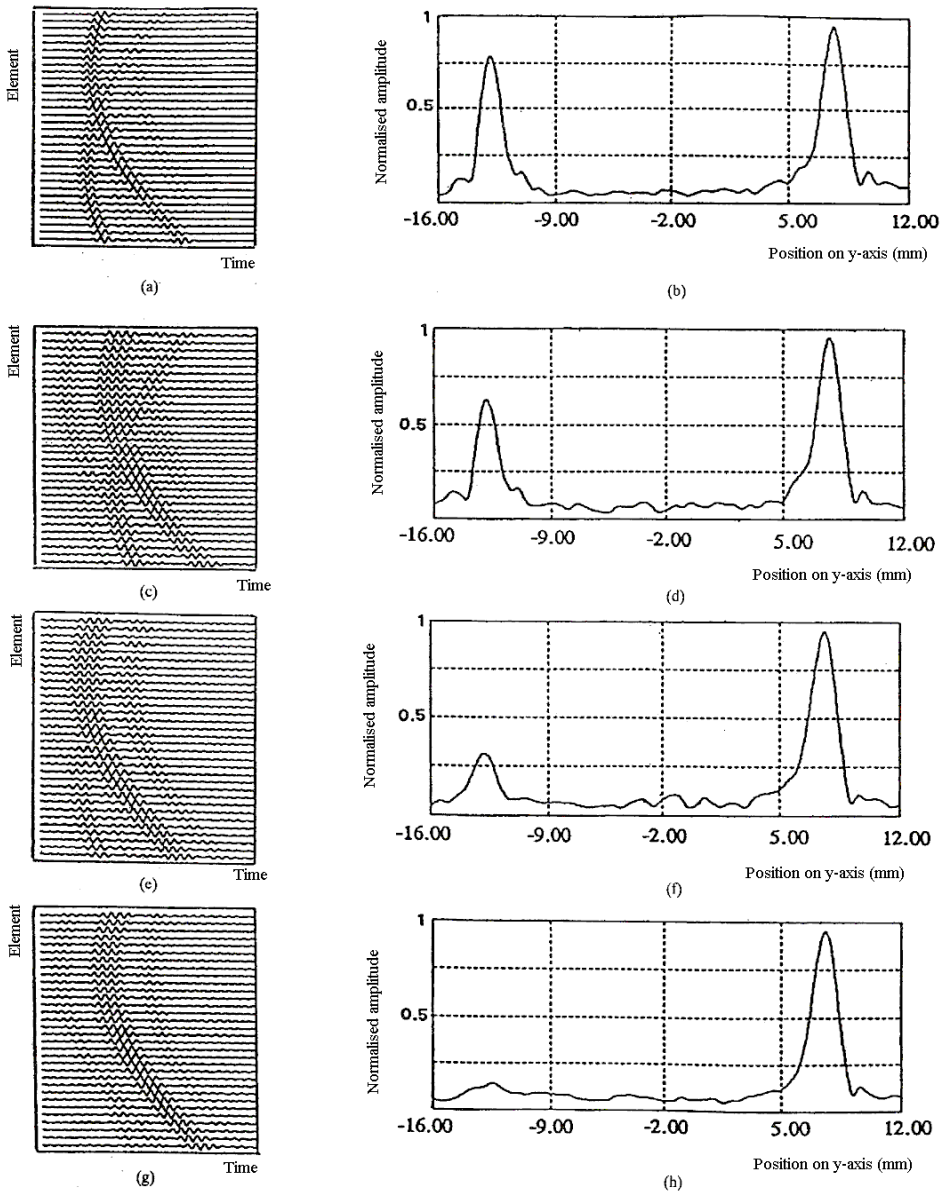

Fig 2.8: Iteration of the time reversal process, (a), (c), (e), (g) show the signals recorded on each element of the TRM after each iteration after the initial illumination (a), and the first, second and third

iterations. (b), (d), (f), (h) show the pressure observed in the y-axis after the initial illumination (b), and its iterations. From [8]

This experiment also showed that:

1) The echo duration became longer with each iteration. This was due to multiple convolutions of the pressure signals by the acousto-electrical impulse response of the transducer elements.
2) The echo pattern was more complex than simple single scattering. The two waveforms were followed by weaker replica, corresponding to the acoustic resonances of the two wires. The wires were not behaving as point sources, but rather as extended sources.

A further experiment demonstrating iterative time reversal was performed by Fink *et al.* [8]. The TRM was the same as before, but the scatterers were now a 0.2mm copper wire, and a 0.4mm copper wire. In addition to these, an aberrating layer was placed between the two wires and the TRM, made up of a 1-D line array. As with the previous experiment, iteration of the time reversal operator provided selective focusing on the brightest wire. This experiment demonstrates that, as previously shown for time reversal experiments the time reversal operator is able to compensate for any aberrations in the medium, and so allows use of a TRM in iterative (or pulse-echo) mode even in the presence of aberrations.

Wu *et al.* [10] performed several lithotripsy experiments to determine the effectiveness of iterative time reversal. The first experiment was to determine the effectiveness of using time reversal as a method of focusing on a single kidney stone. The kidney stone was irregularly shaped, with dimension ~10mm. This experiment demonstrated that due to the complex resonances present within the stone, it was not possible to successfully focus on the stone by time reversing the signal scattered from

it. However, this problem can be overcome by iteration of the time reversal operator. After 2 iterations, the –6dB beamwidth was 4.2mm (cf. stone dimension of 10mm). This experiment has been performed on many stones, and this appears to be a general result. A possible explanation for this effect is to consider each side of the stone to be a different target, and the iterative time reversal process focuses on the brightest (for a particular orientation).

A further experiment was performed where the selective properties of iterative time reversal were tested on 2 kidney stones. These were attached to a nylon wire, and suspended in water. A non-uniform unspecified aberrating layer was placed between the TRM and the kidney stones (to simulate the effect of transmitting into tissue), as summarised in Fig 2.9.

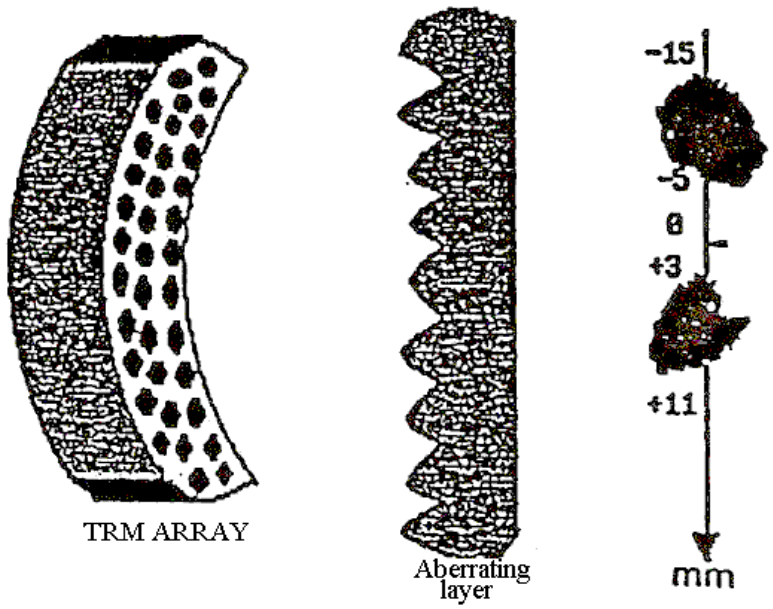

Fig 2.9. Experimental set-up for kidney stones experiment. From [10].

The directivity patterns for the first time reversal and the first three iterations are shown in Fig 2.10.

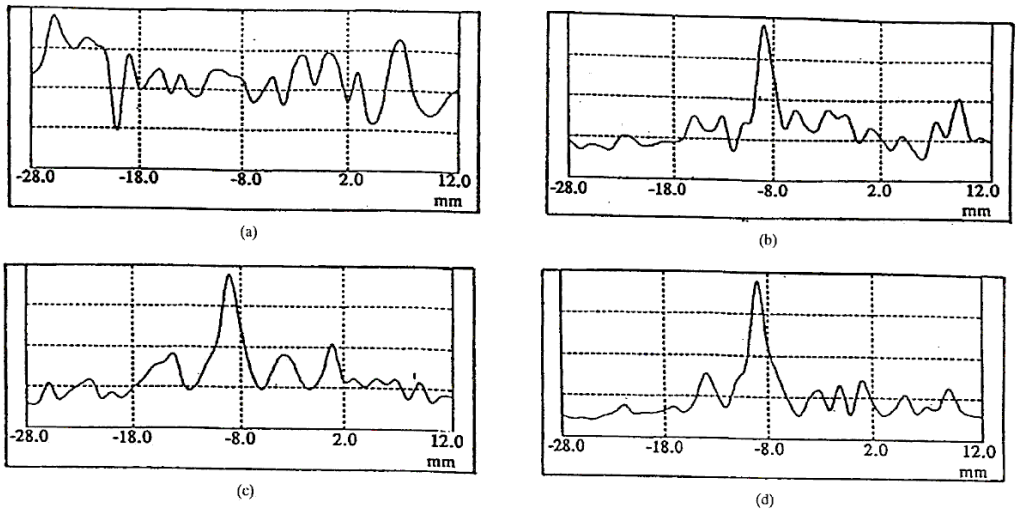

Fig 2.10. Directivity patterns for the TRM after initial time reversal (a) and for the first three iterations (b-d) (from [10]). The x-axis represents position on the y-axis (as in Fig. 2.8).

If we examine the directivity pattern of the TRM we see that the time reversal is focusing energy back at the position of both kidney stones (one at ~ -9mm and the other at ~+7mm). After the first iteration of the time reversal process, the majority of the energy is now focused on a single kidney stone (at ~–9mm), with a much-reduced pressure at +7mm. Two further iterations reduce the sidelobe levels of the peak at –9mm. This experiment clearly demonstrates the automatic target selection and focusing properties of iterative time reversal even in a complex experimental set-up.

2.2.5 The DORT method.

Iterative time reversal showed that, in the presence of two (or more) targets, it focuses on the most reflective of these targets. This leads to the problem of how to focus on weaker targets within a medium. It has been shown [10] that, for well resolved scatterers of different reflectivities, selective focusing can be obtained by determining the invariants of the time reversal operator. The detection and focusing

using this method is known as DORT ("Décomposition de l'Opérateur de Retournement Temporel"). A brief overview of how the DORT method works is shown below, and a full mathematical proof is presented in [11].

The time reversal operator

To begin, we define an L-element transfer matrix, **k**, where L is the number of elements in the time reversal array. Each array element $\mathbf{k}_{lm}(t)$ is the signal received on element *m* when a δ signal is applied to element *l,* propagates through the medium and is scattered. **k** therefore, is an array storing the signal received *from* each element *to* each element and includes all the effects of the propagating medium. It is normally more convenient to work in the frequency domain, so the matrix **K** is used. The elements of **K** are those of **k** after a temporal Fourier transform. According to the reciprocity theorem, replacing the positions of the source and receiver will not alter the measured signal, so $\mathbf{K}_{lm}=\mathbf{K}_{ml}$, and the matrix K is symmetrical.

The time reversal process is equivalent to a phase conjugation in the frequency domain, so, for an arbitrary input signal E^0 (the zeroth iteration), the received signal is:

$$\mathbf{R}^0 = \mathbf{K}\mathbf{E}^0 \tag{2.3}$$

The new input signal $\mathbf{E}^1$ is the phase conjugation of the output signal $\mathbf{R}^0$:

$$\mathbf{E}^1 = \mathbf{R}^{0*} = \mathbf{K}^*\mathbf{E}^{0*} \tag{2.4}$$

So the received signal after time reversal $\mathbf{R}^1$ is:

$$\mathbf{R}^1 = \mathbf{K}\mathbf{E}^1 = \mathbf{K}\mathbf{K}^*\mathbf{E}^{0*} \tag{2.5}$$

The symmetry of **K** implies that $\mathbf{K}^*\mathbf{K}$ is Hermitian. The properties of **K** are:

$${}^t[\mathbf{K}^*\mathbf{K}^*] = {}^t[\mathbf{K}\mathbf{K}^*] = {}^t\mathbf{K}^{*t}\mathbf{K} = \mathbf{K}^*\mathbf{K} \tag{2.6}$$

Therefore $\mathbf{K}^*\mathbf{K}$ can be diagonalised, its eigenvectors are orthogonal, and its eigenvalues are real (and positive). The operator **K*K** has p distinct eigenvalues (where $p \leq L$), $\lambda_1, \lambda_2, \ldots\lambda_p$ with associated eigenspaces[4] $F_1, F_2, \ldots F_p$.

If a signal is an eigenvector of the time reversal operator, then it is invariant under the time reversal process. The decomposition of the time reversal operator is therefore deeply linked to the scattering properties of the medium. For the case of point-like scatterers, the number of significant eigenvalues is equal to the number of scatterers resolved by the system, and each associated eigenvector corresponds to focusing energy on one particular scatterer within the medium [12]. A significant eigenvalue is an eigenvalue with associated eigenvector that will focus energy on one of the scatterers within the system. There will typically only be as many significant eigenvalues as there are acoustic 'bright spots' in the medium. All the remaining eigenvalues will be smaller in magnitude, and will not focus energy within the medium.

Experimentally performing the DORT method.

The DORT method is experimentally deduced from the complete theory, outlined above. It includes mathematical processing of the measured signals and allows focusing on any scatterer within an inhomogeneous medium. It is performed in three stages.

Stage 1

The first stage involves measurement of the inter-element impulse responses. Typically this is performed in parallel (i.e. the signal is recorded on all receiving channels simultaneously), and so requires L transmit-receive operations (where L is

[4] An eigenspace is a set of eigenvectors with a common eigenvalue.

the number of elements). The components of the transfer matrix K are obtained by Fourier transforms of each signal.

Stage 2

The matrix $\mathbf{K}^*\mathbf{K}$ is diagonalised at the chosen frequency. This diagonalisation requires that the matrix **K** is symmetrical, which is not typically the case for experimental data. (Reciprocity is not satisfied due to differences in electroacoustic response between elements, and noise). The matrix is made symmetrical by taking pairs of elements $\mathbf{K}_{lm}$ and $\mathbf{K}_{ml}$ and replacing them with the average of their two values. Provided that the values of $\mathbf{K}_{lm}$ and $\mathbf{K}_{ml}$ are not significantly different, this is not considered to introduce significant error. $\mathbf{K}^*\mathbf{K}$ is now calculated and diagonalised. The eigenvalue distribution provides useful information. The number of significant eigenvalues is the same as the number of bright spots in the set of targets. As stated previously, for point-like scatterers, this corresponds to the number of targets resolved by the system.

In the case of spherical scatterers, this becomes more complex because each scatterer can produce up to four distinct eigenvectors, each corresponding to a different mode of vibration. These modes are a monopole and up to three orthogonal dipole modes. This breaks the one-to-one relationship between eigenvectors and scatterers. However, as different scatterers would have different phases, there remains the possibility of distinguishing between scatterers [12].

Stage 3

Each eigenvector is now back-propagated. This can be performed numerically or experimentally. Experimental back-propagation requires programmable generators, as for the standard TRM. Pulsed signals can be built from linear superposition of the monochromatic data given by the eigenvectors.

This back-propagation allows us to transmit a focused wave on any one of the targets within the region of *interest without any knowledge of the geometry of the transducer array and/or properties of the propagating medium.*

Experiments involving the DORT method.

Several experiments were performed by Prada *et al.* [11] to evaluate the performance of the DORT method. These experiments used two wires as targets in a similar way to the early iterative time reversal experiments.

Two wires of different diameter

In this experiment, a 128-element line array with a centre frequency of 3 MHz was used as the TRM, and two coated brass wires of diameter 0.2mm and 0.1mm (wires (1) and (2) respectively) were used as targets. One was placed at –7mm on the y-axis, the other at +1.5mm. The relative reflectivities of the two wires were very close (~0.97). Initially iterative time reversal was performed on the two wires. The ratio of heights of the second lobe (the one iterative time reversal will reduce to zero) was 0.9 between the first and fourth iteration. In this case, the proximity of the reflectivities meant that the convergence was slow (it would take more than 20 iterations [11] to completely remove the echo from the second wire).

The DORT method was performed on the two wires, and diagonalisation of the time reversal operator produced 2 significant eigenvalues (corresponding to the

two scatterers in the medium), and 126 ‘noise’ eigenvalues (the remaining eigenvalues of the array) that were several orders of magnitude lower. Fig 2.11 shows the directivity of these two eigenvectors. Each one focuses energy on one of the two wires and not the other. In comparison, iterative time reversal found it difficult to focus on wire 1 due to the slow convergence of the process, and focusing on wire 2 would not be possible, as iterative time reversal can only focus on the brightest scatterer.

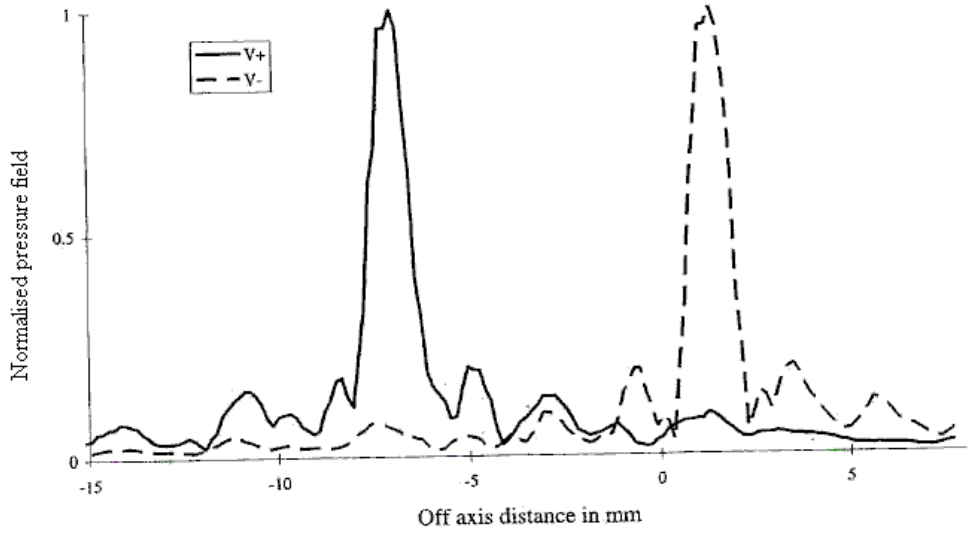

Fig 2.11. Directivity patterns for the two significant eigenvectors V+ and V-. Each eigenvector focuses energy on one wire with no significant amount of energy focused on the other. From [11].

Focusing through an aberrating medium

The experiment was performed again, with the addition of an aberrating layer between the wires and the TRM. The aberrating layer was made from a rubber sheet of non-uniform thickness. As for the previous experiment, diagonalisation of the time reversal operator produced two significant eigenvectors, each focusing energy on one wire and not the other. The directivity patterns are shown in Fig 2.12.

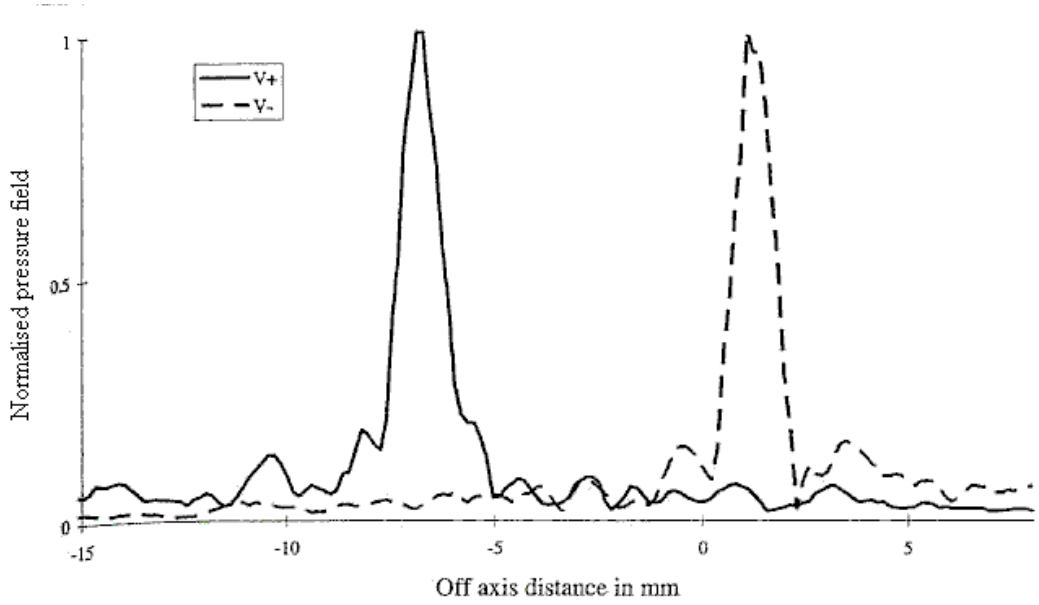

Fig 2.12. Directivity patterns for the two significant eigenvectors V+ and V- when focusing through an aberrating layer. As in Fig.2.10, each eigenvector focuses energy on one wire with no significant amount of energy focused on the other. From [11].

Focussing on two identical wires

Focussing on one of two identical wires is more problematic because the eigenvalues produced by the DORT method do not focus exclusively on a single scatterer. One of the eigenvalues corresponds to in-phase focusing on the two wires (V_+), and the other to opposite-phase focusing (V_-). A linear combination of these two eigenvalues can be used to selectively focus on one of the two wires. (V_-+V_+) will focus on one wire, and (V_+-V_-) will focus on the other.

When the wires are no longer well resolved, it becomes impossible to focus on one wire only, but the number of significant eigenvalues is still able to indicate the number of scatterers (assuming that they are point-like in behaviour).

2.3 Time reversal and underwater acoustics

Acoustic waveguides are often found in underwater acoustics, especially in shallow water regions, where the effect of multipath propagation acts to limit the effectiveness of underwater communication systems. The problem arises because the acoustic transmission bounces off the ocean surface and floor, causing multiple arrivals on the receiver. Section 2.2.3 shows how time reversal techniques can be used to negate the problems of multiple arrivals, and even use them to improve the spatial resolution of an array.

Roux *et al*. [13] studied the temporal and spatial focusing properties of time reversal mirrors in a waveguide. They analysed focal spot size, and temporal and spatial sidelobe levels. In particular they found that the spatial sidelobe level around the focal spot depended on $\frac{NL}{H}$ where L and H are the height and length of the guide, and N is the number of transducers of the TRM. They found that some of their results were applicable to underwater acoustic channels, and also found that the temporal compression observed suggested its use in the field of underwater acoustic communication.

In addition to this, Roux et al. [13] studied time reversal in a non-static waveguide by adding surface waves to the waveguide. They remarked that the direct signal and first bottom reflection, which are the most energetic waves, remain unaffected by this and so should not have a large effect on time reversal in the ocean. To explore the effect of the waves, they time-windowed their signal to select only waves that had reflected off the surface at least once. They performed their analysis in two modes; slow, where the surface waves would move between reception and retransmission, and fast, (~2ms), where the surface could be considered ‘frozen’ for the duration of the time reversal process. They found that when the time reversal

process was slow, there was a four-fold reduction in the average peak amplitude of the time reversed signal. When the process was fast, the surface could be considered as rough, and was similar to a static waveguide.

Mordant *et al*. [14] investigated the use of DORT in a waveguide. They found that DORT was capable of taking advantage of the multiple reflections to produce a spatial resolution at least 9 times better than in free space (cf. section 2.2.3). They also found that they were able to detect objects close to the water/air interface with a resolution of $1/20^{th}$ of the free-space diffraction spot.

The effect of surface waves on the significant eigenvalues of $\mathbf{K}^*\mathbf{K}$ was examined. They found that by averaging they were still able to retain a spatial resolution three times finer than in free space.

The findings of [8] and [9] demonstrate the attractiveness of using time reversal in underwater acoustics, where it offers improvements in both communication and detection, in regions (like shallow water waveguides) where the effectiveness of conventional methods is reduced,.

One potential problem in using time reversal in underwater acoustics is that over such a large scale, it is possible that non-linear propagation effects will become significant, and thus break the time invariance required for time reversal. Cunningham *et al*. [15] investigated this effect, placing emphasis on non-linear propagation in the time reversal beam, and specifically its effect on field reconstruction. It was shown that even in the presence of shock formation, the ability of time reversal to retarget most of the energy on the source/focal region is quite robust.

Experiments into time reversal in the ocean were first performed in the early 1960's by Parvulescu and Clay [16,17]. Their shallow water experiments used a single transducer operating in time reversal mode. They found that they could produce

temporal compression, but could not demonstrate the spatial focusing property of TRMs.

In recent years, several experiments have been performed [18,19] that experimentally demonstrate the robustness of the time reversal technique in the ocean, provided that the time reversal array adequately samples the water column.

Song *et al*. [18] performed an experiment examining iterative time reversal in the ocean. They found that, for a single target, iterative time reversal results in a minor improvement in spatial focusing. They also demonstrated the importance of the waveguide and source transducer in the single target case. In the case of multiple targets, iterative time reversal focuses on the target corresponding to the largest eigenvalue of the time reversal operator, which depends on the reflectivity of the target, and also on the complex propagation effects between target and TRM.

Hodgkiss *et al*. [19] went on to perform another time reversal experiment in the ocean, which (1) extended the range of the focus from ~6km to ~30km; (2) verified a new technique for focusing at ranges other than the source range (as in [17]); (3) demonstrated that time reversed pulses up to 1 week old can still be refocused successfully.

In [20], Song *et al*. also outlined a method of focusing at ranges other than the source. They found that, as increasing or decreasing the source frequency could shift the position of the sound field maxima, they could apply focal range shifts to a TRM provided that the bandwidth of the signal was relatively small compared to the carrier frequency.

Edelmann *et al*. [21] have provided an initial demonstration of acoustic communication using time reversal. They used a TRM to generate binary phase shift keying communication sequences (see [2] for basic explanations of the process). They

show time reversal to be an effective approach for mitigating the effects of intersymbol interference caused by multipath propagation.

Finally, Dungan *et al*. [22] have investigated through simulations the effect of wave propagation on time reversal in a shallow ocean. This is because the unique capability of time reversal may be degraded in time-dependent or noisy acoustic environments. They performed simulations of a monochromatic signal in a waveguide with a linear superposition of time-varying surface waves. They then show that in some circumstances these surface waves can limit the effectiveness of a TRM's refocusing ability.

The effect of surface waves on time reversed pulses seems particularly important, and it warrants further experiments. It was therefore decided to design a new experiment to determine the practical limits imposed by surface waves on the time reversal process. This is the subject of the next chapter.

Chapter 3.

Description of time reversal experiments

3.1 Outline of experimental technique.

Chapter 2 showed that time reversal is typically achieved using dedicated hardware that consists of a receiver amplifier, an Analogue/Digital (A/D) converter, storage memory (for storing the digitised waveforms), and a programmable transmitter (for transmitting the time reversed digitised waveform). It is possible to use dedicated hardware to produce a system that is very fast at time reversing and re-transmitting the incoming signal, allowing the time reversal to be performed in real time with very little (~μs) processing time, but this is (often) expensive to produce. Due to budget constraints, and also initial uncertainty as to the most suitable frequency range, it was decided to adopt a more flexible approach and use 'off-the-shelf' equipment similar to that of the earlier experiments presented in chapter 2. The main difference between the experiments in chapter 2 and those presented here is the operating frequency (100 kHz as opposed to ~3 MHz for most of the experiments in chapter 2), selected as to suit both laboratory and field experiments.

This experimental set-up was tested to verify that time reversal was being performed adequately. This is presented in section 3.2. The experiments investigating the effect of surface motion on time reversal are then presented in section 3.3. A summary and discussions are presented in section 3.4.

3.2 Experimental set-up.

3.2.1 Description of the original method

In order to perform time reversal, the experiment can be split into three separate stages:

1) Transmission of a waveform, propagation through the medium and reception.

2) Time reversal of this waveform for each receiving channel, i.e. each hydrophone.

3) Re-transmission, back-propagation and reception of the (summed) time reversed waveforms at the source.

This is shown in Fig. 3.1, showing a generic time reversal cavity (TRC).

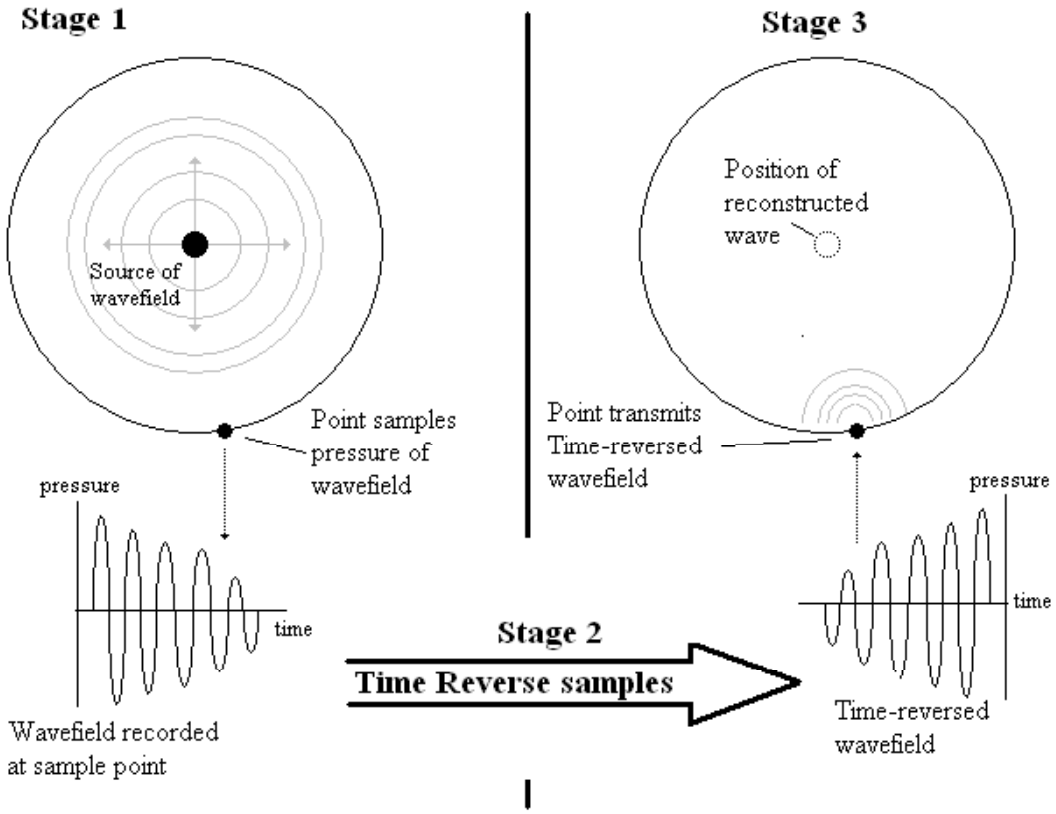

Fig.3.1. Three stages of time reversal, for a generic time reversal cavity.

For my experiments, time reversal is achieved using an oscilloscope to measure the received signals, and an arbitrary waveform generator to transmit signals (both the original pulse and the several time reversed pulses). So the experimental procedure used here can be summarised as follows:

1) The parameters of the initial pulse are set, and the pulse transmitted using the arbitrary waveform generator in triggered mode. The trigger is internal to the arbitrary waveform generator, and is used to control the pulse repetition frequency (PRF) of the initial pulse (Stage 1). (It is also used to control the PRF of the time reversed pulses in stage 3).
2) The signals received at the hydrophones that make up the TRM are amplified and checked using a lowpass filter. (Stage 1)
3) A digital oscilloscope captures the amplified signals on each receiving channel. (Stage 1)
4) Each received signal is placed into an array, and the array reversed in time. The typical size of an array was 50,000 x 2 samples. (Stage 2)
5) Each (time) reversed array is transferred into the arbitrary waveform generator. (Stage 2).
6) The arbitrary waveform generator creates the time reversed signals at the same PRF (pulse-repetition frequency) as the pulse originally transmitted. These pulses are transmitted by the TRM and propagate back through the medium. This is achieved by using the same internal trigger as previously used in (1). (Stage 3)
7) The time reversed field is investigated using a hydrophone using the digital oscilloscope to capture the time reversed pulse. (Stage 3)

These steps are summarised in Fig 3.2.

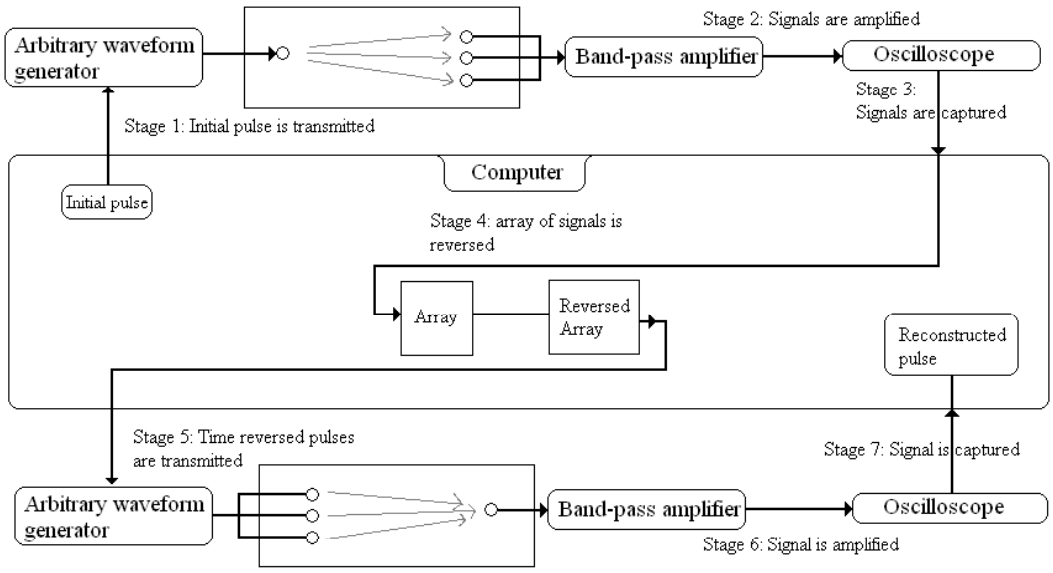

Fig. 3.2. The seven stages used to achieve time reversal in these experiments.

The electrical set-up

The main electronic components used in this experiment consist of a LeCroy 9304C 4-channel oscilloscope (200 MHz, 100 MS/s, 50 kpts/channel), a TTi TGA1244 4-channel arbitrary waveform generator (64k points/channel, 8-bit dynamic range/channel, 0.1m Hz-16 Mhz), and a stepper-motor controller that controls the position of the source hydrophone. It was decided to use 4 channels, as this was the largest number that could be effectively utilised (i.e. the most that could be sampled using a single oscilloscope and arbitrary waveform generator).

In addition, a 4-channel switch/amplifier circuit was required to amplify the voltages of the hydrophones in receive mode. This was to increase the signal-to-noise ratio of the received signals. The amplifiers have a fixed gain of ~1000 over the frequency band of interest (~90-110 kHz). The amplifier's frequency is shown in Fig. 3.3. The response was measured by taking the average gain of 3 measurements at each

frequency. The standard deviation of the gains can be considered to be negligible (it was typically ~4). The frequency response of the amplifier is shown in Fig. 3.3.

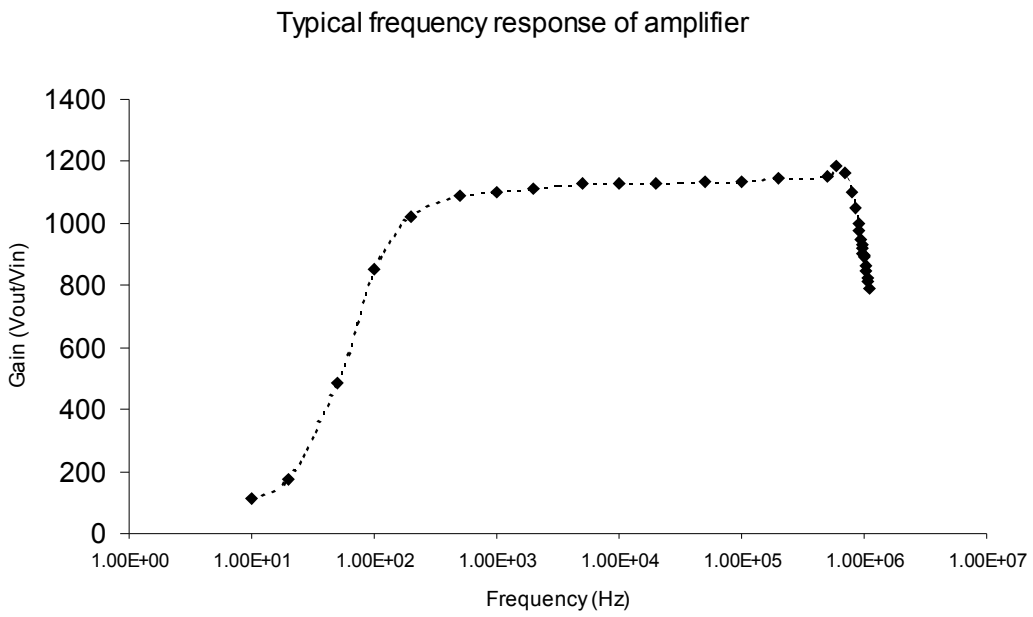

Fig 3.3: Amplifier response curve.

Each transmitting/receiving channel also contains a switch, which is used to manually change between the three different modes of operation available (Table 3.1).

Tx	The output of the arbitrary waveform generator is connected to the corresponding hydrophone. This is the transmitting mode.
AMP	The hydrophone output is passed via the amplifier and lowpass filter to the input of the oscilloscope. This is the receiving mode.
Mon	The output of the arbitrary waveform generator is connected to the input of the oscilloscope. This mode is used to check that the correct pulse is being applied to the hydrophone, and is not used during the time reversal process.

Table 3.1: Summary of switch/amplifier box modes

The switch/amplifier box is controlled manually, and is used to set which transducers are used to transmit and which to receive for each stage of the experiment. The oscilloscope, the arbitrary waveform generator, and the stepper controller are linked and controlled by computer via RS232 and IEEE interfaces. A LabVIEW

program was written for this purpose, controlling all communication between these components and is used to control the experiment.

The control and data flow of the experimental set-up is summarised diagrammatically in Fig. 3.4.

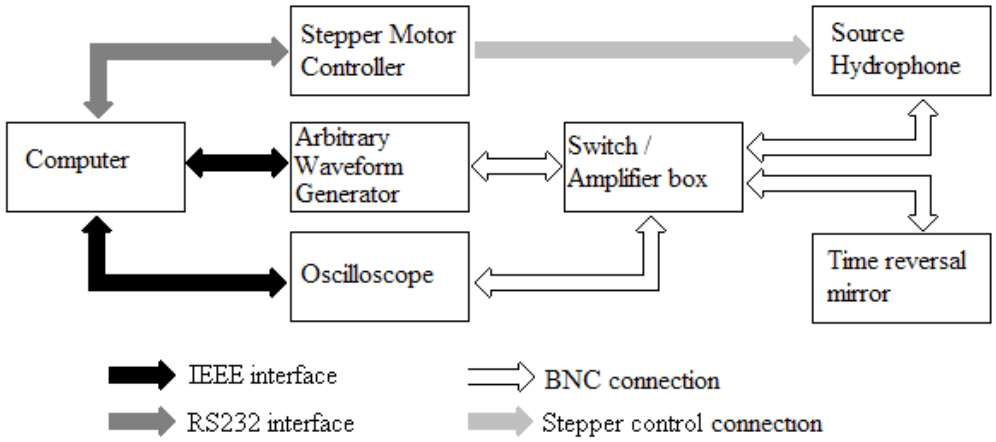

Fig 3.4: Indication of data flow and control, arrows indicating direction of flow/control.

The Acoustic Set-up

The initial time reversal experiments were carried out in a glass tank of internal dimensions 905mm x 290mm x 305mm. The water depth was typically between160-170mm. A single Reson TC-4013 hydrophone was used as the source for the initial pulse.

The frequency of 100k Hz was chosen for these experiments, for the reasons outlined above. The time reversal mirror (TRM) consists of 3 TC-4013 hydrophones identical to the original transmitting/receiving hydrophone. The hydrophones were mounted on the end of a hollow metal rod with their connecting wires running through the tubing to the instruments. The 3 hydrophones that form the TRM were mounted directly to the frame that surrounds the tank, and can be considered fixed for each

time reversal experiment. The source hydrophone is mounted on the stepper controller rig, which is itself mounted on the frame. The source hydrophone could be moved relative to the TRM, and was moved when performing a scan of the time reversed field surrounding the source hydrophone.

Due to the highly reflective nature of the glass walls, the acoustic environment inside the water tank produced a large amount of signal reverberation. A sample 3-cycle 100 kHz signal (taking 30μs to transmit) would produce a signal that would take approximately 100ms to die, reduced in amplitude to the level of background noise. In this case, it is reasonable to assume that the system is closed, i.e. that no acoustic energy is lost from the system. For a closed system, a hydrophone placed at any point in the tank will sample the entirety of the transmitted waveform. In this case, the position of the 3 hydrophones is (in theory) of no consequence, and they can be placed randomly in the tank, though, for convenience, the three hydrophones forming the TRM were placed in a line as shown in Fig. 3.5. The water depth for these experiments was ~300mm.

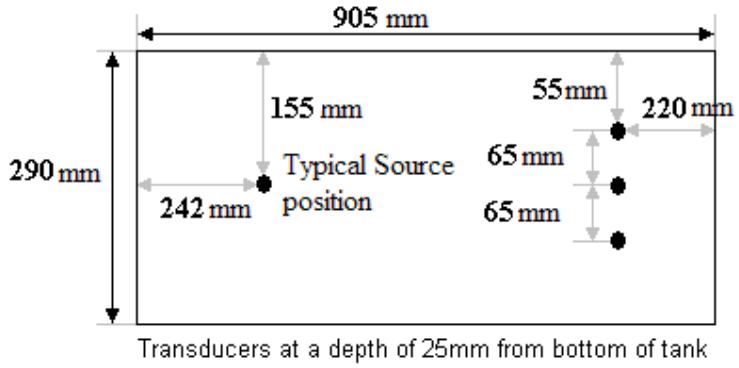

Fig 3.5: Plan view showing the position of the transducers (black circles) in the tank, whose water depth was ~300mm.

3.2.2 Validation of the original method.

Preliminary results

The first step was to measure the signal received from a single-cycle sine wave pulse, to determine how long the pulse reverberated in this tank, and therefore deduce the required pulse repetition frequency and the required time scale for measuring the pulse for time reversal. Fig. 3.6 shows a typical received signal when a single-cycle sine wave pulse, with peak-to-peak amplitude of 20 Volts, and a frequency of 100 kHz is transmitted from the source position.

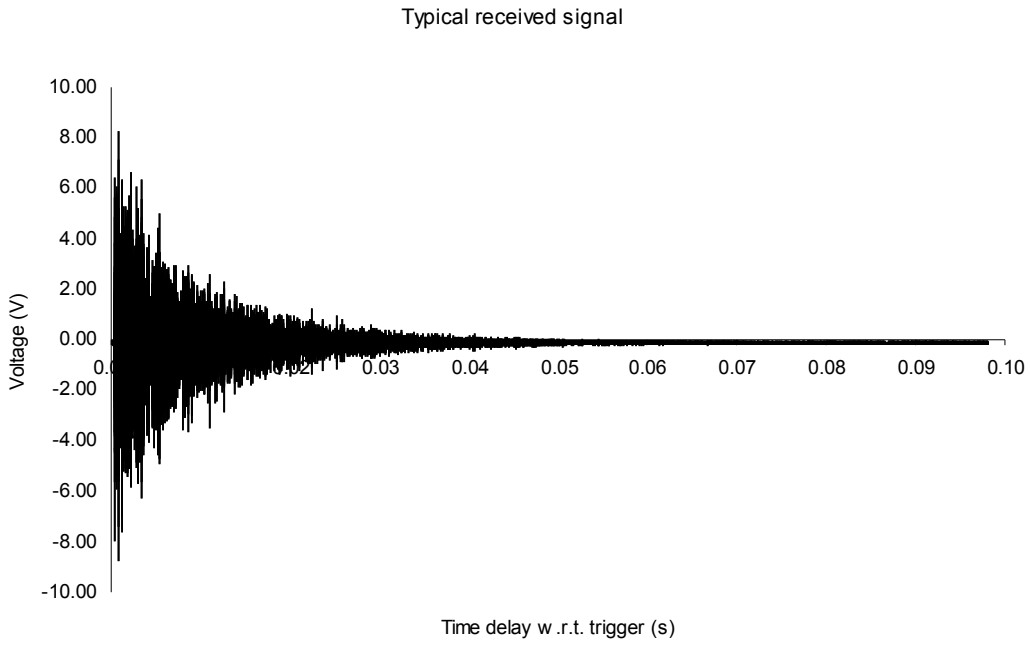

Fig 3.6: Typical received signal. The trigger is the point at which the signal is transmitted.

The signal initially transmitted typically took approximately 80-100ms to die away completely, and the system took ~34ms to reach a voltage level of -30dB. This time delay implies a maximum path length of ~50m. A signal travelling for this distance in the tank will have been reflected between 50 and 160 times depending on

the ray path. This indicates that a large number of wavepaths are present in the received signal, so it is not unreasonable to assume that this system is closed, i.e. has a low rate of energy loss

If this is indeed the case, we should be able to reconstruct the pulse using the time reversal of this signal alone, as it will contain sufficient information about the propagation paths of the signal to adequately reconstruct the original pulse. Fig. 3.7 shows the time reversed signal received at the origin when using the signal shown in Fig. 3.6.

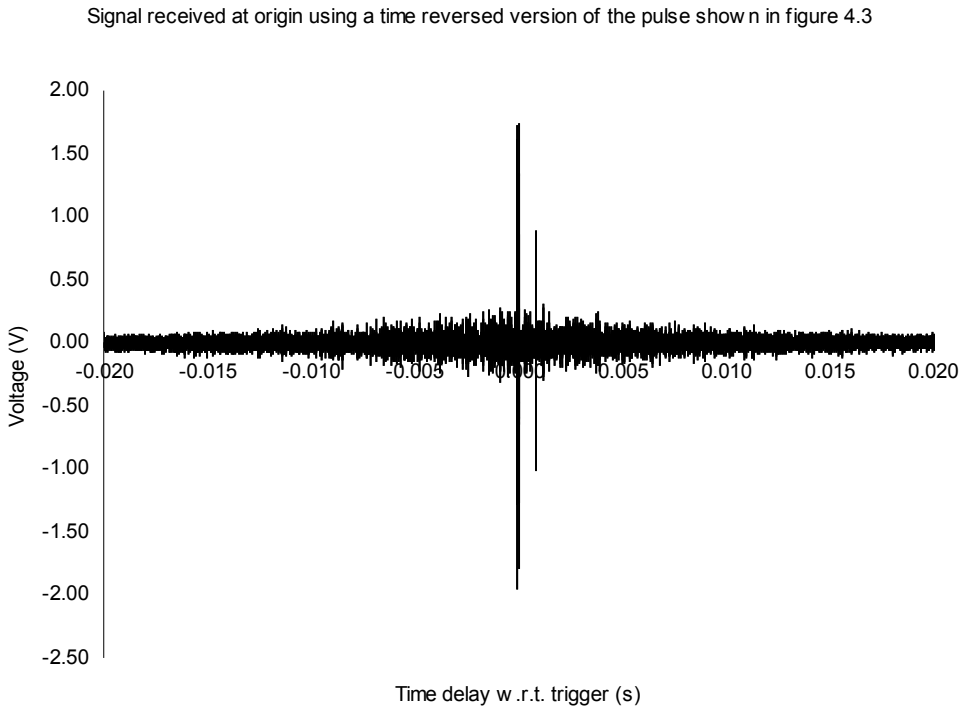

Fig 3.7: Signal received at the origin using a time reversed version of the pulse shown in Fig 3.6.

Fig. 3.7 demonstrates that the time reversed signal shown in Fig 3.6 has reconstructed the initial transmitted pulse. We can see the original pulse (a single cycle sine wave), and background noise, plus a secondary (undesired) signal peak.

The signal level used for the time reversed pulse was a maximum output of 0.25V. This was scaled down from the measured maximum of ~8V peak-to-peak, to

prevent saturation of the amplifier due to high peak voltages on the time reversed signal.

If we consider the secondary signal peak, we find the time delay between the two peaks is ~0.9ms which implies it has travelled a further ~1350 mm, the distance between the origin and the far wall of the tank. The most likely cause of this peak is a reflection of the time reversed signal from the receiver, off the far wall and back again. This is a reasonable assumption because the situation is not a true time reversal. In order to produce a true time reversal we would have to replace the original acoustic source (our source transmitter) with an acoustic *sink* to remove the energy from the system after the pulse has been reconstructed. This was not achievable in these preliminary experiments, this energy remained in the system, allowing it to propagate further and produce the second, undesired peak. However, even accounting for this undesired secondary peak, *we are clearly seeing the time reversal effect, already for only one time reversed sample.*

Fig. 3.8 shows the original signal reconstructed when several time reversed pulses are used (see chapter 2.1). Here we see the pulse increasing in amplitude as more channels (hence more signals) are used to reconstruct the initial pulse. We also notice how the noise level (left and rightmost on the plot) remains at approximately the same level. This is in good agreement with the expected results, in that the signals sum together constructively at one particular time to re-create the original pulse, but not at any other time.

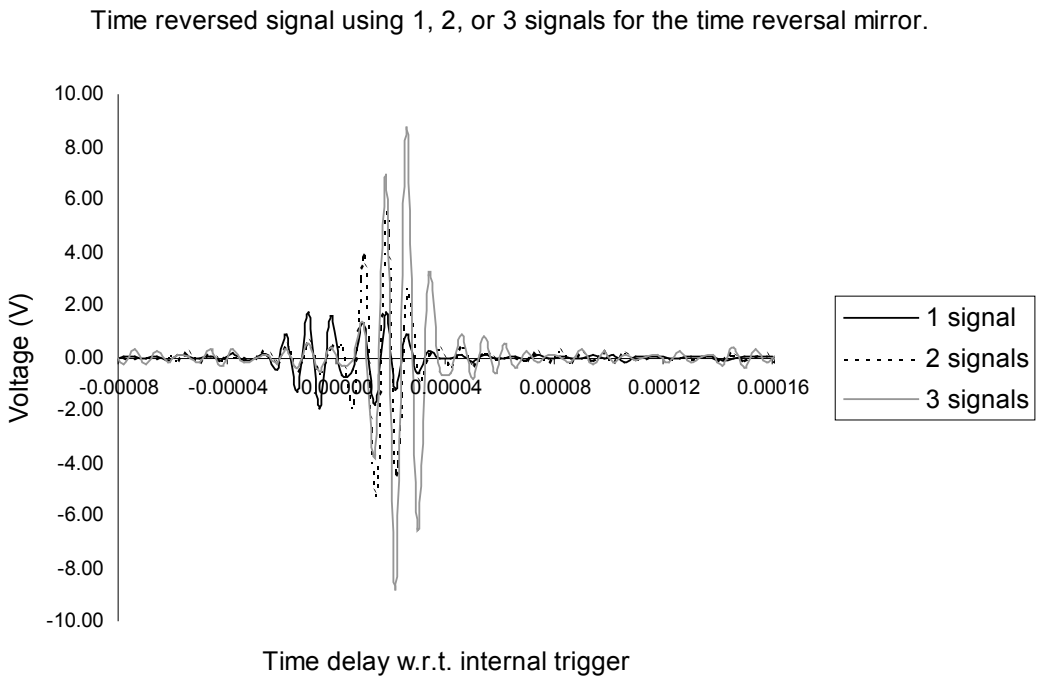

Fig 3.8: Close up of the time reversed signal for 1, 2 or 3 signals.

Temporal properties of the time reversed pulse

Now that it has been demonstrated that time reversal was possible using this experimental apparatus and technique, it is important to measure the duration of the time reversal effect. The initial experiments would take ~5 minutes to perform, so it was important to know how long time reversed pulses remained valid and whether or not the time taken to perform the experiments became significant. The initially long time was almost entirely due to the writing of the signals to the arbitrary waveform generator, which acted as the 'bottleneck' in these experiments. The time reversal technique relies on the time invariance of the propagating medium, i.e. that there are no changes in the medium over the duration of the time reversal process. Therefore, it was important to verify that this was the case in order for my experiments to be valid.

Variations of the time reversed pulse with time are shown in Fig 3.9. These plots show that there is very little difference in the appearance of the time reversed signals over the time period shown.

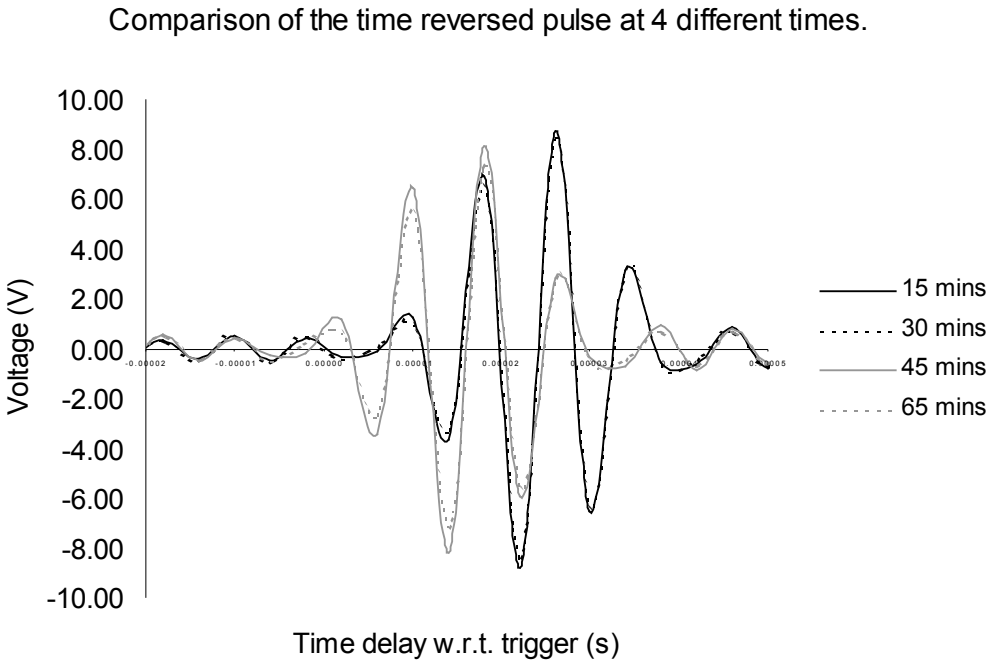

Fig 3.9: Comparison of the signal at 4 different times.

Fig. 3.9 shows that the pulse remains constant for up to 30 minutes but changes by 45 minutes. This implies that the system's acoustic properties vary very little with time (with no discernable change within half an hour of the experiment taking place). This is what we would expect, since the only cause of change would be variations in the water temperature, expected to remain relatively constant. This set of results shows that, even after an hour, the signal is still being reconstructed at the origin (albeit with some distortion). It was found that in some cases, the signal was still present up to 2 hours later, although in general the signal was seen to reduce after approximately 1 hour. *In conclusion, these results demonstrate that the time taken to*

perform the experiment is unlikely to affect the time reversal process, at least with the present settings.

Spatial properties of the time reversed pulse

According to the theory of time reversal (see Chapter 2), the reconstructed pulse should only appear at the origin in space of the transmitted pulse. A single-cycle 100 kHz sine wave pulse was time reversed, and the resulting time reversed field was scanned to determine the localisation of the reconstructed pulse. An area of 200mm x 200mm was scanned at 20mm intervals and the maximum peak voltage was measured. Fig. 3.10 shows the resulting two-dimensional surface plot. The origin of the scan grid (X=0 Y=0) corresponds to the origin of the original pulse.

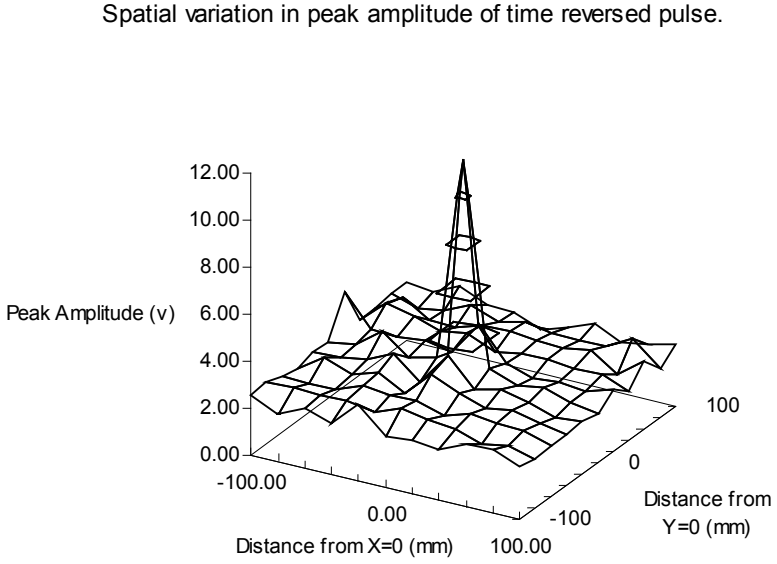

Fig.3.10: 2-d scan of area around the origin of the transmit pulse, at 20mm steps.

Fig 3.10 shows that the time reversed pulse is localised to a small area around the origin of the transmit pulse. The peak voltage drops off at a distance of 20mm (approximately 4/3 of a wavelength) in any direction from the origin in the x-y plane.

Theory predicts (see section 2.2.1) that the best possible resolution for a reconstructed signal is ~ $\lambda/2$ of the origin (at most), so the experimental results are in reasonably good agreement with the theory.

3.3 Experiments into the stability of time reversal in a waveguide

3.3.1 Description of the new time reversal experimental set-up.

In order to determine the practical limits imposed by surface waves on the time reversal process, several changes were made to the experimental set-up. These are described below.

Tank change

It was decided that a suitable method of investigation would be to examine the effects of surface waves using a shallow water tank. This was to emulate as closely as possible the experiments performed in the ocean by Kuperman *et al*. [18-21]. These experiments were performed over long distances (~14.5km) in water depths of ~110-130m. In these experiments, we can consider the ocean to be acting like an acoustic waveguide. Using an acoustic waveguide should also prove useful in quantifying the effect of surface waves because all but two ray paths (the direct transmission and the first reflection of the bottom) will interact with the (wavy) surface. To achieve this, another water tank was used. This new water tank was much more suitable for this set-up, having internal dimensions of ~1980mm x ~1720mm. The water depth was approximately 170mm, however the water depth varied across the tank due to the weight of the water causing the bottom to sag in the middle. The actual water depth was sampled at intervals of 100mm in the x and y direction (taking one corner of the tank as the origin), to the nearest millimetre. The results are summarised in Fig. 3.11.

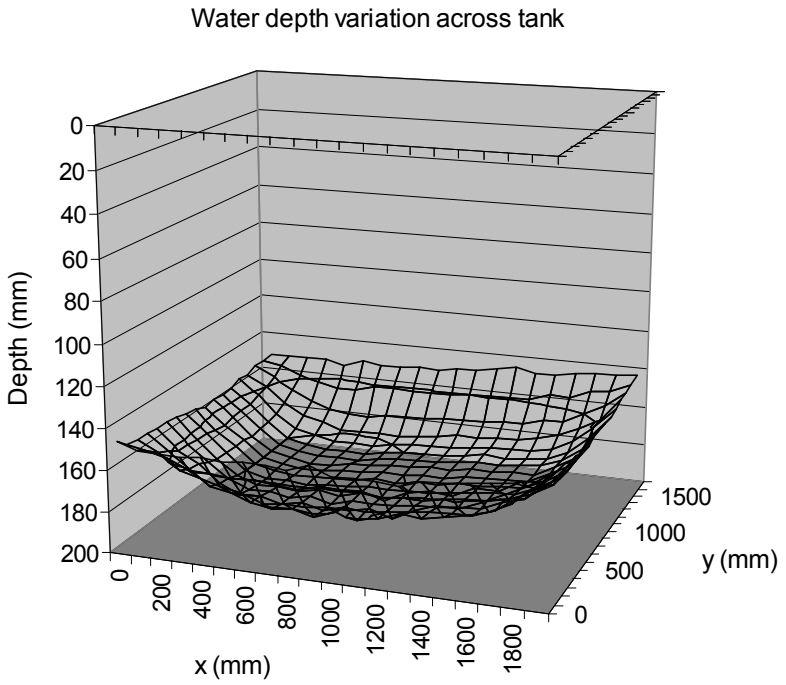

Fig. 3.11: Water depth variation across the new tank

Use of a wavemaker

To produce surface waves, a flat paddle wavemaker was used. This wavemaker consisted of a heavy-duty 3-phase electrical motor connected to a flat wheel. This wheel was linked to a crankshaft, connected to a flat steel paddle.

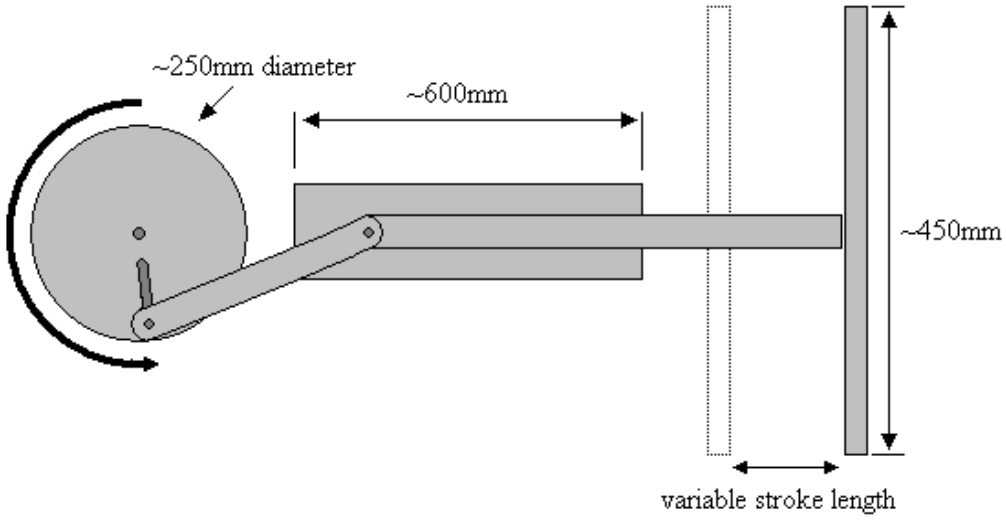

Fig. 3.12: Diagram of the wavemaker used in the new experiments.

The wheel contained a cutout that allowed varying the stroke-length of the paddle, and the motor had a variable speed controller, allowing changes to the frequency of the surface waves.

Two additional metal bars were attached to the wavemaker, so that it could be attached to the middle of one of the short sides of the tank. The wavemaker was clamped to the tank's frame to ensure it remained stationary with respect to the tank. The wavemaker was positioned so that it sat outside the tank, with the drive shaft running over the lip, and the paddle dipping into the water. The depth of paddle in the water was ~5.3 cm.

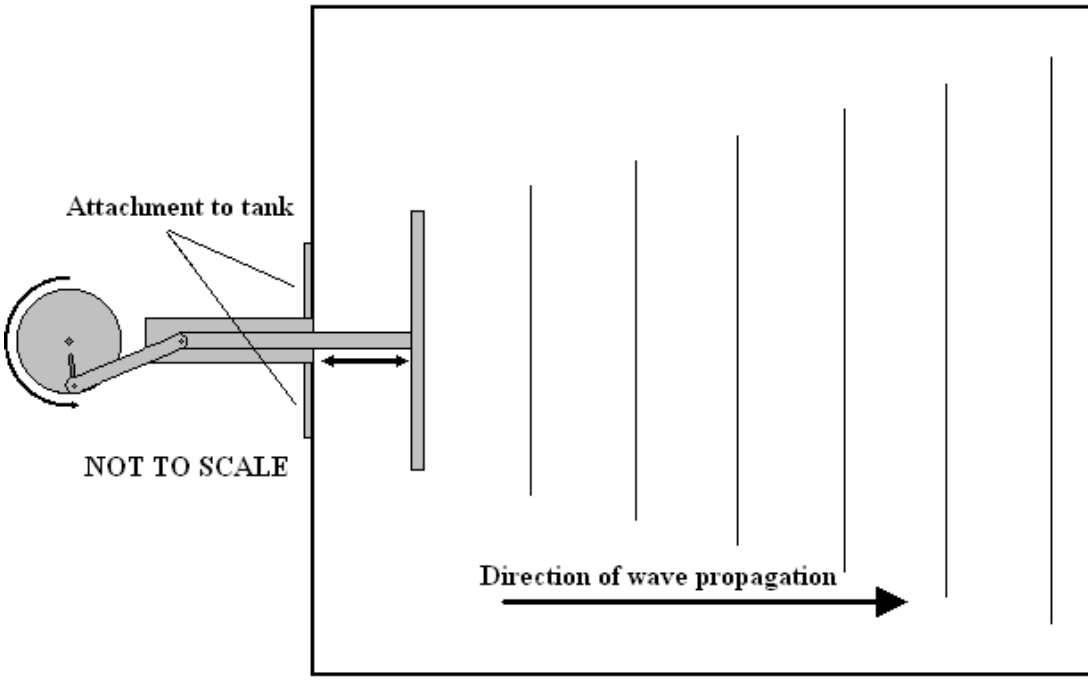

Figure (3.13): Diagram of the wavemaker attached to the tank (view is from above looking down).

Changes in experimental technique.

When moving from the initial (smaller) tank experiments to the large shallow tank used for the surface wave experiments, several changes were made to the experiment. These are summarised below:

1) The LabView code used to control the experiment was modified so that the experiments would run faster. For example all three waveforms were captured simultaneously rather than one after another.
2) The voltage auto-scaling subroutine (which altered the vertical scaling so that the signal fit the screen) was removed, as it was not appropriate for a time varying signal.
3) The signals were no longer time averaged, as it was not appropriate for a time varying signal.
4) When capturing the time reversed signal, 50 samples with no averaging were taken rather than 1 sample of 100 sweeps. This gave an idea of the variations of the time reversed signal with time.
5) The transducers were re-mounted so that they pointed in the horizontal plane, rather than the vertical. This ensured that the main contributions to the received signal(s) came from the direct path and the first few multiples.

Transducer positioning.

The single transmitting hydrophone, and the 3 hydrophones used for the time reversal mirror were all mounted in a fixed position on a metal frame.

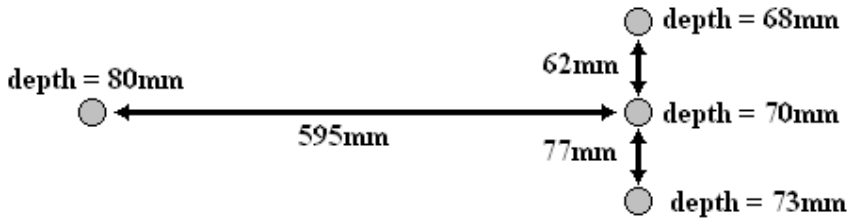

Fig. 3.14: Relative transducer positions (grey circles).

The metal frame was supported above the tank so that only the metal tubes that held the transducers entered the water. The positioning of the metal frame was not fixed, and varied for different experiments (notably the variation in the direction of surface waves with respect to the transducers was achieved by rotating the fixed metal frame relative to the tank). Sections 4.5 and 4.6 give full details of the positioning of the frame and the transducers for each set of experiments.

3.4. Chapter summary

This chapter described the experimental apparatus and procedure used in the time reversal experiments. The time reversal method was tested to determine its validity by comparing its performance with theoretical and/or practical results, such as the temporal and spatial resolution of time reversed pulses. Due to the slow nature of the experimental process (due to data exchange between the computer and the arbitrary waveform generator), the long-term stability of the time reversed pulse was also investigated. Once it was established that the method could be used to perform time reversal experiments, a final experimental set-up was designed. This incorporated several changes, making measuring the effects of surface waves easier to achieve.

3.5 Discussion

The major limiting factor of the time reversal method used was the long time delay, typically 1-1½ minutes per signal (~3-5 minutes for all 3) in writing the time reversed signals to the arbitrary waveform generator before they could be re-transmitted to reconstruct the original pulse. This meant that all the experiments into the effect of waves had to be designed to perform in a (pseudo-) steady state, i.e.

although the surface would be wavy, the frequency and amplitude of the waves would not be varying with time. It also meant that the experiments were limited to examining the performance of a *single* time reversed signal for each configuration. Although less than ideal, it this is not the first time that a single time reversed signal has been used for such length of time, and Hodgkiss *et al.* [19] mention that some signals remain valid in calm conditions for up to a week.

Another limiting factor was the dimensions of the tank used. In the early oceanic experiments [19], the water column was ~37 wavelengths deep (120m with $\lambda \approx 3.3$m) and the distance between source and receiver was ~1840 wavelengths (6km with $\lambda \approx 3.3$m). To achieve this, scaling at 100 kHz ($\lambda \approx 15$mm) would require a distance between the source and receiver of ~2.76m and a depth of ~0.55m. The tank available provided a depth of ~13 wavelengths and range ~40 wavelengths. This was not ideal but should still produce worthwhile results.

Although the experiments are more limited in scope than originally desired, they are valid and provide a vital 'first step' into examining time reversal's performance in wavy conditions. The results of these experiments are presented in detail in Chapter 4.

Chapter 4
Results of surface wave experiments.

4.1 Introduction to experimental variables

4.1.1 Summary of experiment

The purpose of these experiments was to examine the effect of surface waves on the signal level and stability of time reversed pulses. They also investigated different wave frequencies and the role of the angle of arrival of these waves relative to the source/TRM central axis (not previously studied, or at least not previously published). A pulse was transmitted from a single source hydrophone and sampled by a 3-element time reversal mirror. The signals were time reversed, and re-transmitted back to the origin of the original pulse where the original pulse was re-constructed. This was performed in a shallow tank with surface waves produced by a wavemaker (Fig 4.1).

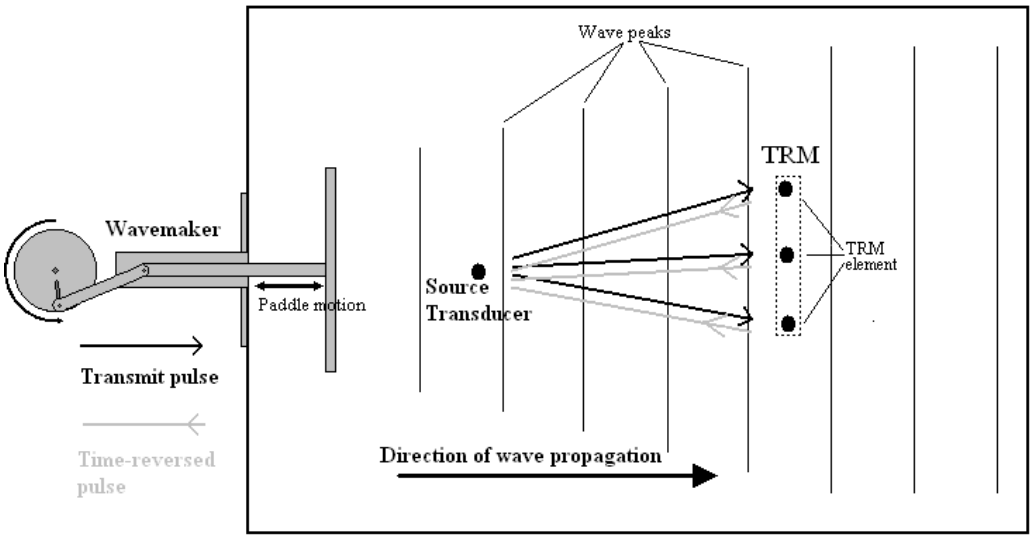

Fig.4.1 Summary of experimental set-up and technique.

Note that in Fig 4.1 the angle between the direction of wave propagation and the angle of direct propagation is 0^{o}.

4.1.2 The Experimental Variables

The experimental set-up of the time reversal experiments provided 3 independent variables:

1) The frequency of the waves.

This is equal to the rotational speed of the wavemaker. It is set electronically and alterable quickly (within seconds).

2) The stroke length of the wavemaker.

It is proportional to the wave height produced [23]. Sliding the drive-rod up and down the notch cut into the wavemaker's wheel could alter the stroke length of the wavemaker. This could only be performed between experimental runs.

3) The angle of the wavefronts with respect to the direction of direct propagation from the source hydrophone to the time reversal mirror.

This was achieved by rotating the metal frame holding the 4 hydrophones (the source and the TRM). This rotated the direction of propagation with respect to the direction of the surface waves while keeping the relative positions of the source and TRM constant. This could only be performed between experiments.

As the frequency of the waves was the only variable that could be altered during an experiment, it was decided to break the investigation into two different series. The first was designed to examine the effect of stroke length (proportional to wave height) for a range of wave frequencies, with the angle of signal propagation relative to the direction of surface wave propagation fixed. The second series of experiments was designed to examine the effect of the angle between the direction of signal propagation and the direction of surface wave propagation, with the stroke length fixed, again for a range of wave frequencies. Their results are shown in sections 4.5 and 4.6.

4.1.3 Frequency measurements

The electronic controller for the wavemaker consisted of a 3-phase power supply and a variable voltage controller, used to control the speed of rotation of the wavemaker's wheel. In the absence of any documentation, it was important to determine the relationship between the settings on the controller and the rotational frequency of the wheel. To do this, the controller was set, and the time taken to perform a number of complete revolutions was measured manually using a stopwatch. This was repeated twice more at each speed setting to provide an average value. The results of these measurements are displayed in Table 4.1.

Controller speed setting	Time for N revolutions (s) (±0.1s)				Average time for one revolution (s)	Frequency (Hz)*
5	N = 10	78.83	79.61	79.75	7.94 ± 0.01	0.126
10	N = 10	36.69	36.65	36.75	3.67 ± 0.01	0.273
15	N = 10	23.96	23.94	23.84	2.39 ± 0.01	0.418
20	N = 10	17.79	17.79	17.78	1.78 ± 0.01	0.562
25	N = 10	14.09	14.12	14.12	1.41 ± 0.01	0.709
30	N = 10	11.73	11.67	11.65	1.17 ± 0.01	0.856
35	N = 10	10.00	9.97	9.96	0.998 ± 0.01	1.002
40	N = 10	8.68	8.71	8.69	0.869 ± 0.01	1.150
45	N = 10	7.74	7.70	7.73	0.772 ± 0.01	1.295
50	N = 20	13.85	13.81	13.86	0.692 ± 0.005	1.445
55	N = 20	12.68	12.60	12.64	0.632 ± 0.005	1.582

*Table 4.1: Relationship between controller speed setting and rotational frequency. *: the errors for frequencies were all less than 0.8% of the frequency value, and are not considered to be significant. This is summarised in Fig 4.2.*

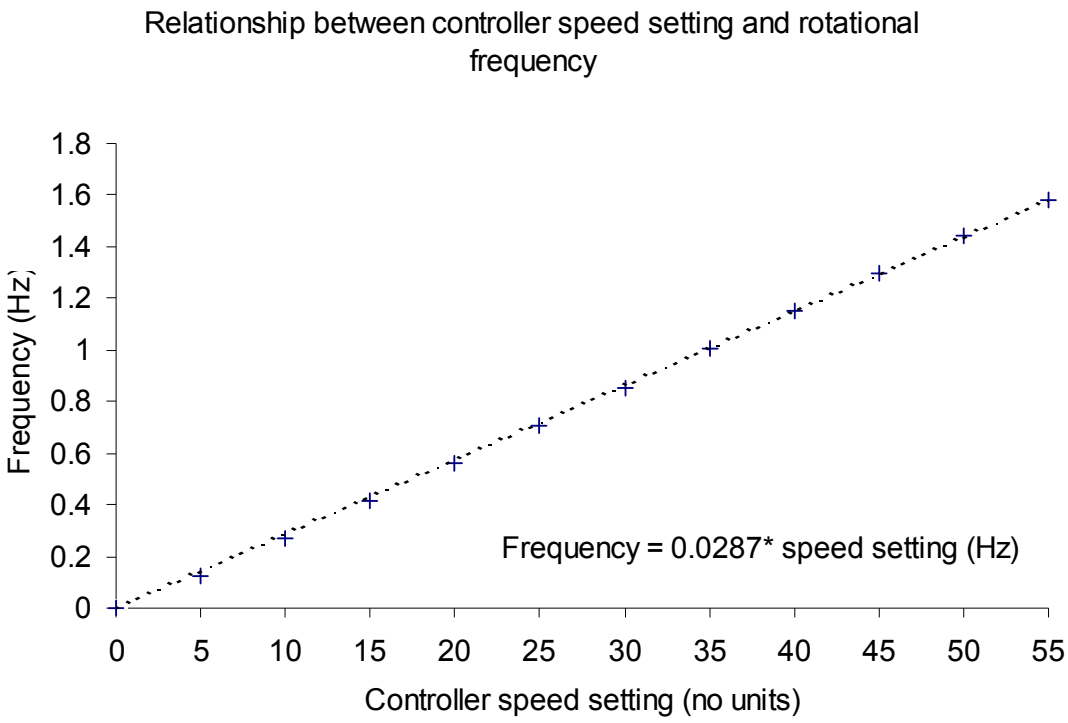

Fig. 4.2: Linear relationship between controller setting and frequency. Frequencies are accurate to 0.8%. See text for details.

Fig. 4.2 shows that the relationship between the controller speed setting and the rotational frequency of the wavemaker's wheel (and therefore the frequency of the water waves) is linear, and regression with Excel yields:

F = 0.0287 * speed setting (Hz) (4.1)

This relationship will be used throughout these experiments when displaying the wave frequency.

4.2 Preliminary measurements

4.2.1 The experimental time window

With the transducers positioned approximately in the centre of the water tank, a test pulse was used to determine the lengths of time taken for the signal to travel along various different path routes. This was important because only the signal that

had travelled from the transmitter to receiver either directly or after reflection off the bottom and/or surface (i.e. caused by the 'waveguide' nature of the set-up) was desired for the time reversal.

Initially a test pulse of a single-cycle 100-kHz sine wave was used to determine the arrival times for the direct signal(s) and the first reflections from the walls. A single-sine wave cycle was used in many of the earlier time reversal experiments, such as those outlined in section 2.2. It became apparent that a single cycle would not produce a large enough voltage to allow useful measurements to be taken. (It would often reduce to a level similar to the level of background noise when surface waves were manually applied, preventing any useful measurements of signal loss being taken). The number of cycles was increased to three, which increased the received signal voltage from ~1V peak to peak to ~6V peak to peak. Increasing the number of cycles further increased the amplitude further, but the longer duration pulses made it difficult to resolve the direct signals from reflected signals, so 3 cycles was deemed a suitable compromise. (The signal voltage was also increased due to problems with electrical noise; see section 4.2.2 for more details). Fig. 4.3 shows a plot of the arrival times for these signals, typical of the signal arriving at any of the three TRM elements.

The signals reflected from the tank walls typically arrived ~1.1-1.4 ms after the transmission of the 3-cycle test pulse. This left a useful time window of up to ~1ms after the transmission of the original pulse. Using the transducer position displayed in Fig 4.1, geometrical calculations suggest that the time reversed signal will contain the direct signal, and signals that have reflected up to eight or nine times off the surface and/or bottom (see Appendix 1 for details).

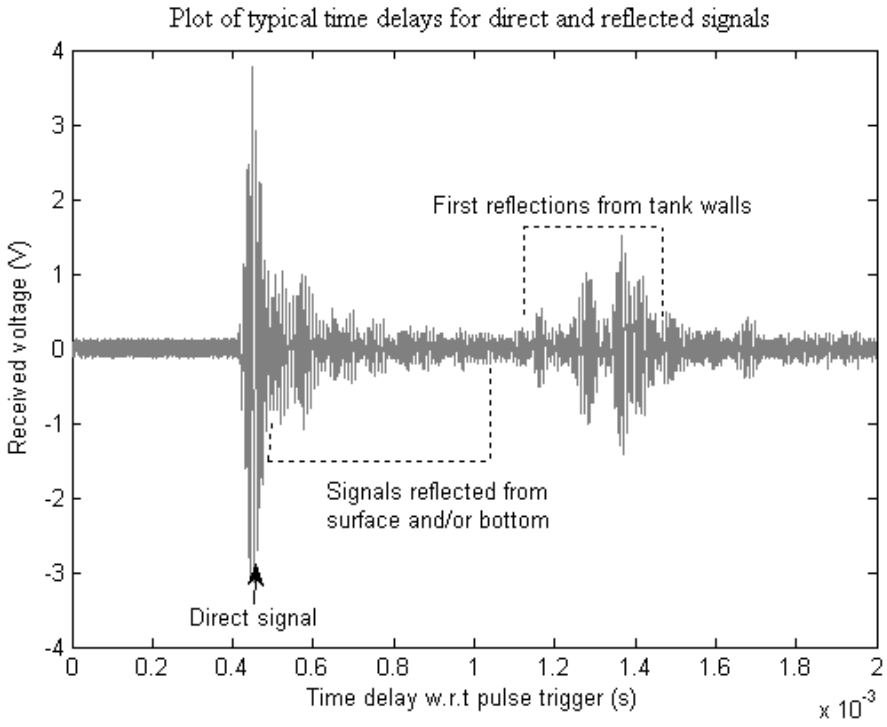

Fig. 4.3: Typical times of arrival for direct signal and its first reflections from the tank walls.

4.2.2 Electrical noise

An unexpected problem in the preliminary experiments was the presence of a large amount of high-amplitude electrical noise. After investigation, it was attributed to the electrical controller used to power the wavemaker. This controller was creating a large amount of electrical noise, picked up directly at the oscilloscope inputs. This noise consisted of two parts; a constant low-level noise of ~4V peak-to-peak amplitude, and a series of peaks of ~8V peak-to-peak amplitude. This electrical noise made capture and time reversal of any signals unfeasible (aside from the direct signal return, all other signals had a lower voltage level than the electrical noise). This was rectified by adding a noise-suppressing circuit. Some examples of the amount of noise produced after the noise suppressor was installed are shown in Fig. 4.4.

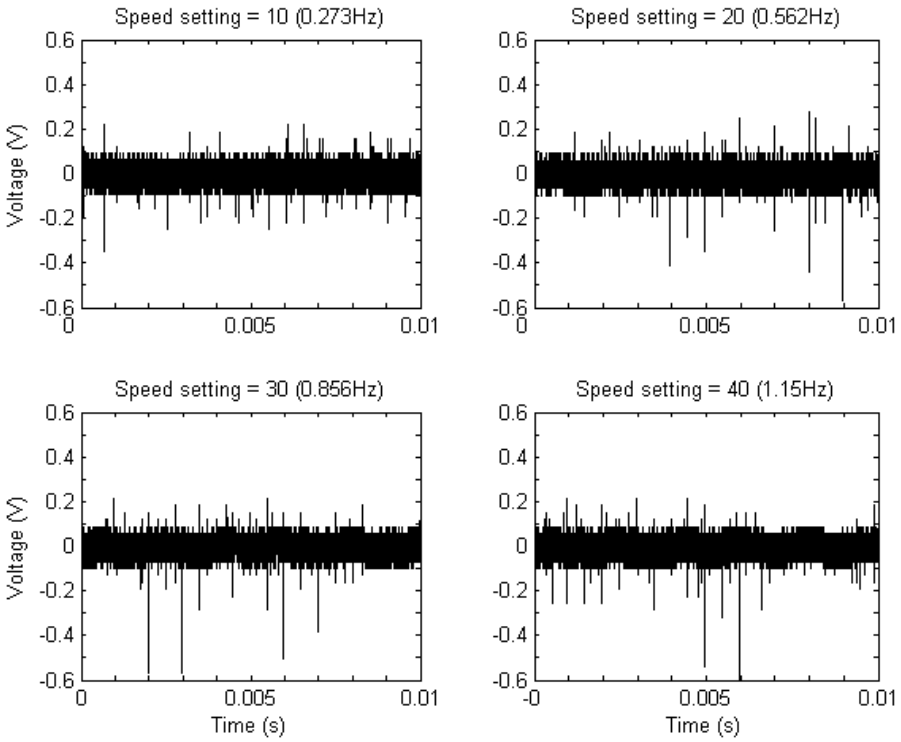

Fig 4.4: Examples of electrical noise produced at different speed settings, after introduction of the noise-suppressing circuit.

Fig 4.4 shows that the noise levels were reduced significantly, and not linked to the speed setting of the wavemaker. (The electrical noise produced before the electrical noise suppressor was fitted had the same general shape but with much greater amplitude). The addition of the suppressor allowed the experiments to be performed without any further alterations to the experimental set-up.

4.3 Method of analysis

The focus of these experiments was to measure the signal loss caused by the addition of surface waves on time reversed signals, so the analysis of these signals centred on the measurement of the peak voltage levels of the time reversed signals.

As explained previously (section 3.3.1), each experimental run contains 50 samples. The analysis for each experimental run was broken into several stages, summarised below:

1) The first of the 50 samples is plotted, and the time window in which the time reversed signal appears is manually determined.
2) The maximum absolute voltage (which is assumed to have been produced by the peak of the time reversed signal) is measured and stored in a 50-element array.
3) In turn, the file containing each sample of the run is opened, and the peak voltage within the time window specified in step 1 is measured and stored in the array.
4) Once the peak amplitude for all the samples has been measured, the array is written to file.

This produces a file containing 50 instantaneous measurements of the peak voltage, plotted for visual inspection. This was to examine the data for any abnormally high voltage points, which were possibly contaminated by electrical noise. A typical array with no noise contamination is shown in Fig 4.5.

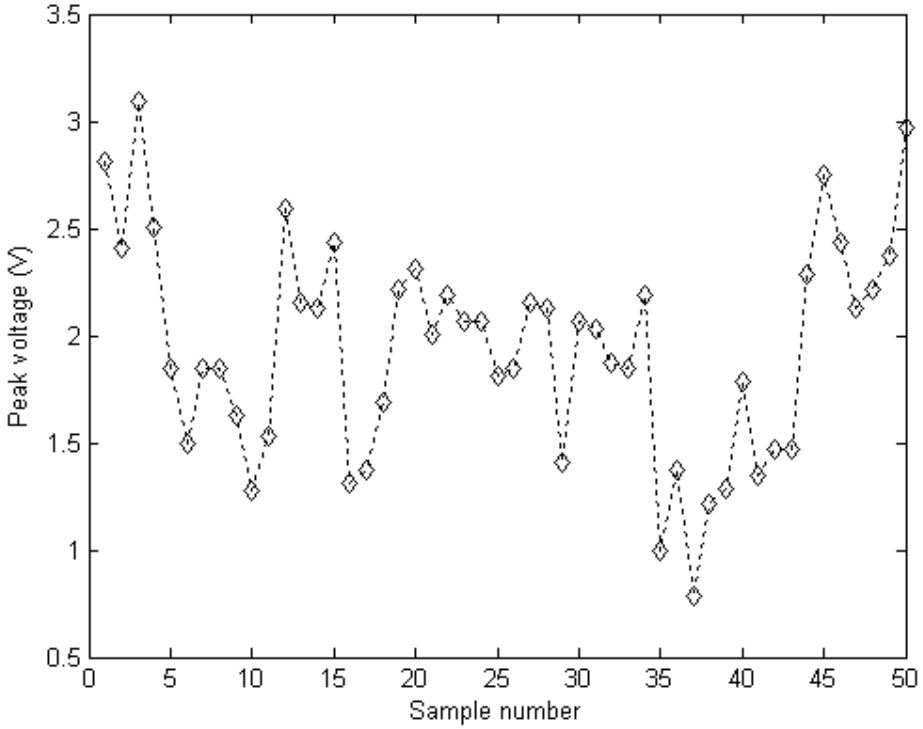

Fig 4.5 Typical array of peak voltages (see text for details)

Unfortunately, some of the samples in some runs were contaminated with electrical noise that produced erroneously high peak voltage measurements. These points would induce errors in any further analysis of the data, so had to be removed. In order to do this, the following procedure was carried out:

1) The array of the 50 peak voltage samples was plotted in a graph.
2) Any samples that produced suspiciously high peak voltages were noted.
3) All suspicious samples were individually plotted and visually examined to determine if any electrical noise was present.
4) All voltage samples confirmed to be contaminated with noise were removed from the file of the voltage samples before further analysis was performed.

Fig 4.6 shows an array with several points contaminated with electrical noise.

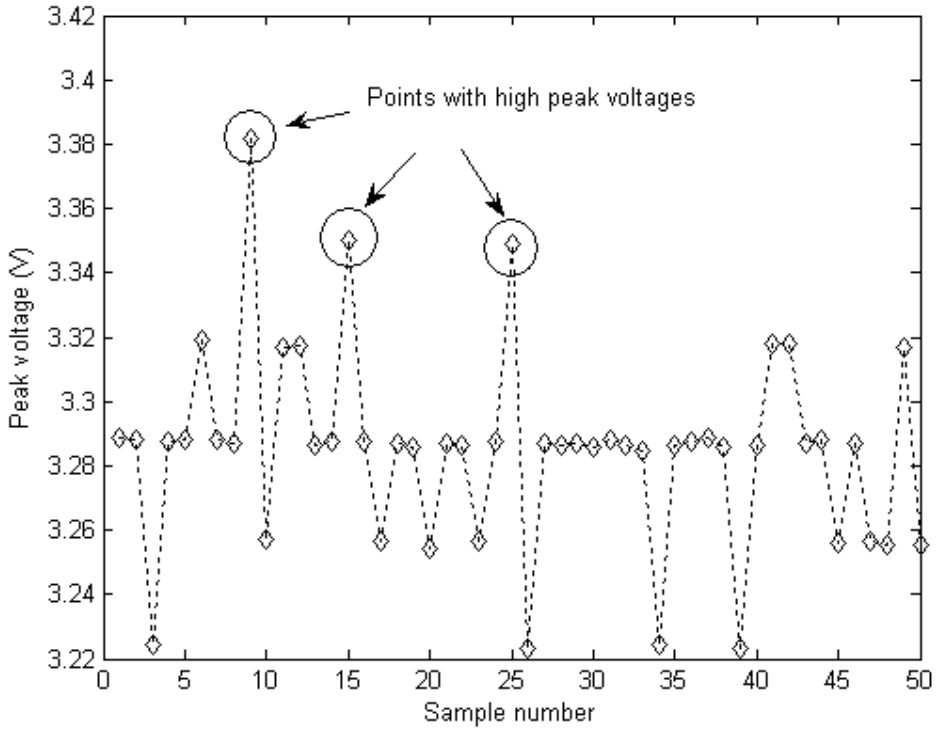

Fig 4.6: Voltage array with several points contaminated with electrical noise.

In Fig 4.6 the peak voltages from sample 9, 15 and 25 all have high peak voltages. These samples would all be individually plotted and visually examined for noise. Approximately half of all suspicious samples were found to contain electrical noise, the other half were valid measurements. Only the high peak voltages were considered for electrical noise, as this noise always increased the signal level (i.e. did not reduce it). Therefore all the lower voltage measurements are considered valid.

Fig 4.7 shows the noise contamination present on sample 9 from Fig 4.6. Note that the electrical contamination is present on most of the cycles of the sine wave. Only one contaminated peak is indicated for clarity.

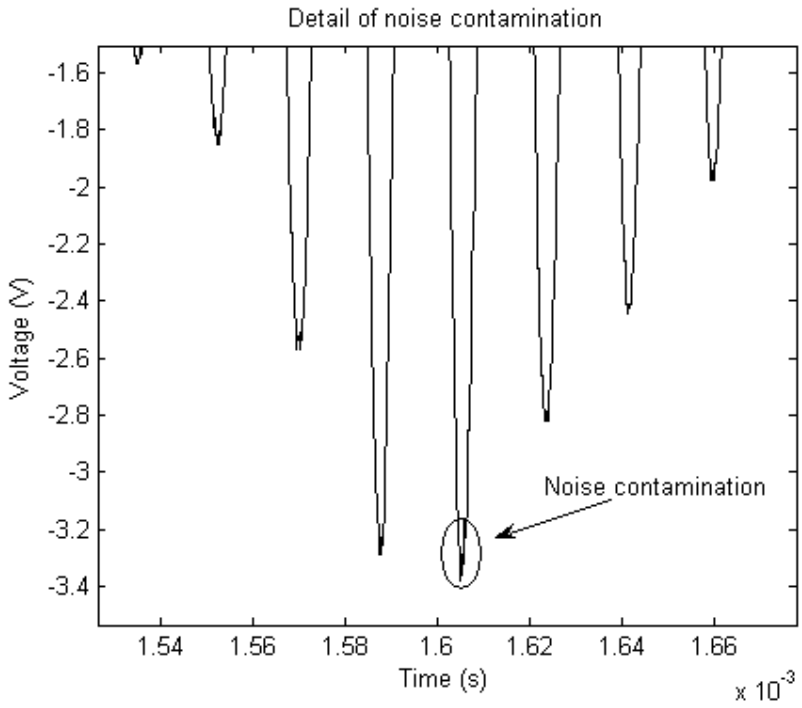

Fig 4.7: Example of a time reversed signal contaminated with electrical noise

On average, 1-2 samples per 50 were found to contain electrical noise and were removed. Once any samples containing electrical noise contamination had been removed, the final stage was to gain a measure of the signal level, and the variation in signal level caused by the effect of waves. This was achieved by measuring the mean and standard deviation of the voltage samples.

4.4 Wave height measurements.

According to [23], in shallow water, we can reason that the volume of water displaced by the wavemaker should equal the crest volume of the propagating waveform. This is shown in Fig. 4.8.

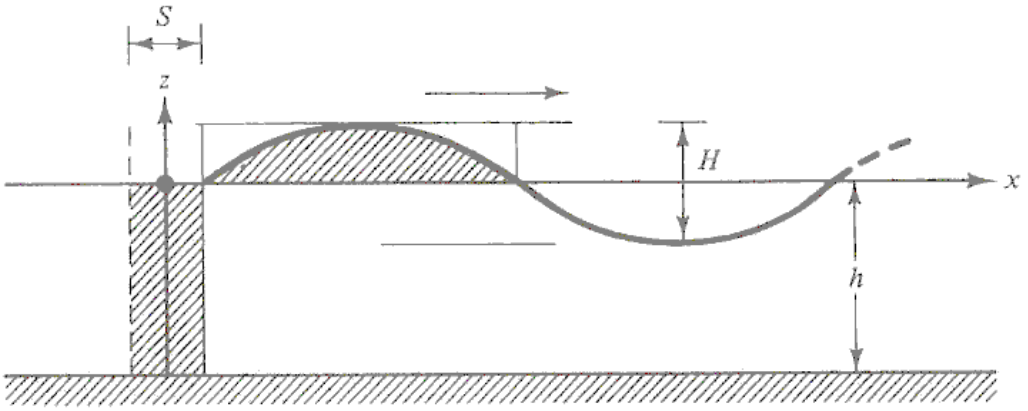

Fig. 4.8: Simplified wavemaker theory. Taken from [23].

This can be expressed as:

$$\left(\frac{H}{S}\right)_{piston} = kh \tag{4.2}$$

where H is the peak-to-peak wave height, S is the stroke length of the wavemaker, *h* is the height of the water column, and *k* is the wavenumber of the water wave.

Rearranging this, we find

$$H = S\,k\,h \tag{4.3}$$

The wave height is linearly dependant on the wavemaker's stroke length.

This was the original motivation behind the design of these experiments. It quickly became apparent, however, that the height of the water waves produced was not related to the stroke length in the manner predicted by Equation. 4.2. This is because two assumptions made in formulating Equation 4.2 were not valid:

1) The paddle of the wavemaker does not actually span the entire water column. As the paddle only dipped into a small area within the tank, it allowed water to travel around it as it moved, negating the effect of the paddle's stroke. This effect was most apparent at low frequency settings (slowest paddle speed).
2) There is in fact interference from the wave reflections.

Due to the relatively small size of the tank, reflections from the boundaries would interfere with the waves produced by the wavemaker. This meant that rather than producing a single set of waves from the wavemaker (as shown in Fig. 4.1), a set of standing waves would be produced for each particular wavemaker setting.

This meant that it would not be possible to use Equation 4.3 to estimate wave heights. To remedy this, it was decided to perform a further set of experiments to adequately determine the wave heights at different points in the water tank for the wavemaker settings used in the stroke length and wave height experiments. The details of these experiments are outlined below.

The experiment was set up using just the tank and the wavemaker, removing the rig containing the source probe and TRM elements. Four points were chosen to measure the wave heights, specific distances away from the wall with the wavemaker, and placed centrally between the two side walls of the tank. The distances away from the front wall were chosen as ~800mm, ~930mm, ~1000mm, and ~1200mm (Fig. 4.8).

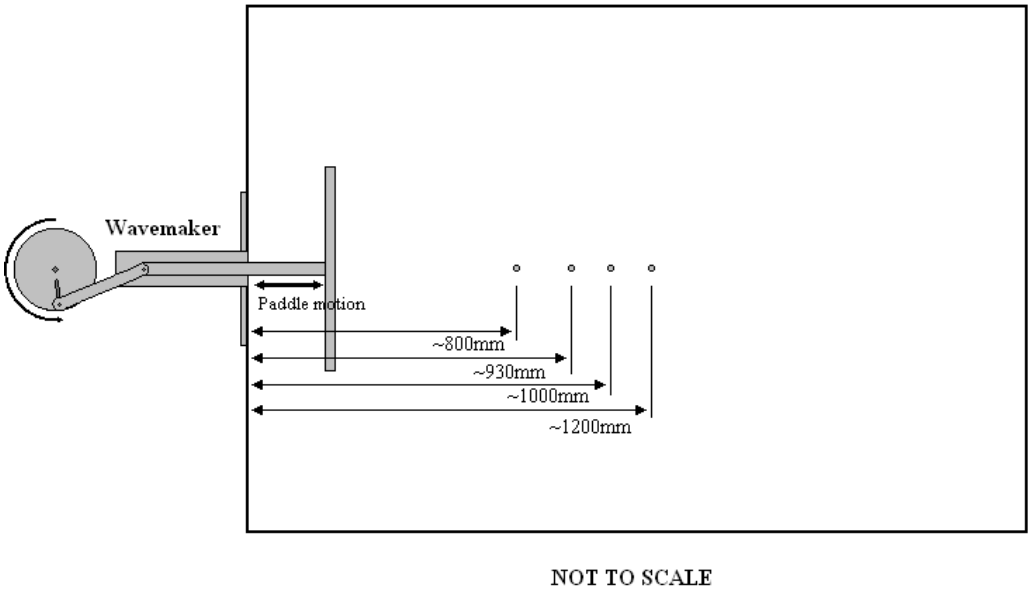

Fig. 4.9. Position of points where wave heights were measured.

At each of the positions, the wave height produced for every configuration of the wavemaker used for the other experimental runs (see sections 4.5 and 4.6) was measured. The wave's peak and trough were each measured to the nearest millimetre, so the total error in the peak-to-peak wave heights was ±1mm.

These measurements allow comparison between the measured wave height and the corresponding change in signal level for time reversed signals. They are summarised below (Figs 4.10 to 4.14). The averaged values of wave heights, as shown in Fig. 4.14, will be used in Sections 4.5 and 4.6.

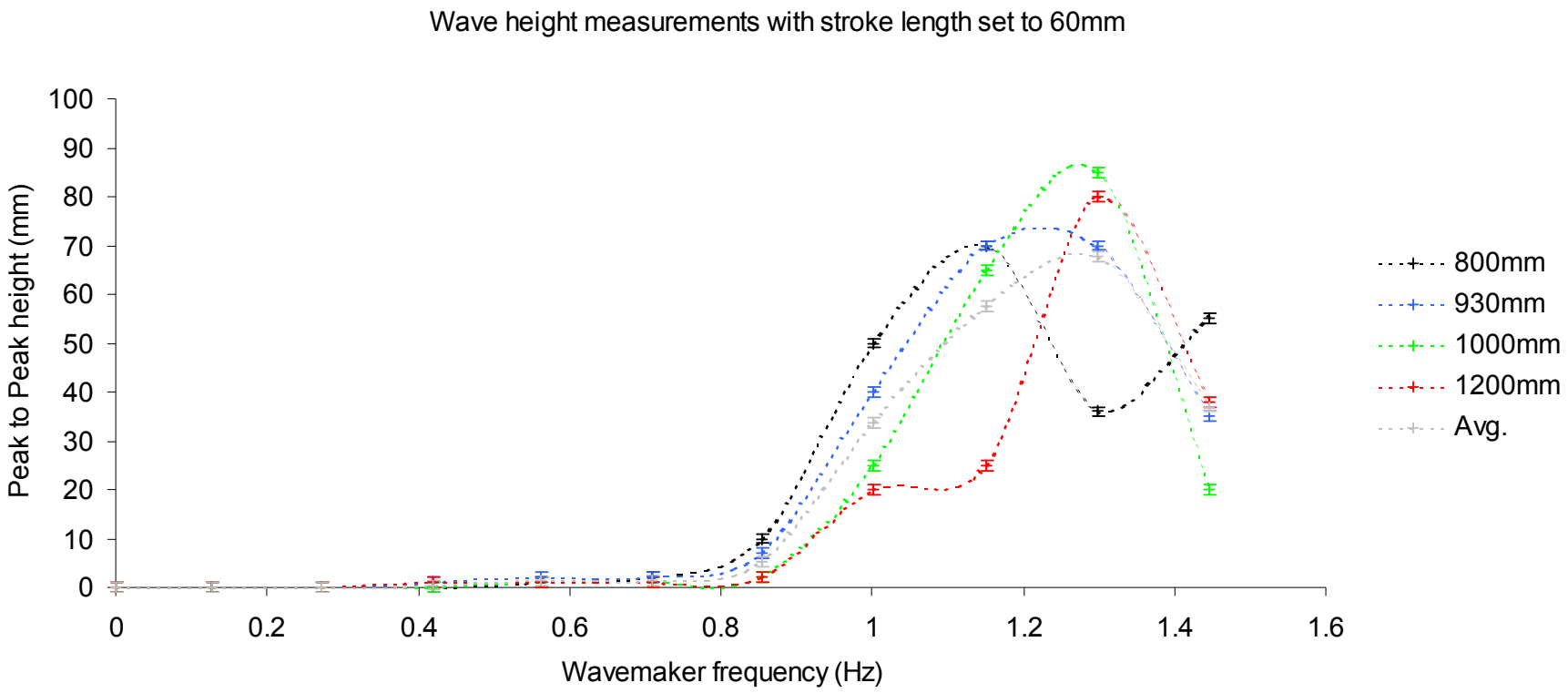

Fig. 4.10. Wave height measurements at different positions with the stroke length set to 60mm

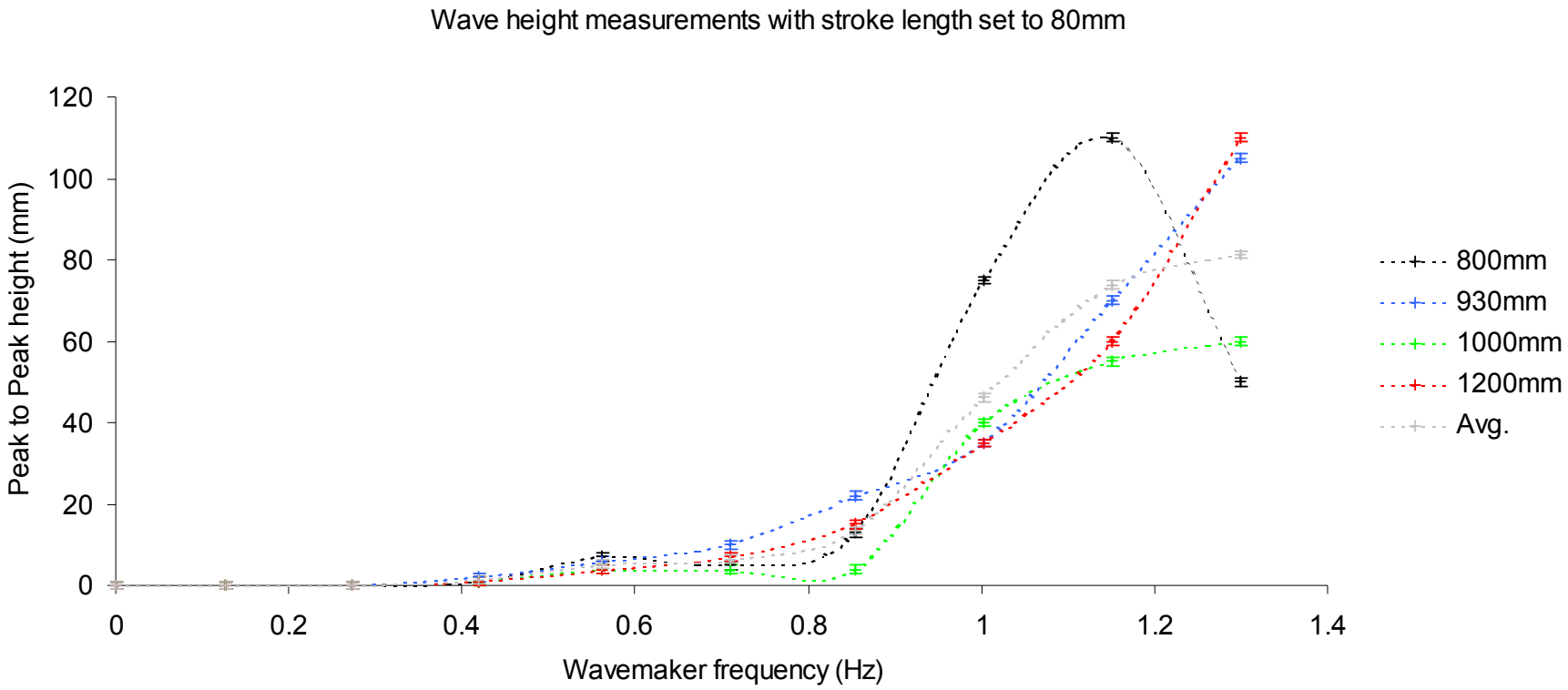

Fig. 4.11. Wave height measurements at different positions with the stroke length set to 80mm

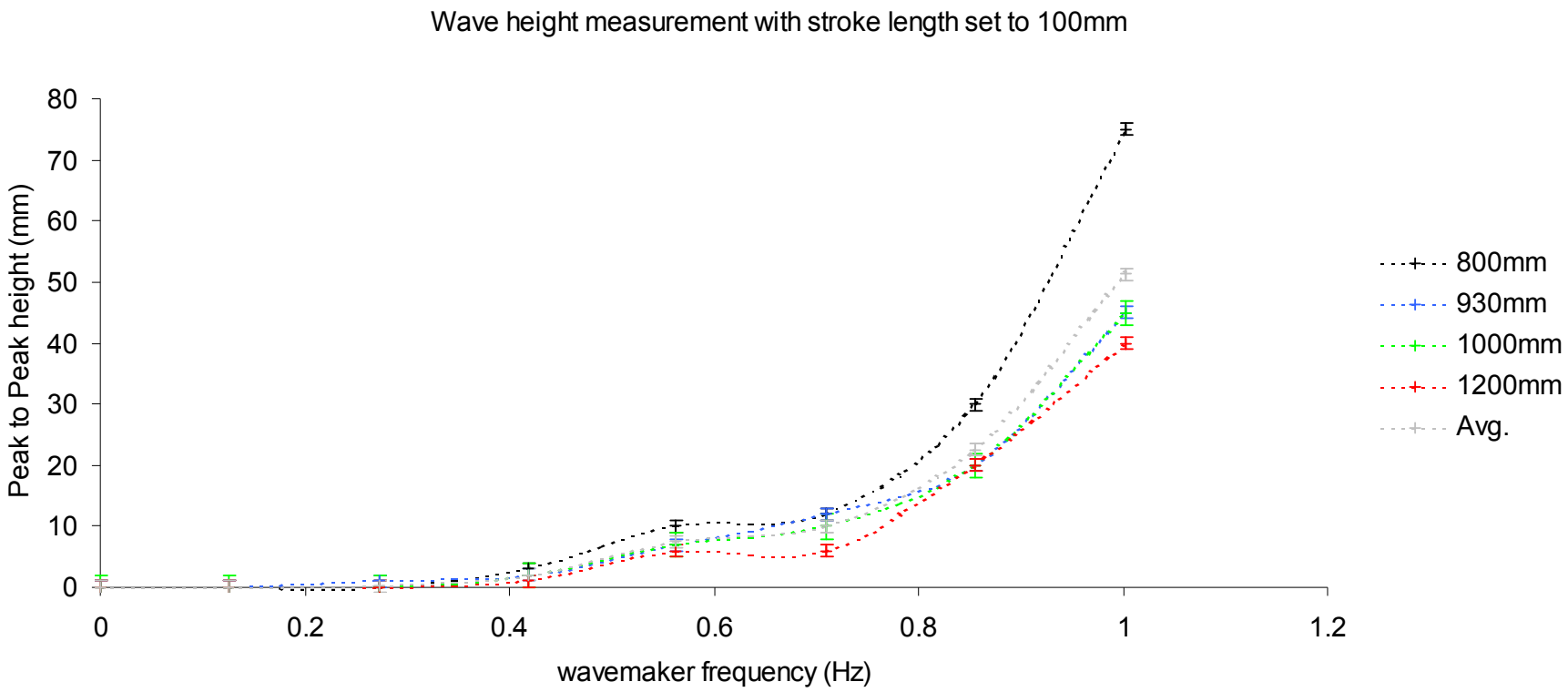

Fig. 4.12. Wave height measurements at different positions with the stroke length set to 100mm

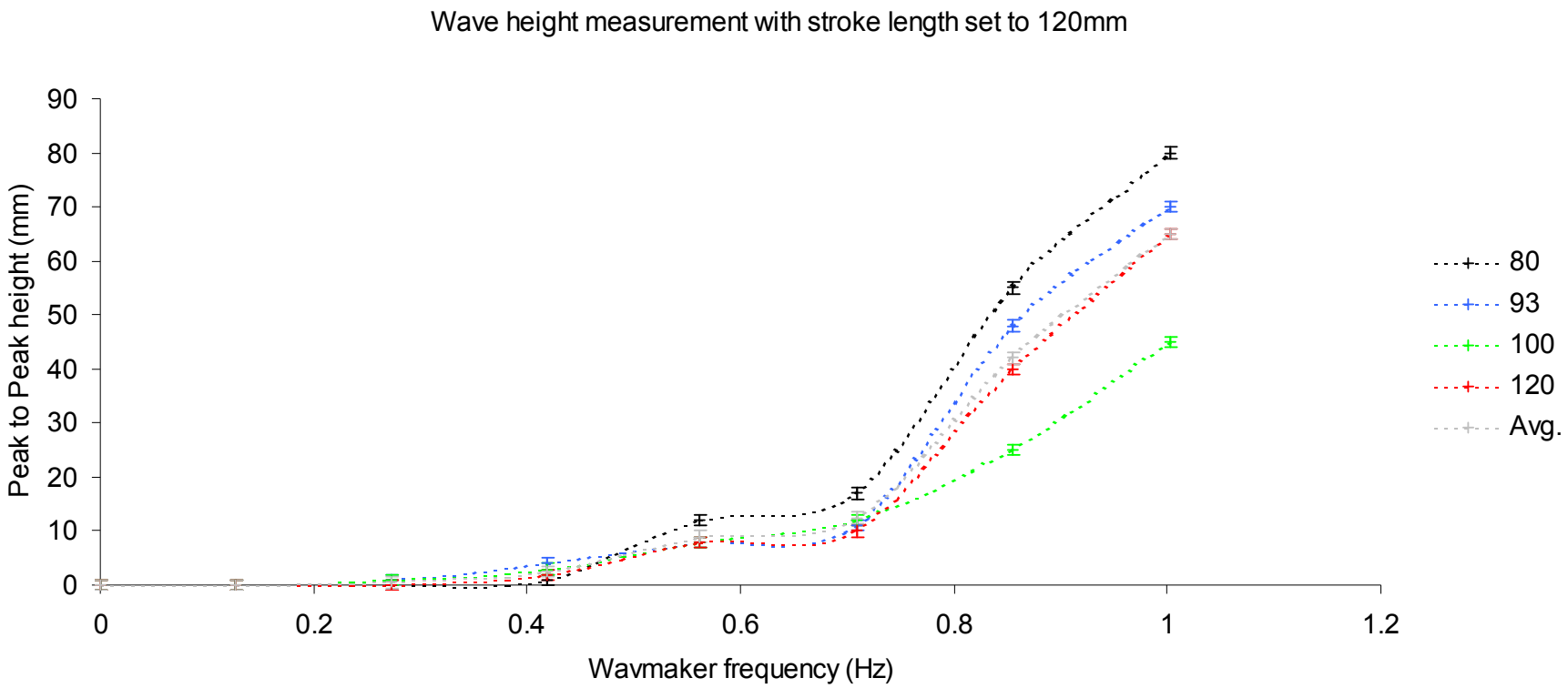

Fig. 4.13. Wave height measurements at different positions with the stroke length set to 120mm

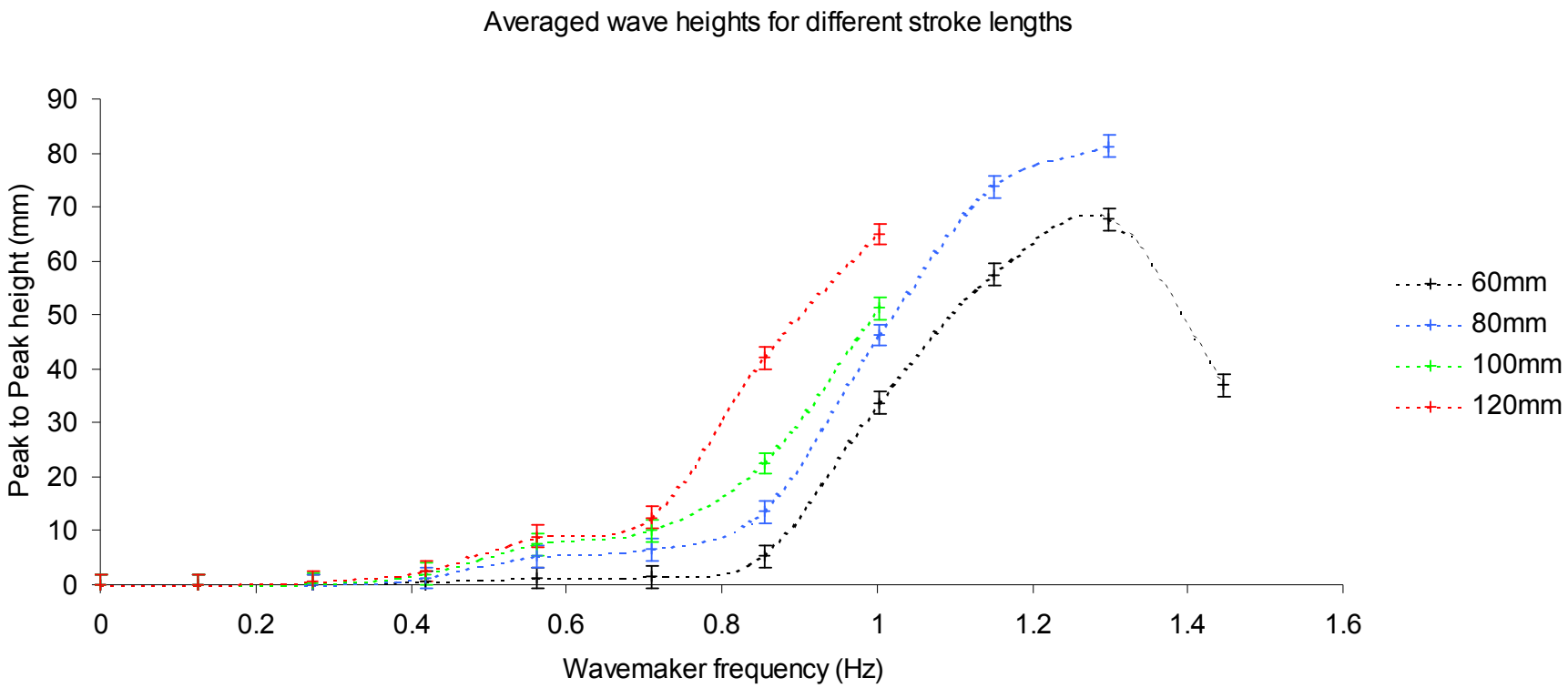

Fig. 4.14 Average measured wave heights for different wavemaker stroke lengths.

Comparison of theoretical waveheights with experimental measurements

Fig 4.15 shows the difference between the experimentally measured waveheights measured in the tank, and the theoretical predictions obtained from eqn. 4.3.

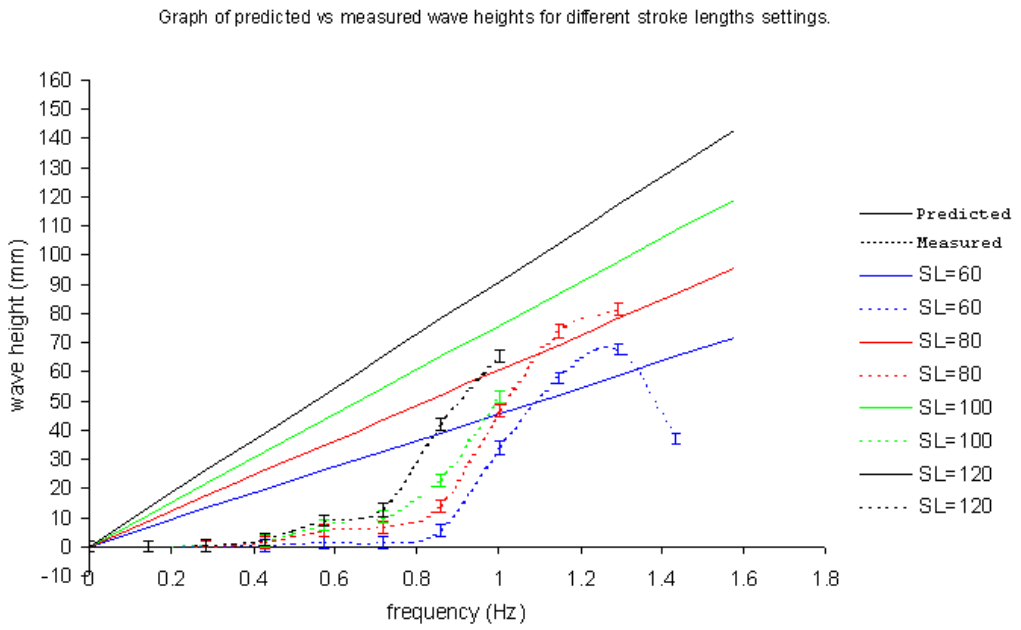

Fig. 4.15: Predicted vs. experimentally measured waveheights for different stroke lengths

This demonstrates the inadequacy of the theoretical model that was used. In all the experimental results shown in this chapter, the experimental values for waveheight are used.

4.5 Stroke length measurements.

To determine what effect the stroke length setting on the wavemaker had on time reversed signals (by altering the height of the water waves produced), time reversal experiments were carried out at 4 different stroke length settings. The stroke length settings were 60, 80, 100, and 120mm. For each stroke length, the signal would be time reversed at a particular wavemaker speed setting, and then the speed setting would be varied in steps of 5 (0.126 Hz), from 0 (no surface waves) to a maximum value (the maximum speed setting that could be used without the water waves spilling over the sides of the tank). The source and TRM were orientated so that the waves produced by the wavemaker travelled parallel to the direction of a direct transmission and return from the source to TRM (Fig. 4.16).

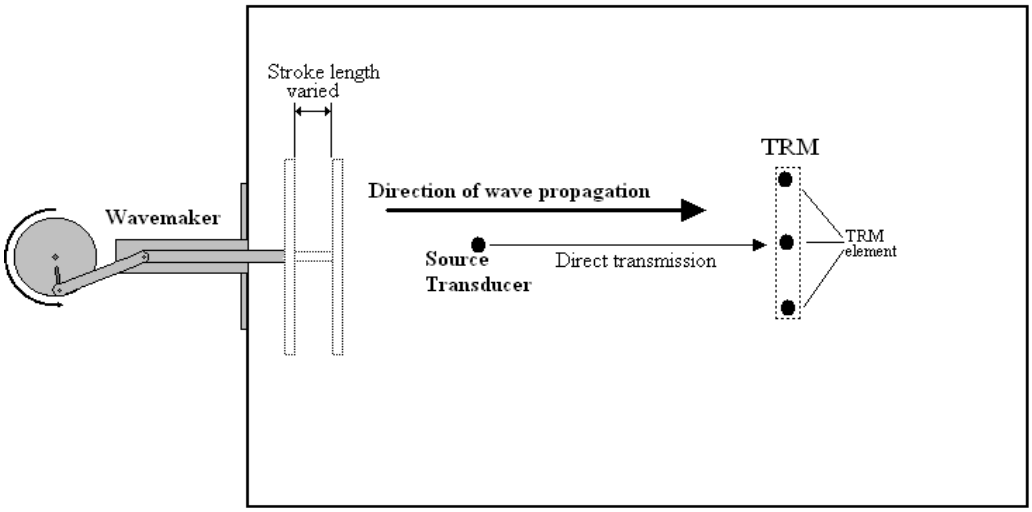

Fig. 4.16. Experimental set-up for stroke length experiments.

The results of the peak voltage outputs measured for each stroke length are summarised in a single plot per stroke length. Individual plots for each time reversed signal are presented in Appendix 2.

The results are then plotted, comparing the performance of each pulse across the range of wave heights to the signals at the wave heights the pulse was time reversed at. For example, a signal time reversed with 0-mm waves would see all its measurements compared to the voltage measured in the absence of surface waves. Figs. 4.17 to 4.20 present the results of the measured peak voltages. Figs. 4.21 to 4.24 display the relative performance of the different time reversed pulses. Here, at each waveheight the voltage level of each signal is compared with the voltage level of the signal time reversed *at that waveheight*. Note that any increase in performance (i.e. a positive relative performance) is an unexpected result, as we would not expect a signal time reversed with a large amount of surface waves to produce a higher peak voltage in calm conditions than the signal time reversed in calm conditions (for example).

Stroke length set to 60mm

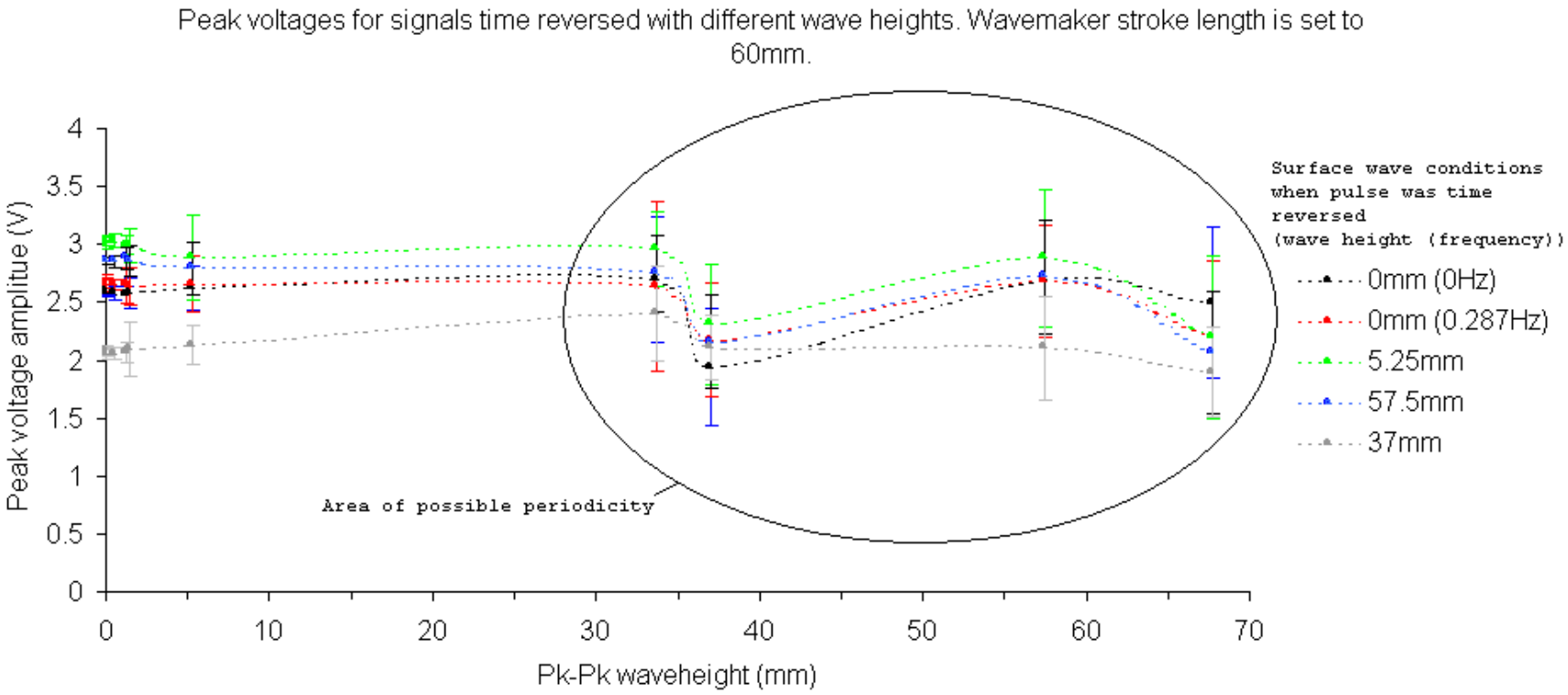

Fig.4.17: Peak voltages for signals time reversed at different wave heights for a wavemaker with a 60mm stroke length (Note that the dataset for the signal time reversed at 0.574 Hz(~1.25mm) was corrupt and so is not shown).

Stroke length set to 80mm

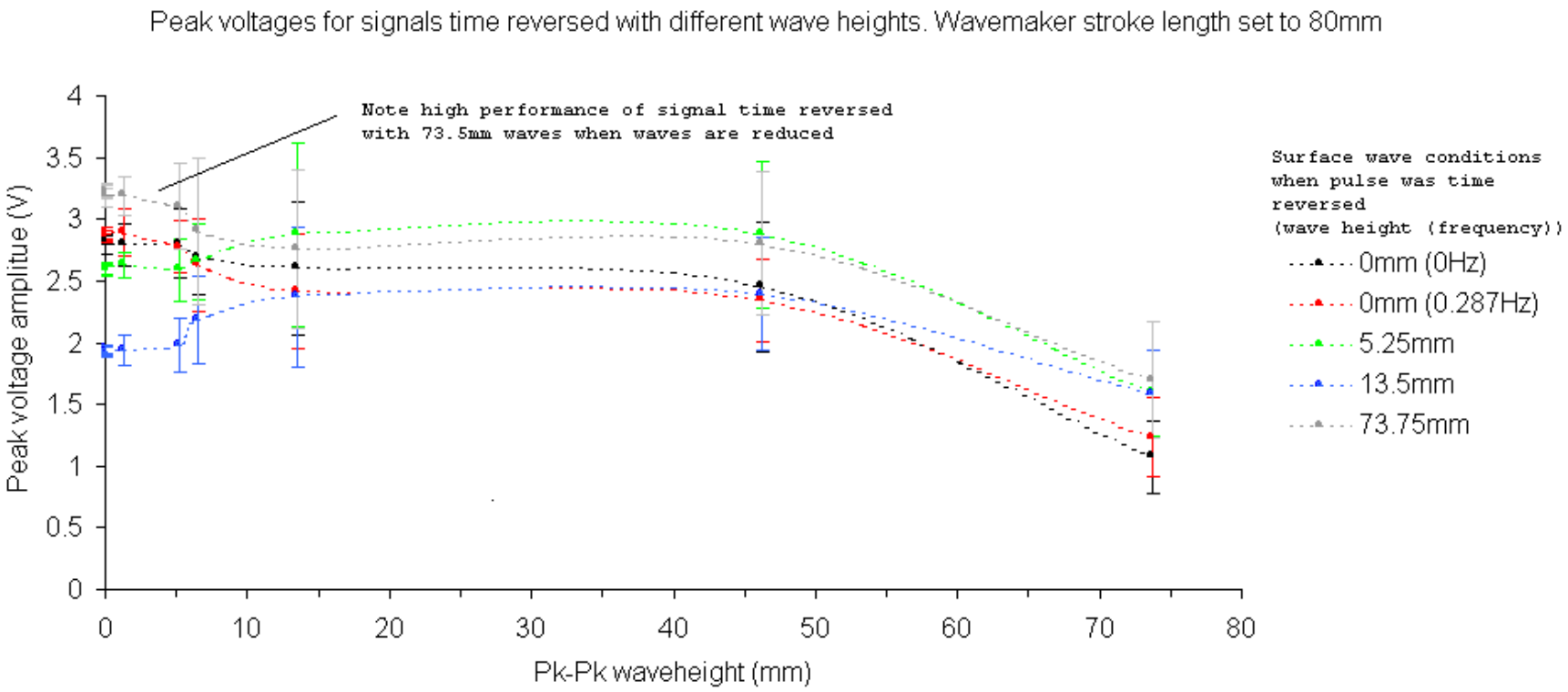

Fig. 4.18: Peak voltages for signals time reversed at different wave frequencies for a wavemaker with a 80mm stroke length

Stroke length set to 100mm

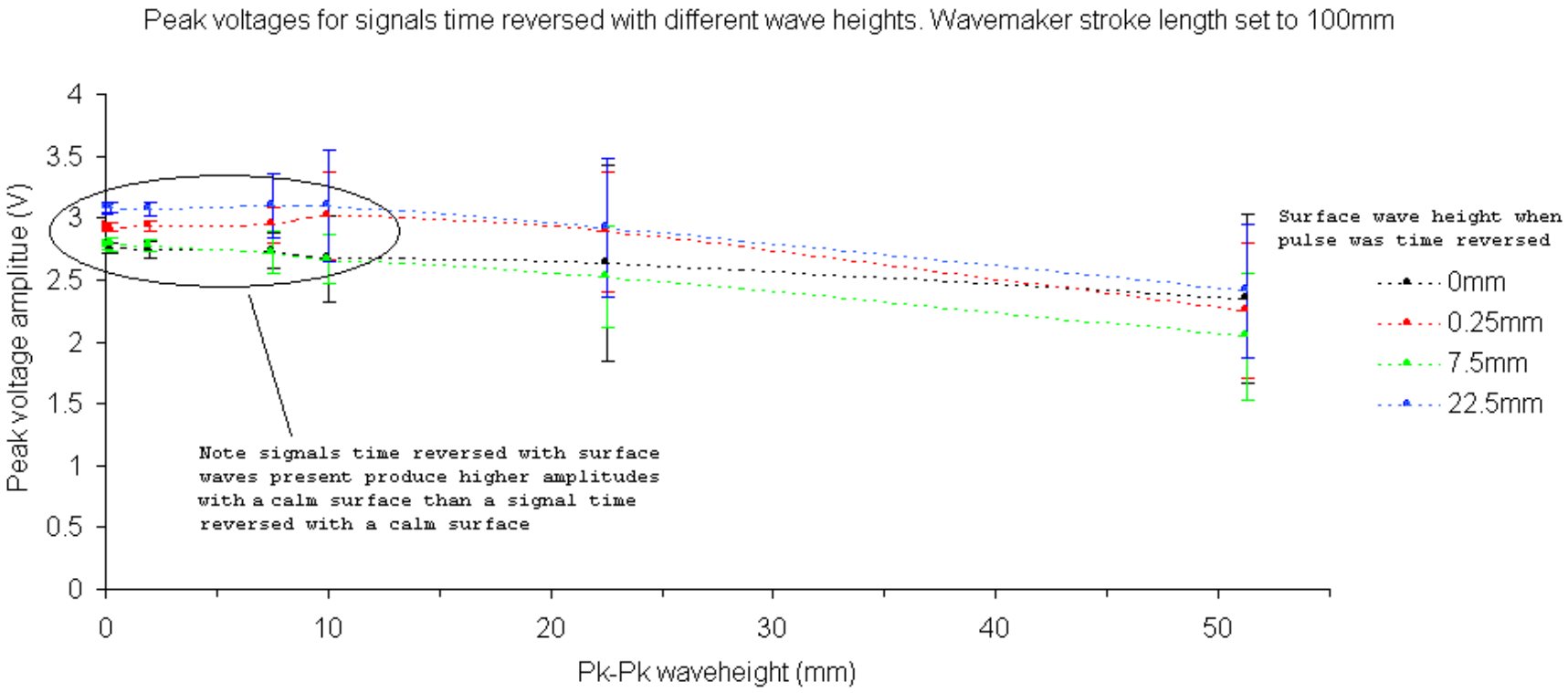

Fig. 4.19: Peak voltages for signals time reversed at different wave frequencies for a wavemaker with a 100mm stroke length

Stroke length set to 120mm

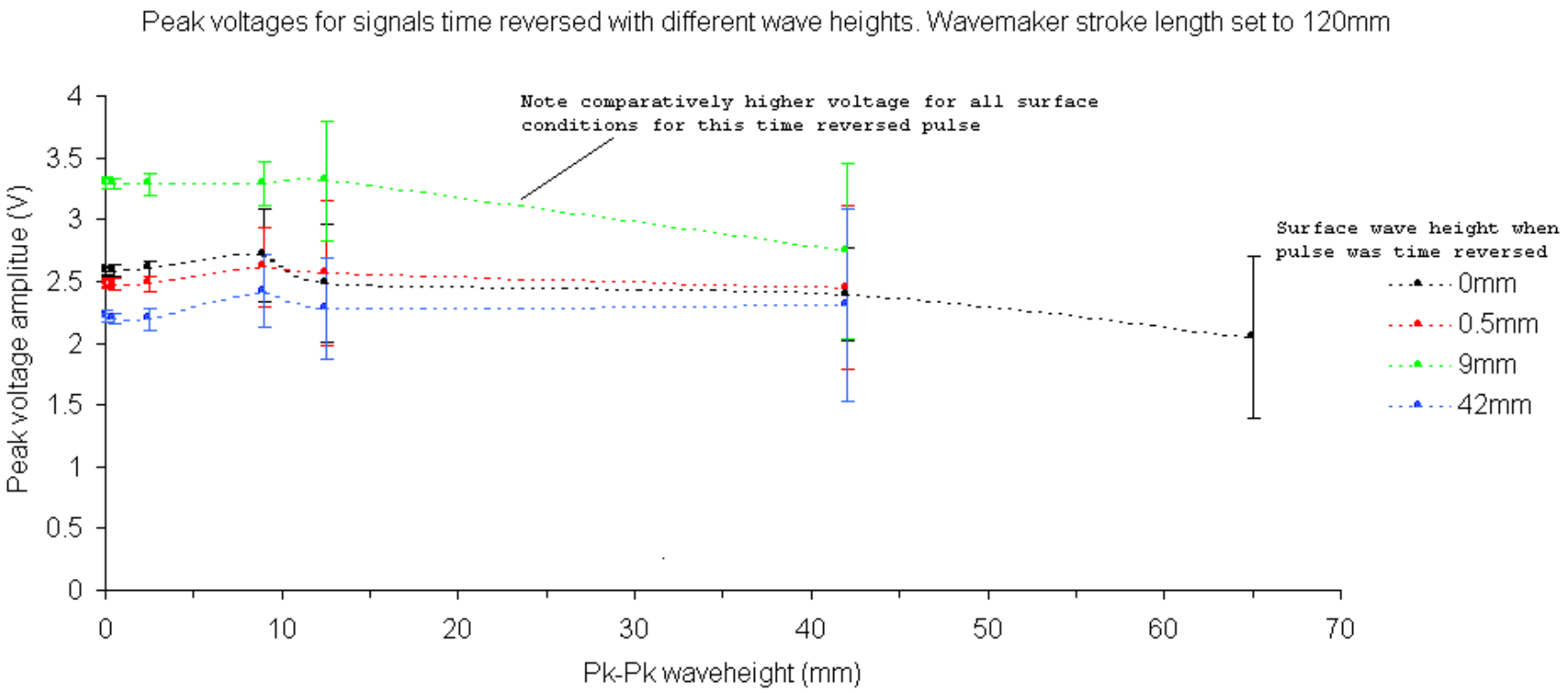

Fig. 4.20: Peak voltages for signals time reversed at different wave frequencies for a wavemaker with a 120mm stroke length

Stroke length set to 60mm

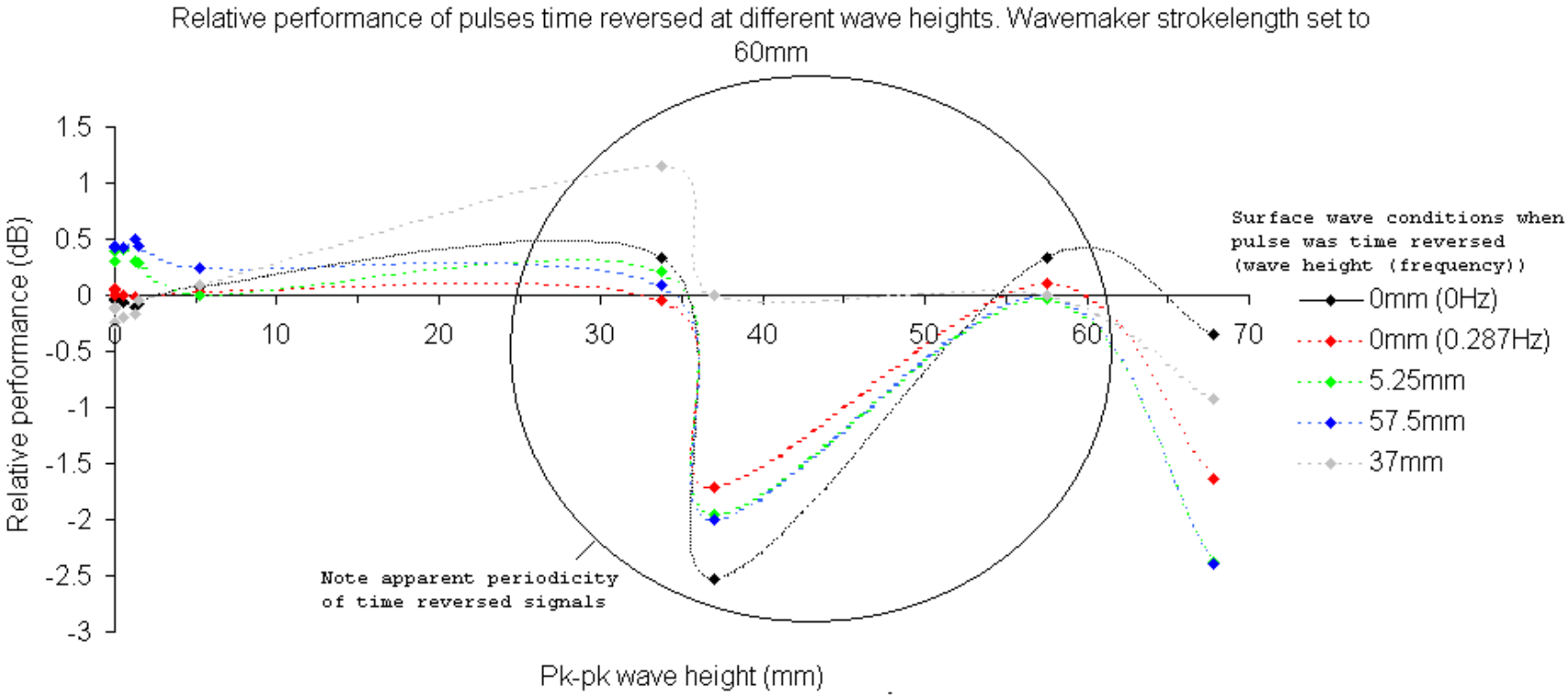

Fig. 4.21: Relative performances for time reversed signals with the wavemaker set to a stroke length of 60mm

Stroke length set to 80mm

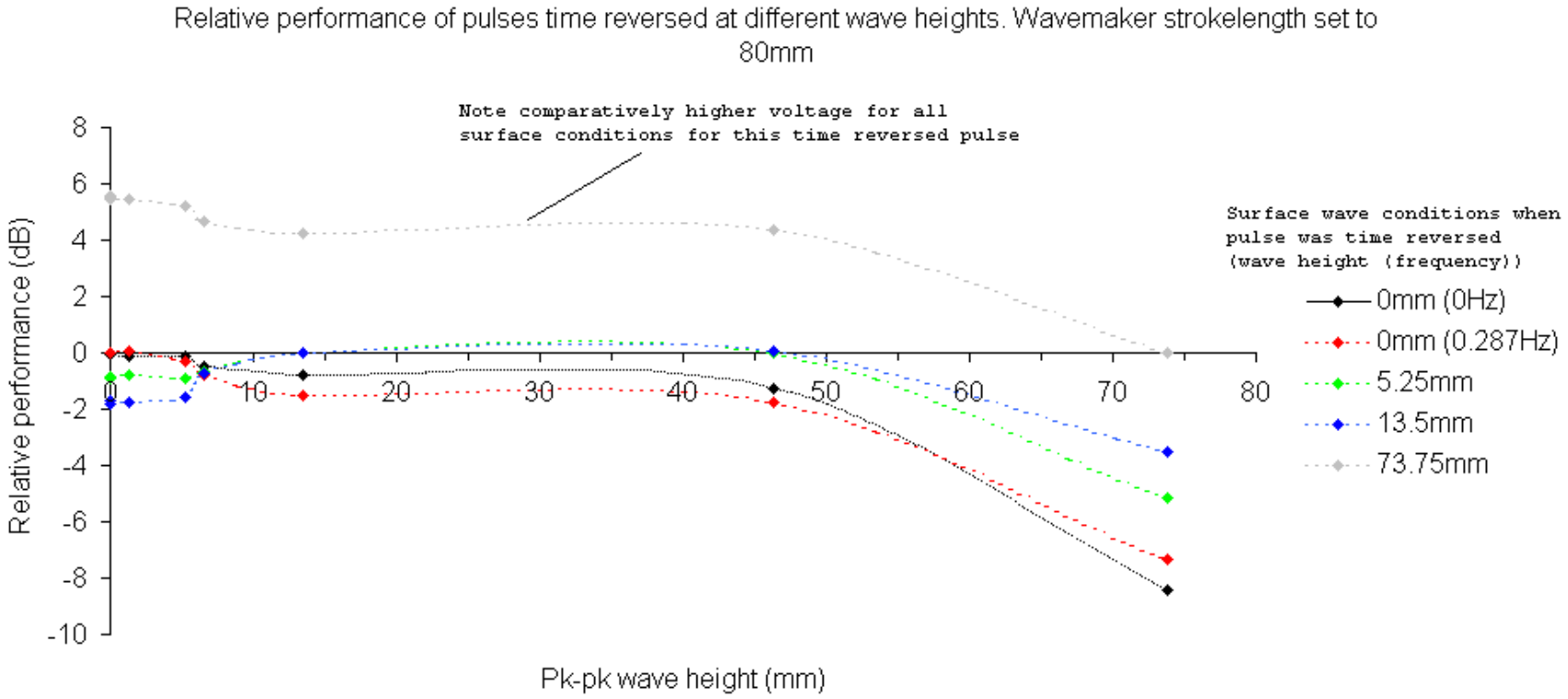

Fig. 4.22: Relative performances for time reversed signals with the wavemaker set to a stroke length of 80mm

Stroke length set to 100mm

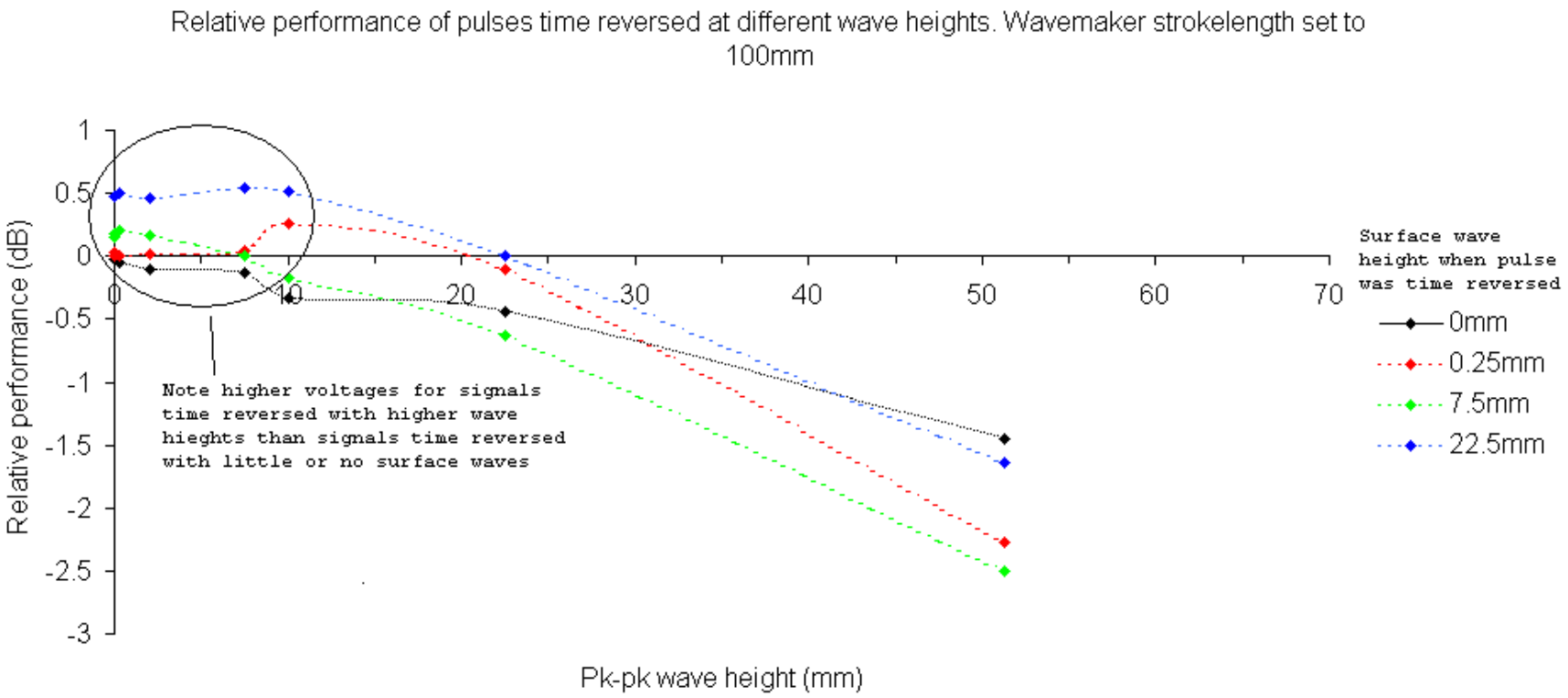

Fig. 4.23: Relative performances for time reversed signals with the wavemaker set to a stroke length of 100mm

Stroke length set to 120mm

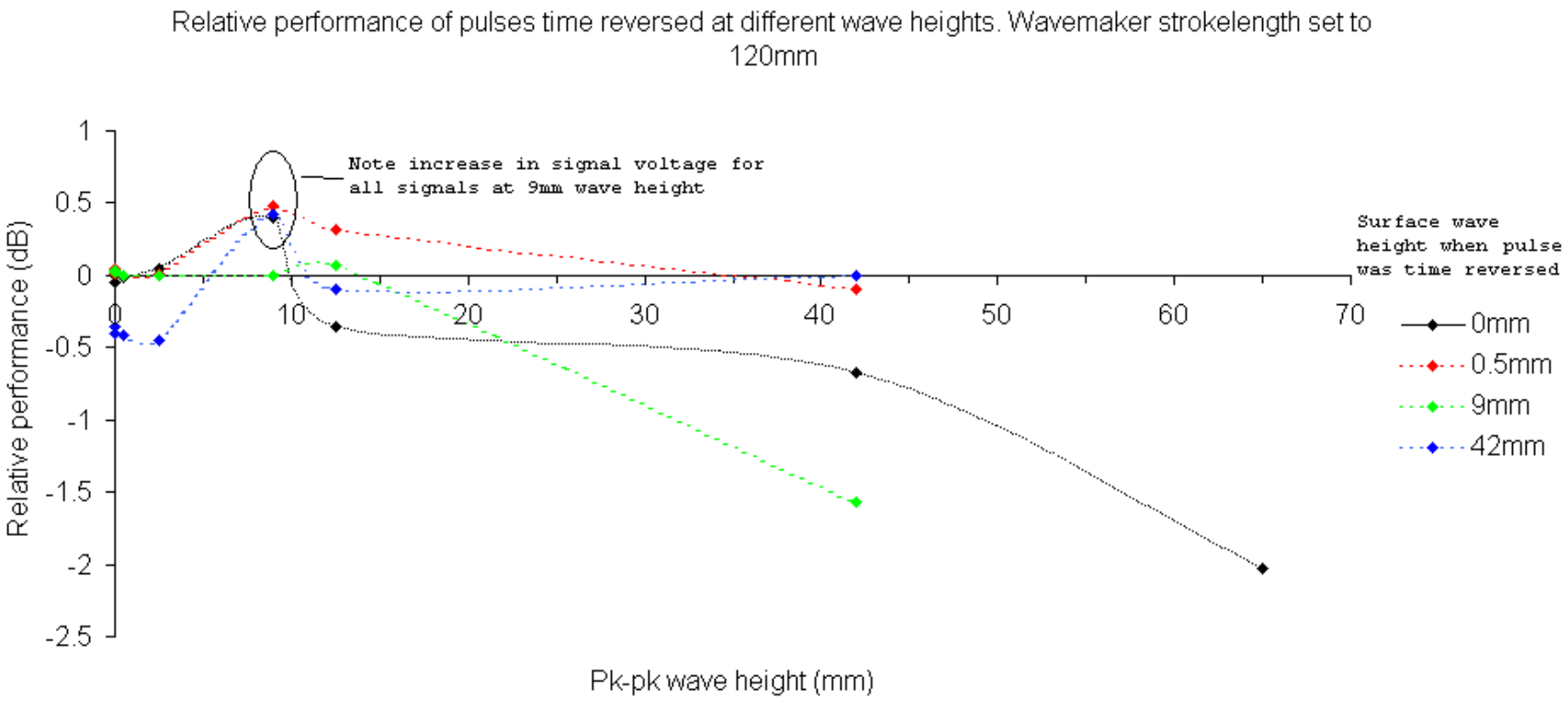

Fig 4.24: Relative performances for time reversed signals with the wavemaker set to a stroke length of 120mm

4.6 Wave angle measurements

Once a series of experiments into the effects of different stroke lengths (therefore wave heights) had been performed, the next step was to investigate the effect of the angle between the direction of propagation for the surface waves and the direction of direct transmission. Due to time constraints it was decided to perform these experiments at a single stroke length setting (i.e. a single set of wave heights). Examining the results from the stroke length experiments, it was decided to use the wavemaker with an 80mm stroke length. It was felt that this setting allowed a wide range of wave heights and a reasonable number of data points. (Although we could achieve higher waves using a larger stroke length, there would be less available speed settings before the water would spill out of the tank).

The angle was achieved by rotating the entire rig (the source and TRM and frame), the rig was positioned manually, and the angle was correct to the nearest degree (i.e. $\pm 0.5^{o}$). This is shown in Fig. 4.25.

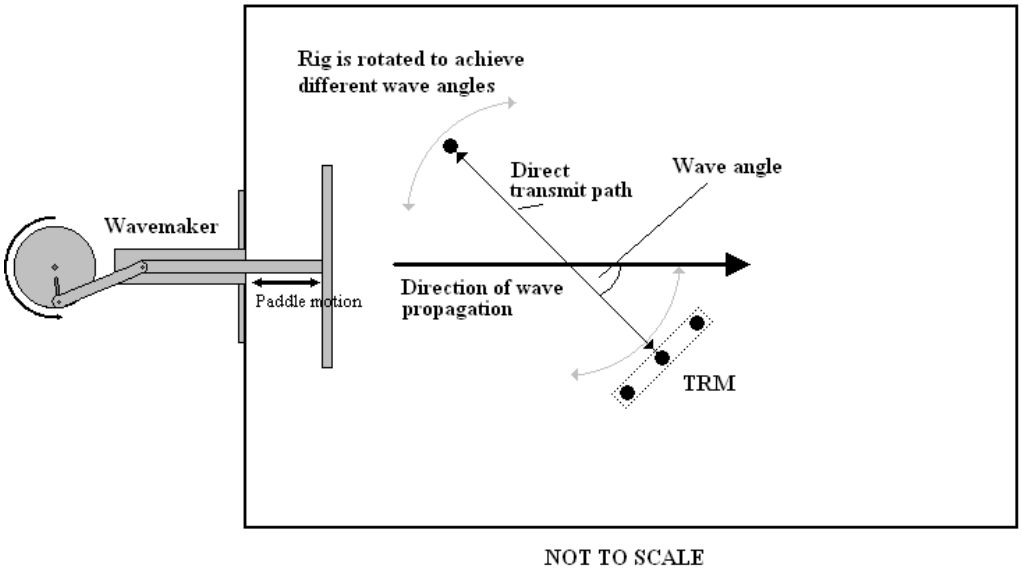

Fig. 4.25 Experimental set-up for wave angle experiments.

The wave angle was varied from 0° to 90° in steps of 10°. The results for wave angles of 10° to 90° are shown in Fig. 4.26 to 4.34. (The results for 0° have already been presented in Fig 4.18). Also, as with the stroke length measurements, the relative performance of each signal at different wave heights is shown. The results for angles 10°-90° are shown in Fig 4.35 to 4.43 (the results for 0° being displayed in Fig. 4.22).

Wave angle set to 10 degrees

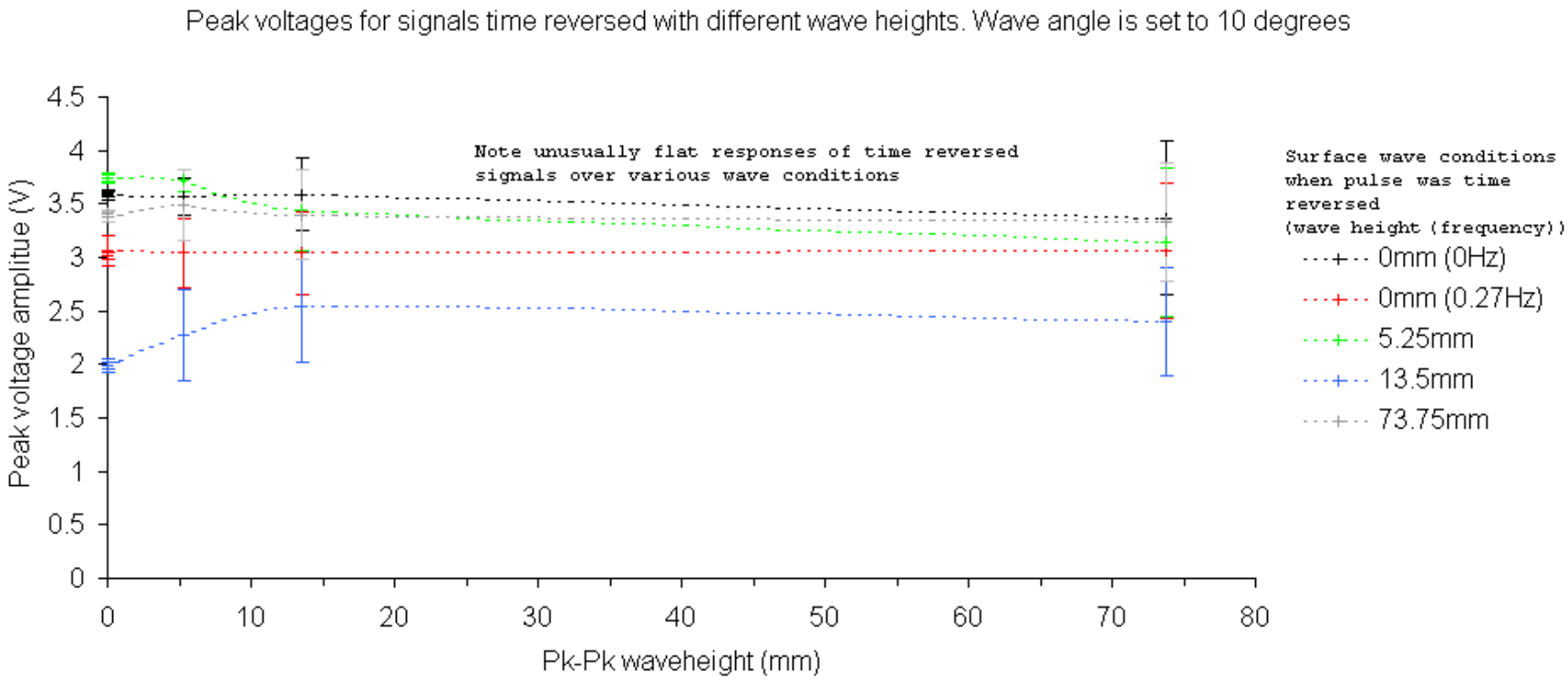

Fig. 4.26. Peak voltages for signals time reversed at different wave frequencies for a wavemaker with a 10 degree wave angle.

Wave angle set to 20 degrees

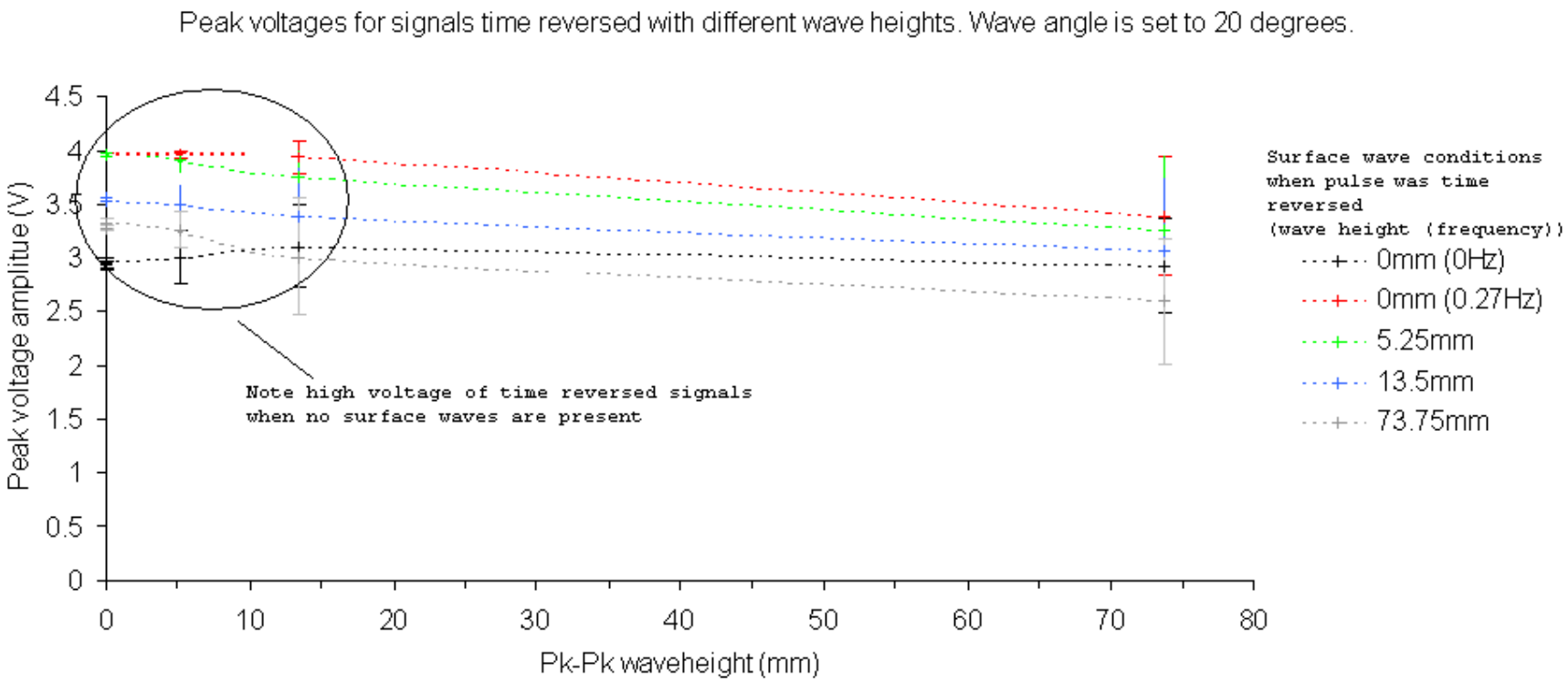

Fig. 4.27. Peak voltages for signals time reversed at different wave frequencies for a wavemaker with a 20 degree wave angle.

Wave angle set to 30 degrees

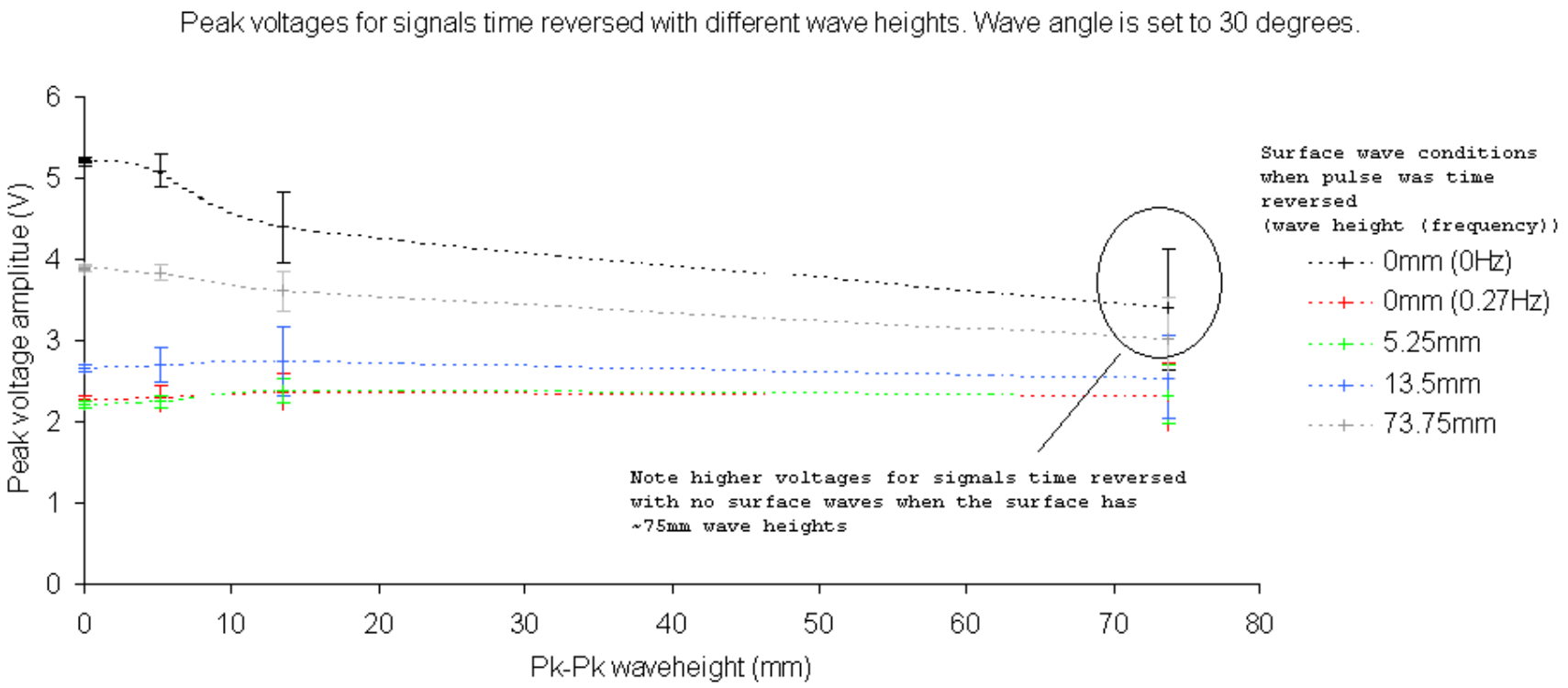

Fig. 4.28. Peak voltages for signals time reversed at different wave frequencies for a wavemaker with a 30 degree wave angle.

Wave angle set to 40 degrees

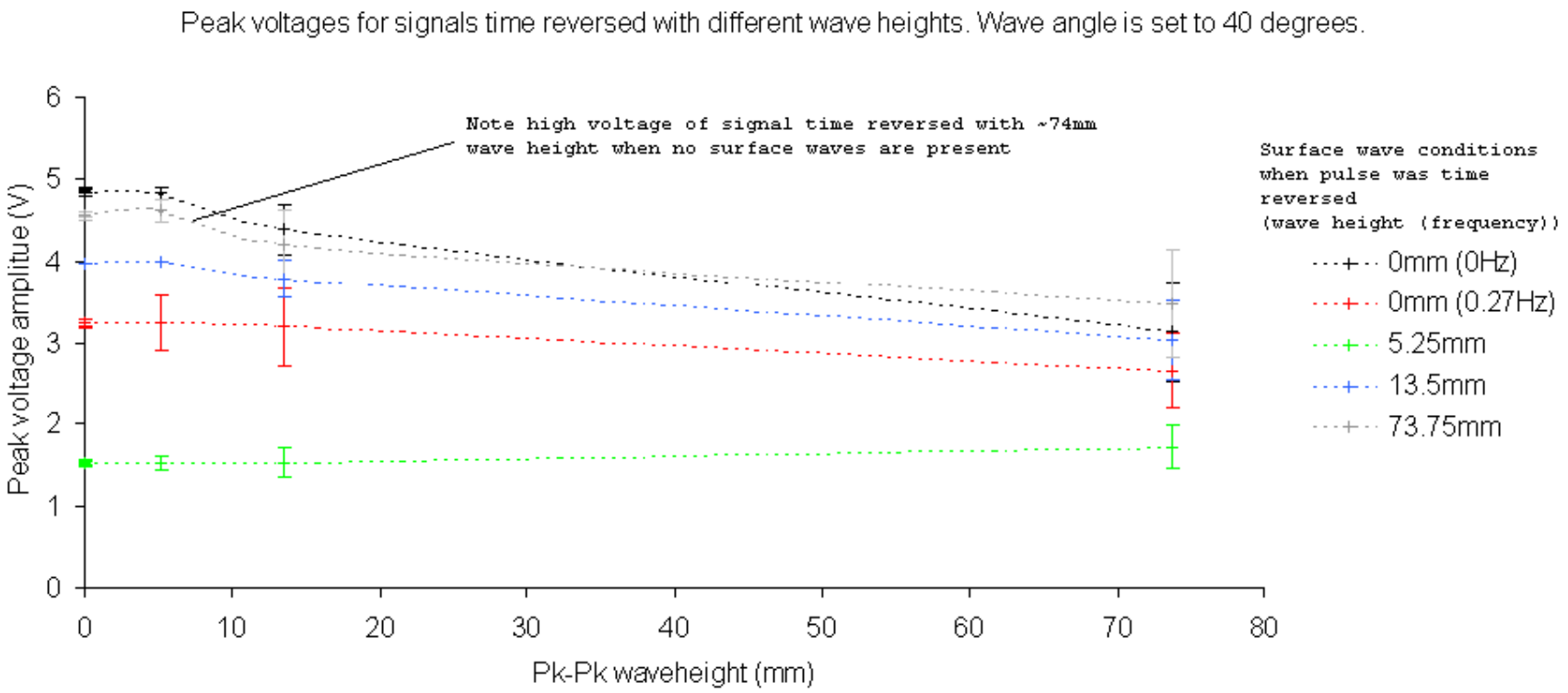

Fig. 4.29. Peak voltages for signals time reversed at different wave frequencies for a wavemaker with a 40 degree wave angle.

Wave angle set to 50 degrees

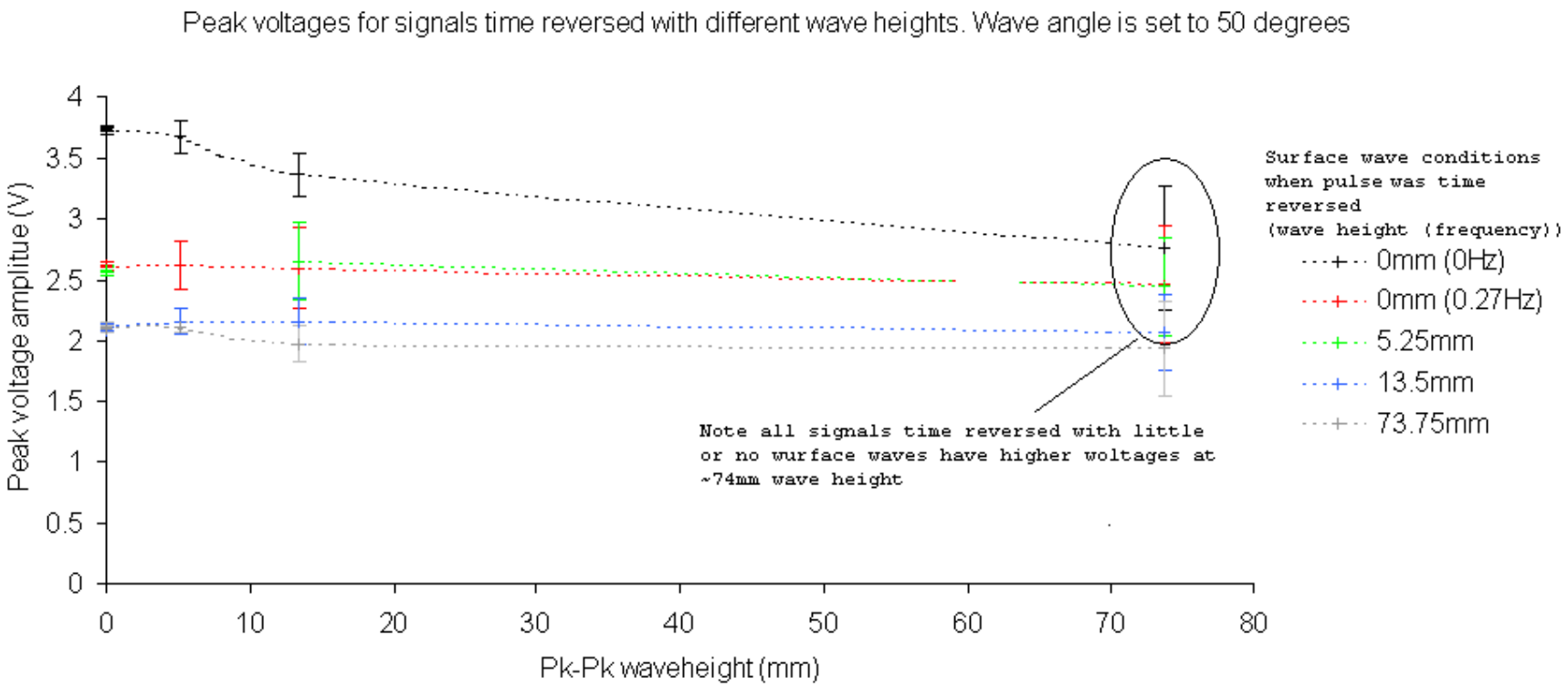

Fig 4.30. Peak voltages for signals time reversed at different wave frequencies for a wavemaker with a 50 degree wave angle.

Wave angle set to 60 degrees

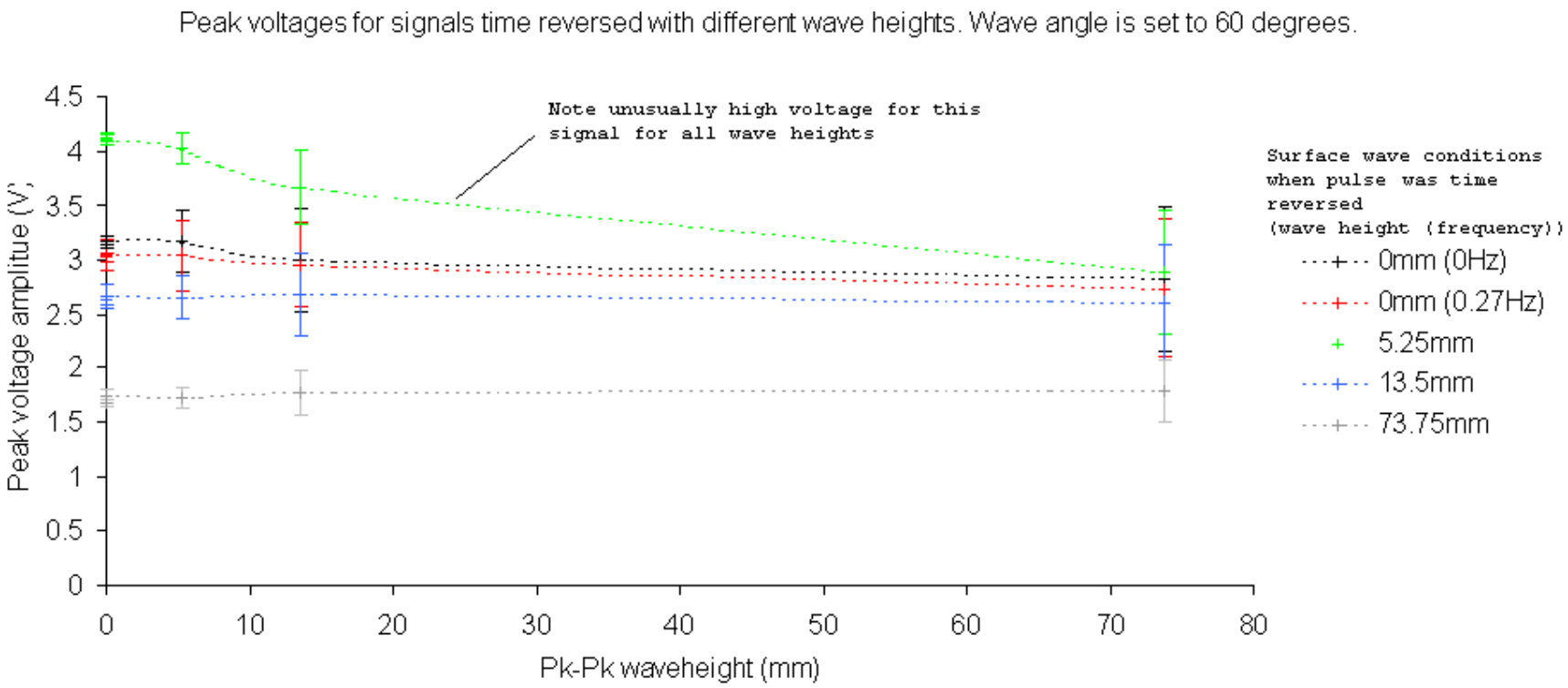

Fig.4.31. Peak voltages for signals time reversed at different wave frequencies for a wavemaker with a 60 degree wave angle.

Wave angle set to 70 degrees

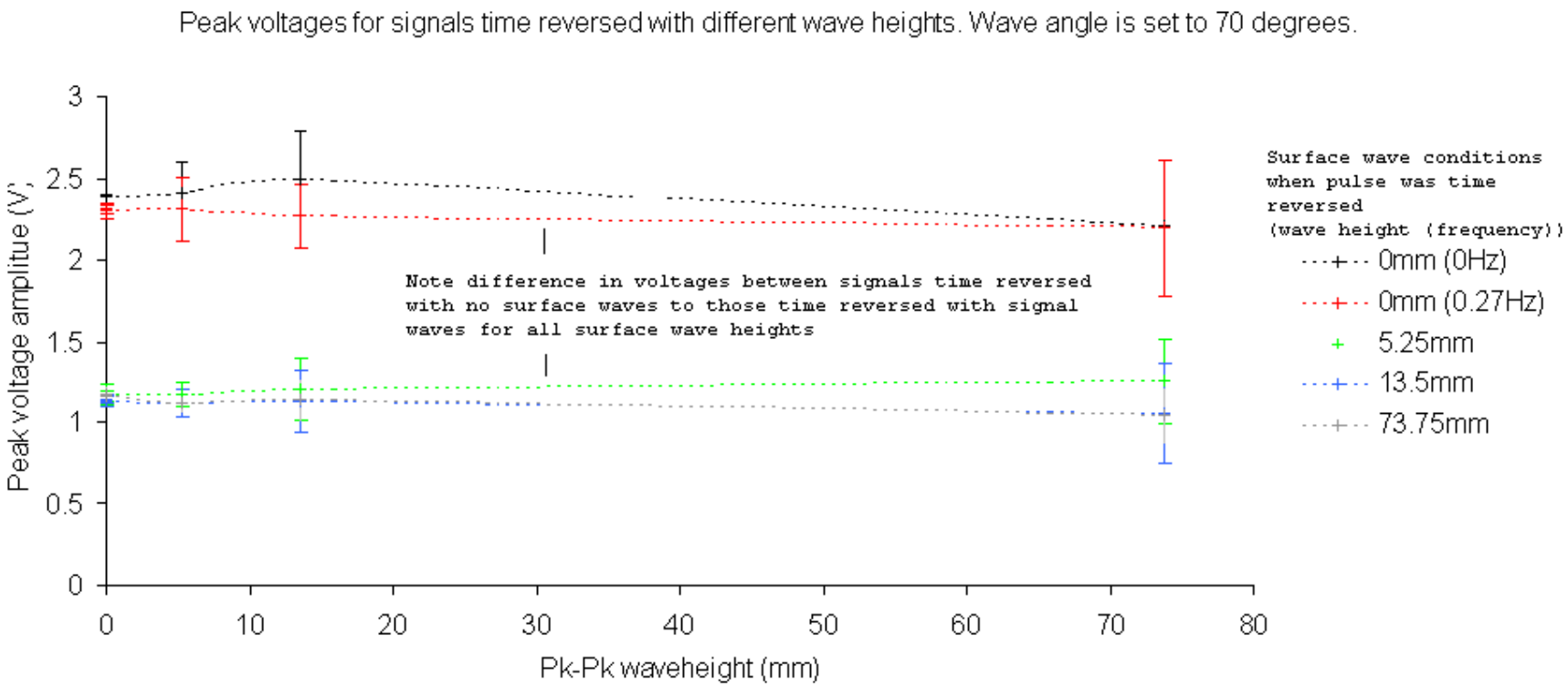

Fig. 4.32. Peak voltages for signals time reversed at different wave frequencies for a wavemaker with a 70 degree wave angle.

Wave angle set to 80 degrees.

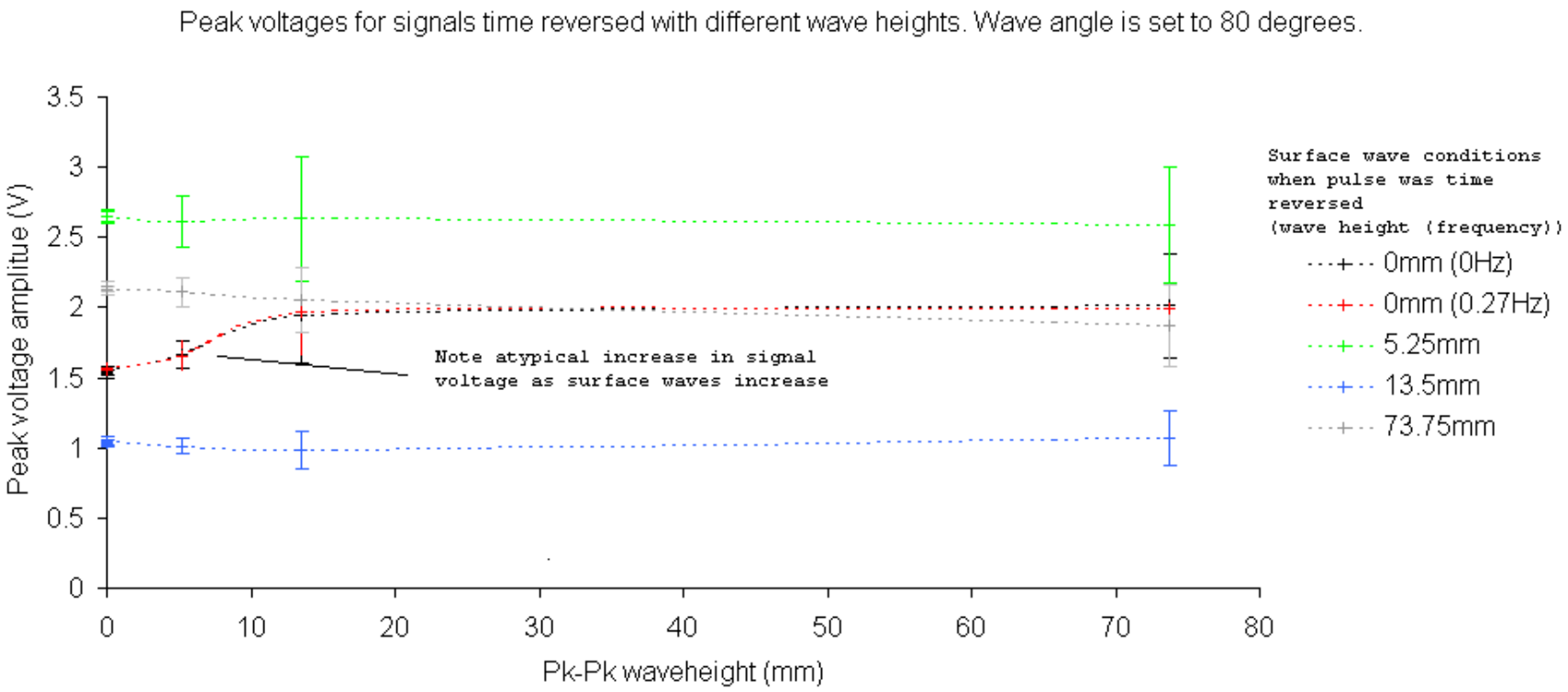

Fig. 4.33. Peak voltages for signals time reversed at different wave frequencies for a wavemaker with an 80 degree wave angle.

Wave angle set to 90 degrees

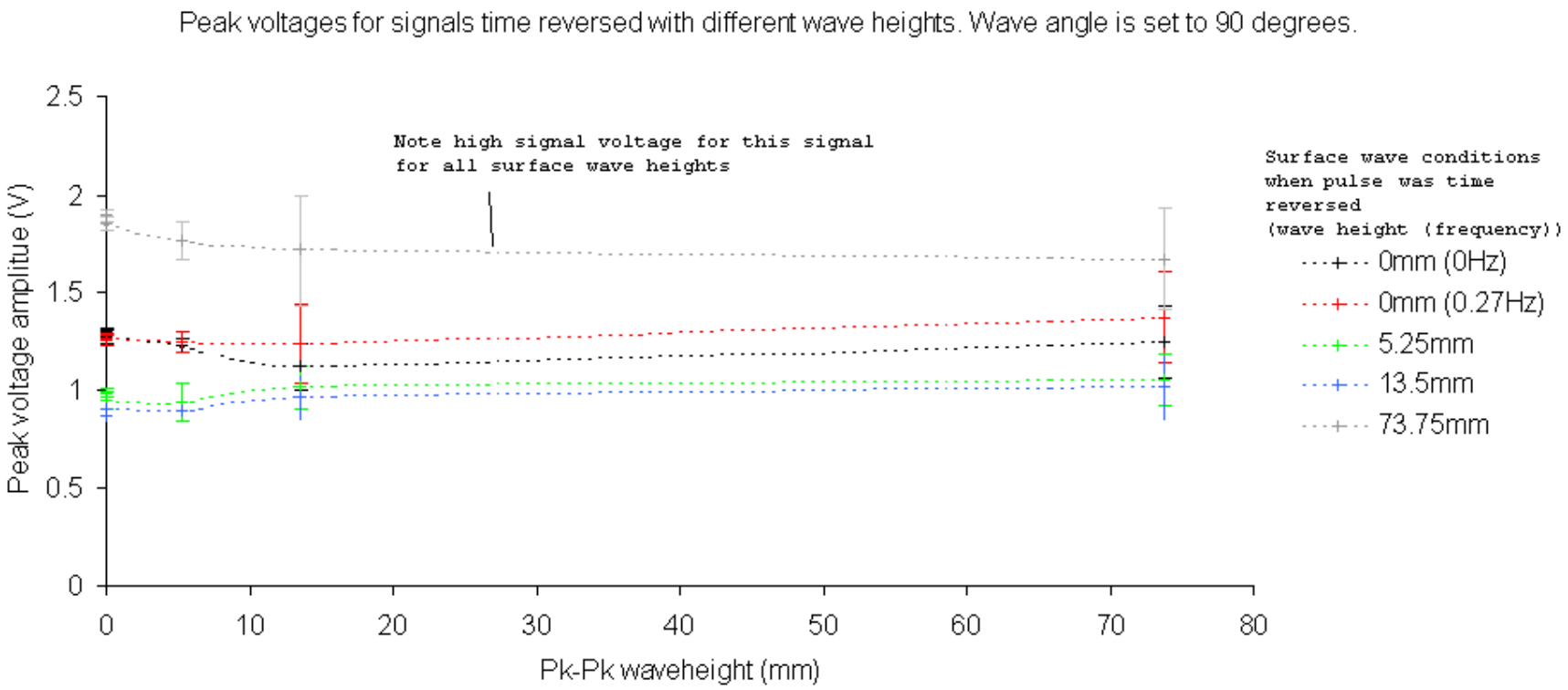

Fig. 4.34. Peak voltages for signals time reversed at different wave frequencies for a wavemaker with a 90 degree wave angle.

Wave angle set to 10 degrees

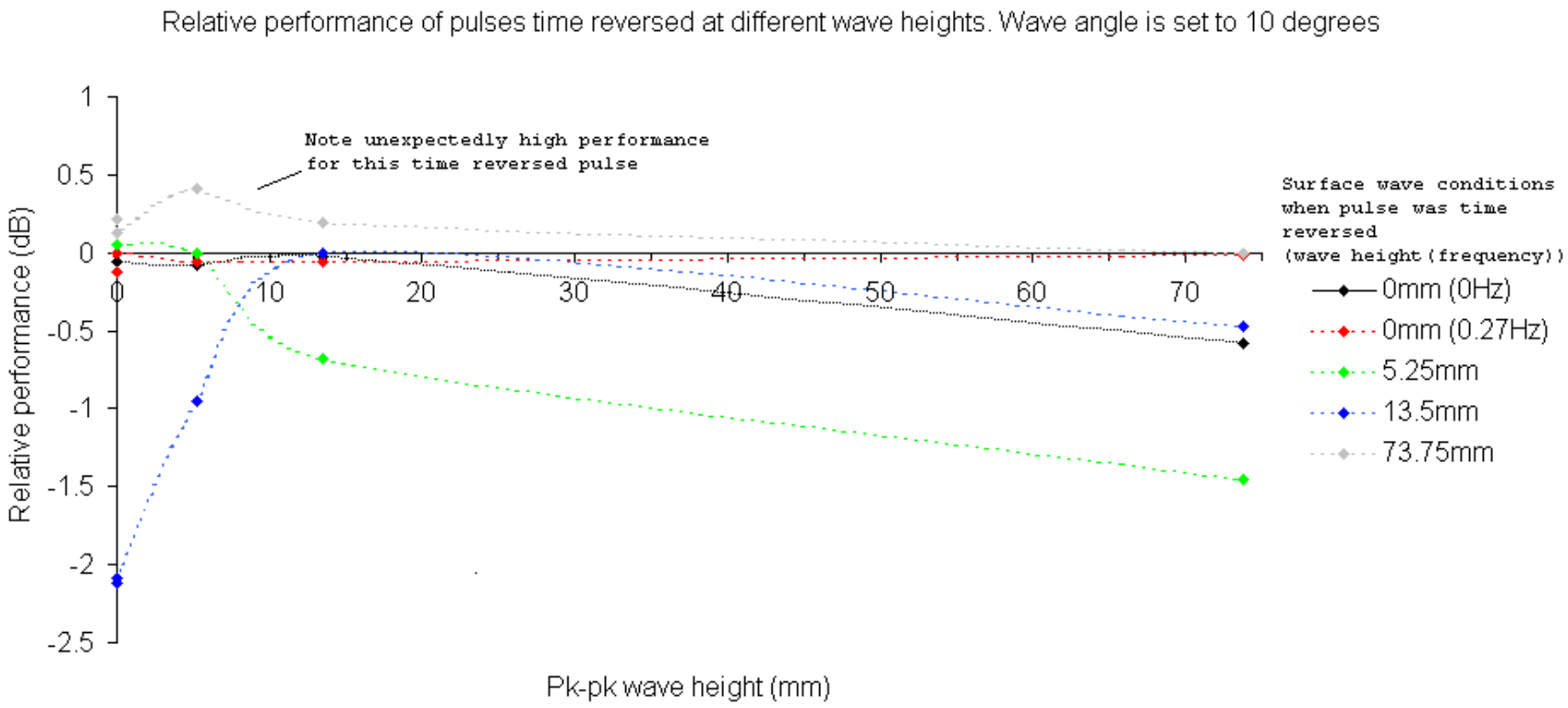

Fig 4.34: *Relative performances for time reversed signals with the wave angle set to 10 degrees.*

Wave angle set to 20 degrees

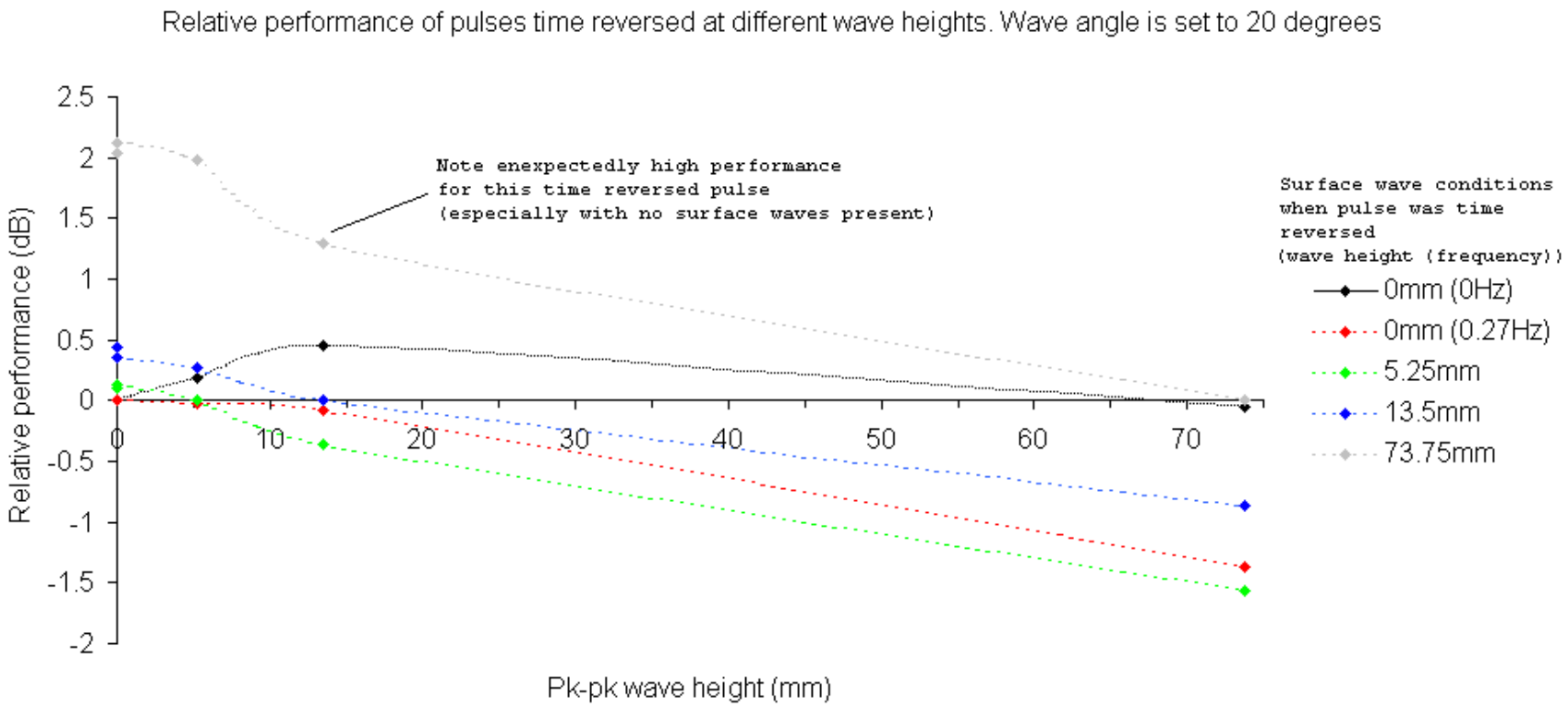

Fig. 4.35: Relative performances for time reversed signals with the wave angle set to 20 degrees.

Wave angle set to 30 degrees

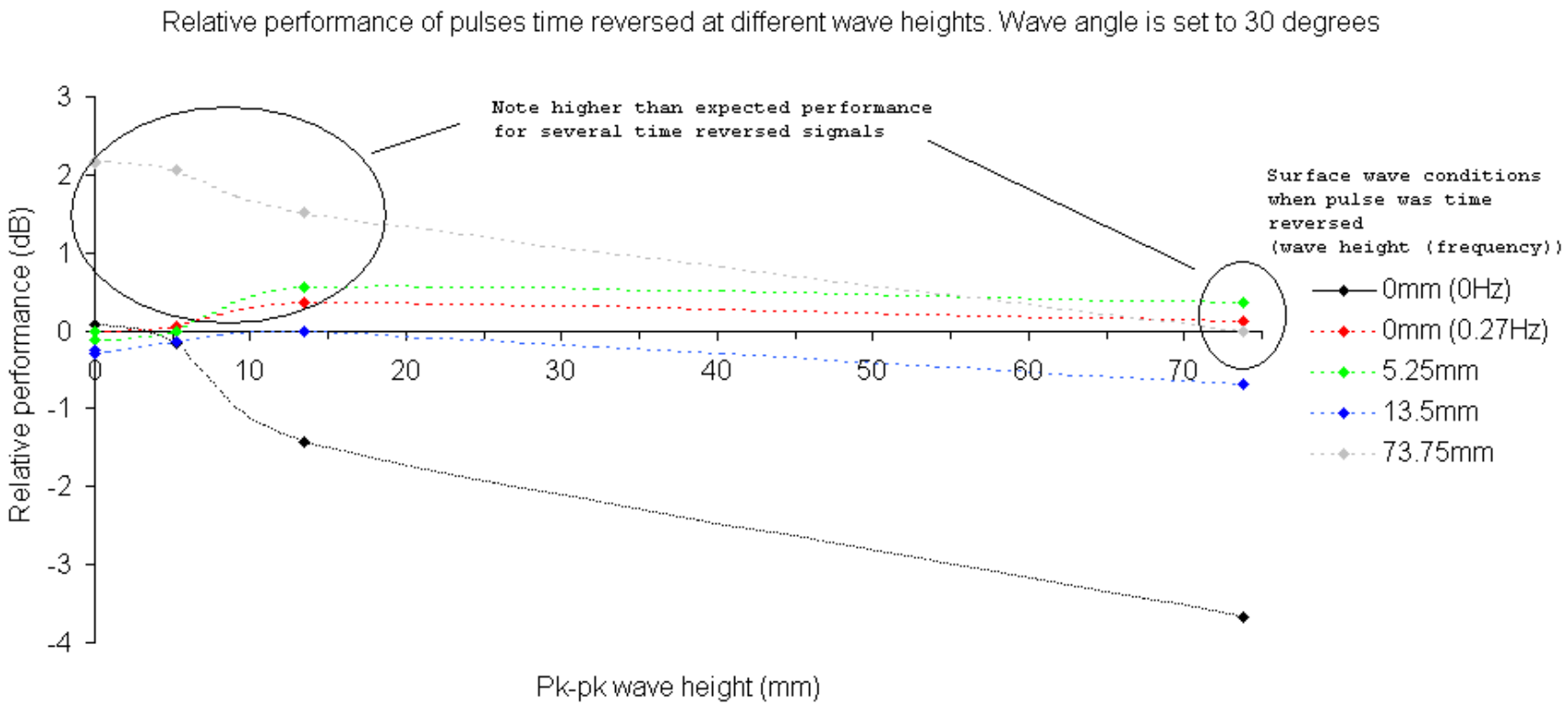

Fig. 4.36: Relative performances for time reversed signals with the wave angle set to 30 degrees.

Wave angle set to 40 degrees

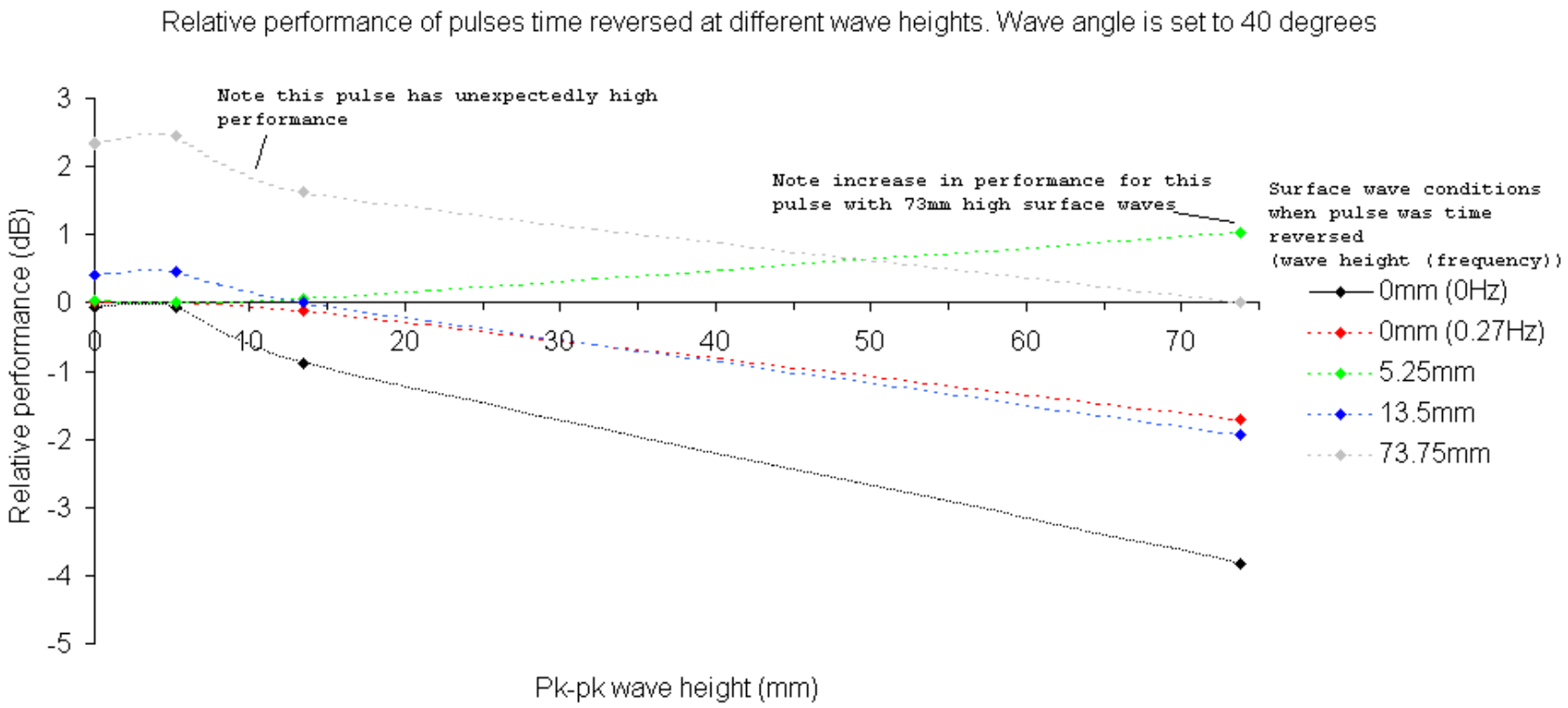

Fig. 4.37: Relative performances for time reversed signals with the wave angle set to 40 degrees.

Wave angle set to 50 degrees

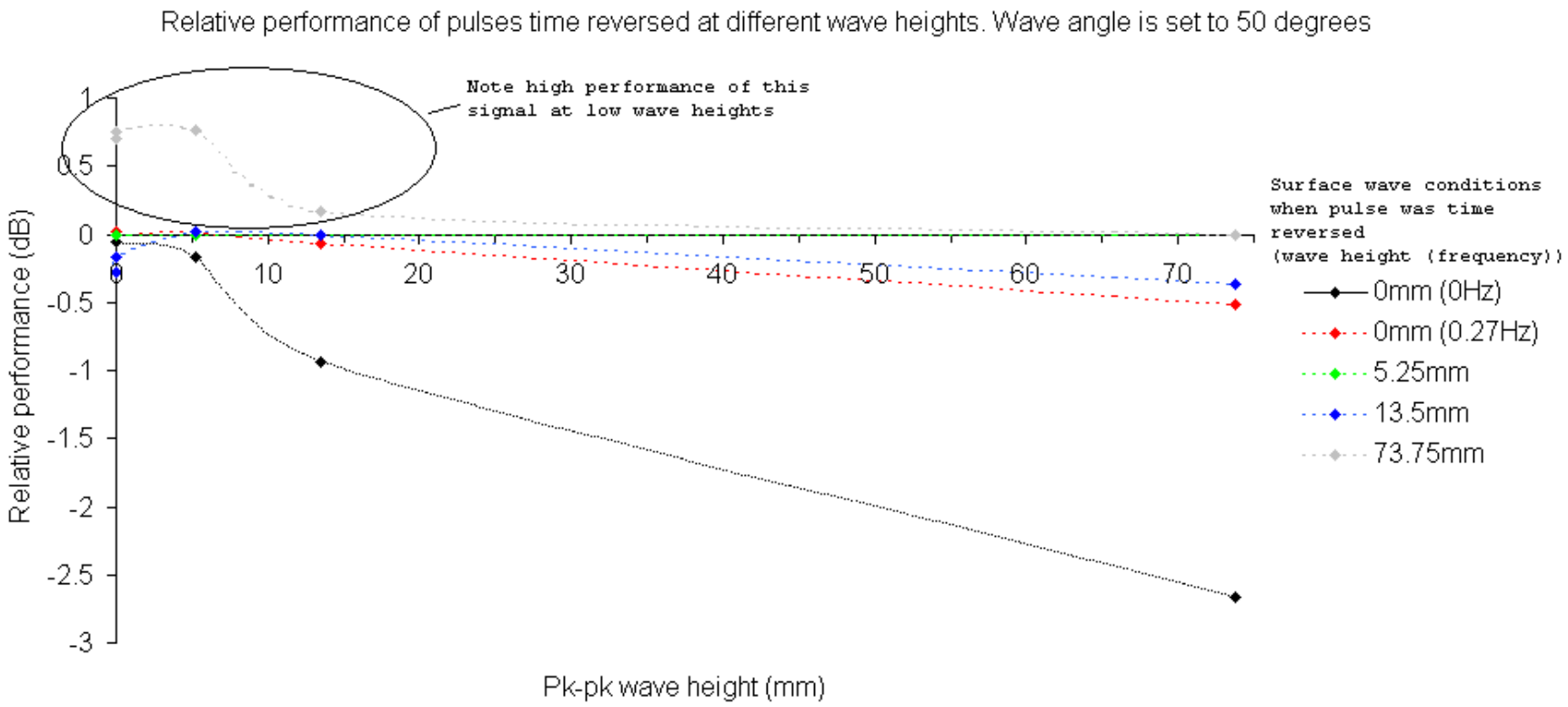

Fig. 4.38: Relative performances for time reversed signals with the wave angle set to 50 degrees.

Wave angle set to 60 degrees

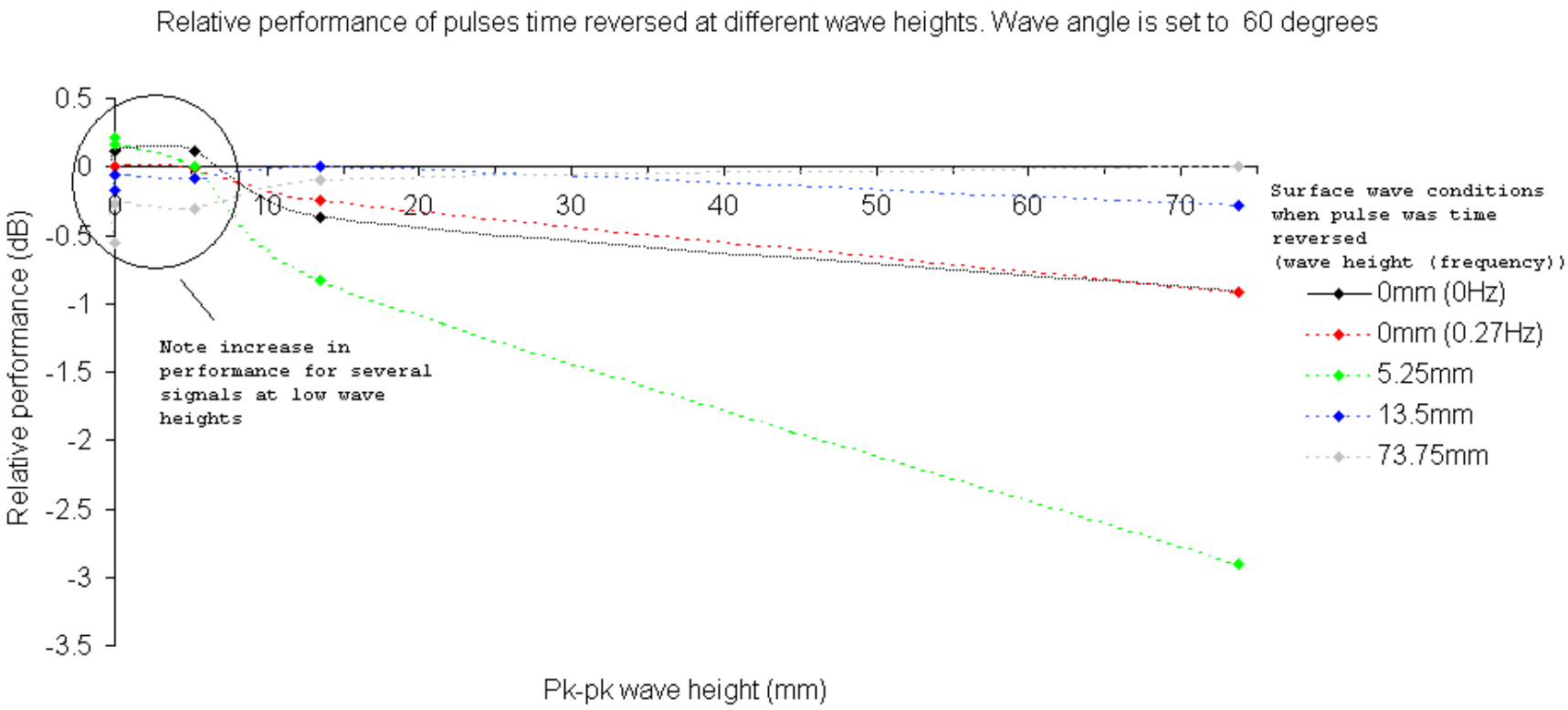

Fig. 4.39: Relative performances for time reversed signals with the wave angle set to 60 degrees.

Wave angle set to 70 degrees

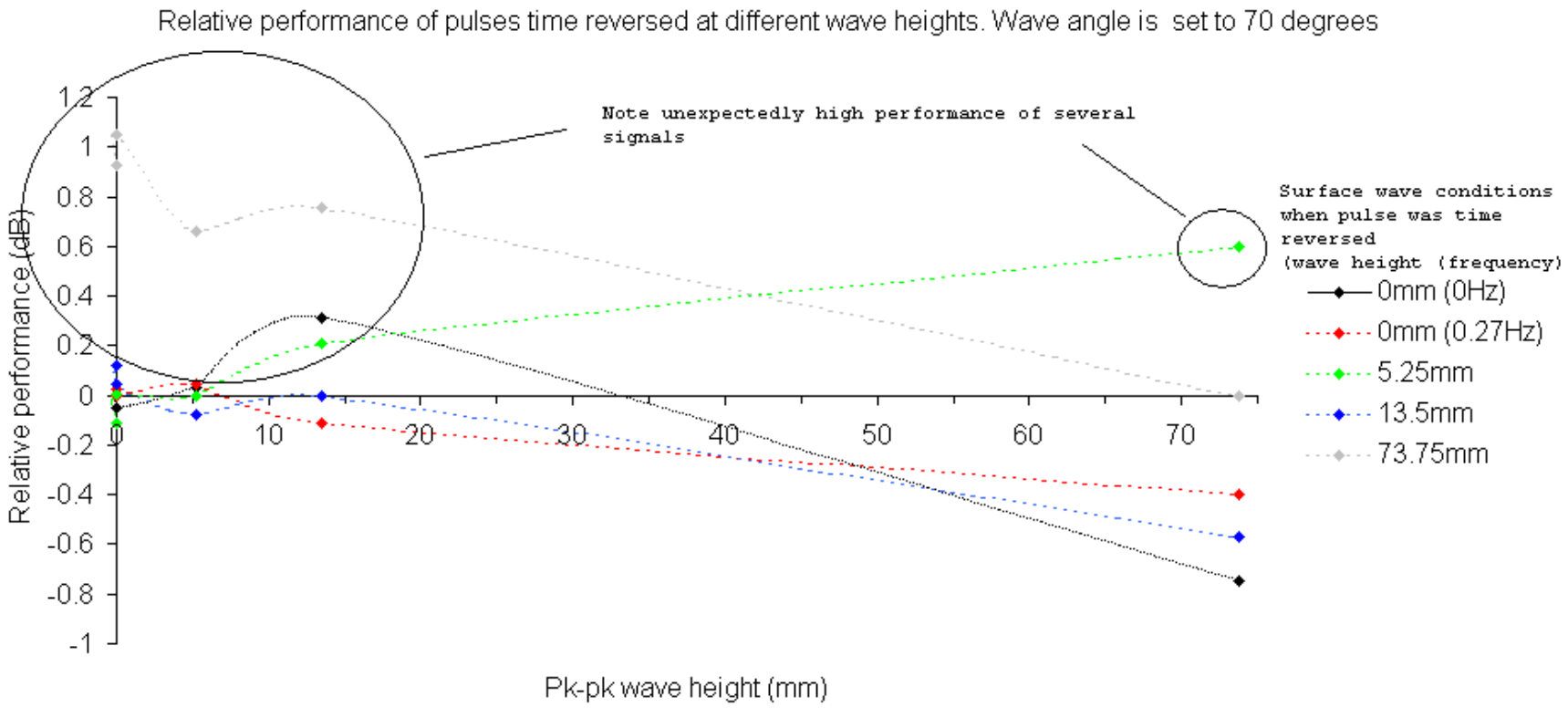

Fig. 4.40: Relative performances for time reversed signals with the wave angle set to 70 degrees.

Wave angle set to 80 degrees

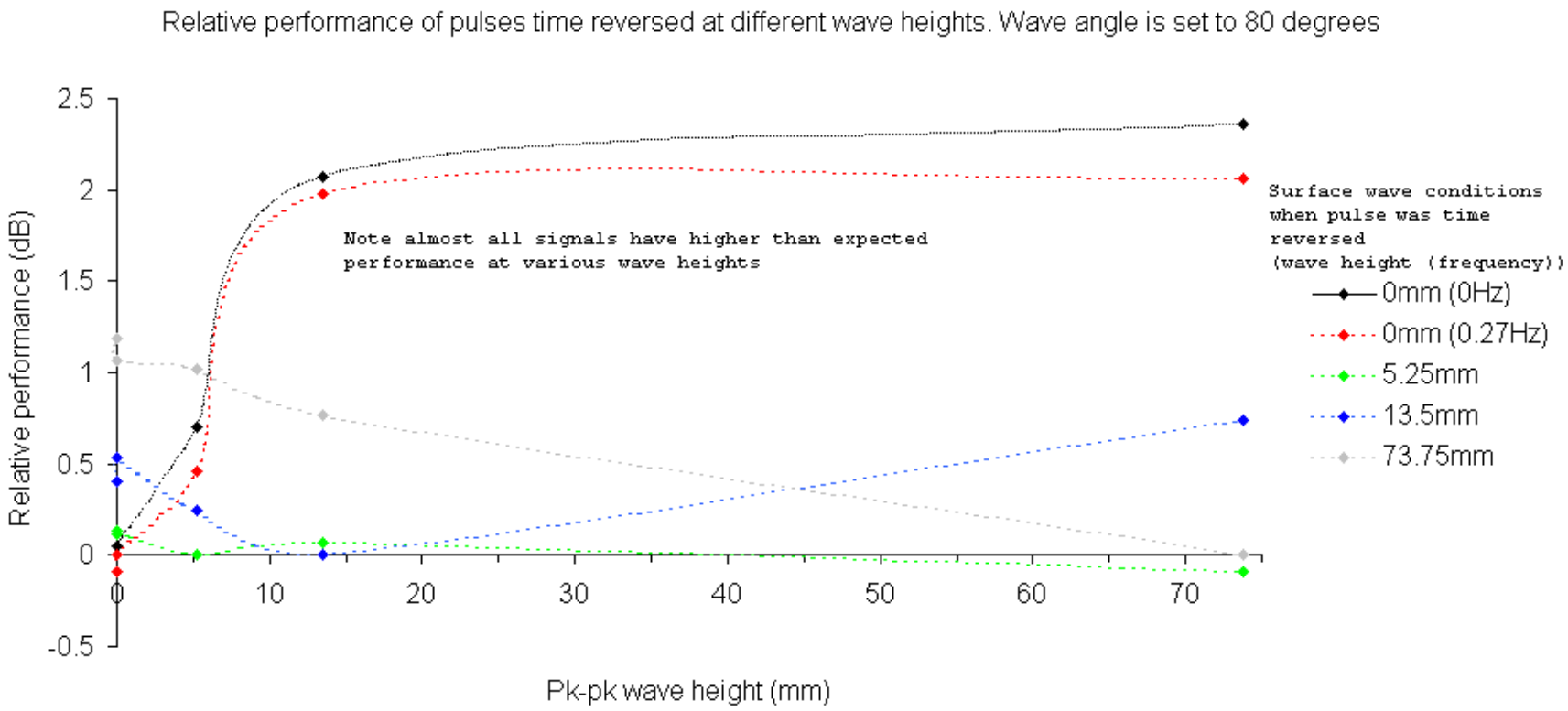

Fig.4.41: Relative performances for time reversed signals with the wave angle set to 80 degrees.

Wave angle set to 90 degrees

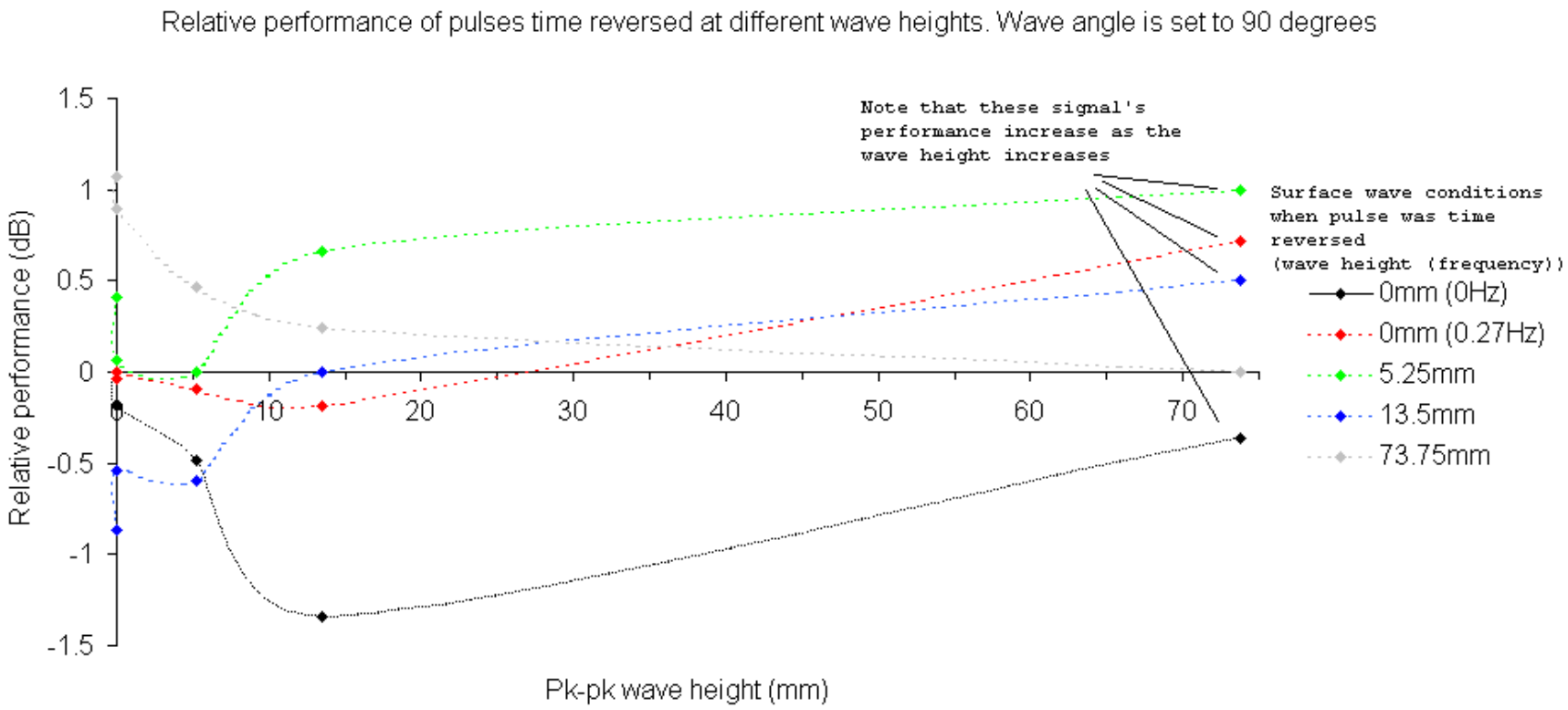

Fig.4.42: Relative performances for time reversed signals with the wave angle set to 90 degrees.

4.7 Conclusions

4.7.1 Wave height measurements

The experiments examining the wave heights produced by the wavemaker demonstrated the simple wavemaker equation was not valid, i.e. that the relationship between the frequency setting and wave height was not linear. These measurements characterised the output wave heights for all wavemaker configurations used in the subsequent experiments. They also demonstrated that, due to the nature of the experimental set-up, the wavemaker waves were more consistent with a standing wave pattern, rather than plane waves of constant height with a single direction of propagation. This had several repercussions on the rest of the experiments:

1) As the relationship was not linear, the wave heights used in the other experiments were not sampled at regular intervals, as originally planned (by choosing regularly spaced frequency settings for the wavemaker). This is not that important, as a wide range of wave heights were still investigated.
2) The standing wave pattern means that the experiments examining the effect of the angle of the incoming waves with respect to the direction of propagation are less meaningful, as they are not examining pure plane waves. However, there still was a directional component to the wave pattern, so the results remain of value.

4.7.2 Wave height conclusions

The experiments have shown that there is a general trend for the voltage level of a time reversed signal to decrease as the height of the surface waves increase, i.e. the voltage level is inversely proportional to the wave height. This is accompanied by

an increase in the standard deviation of the voltages of each time reversed signal. This increase in the standard deviation shows that increasing wave height acts to increase the range of voltages that are received at the focus of the time reversed signal. Conversely, it can be said that decreasing the height of the surface waves will in general increase the received voltage of the time reversed signal. This increase in voltage appears to be a general result of all the time reversed signals, *irrespective of the conditions under which the original time reversal took place*.

In terms of the relative performance of the time reversed pulses over a range of wave heights, generally the time reversed signals remained within ~3-4dB of the signal at its time reversed wave height (the notable exception being the 80mm stroke length experiment where the signals varied by nearly 10dB). This demonstrates that these time reversed signals are remarkably stable, even when surface waves are ~ 5 times the wavelength of the pulse. (If we consider [21], where a 3.5k Hz signal was used, then if these results are 'scaleable', this would correspond to peak-to-peak wave heights of ~2m) (Equivalent to Sea State 4 ("moderate") on the Beaufort scale). These results, and their possible interpretations, are detailed in section 4.8.

4.7.3 Wave angle conclusions

The wave angle experiments demonstrated a decrease in signal levels for all pulses used as the angle increased. This is attributed to the changing orientation of the bottom of the tank, curved by the weight of the water. This rotation will have the effect of changing the curvature of the bottom in relation to the signal path, so altered the directions of the rays reflected off the bottom of the tank. As this reduction took place across all the signals, it is not thought to be a feature of the surface waves.

The results of the wave angle experiments are in general agreement with the stroke length experiments, in that they show an inverse relationship between received voltage levels and wave heights. However, this inverse relationship appears to break down at wave angles approaching 90 degrees. Figs. 4.40-4.42 show that some of the time reversed signals *increase* in voltage level as the wave heights increase. These results, and their interpretations, are also discussed in more details in section 4.8.

4.7.4 Overall conclusions

Even with significant surface wave heights (~5 times the wavelength of the pulse) the signal loss is rather small (~-3-4dB). This shows the remarkable robustness of time reversal.

4.8 Discussion.

4.8.1 Time reversal experimental apparatus.

As previously stated in the discussion section of chapter 3, there was an approximately 3-5 minute delay between the transmission of the 3-cycle sine wave pulse, and the re-transmission of the time reversed samples captured by the TRM. This has restricted these experiments to steady-state measurements at each selected wave height. This, as stated in 4.7.1 means that rather than examining plane waves on the surface of the water, a more complex standing wave pattern was used.
A time period of ~1-2 minutes was allowed from setting a new speed on the wavemaker before taking any measurements, to allow the system to reach the desired steady state. The experiments would then take ~5-8 minutes for a set of results, and it has been assumed that there is no further change in the water in that time. This is not strictly true, as a small amount of water was lost on several of the runs where high-

amplitude water waves were used. (The maximum speed setting used was that which produced waves just below the height of the tank). This water loss did not produce any measurable reduction in the depth of the water, and it is assumed that any error caused by this very slight reduction in water depth is negligible.

4.8.2 Wave height measurements.

Due to the nature of the relationship between wave amplitudes and speed setting of the wavemaker, the sampling of wave heights for these experiments is not linear, as intended. This meant that there are more data points at lower amplitudes (especially <5mm) than those at higher amplitudes. This means that the behaviour of time reversed signals at low wave heights has been reasonably well measured, but at higher amplitudes, where the data is sparser, the behaviour is much less clear. This is discussed further in the next section.

4.8.3 Time reversal at different wave heights.

General trend

The results indicate an inverse relationship between wave height and time reversed signal voltage. This implies that all time reversed signals improve as surface waves are reduced (and reduce as surface waves increase)*, regardless of the amount of surface waves present when the time reversal took place*. This result appears to go against one of the basic ideas of time reversal that changes in the environment after a signal has been time reversed will *reduce* the signal level.

The expectation was a peak in signal voltage at the same wave height as the signal was time reversed, and a reduction in signal level as the wave height moves away from this value, (i.e. as the wave height is increased or decreased).

This relationship may be caused by an intrinsic property of time reversed pulses where the performance of any time reversed pulse is degraded with wave motion, regardless of the circumstances in which it was time reversed. If this is the case, then it implies there will be little to no advantage in time reversing at specific wave amplitudes, as any pulse time reversed in the same channel should have comparable performance. (Although this does not explain the difference in the relative performances, discussed below.)

Relative performance of time reversed pulses

Another area yielding unexpected results is the relative performance of different signals. We would expect that the best possible signal for any particular wave height would be produced by time reversing a test pulse at that wave height (including no surface waves). What the results have shown is that in some cases, (see Fig. 4.16 for example) pulses time reversed with surface waves present have a higher signal voltage with no waves than a signal time reversed with no surface waves.

One possibility for this disparity could be in the method used for time reversing and then re-transmitting. In the process of writing the time reversed pulses to the arbitrary waveform generator, the pulses were all scaled to the maximum output the arbitrary waveform generator could produce. If a pulse is relatively 'flat', in that the voltage received from the direct transmission and its reflections have approximately the same value, then it will have more energy than a pulse that has a higher peak from the direct transmission and lower scattered voltage levels. This may go some way to explaining the increase in voltage levels for some pulses. (A preliminary examination of several pulses does not demonstrate much difference in

the relative levels of the direct transmission and first reflections of several pulses, so it seems unlikely that this is the sole cause for this result).

Another possibility could be that those pulses time reversed with high amplitude surface waves will have a much reduced level of scattered returns, so it is possible that the time reversal process has acted in some way to focus more energy along the direct transmission and bottom scatter (as those should remain relatively constant), meaning that less energy will be lost through attenuation than a signal that is using multiple reflections (which have a longer distance to travel). Although as with the general trend, this would appear to go against what we understand about time reversed pulses in that we would expect a signal time reversed with no surface waves to be composed of the direct path, the bottom reflection (like those time reversed with surface waves) *plus* multiply scattered rays, so it should still produce a higher amplitude. Further experimentation is required to determine its exact cause.

Scarcity of data points at high surface wave amplitudes

Due to the nature of the relationship between the wavemaker's speed setting and the amplitude of the surface waves produced, most of the samples occurred at low surface wave amplitudes, with only a few at higher amplitudes. This means that much of the trends observed in these results are reliant on very few data points, which increases the risk of error. (For example, in the case of the wave angle measurements, the trend with increasing surface wave amplitude appears to be inferred by a single data point for most of the datasets.) Clearly there is a need for more experimentation to collect more points at surface wave amplitudes from 15mm peak to peak to 70mm peak to peak to determine the true behaviour of time reversed signals.

Possible periodicity of amplitudes

The results for the wavemaker set to a 60mm strokelength (Fig. 4.16) show an unexpected increase in amplitudes across all time reversed pulses at ~33-38mm surface wave peak to peak amplitude. This is not visible at other settings, but given the lack of data points, it remains a possibility that there is a certain amount of periodicity in the relationship between time reversed signals and surface wave amplitude. Further experiments with a closer spacing between sample surface wave amplitudes would show if this periodicity exists as a general result for all signals, or if it is specific to the set-up for the 60mm stroke length experiment.

Wave angle results

The results for the angle of wave propagation with respect to the direct transmission gave the unexpected result that when the direction of propagation is approximately perpendicular to the direction of surface wave propagation, time reversed signals increase with wave amplitudes. This contradicts not only to what might be expected, but also all the other results. If these results are true, this would imply that in some cases time reversed pulses perform better in changing environments. This is opposed to a basic assumption of time reversal, that there is no change in the environment over the time taken to perform the time reversal.
Given that, in most of these cases, this trend is inferred from a single data point, it is probably not a general trend. Further, closer sampling of surface wave amplitudes is needed. It is possible that these high voltage responses could be peaks in a periodic relationship, suggested by the results of Fig. 4.16.

These wave angle experiments did differ from the previous experiments in that as the rig was rotated, the curvature of the bottom of the tank changed. There is a

small possibility that this would account for the measured signal increase as the wave angle approached 90°.

4.9 Chapter summary

This chapter has shown the performance of the time reversal process in a shallow water waveguide for a range of surface wave conditions. The results presented show the robustness of the time reversal technique in this environment.

This concludes the work carried out on time reversal, which was introduced in chapter 2, and discussed further in chapter 3. The next chapter introduces mine warfare and countermeasures, where we are looking at the interaction between chaotic signals and resonant targets, which is the other area of research in this thesis. Chapter 7, (section 7.7 specifically) discusses the possibility of using the two techniques in unison to provide an enhanced method for mine hunting.

Chapter 5.

Introduction to naval mine warfare and countermeasures.

One of the original motivations behind the present research was the applicability of new techniques to mine hunting in shallow-water, complex environments. Whilst Chapters 2-4 presented time reversal and its application to changing environments in a shallow-water waveguide, the next part of my research concentrated on the novel use of chaotic signals to investigate target resonances. To place more firmly this research in its context, it was felt that a short chapter on the relevant aspects of mine warfare, and the modern trends in mine hunting, was necessary.

5.1 Basic concepts of mine warfare

Mine warfare can be used to achieve two important strategic objectives [24,25]. The first is denial of sections of sea. This can be defensive, when areas like coastlines are mined to prevent enemy approach, forcing enemy ships/submarines into waters that are more easily defended, or away from strategically important areas such as ports. Mines can be placed offensively in enemy waters to hamper their own movements, and even in enemy ports to deny access. The second strategic objective is denial of important (if not vital) enemy supplies. This can be achieved by mining shipping lanes, which can result in losses in shipping, and also dissuade ships from using this route altogether. Often in this case, mines are laid out thinly, to create the impression of randomness in a large area, which can have a psychological effect on the crew of these vessels.

International law states that a nation must declare when it has mined an area, so that civilian shipping can avoid the area, but these warnings do not have be specific. For example, during World War II, Britain simply declared that it had mined the English Channel, North Sea and French coast [24]. It is also possible to declare an area to be mined when no mines have actually been placed. In this situation, the threat of mines proves as effective as the mines themselves. This is why most countries with a coastline routinely check their seabeds for out-of-place objects, which could be mines. Called MLOs (Mine-Like Objects), these are identified on sonar maps and checked with mine hunting. Because it is not practical to survey the whole coastline of a country, navies around the world tend to focus on shipping lanes and access routes to particularly important areas. The areas routinely checked and known to be clear of mines (to a certain degree of confidence) are often referred to as "Q-routes".

5.2 The advantages and disadvantages of using naval mines.

Naval mines have several key advantages and disadvantages [24]. The main advantages are:

1) Naval mines are relatively cheap, and so represent a cost-efficient way of waging war. They can cause many times their own cost in damage on enemy vessels.[5]
2) Mines can be laid using a variety of methods such as minelayers, submarines, aircraft, and even by hand (in harbours and coastal approaches).
3) It takes much longer (up to 200 times longer) to remove a minefield than it does to lay it, and it also costs much more (typically between 10 to 200 times) to remove than to lay.

[5] . During the First Gulf War, USS Princeton was struck by two bottom influence 'Manta' mines, each costing ~$10k. Between them, they caused approximately $24m damage to the ship [26].

4) Once a minefield has been laid, it requires no further attention (although it may require replenishment should the mines be removed by minesweeping and/or mine hunting).

The disadvantages of naval mines are:

1) Naval mines are to a certain extent indiscriminate. Although they can often be set to be triggered by certain types of target (see section 5.4), there is no guarantee that these mines will not damage one's own fleet.
2) Naval mines are very robust, and will usually outlast the conflict during which they were placed. (There are still areas of ocean where mines laid during the WWII still exist, because they are too spread out and expensive to clear—and, theoretically, some of these mines might remain active for hundreds of years). These mines still represent a real threat to civilian and military shipping, more than 60 years after the end of the war.

This continued presence of active naval mines, often long after the end of the conflict they were intended for, means that mine-hunting and minesweeping remain essential in times of both war and peace.

5.3 Types of mine

Mines can be broadly placed into one of three categories [27] (Fig. 5.1).

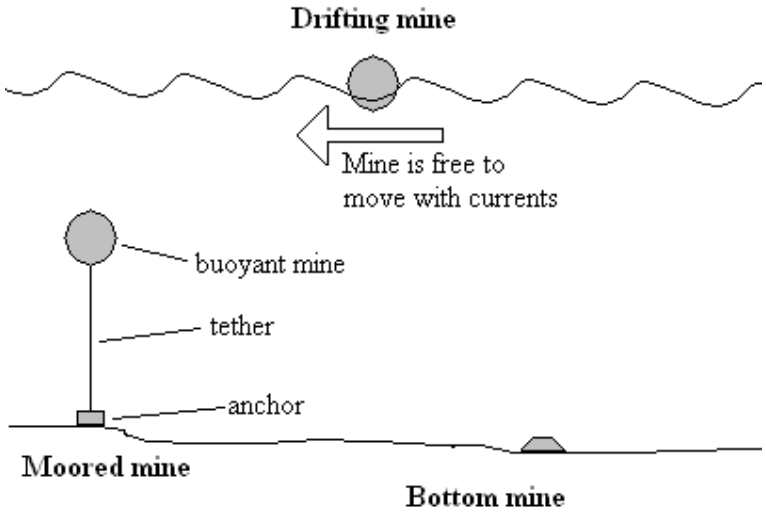

Fig. 5.1: The three basic types of naval mines. The additional effects of mine burial (for bottom mines) are beyond the scope of the present work, and will not be detailed here.

These three types are:

1) Moored/Tethered mines.

   These are buoyant mines that are connected with a wire to an anchor on the bottom. The length of cable used to attach the mine to the anchor determines the vertical height off the bottom of the water. Mines placed near the water surface are more effective against surface vessels, while mines near the bottom are more effective against submarines. These mines tend to be used in deeper water, and can be effective against both surface ships and submarines. A moored mine that loses its tether becomes a drifting mine.

2) Drifting mines.

These are buoyant mines that float on the surface of the water, and are free to move with water currents. The use of drifting mines was banned under the Hague Convention of 1907 [25], however they have been used since then.[6]

3) Bottom mines.

These mines are designed to sink and rest on the ocean floor. Over time, they can become partially or totally covered with silt/mud etc., making detection harder. Additional effects during burial (such as scouring or sediment liquefaction in the close vicinity of the mine) are beyond the scope of the present work and therefore not envisaged. These mines are most effective in shallower waters. In deeper water, it may be possible for surface ships to pass over the mine without triggering it, although it will still remain effective against submarines.

5.4 Types of trigger

There are broadly speaking four different triggering mechanisms for naval mines (Fig. 5.2), although some mines may contain more than one triggering method. The four types are [25]:

1) Contact

The target vessel must physically touch the mine. This is the oldest type of activation, but is very effective as the explosive charge goes off very close to the hull.

2) Magnetic

The magnetic signature given off by a ship's hull as it passes the mine activates it. These signatures can be specific enough for the mine to be able to

[6] In 1940 and 1944, floating contact mines were used by the British as part of 'Operation Marine', where floating mines were dropped into the Rhine in France with a timer set to become active once they reached German territory [23].

target 'High Value Units' such as supply tankers and aircraft carriers, while leaving smaller (lighter) vessels unharmed.

3) *Acoustic*

Acoustic mines are triggered by the amount of noise produced by a ship (this is normally through its engines and propellers). This can be very specific, allowing specific types of units to be attacked and others to pass without incident.

4) *Pressure*

The amount of water that a vessel displaces creates a surrounding pressure wave (with heavier ships producing a larger pressure wave). This can be detected by mines and cause them to activate.

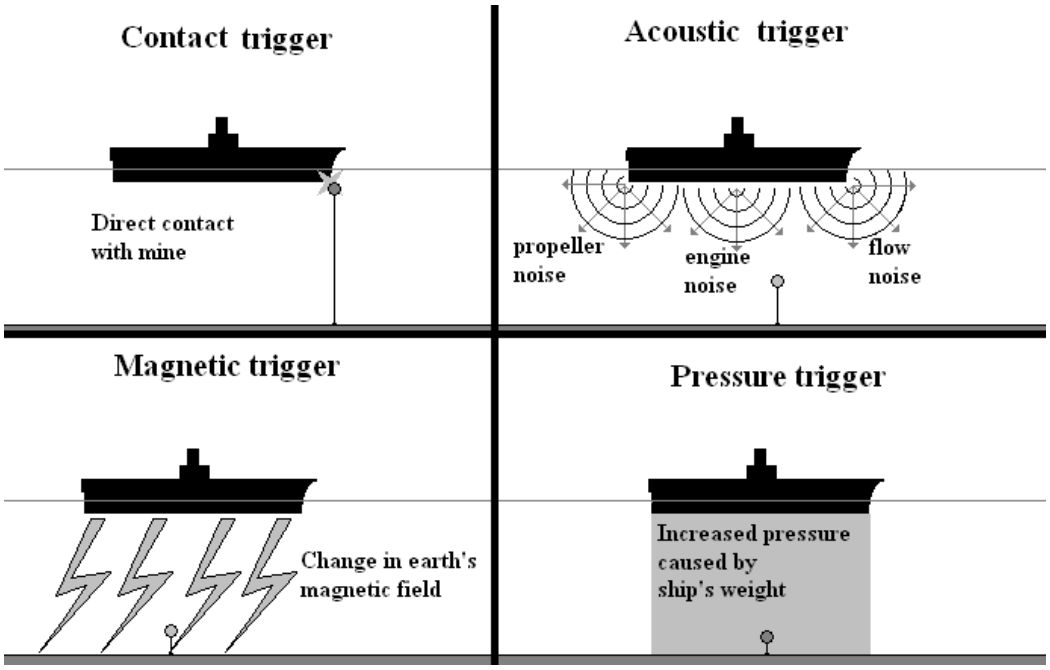

Fig. 5.2 Main triggering mechanisms for naval mines. Some mines may combine several different triggers.

5.5 Mine countermeasures

There are two ways of dealing with mined areas, namely minesweeping and mine hunting.

5.5.1 Minesweeping

Minesweeping can take one of two forms, either a contact sweep or a distance/influence sweep [28].

Contact sweeping.

Contact sweeping is achieved using a metal wire dragged behind the ship to cut the cables of moored mines. The cables are cut either by abrasive action between the sweep wire and the cable, or by one of several cutters positioned along the sweep wire (Fig. 5.3).

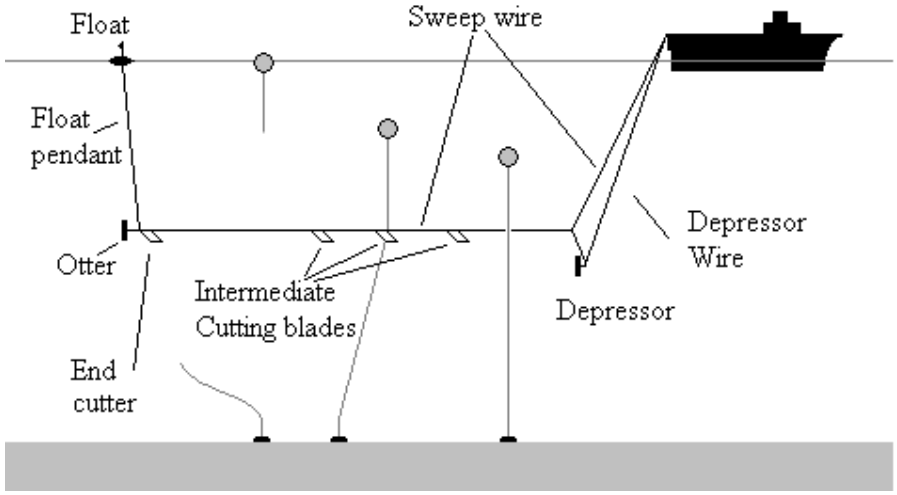

Fig.5.3. Basic configuration of contact minesweeping.

The depth of the sweep cable is controlled using a float and a depressor. The end farthest from the minesweeper is attached to a float via a float pendant which acts to set its depth, while the end closest to the mine sweeper is attached to another wire known as the depressor wire, which in combination with a depressor also sets the

depth of the sweep wire. Using both a depressor wire and a float has the effect of keeping the depth of the sweep wire approximately constant over the length of the sweep wire. An otter is attached to the sweep wire to steer the wire either port or starboard, to increase the width of the areas swept during a single straight-line sweep by a minesweeper [29]. This is shown in Fig 5.4.

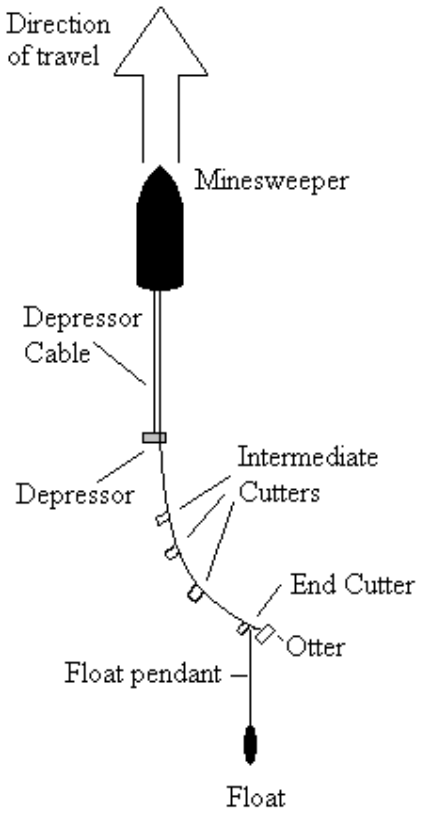

Fig. 5.4: Use of otter to steer sweep wire to starboard. (view from above).

Using otters to steer the sweep wires allows the use of two sweep wires (one to port, and one to starboard), increasing the area a minesweeper can sweep at any one time. It is also possible to link sweep wires together between ships further increasing the area swept [29].

Once a mine has been swept, and its cable cut, the mine will then float to the surface where it can then be either destroyed or picked up for close examination.

Minesweeping in this fashion requires the ship to move at slow speed in a straight line, making it very vulnerable to enemy attack [24]. Contact sweeps are also ineffective against bottom mines. (It is also possible to sweep for bottom mines by dragging a net across the sea floor, but this is seldom performed [25]).

Distance/influence sweeping

When performing a distance/influence sweep, a minesweeping vessel will mimic the characteristics of another (usually larger) type of vessel in order to 'trick' the mine into detonating. This is achieved using a noisemaker and an electric cable or solenoid generating an acoustic/magnetic field, either attached to the hull of the minesweeper or in an array towed behind the ship. These signals simulate the acoustic and magnetic properties of the mine's target ship. If successful, these signals trick the mine into exploding under the sweeping gear (Fig 5.5).

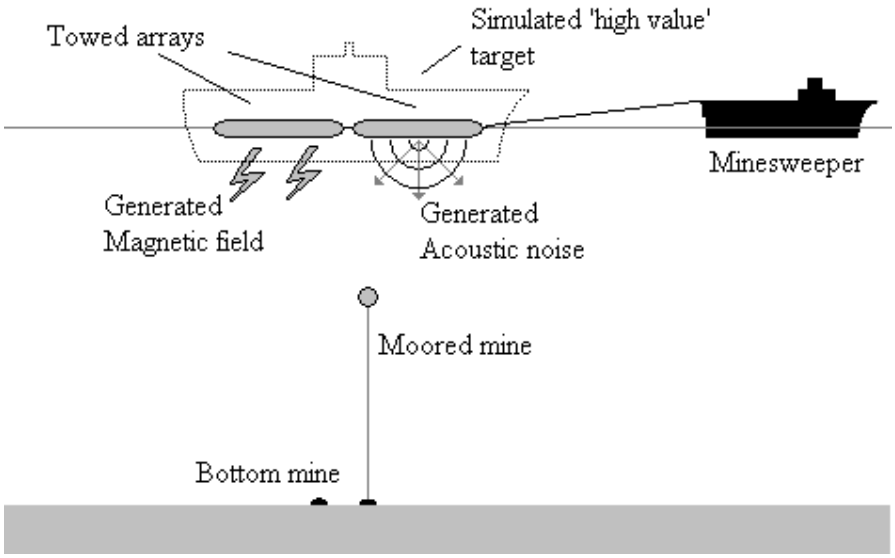

Fig. 5.5: Diagram of a simplified influence sweep set-up.

Influence sweeps are effective against both tethered and bottom mines, but they are unable to reproduce the pressure waves of larger ships, and so are incapable of activating mines with pressure triggers [25]. It is possible to use a heavily laden barge or a derelict vessel to produce a large pressure field to trigger this type of mine, but this technique is not used [25].

5.5.2 Mine hunting

Mine hunting uses high definition sonar arrays to search for mines [24,29,30]. Mine hunting is slow, but is considered the most secure method of neutralising mines [1]. Typically this is performed using an array attached to the hull of the minesweeper, although it can also be performed using a towed array. This array uses active sonar to locate objects either on the bottom or floating in the water. Once located, these objects are classified as either mine-like or non-mine-like. Mine-like objects (MLOs) are then examined and, if confirmed, destroyed (Fig. 5.6).

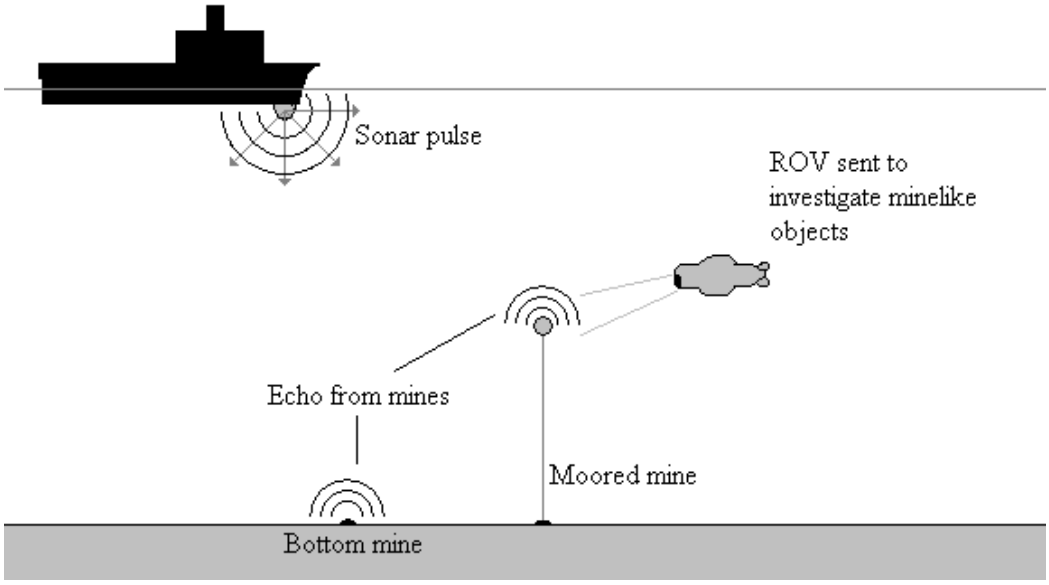

Fig. 5.6: Basic principles of mine-hunting. Note that a diver could have been shown instead of the Remotely-Operated Vehicle (ROV).

A major advantage over minesweeping is that it is capable of locating and in some cases classifying mines [29]. (Minesweeping does not locate mines, it merely attempts to neutralise those in its sweep path). In addition, as location and neutralisation are two separate stages, it is possible to locate mines without neutralising them.

Mine-hunting is currently the most important method of neutralising mines. Also, especially as many mines are now fitted with anti-sweep mechanisms [24], mine-hunting will remain the best method of neutralising naval mines.

This method is however slow [e.g. 24] and not infallible. Therefore, improving the ability to find and classify mines remains an important area of research. The research shown in Chapter 6 gives information on research into a new method of mine hunting, which involves chaotic pulses for acoustic detection.

Chapter 6

The use of chaotic pulses for acoustic detection

6.1 Background to research.

Associated to part of this research, Dr A.J. Fenwick (QinetiQ, UK), carried out the initial studies in this area [31]. The aim of this part of the thesis was to investigate potential new methods of acoustic detection using novel types of signal. The initial stages of the research were performed using computer simulations carried out using MATLAB. Part of this research investigated the use of chaotic signals, and the possibilities of exploiting their behaviour when interacting with resonant objects. The work presented here is the experimental validation of the original simulations, performed in collaboration with Dr Fenwick, followed with an investigation into methods of detection of acoustic resonances using chaotic signals, and finally presenting a large-scale trial of the detection process.

6.1.1 Introduction to chaotic signals.

A system can be described as *chaotic* if it has the following characteristics [32]:

1) It is *aperiodic* (i.e. it never repeats);

2) It exhibits *sensitive dependence on initial conditions* (hence becoming unpredictable in the long term);

3) It is governed by one or more *control parameters*, a small change in which can cause the chaos to appear or disappear;

4) Its governing equation is *non-linear*.

Several different types of chaotic signal were investigated initially, but it was decided to focus on a single type of chaotic signal as they generally all possessed the same qualitative properties. The chaotic system used in this research is a 'Duffing oscillator', described by the equation:

$$\frac{d^2x}{dt^2} + b_d \frac{dx}{dt} + k_d x + k_{nl} x^3 = 0 \qquad (6.1)$$

Where x is the displacement from the equilibrium position, b_d is the damping constant, k_d is the spring constant, k_{nl} is the weighting on the non-linear term and t is time.

If a simple harmonic oscillator is used to drive this Duffing oscillator, the equation becomes

$$\frac{d^2x}{dt^2} + b_d \frac{dx}{dt} + k_d x + k_{nl} x^3 = F\cos(\omega t) \qquad (6.2)$$

where F is the (constant) amplitude and ω is the angular frequency of the drive.

The specific equation used in this research was:

$$\frac{d^2x}{dt^2} + 0.3\frac{dx}{dt} - x + x^3 = 0.5\cos(1.2t) \qquad (6.3)$$

With initial conditions x = 0 and $\frac{dx}{dt} = 1$.

This was the equation and initial conditions used in Dr Fenwick's simulations, so it allows direct comparison between simulated and experimental results. The calculated output of this system provides the chaotic signal used in this research. A typical response from this Duffing oscillator is shown in Fig. 6.1.

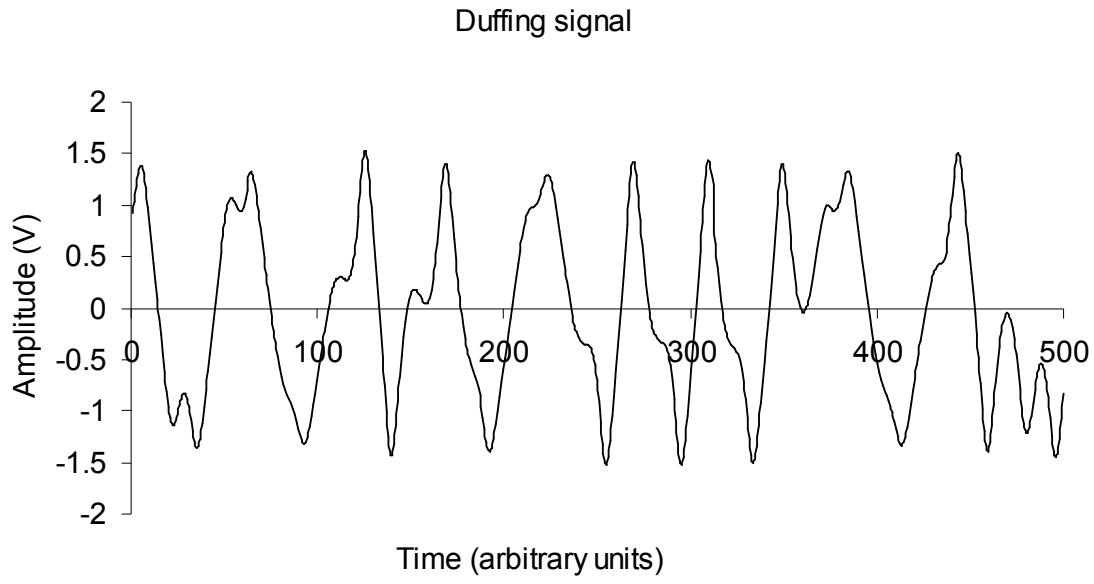

Fig. 6.1: A typical Duffing signal (see text for details)

The time-averaged spectrum of the Duffing signal is similar to random noise in that they both possess a continuous spectrum, although often a chaotic signal also possesses some additional structure [4]. The time-averaged frequency spectrum of the Duffing signal used in these experiments is shown in Fig. 6.2.

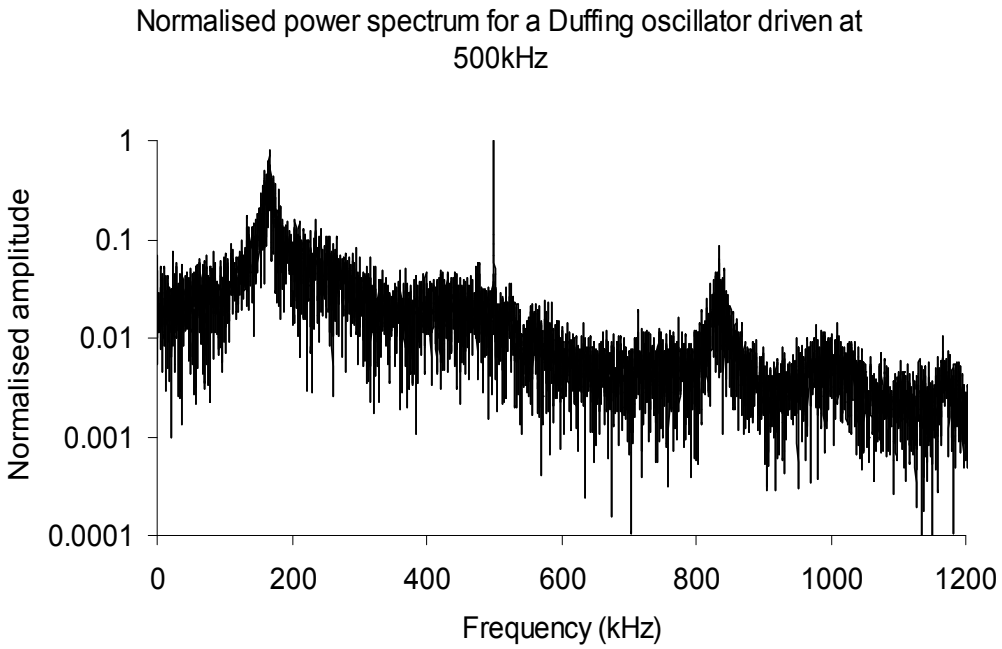

Fig. 6.2: Time-averaged frequency spectrum of a Duffing oscillator at 500 kHz

The time-averaged power spectrum of the Duffing oscillator used in these experiments has two dominant peaks at frequencies of approximately $\omega/3$ and ω where ω is the drive frequency of the harmonic oscillator. In this case $\omega/3 \approx 166$ kHz and ω=500 kHz. This appears to be a general result for the Duffing signal(s) used in these experiments.

The equation that describes the Duffing oscillator is a second-order equation, but may be expressed as two linked single-order equations.

$$\frac{d^2x}{dt^2} + b_d \frac{dx}{dt} + k_d x + k_{nl} x^3 = F\cos(\omega t) \tag{6.2}$$

becomes

$$\begin{cases} \dfrac{dx}{dt} = y \\ \dfrac{dy}{dt} = k_{nl} x^3 + k_d x - b_d y + F\cos(\omega t) \end{cases} \tag{6.5}$$

This 2-dimensional state space is commonly known as *phase space.* [32]. A phase portrait (or phase-space portrait) is considered a useful method of viewing how a dynamical system varies with time. The phase portrait for this Duffing signal is shown in Fig. 6.3.

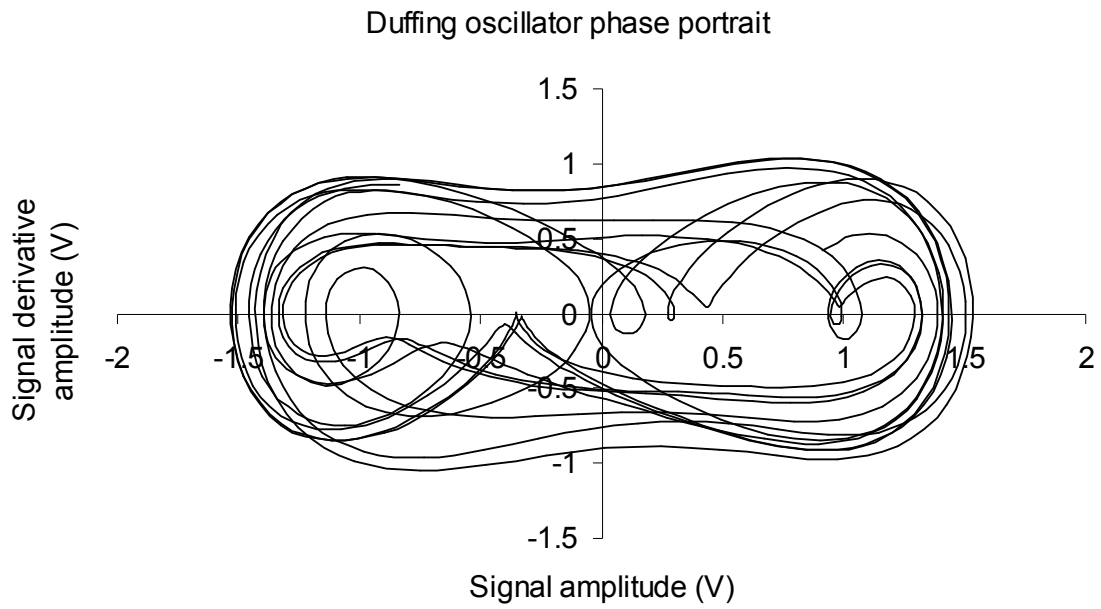

Fig. 6.3: Phase portrait of a typical Duffing signal.

This phase portrait illustrates the chaotic nature of the signal, as its trajectory through phase space does not follow a regular loop (showing its dependence on starting conditions), and does not repeat. This phase portrait is typical of a Duffing oscillator.

6.1.2 Simulations of simple harmonic coupled systems.

The original simulations, performed by Dr Fenwick [31], simulated the simplest of physical situations, where the chaotic signal of Section 6.1.1 is used to excite a simple harmonic oscillator. The results of these simulations are summarised below.

A typical time domain signal for a Duffing signal coupled with a harmonic oscillator is shown in Fig. 6.4.

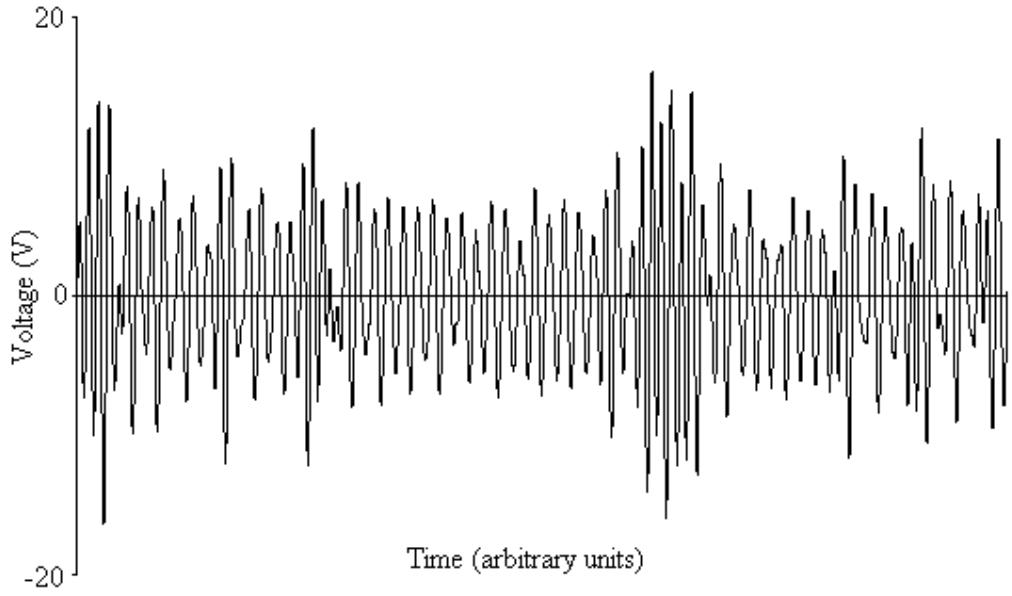

Fig. 6.4: Typical time domain response for a Duffing oscillator coupled with a simple harmonic oscillator

Here we see that the output from the simple harmonic oscillator is broadly similar in character to the input Duffing signal, but that the peak voltages have changed. Whereas previously the peak voltage of the Duffing signal was constant throughout the signal, here we see that the voltage level contains periods where the peak voltage is nearly constant, and periods where the peak voltage becomes significantly higher. The brief periods when the voltage is significantly higher are known as ‘bursts’. The phase portrait of this signal is shown in Fig. 6.5.

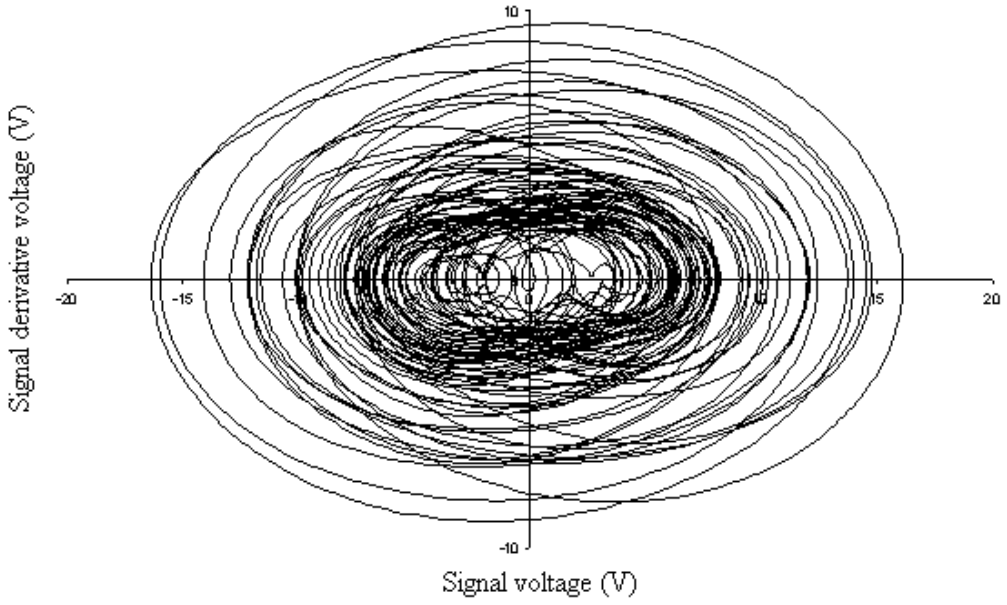

Fig. 6.5: Phase portrait of response for a Duffing oscillator coupled with a simple harmonic oscillator.

As with the time domain result, the phase portrait shows us that the signal spends most of the time travelling through phase space at approximately constant amplitude, with brief periods at much higher amplitude (bursting).

These initial simulations indicated that there is a quantifiable change in the nature of the chaotic signal when it interacts with a resonance, and it was decided to investigate if this 'bursting' phenomenon could be reproduced experimentally. If this is the case, then this has the possibility of providing a method of detecting the presence of resonant objects within the area illuminated by the chaotic signal. If this could be applied to mine detection, it would offer a unique advantage.

6.2 Experimental work.

One aim of this thesis was to validate experimentally the theoretical simulations performed by Dr Fenwick [31], and to collaborate in the development of methods of detection using chaotic acoustic pulses.

6.2.1 Experimental set-up.

The experimental system used is shown diagrammatically in Fig. 6.6.

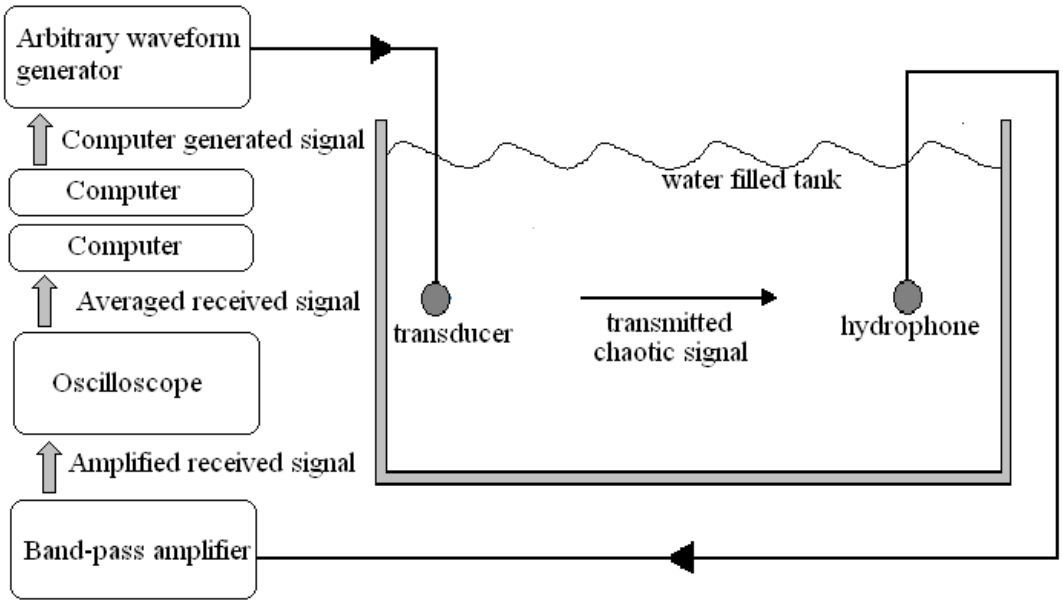

Fig. 6.6: Experimental set-up for transmission of chaotic pulses.

A chaotic signal of finite length was generated numerically with MATLAB (using the parameters outlined in section 6.1.1). The signal was then digitised into 4096 (2^{12}) bits, (the dynamic range of the arbitrary waveform) and stored in the arbitrary waveform generator. The signal was scaled up to 20V, the maximum the arbitrary waveform generator was capable of. The signal was scaled in time to the desired drive frequency (f_d). This signal was then applied to a Panametrics V391-su transducer, which had a resonant frequency of 450 kHz, and a Q-factor of ~1. The receiving hydrophone was a prototype design produced by NPL and provided by Prof. V.F. Humphrey. It had a response that could be considered flat over the frequency range of interest (100 to 1000 kHz). The received signal was then passed through a band-pass amplifier (with the pass band defined as 100 to 1000 kHz) to increase the

signal-to-noise ratio of the signal. This is because the receiving hydrophone had a very low voltage output.

The use of the arbitrary waveform generator enabled the same signal to be transmitted repeatedly and facilitated the use of signal averaging to further improve the signal-to-noise ratio (in a way similar to that used in seismic data processing, e.g. [33]). In the experiments presented here, 100 signals were averaged. Gated pulses of chaotic signal, typically 2.5 ms long, were transmitted at a pulse repetition frequency of 10 Hz, to ensure that the received signals were free from multiple reflections. The distance between the transmitter and receiver was set at ~362mm.

6.2.2. Initial validation of chaotic transmission

Before being able to verify the simulations, it was necessary to determine the effect that the transmit process had on the acoustic signal. This is because the transmitter is itself an object with an acoustic resonance, so by passing a chaotic (electrical) signal through it, we are in effect driving a resonant object with a chaotic signal. This is the case these experiments have set out to investigate, and so it is expected that the output acoustic signal will therefore contain some amount of bursting.

Fig. 6.7 shows an example of a section of the numerically generated chaotic signal, and the resultant signal transmitted through the water and received by the hydrophone for drive frequencies f_d of 500, 700 and 900 kHz. The corresponding spectra are shown in Fig. 6.8.

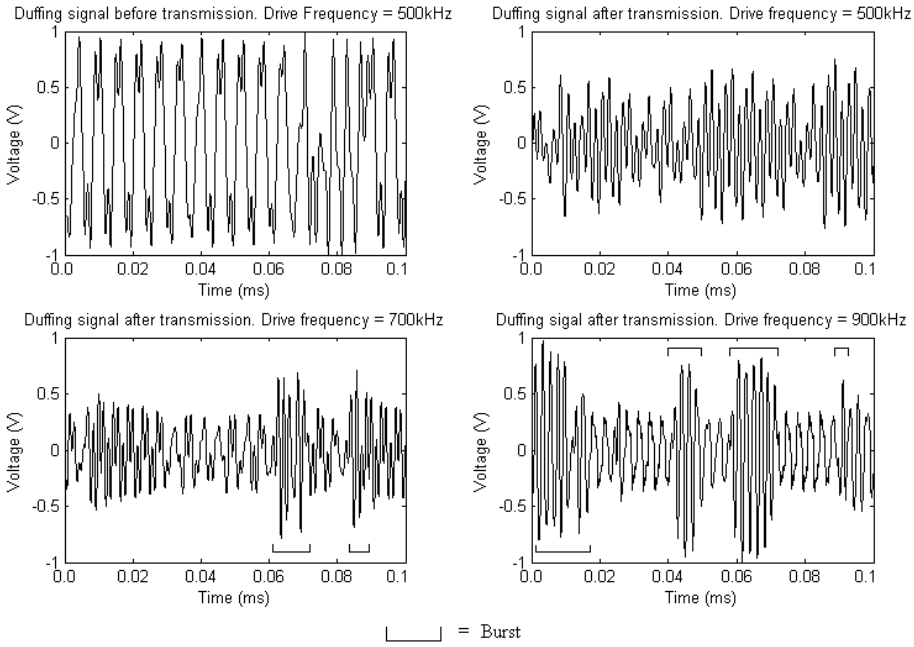

Fig. 6.7: Comparison of initial Duffing signal and transmitted signals in water for drive frequencies of 500, 700 and 900 kHz.

The characteristic features of the Duffing signal are retained in the signals transmitted through the water but there is evidence of bursting in 700 and 900 kHz results (as indicated in the lower 2 plots of Fig. 6.7). This is problematic, as any bursting present on the transmit signal will make it more difficult to detect when bursting is produced by interaction with a resonant object in the region of interest. This underlines the importance of appropriate overall system design to allow for the signal and the transducer characteristics

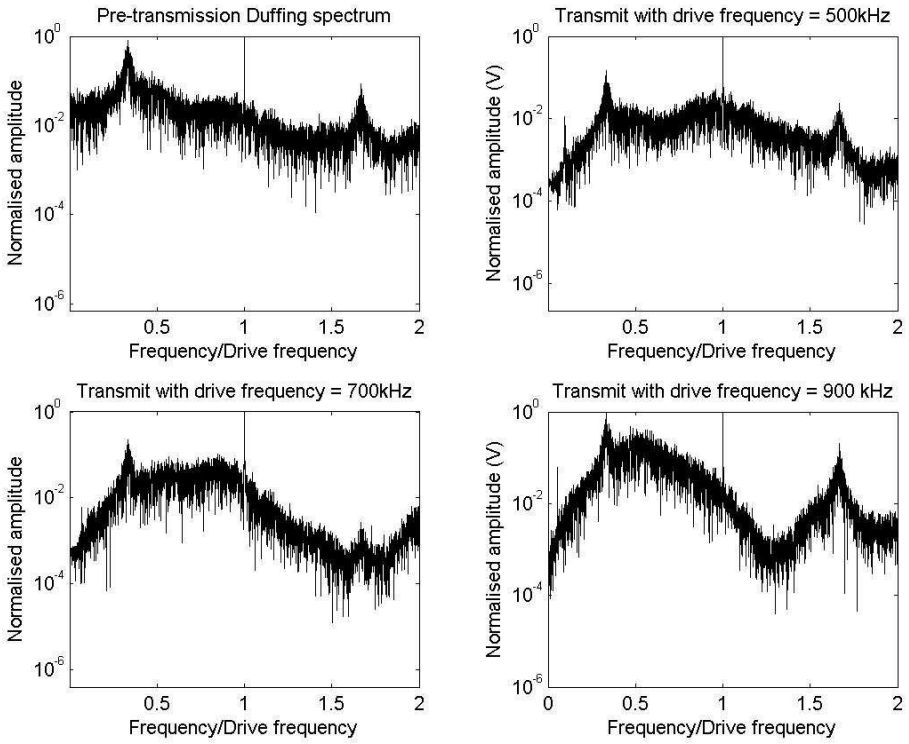

Fig. 6.8: Comparison of the frequency spectra of the initial Duffing signal and transmitted signals in water for drive frequencies of 500, 700 and 900 kHz.

The frequency spectrum, as with the time-domain signal, is changed by the response of the transducer. The two dominant frequencies are the very narrow spectral peak at the drive frequency f_d and a broader spectral peak at about $f_d/3$; the relative amplitude depends on the drive frequency relative to the resonant frequency of the transducer. The peak at ~$1.7f_d$ is also present in f_d = 500 kHz and 900 kHz, it is much reduced in f_d = 700 kHz due to lying in a null of the transducer. It is thought that this peak at ~$1.7f_d$ is of less significance to bursting. It is important that the dynamics of the signal remain relatively unchanged. The spectra indicate that for this transducer there is a range of drive frequencies that may be used without a change in the chaotic nature of the signal.

6.2.3 Transmission through a flat metal plate

Given that an acoustic chaotic pulse could be successfully transmitted, the next step was to investigate if these chaotic pulses could produce the bursting response in resonant objects as predicted by simulations. A flat steel plate of thickness 14.3mm was used as a resonant object. This was chosen as the resonant target because it provided a simple resonance within the frequency range of interest. The equation for the transmission coefficient (the proportion of incident energy that is transmitted) for a steel plate in water (normal incidence) can be approximated as;

$$T = \frac{1}{1 + \frac{1}{4}\left(\frac{r_2}{r_1} - \frac{r_1}{r_2}\right)^2 \sin^2 k_2 L} \tag{6.6}$$

where r_1 and r_2 are the characteristic impedances of water and steel respectively, L is the thickness of the plate, and k_2 is the wavenumber in steel. [34]

The value of T is maximum when $kL=n\pi$ (i.e. $\sin(kL) = 0$). Solving for f we get maximum transmission at frequencies

$$f \approx \frac{nc}{2L}, \tag{6.7}$$

For steel, $c \approx 6374 ms^{-1}$ [5], so the plate used in these experiments had resonant frequencies at ~n*223 kHz.

The second resonant frequency is 446 kHz, and so is ideal for our experiment. The steel plate was placed at right angles to the incident chaotic signal so that the maximum amount of energy would be transmitted through the plate. Fig. 6.9 summarises the changes in the signal, frequency spectrum and phase portrait that occurred when the signal was transmitted into the water with and without the resonant plate, for a drive frequency of 700 kHz. The frequency of 700 kHz was chosen, as it was one where it was easy to see both the change in the Duffing signal, and the

corresponding change in the power spectrum. It shows that bursting is present on the signal with and without the plate, which makes the detection of the resonant object (the plate in this experiment) more difficult than simply looking for high amplitude bursts in the received signal.

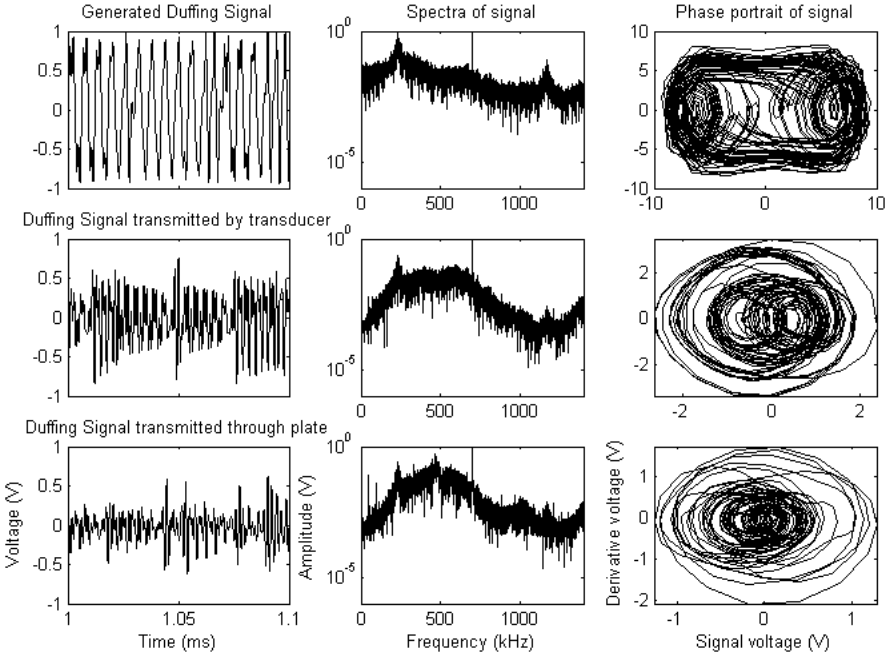

Fig.6.9: Transmission of a Duffing signal through a flat steel plate (f_d = 700 kHz). Time series, spectra and phase portraits: (a) Duffing signal, (b) signal in water and (c) signal transmitted through plate.

If we examine the Duffing signal before and after it has passed through the plate, we can see that they both contain bursts, but that transmission through the plate (i.e. interaction with a resonance) has increased the amplitude of the bursts in relation to the mean peak voltage level. This change in level presents us with the possibility of detecting resonances, by measuring a change in the level of bursting.

6.3 A method for detecting the interaction of chaotic signals with resonant objects

Examination of the chaotic signal before and after transmission through the steel plate suggested that the effect of the steel plate was to increase the amplitude of the bursts. If this were the case, then if we were to examine the distribution of amplitudes for the two signals, there would be a significant difference between the two. Figure 6.10 shows two histograms illustrating the distribution of voltages relative to the mean voltage level for a 700 kHz Duffing signal before and after transmission through a steel plate.

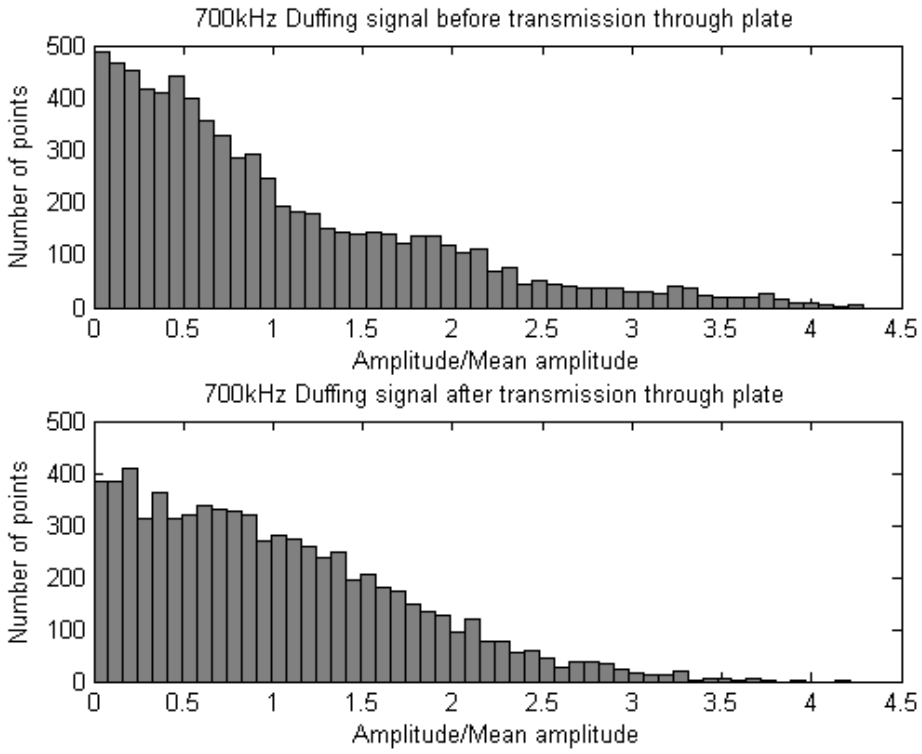

Fig. 6.10: Histogram of amplitude distribution before and after transmission through steel plate.

Fig. 6.10 clearly demonstrates that there is a significant difference in the distribution of amplitudes before and after transmission through the plate. Given that it had been demonstrated that the process of transmitting a Duffing signal through a

resonant object altered the distribution of amplitudes of the signal, it was decided to investigate the 3rd and 4th order moments of the data, the skew and kurtosis.

6.3.1 Definitions of skew and kurtosis.

Skew is the 3rd order moment (the 1st and second order moment being the mean and standard deviation respectively), and is defined as:

$$\frac{\Sigma(X-\mu)^3}{N\sigma^3} \tag{6.8}$$

where μ = the mean and σ = the standard deviation [35].

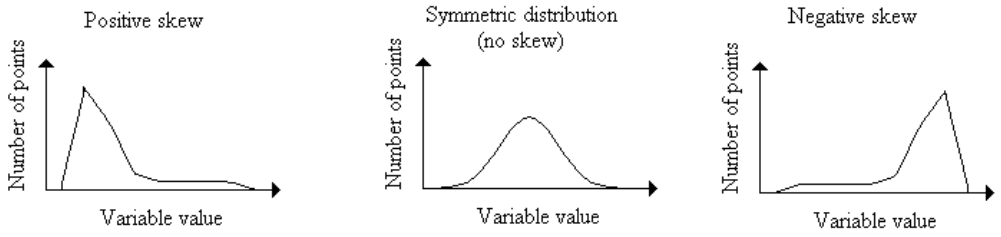

Figure 6.11: example of different types of skew.

Figure 6.11 illustrates the 3 different types of skew. The first distribution, shown on the left in Fig.6.11, has a positive skew; this means that it has a long tail in the positive direction (i.e. to the right). The second distribution is symmetric and has no skew distribution. Finally, the third distribution has a negative skew since it has a long tail in the negative direction (i.e. to the left).

Distributions with positive skew are sometimes called "skewed to the right" whereas distributions with negative skew are called "skewed to the left."

If we evaluate the skew for the two signals shown in Fig. 6.10, we find that before transmission the signal has a skew of ~0.50, and after transmission ~0.99.

Skew can detect and quantify increased bursting caused by the interaction with a simple resonance.

Kurtosis is the 4th order moment, and is defined as:

$$\sum \frac{(X-\mu)^4}{N\sigma^4} - 3 \qquad (6.9)$$

Where μ = the mean and σ = the standard deviation [36].

Kurtosis is a measure of the peakedness (or 'spikiness') of a distribution. It is normally compared to a normal distribution which has a kurtosis of 3, hence the '–3' term. Distributions with relatively large tails are called "leptokurtic"; those with small tails are called "platykurtic". This is illustrated in figure 6.12.

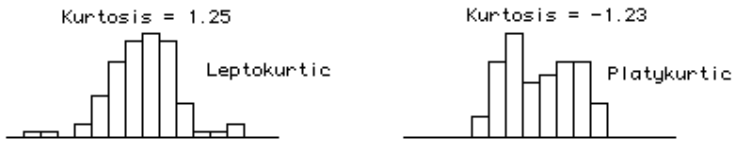

Fig. 6.12: Examples of types of kurtosis.

If we evaluate the kurtosis for the two signals shown in Fig. 6.10, we find that before transmission the signal has a kurtosis of ~ -0.44, and after transmission ~0.69. Kurtosis can detect and quantify increased bursting caused by the interaction with a simple resonance.

6.3.2 Experimental measurements of skew and kurtosis.

The skew and kurtosis of the chaotic signal before and after transmission through a flat steel plate were calculated across a wide range of frequencies (400 kHz – 1000 kHz, by steps of 50 kHz).

The 'incident' waveforms were measured using the experimental set-up shown in section 6.2.1.

The 'transmitted (experimental)' data was measured experimentally using the same experimental set-up as shown in Fig.6.6, with the flat steel plate placed at a distance of ~200mm from the transmitter, and ~162mm from the receiver.

The ‘transmitted (simulated)’ data was produced by taking the waveforms from the direct transmission (the ‘Incident’ data), and multiplying them in the frequency domain with the form function of the flat plate expressed in equation 6.6 using one of my MATLAB programme.

The values of skew and kurtosis were calculated from waveform data using another MATLAB analysis program I wrote.

Splitting each of the waveforms into 4 smaller sections, and measuring the skew of each section produced an estimate of the error. This was to give an idea of how much the statistics might vary with time. The error bars are the standard deviation of the measured values for the 4 separate sections.

The results for skew are summarised in Fig. 6.13, and kurtosis in Fig. 6.14.

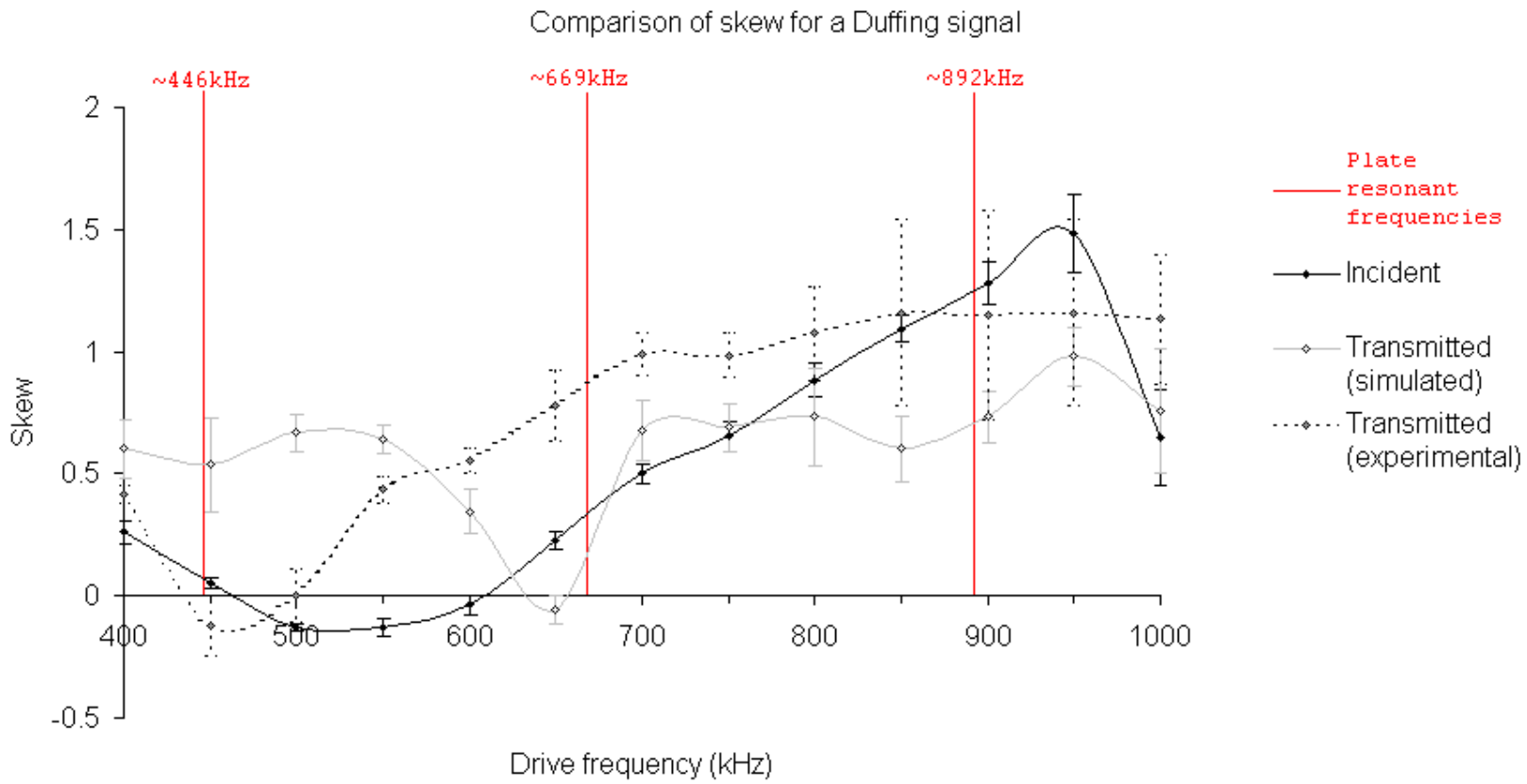

Fig. 6.13: Measured skew for Duffing signals with different drive frequencies

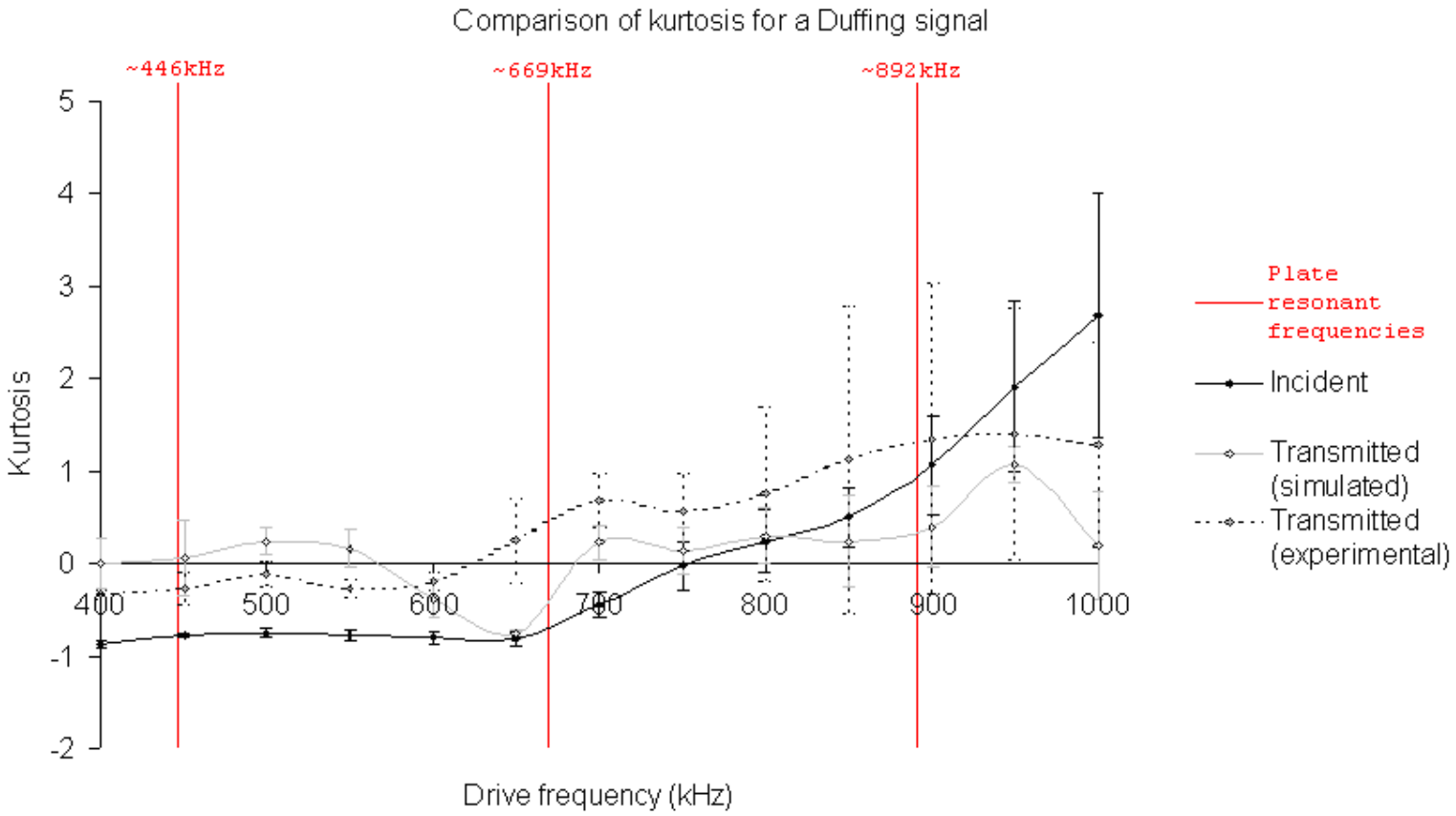

Fig. 6.14: Measured kurtosis for Duffing signals with different drive frequencies.

Fig. 6.13 shows that there is a wide range of frequencies over which there is a detectable increase in skew, equally, Fig. 6.14 shows that there is a wide range of frequencies over which there is a detectable increase in kurtosis. Therefore there is a range of frequencies where this technique would allow us to detect the influence (and therefore presence) of an acoustic resonance.

For a comparison of performance of the detection technique, simulations of transmission of band-limited noise through the same steel plate were carried out. Fig. 6.15 shows one of the noise signals used for the comparison.

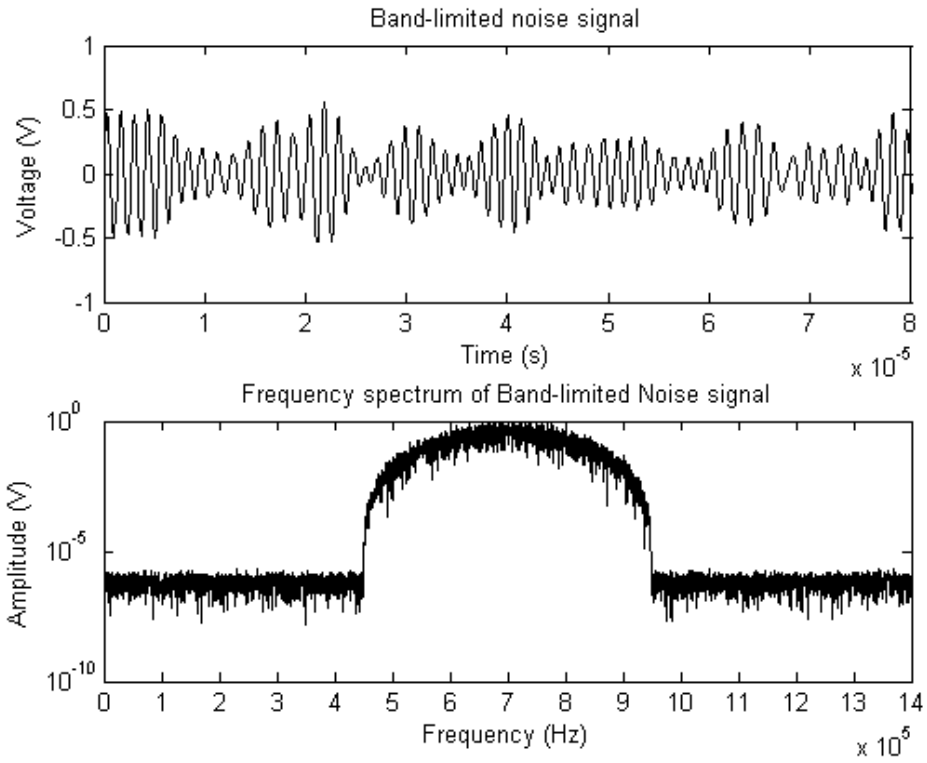

Fig. 6.15: Typical band-limited noise signal used for simulations.

The band-limited noise simulations were carried out in the same way as the Duffing signal simulations. (i.e. the signal was multiplied in the frequency domain with the flat-plate form function from equation. 6.6). The results of these simulations are shown in Fig. 6.16 and Fig. 6.17.

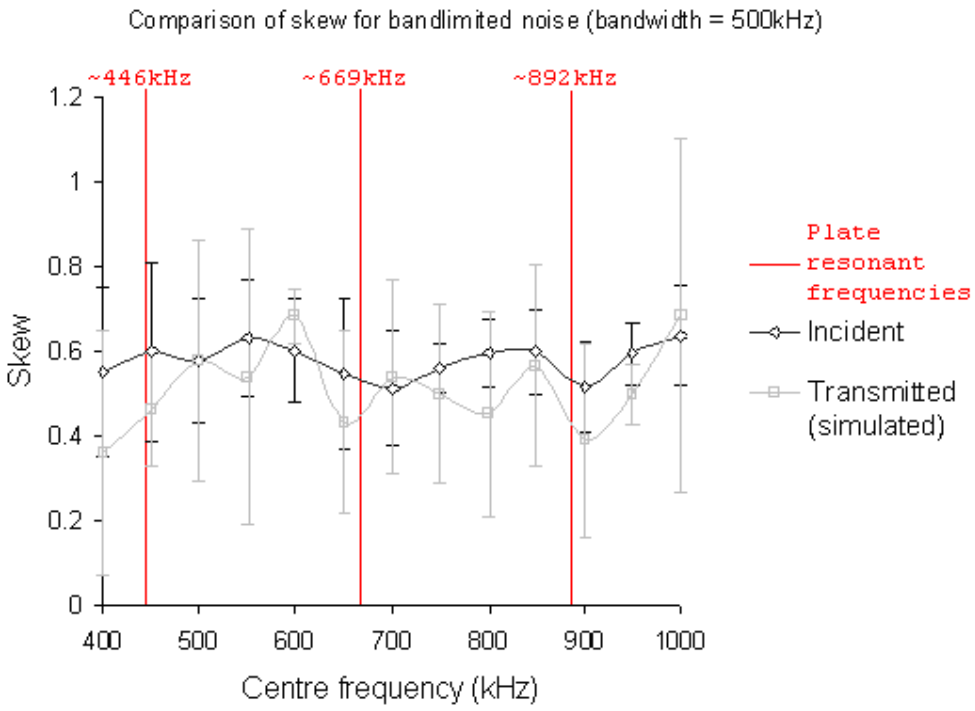

Fig. 6.16: Simulated skew for transmission of band limited noise through steel plate

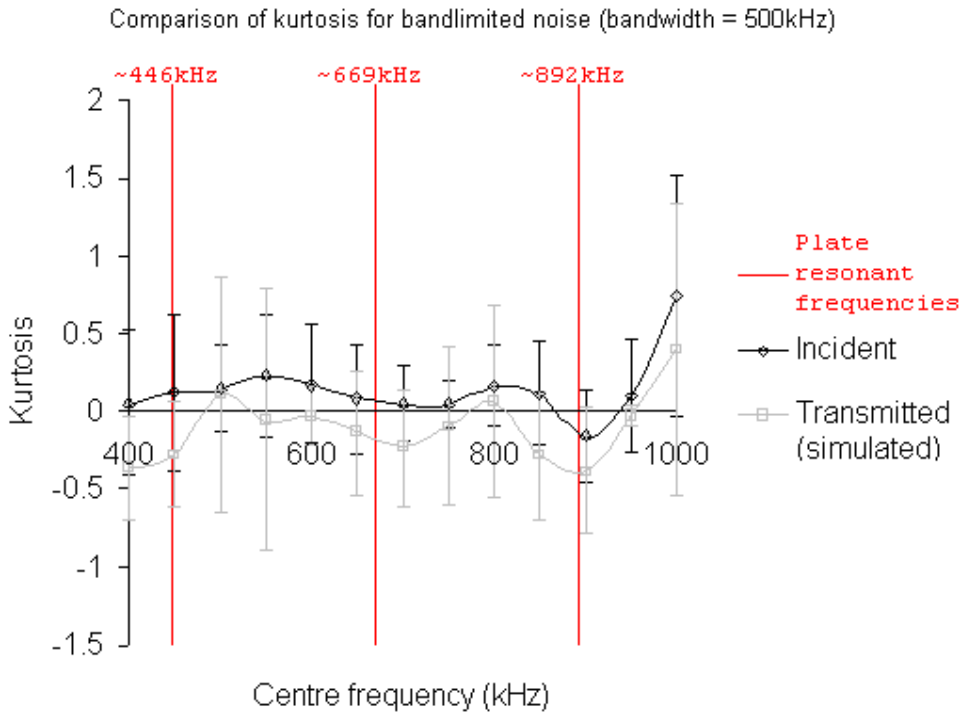

Fig. 6.17: Simulation of kurtosis for transmission of band limited noise through steel plate

Fig. 6.16 and 6.17 show that there is no significant change in the skew of the band-limited noise when it is transmitted through the steel plate. This implies that the change in skew is caused by the nature of the chaotic signal, and not by the wideband nature of the signal.

6.4 Further evaluation of the detection process.

After the initial experiments had demonstrated the effectiveness of chaotic signals for detection, it was decided to try chaotic pulses on acoustic targets with more complex resonances. The results are presented in the following sections.

6.4.1 Plates with non-linear resonances

Two further plates were chosen as resonant targets to test the ability of chaotic signals to detect resonances. These plates were made of a metal composite. Rather than being a solid structure, they were impregnated with densely packed and randomly distributed air bubbles, making a 'honeycomb' type structure. The bubbles within the plate had a range of diameters. This meant that the plate contained a range of resonant frequencies for the chaotic (Duffing) signal could possibly interact with. Plate 1 had a thickness of ~25mm and an average bubble diameter of ~1mm. Plate 2 had a thickness of ~25mm and an average bubble diameter of ~2mm.As with the previous analysis, the skew and kurtosis of the chaotic signal before and after transmission through the plates was calculated across a wide range of frequencies (300/350 kHz – 1000 kHz, by steps of 50 kHz). These results are summarised in figures 6.18 – 6.21. Note that due to the complex nature of the resonances of these plates, simulations of their transmission were not carried out, so the results present experimental values only.

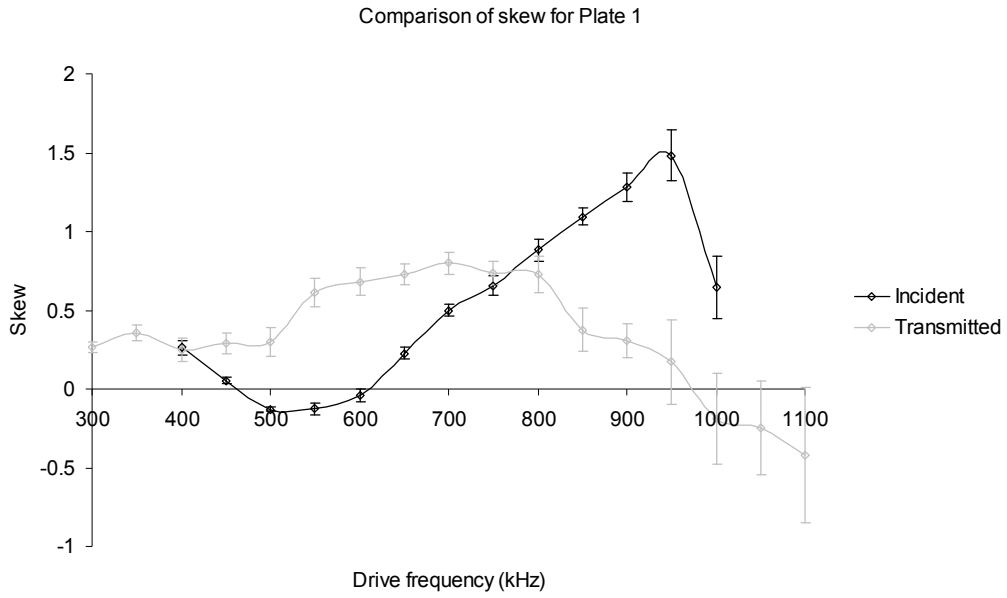

Fig. 6.18: Experimental comparison of skew for plate 1.

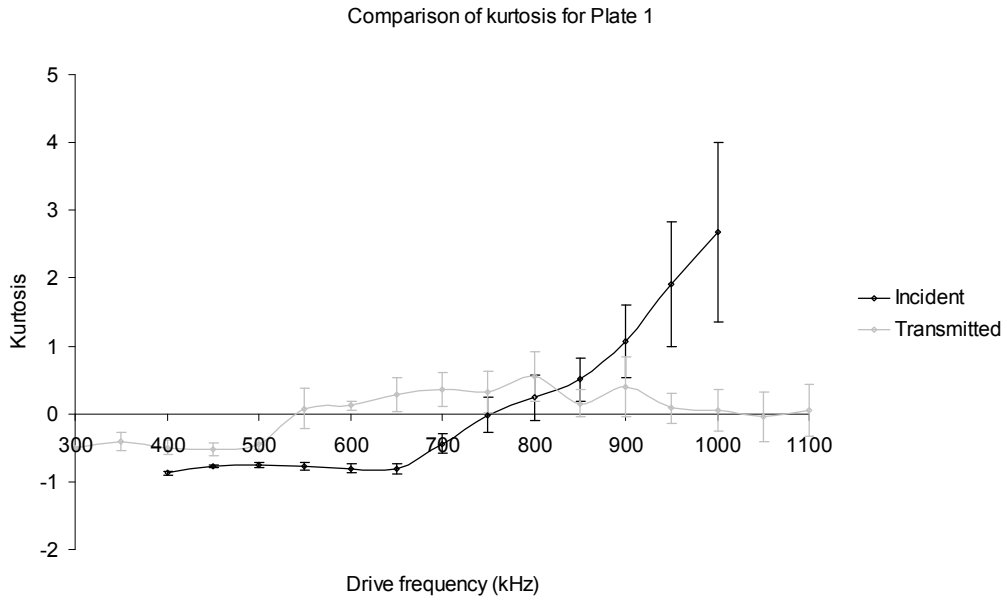

Fig. 6.19: Experimental comparison of kurtosis for plate 1

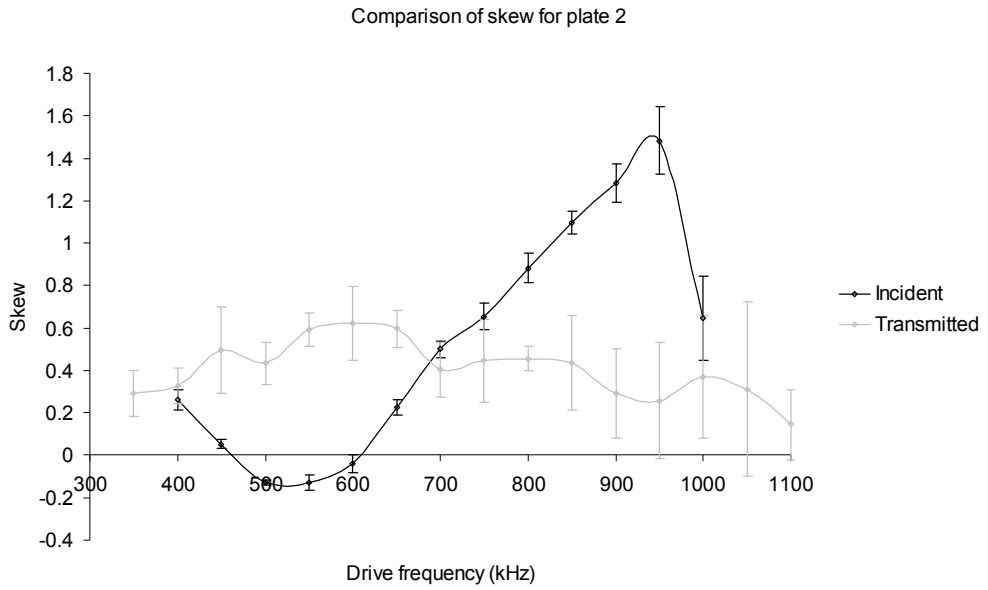

Fig. 6.20: Experimental comparison of skew for plate 2

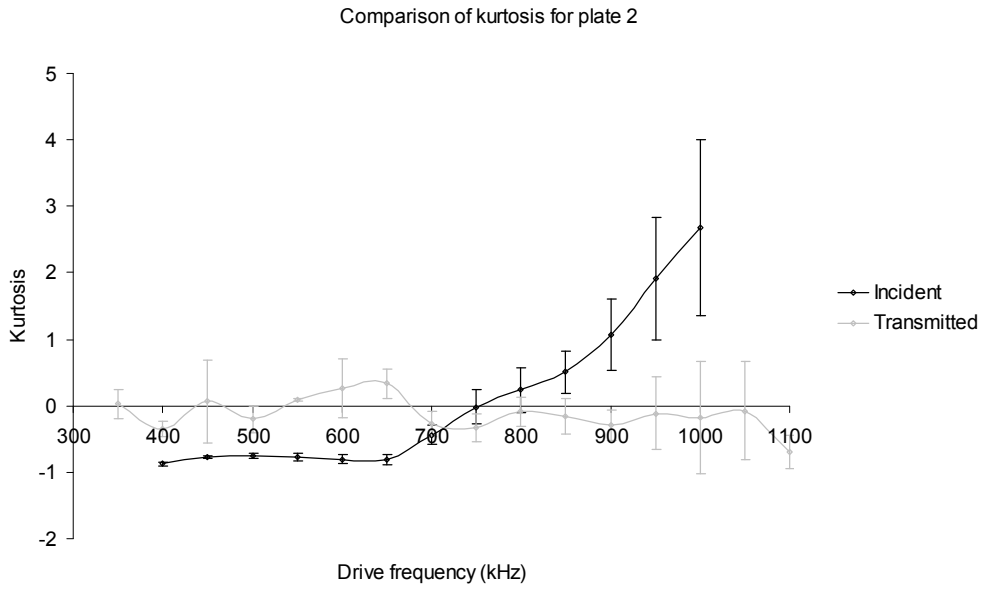

Fig. 6.21:Experimental comparison of kurtosis for plate 2

Figs. 6.18 – 6.21 all show a measurable increase in skew over a wide frequency range, which demonstrates that chaotic signals can be used to detect more complex resonances than the simple flat plate originally tested, allowing this technique to be used for 'real-life' detection.

6.4.2 A large-scale trial of chaotic pulses.

Once the use of chaotic signals had been shown to provide us with a means of detecting acoustic resonances, it was decided that the next step was to perform a large-scale trial. This trial was meant to provide a test of the detection method in a more 'real life' application. As this experiment was part of a larger trial performed at the test site, much of the experimental set-up was dictated by what was on site, and due to time constraints only a small amount of data was collected.

The experimental set-up.

The large-scale trial took place in Waterlip Quarry, Somerset (UK). This disused quarry is ~200m in diameter, with steep slopes and filled with ~12m water (Fig. 6.22). The experiment was performed from a floating laboratory in the centre of the quarry. Most of the electronic equipment and the transmitter and receiver were provided 'on-site' by Thales, the owners of the site.

Fig. 6.22. Aerial view of the Waterlip quarry, showing the steep slopes and the floating platform, put to the centre of the quarry during the experiments. ©GoogleEarth, 2007.

The transmitter used for the experiments was a flat panel array of transmitters provided by Thales. The array dimensions were ~1000mm x 800mm x >500mm. The transmitter had an approximately flat response (with some resonances) over the frequency range 80-180 kHz. The far field of the transducer was 10-20m. The receiver was a Brüel&Kjaer 8103 hydrophone. The target for these experiments was a –20dB hollow steel sphere, ~30cm in diameter.

The transmitter and receiver were both mounted at a depth of 6m beneath the surface of the water. The acoustic target was also set at a depth of ~6m. The positions of the transmitter, receiver and target are summarised in Fig. 6.23.

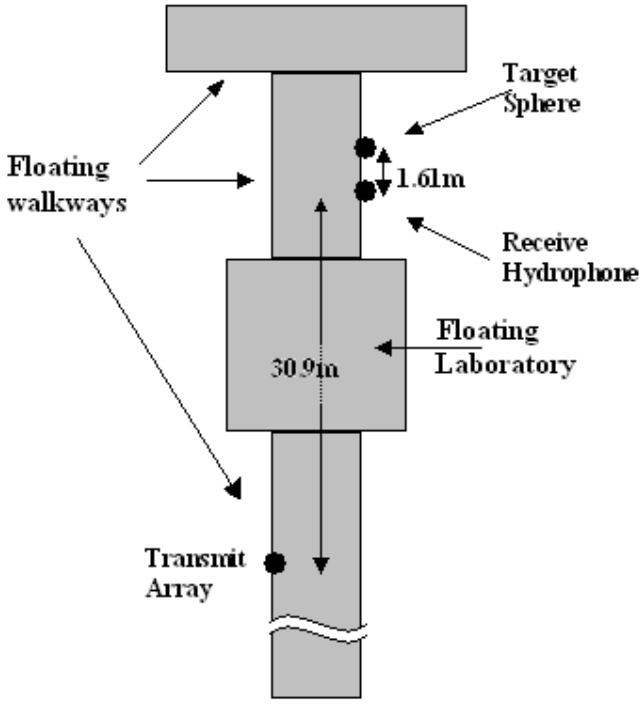

Fig. 6.23: The positioning of the transmitter/receiver/target. All are at ~6m depth.

The target was positioned using a heavy metal (tungsten) sinker. A rope was attached to a loop in the sinker, and was used to submerge the target to the desired depth. This is shown in Fig. 6.24.

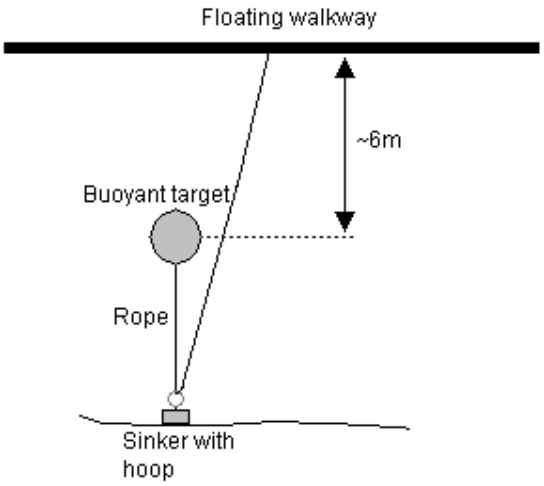

Fig. 6.24: The method of positioning the target.

Carrying out the experiment

The method for carrying out the experiment was the almost the same as that used for the experiments performed in a tank (section 6.2.1), but with the following changes made:

1) The frequency range of the experiment was lowered from ~400 kHz-1 MHz to 100-250 kHz. This was to fit within the resonant frequency range of the transmitter used for the trial.
2) The band-pass frequency range for the amplifier was set to 30-300 kHz.
3) The acoustic target was changed from a flat plate to a spherical target (10" diameter 1.5mm thick air filled stainless steel sphere).
4) The reflected signal, rather than the transmitted signal was used. This was partly to model a more realistic detection scenario (it is typically the reflected signal that is used for detection). This was also due to performing the experiment over longer ranges. At longer ranges, the beampattern will be wide

enough to diffract around the target, making separation of the transmitted signal from the diffracted direct signal difficult to achieve.

5) There was no time averaging of the signals. This was because the motion of the water surface, and the transmitter/receiver made averaging the signals impossible. Instead, the skew and kurtosis were measured for each individual signal, and the mean and standard deviation of these values were used.
6) The signal was captured simultaneously on 2 separate channels of the oscilloscope. This was because the attenuation of the reflected signal meant that a single channel could not adequately represent both the direct and the reflected signal. (Due to the digitisation of the signal).

A typical signal received by the oscilloscope is shown in Fig. 6.25.

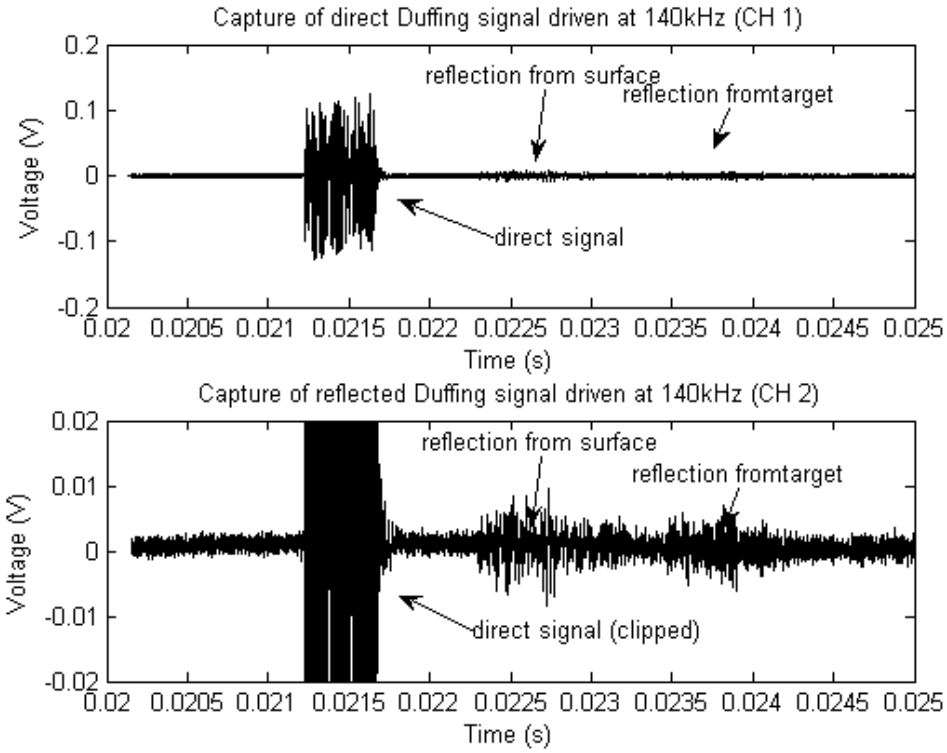

Fig. 6.25: Typical signal captured on channels 1 and 2 of oscilloscope. Note the 10:1 difference in voltage scales between the two channels.

In addition to measuring the skew and kurtosis of the direct signal and the signal reflected from the target, it was decided to also measure the skew and kurtosis from the signal reflected from the surface.

Duffing signals of drive frequencies 100 kHz to 240 kHz in steps of 20 kHz were used in the trial. The measurements for the skew of the signal over the 50 captures for the 100 kHz drive frequency are shown in Fig. 6.26.

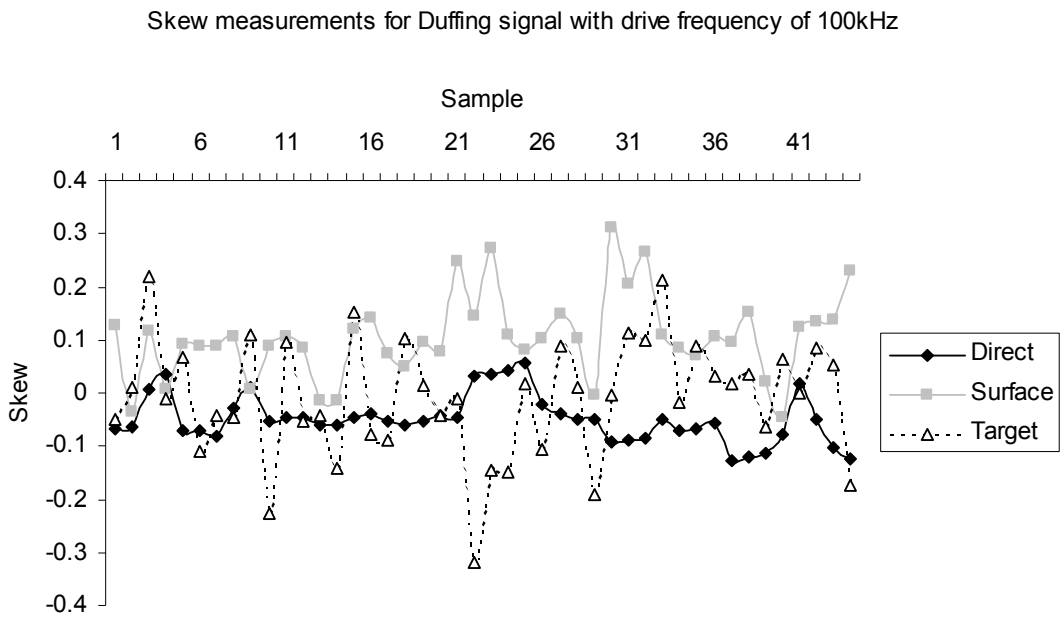

Fig. 6.26: Values of skew for sample of Duffing signal with 100 kHz drive frequency

Fig. 6.26 illustrates the amount of variation in the value of skew that occurred during the trial. Fig. 6.26 only contains 44 data points (50 captures were taken). This is because 6 samples were contaminated with high amplitude electrical noise (which sporadically appeared in the signal), and were removed from the analysis. Every dataset was examined, and any contaminated points were removed before the mean and standard deviation of the skew and kurtosis was calculated.

The results for skew are summarised in Fig 6.27, and kurtosis in 6.28. In addition to the experimental results, the exact Goodman and Stern form function of the sphere used is presented (Pers. Comms. P Atkins)

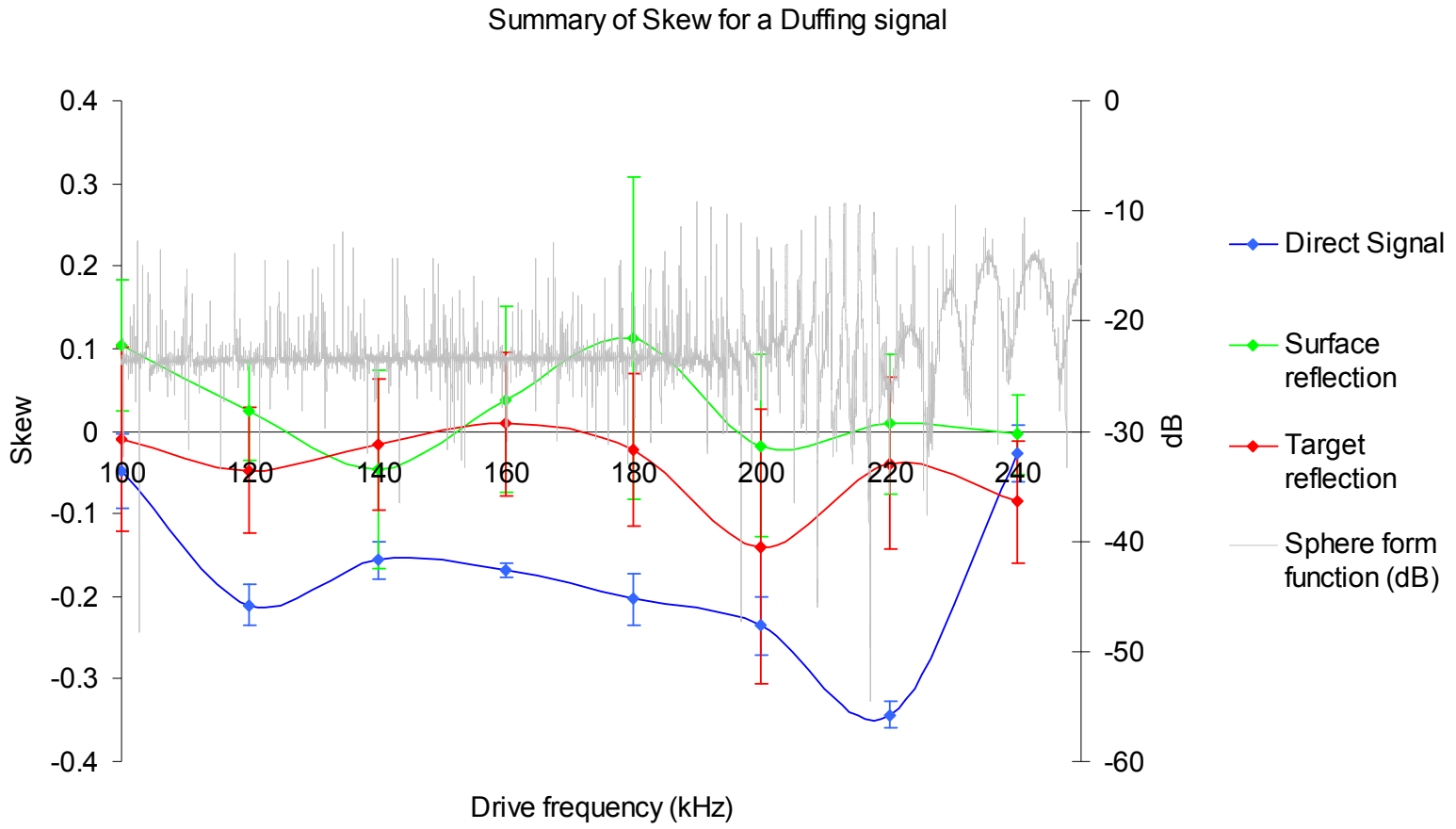

Fig. 6.27: Measured skew for Duffing signals with different drive frequencies.

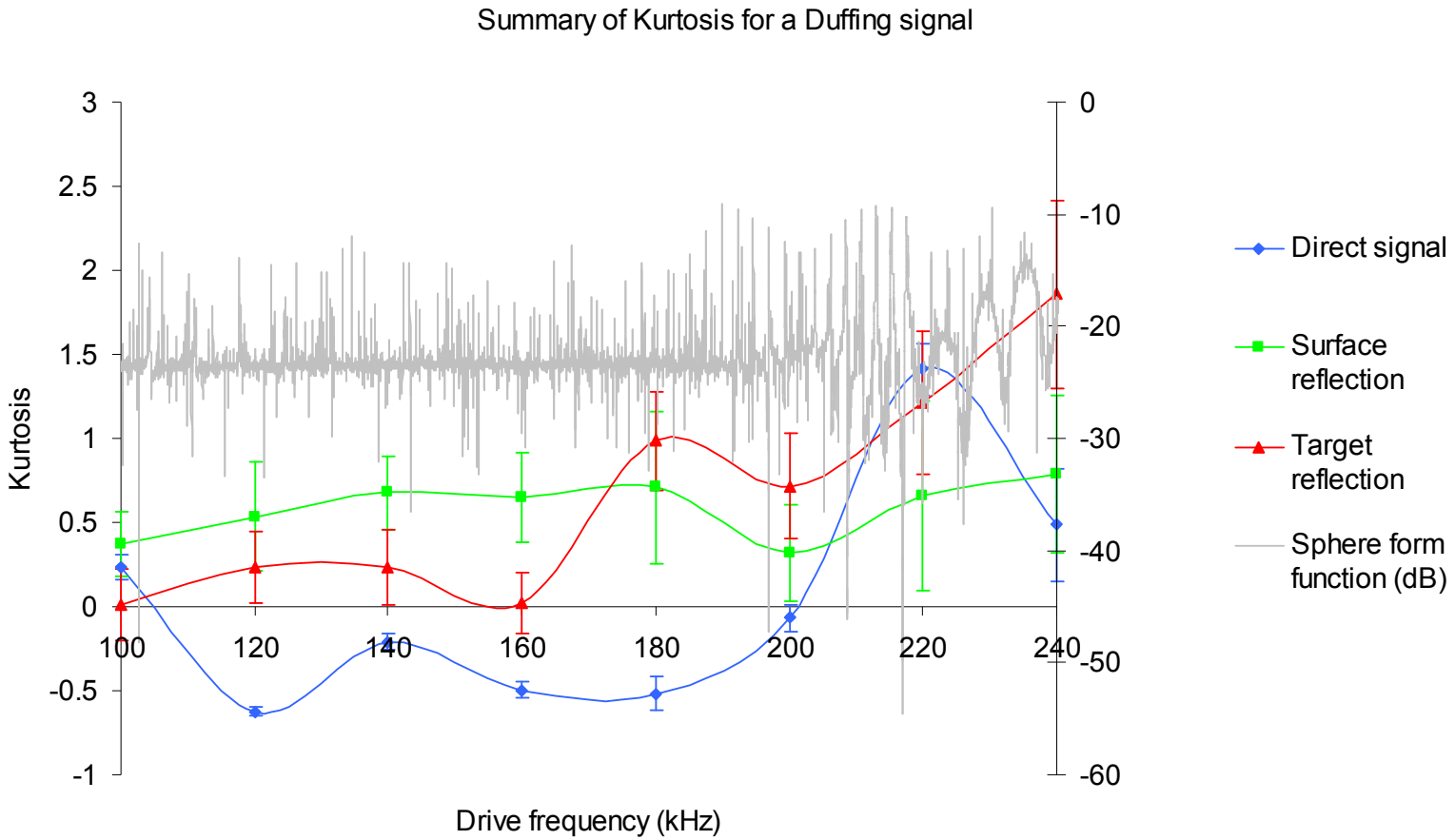

Fig. 6.28: Measured kurtosis for Duffing signals with different drive frequencies

Figs 6.27 and 6.28 again show that there is a range of frequencies over which there is a measurable increase in both skew and kurtosis (120-220 kHz for skew, and 120-180 kHz for kurtosis). However, we also find that there is increase in the skew and kurtosis of the signal that has been reflected from the surface of the water over the same frequency range. This is problematic; as both the target and the surface would appear to be resonant objects, resulting in a correct identification of our target, and an incorrect identification of the surface as a resonant object.

The increase in skew and kurtosis for the signal reflected off the surface is an unexpected result, but can be explained if we consider the reflection off the surface as the sum of several chaotic signals, each attenuated and delayed by a different amount. This is not an unreasonable assumption given that the surface was not completely flat, so there were several different paths (all of slightly different lengths) that the chaotic signal could take from the transmitter to the receiver via reflection from the surface. If we examine such a signal, we find that it also contains a significant increase in both the skew and kurtosis. The air-water interface is likely to change with the weather and surface currents: the frequencies at which skew and kurtosis increase will therefore change too. But the frequencies at which the skew and kurtosis increase will not change if they are associated to a resonant target, allowing definite identification.

A 10,000-point Duffing signal with 20 points per cycle was summed together with a delayed, attenuated copy of itself and the skew and kurtosis was calculated for attenuations of 0 to 1 in 0.1 steps, and delayed in steps of $1/100^{th}$ of the length of the signal (100 points). The results are summarised in Figs 6.29 and 6.30.

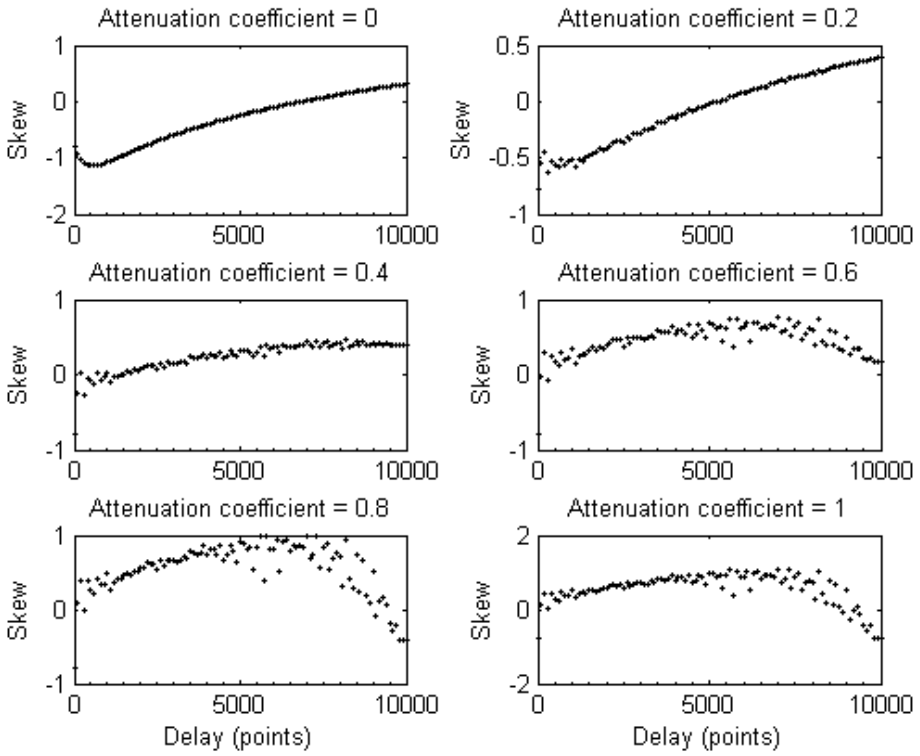

Fig. 6.29: Summary of skew for a signal plus a delayed attenuated copy.

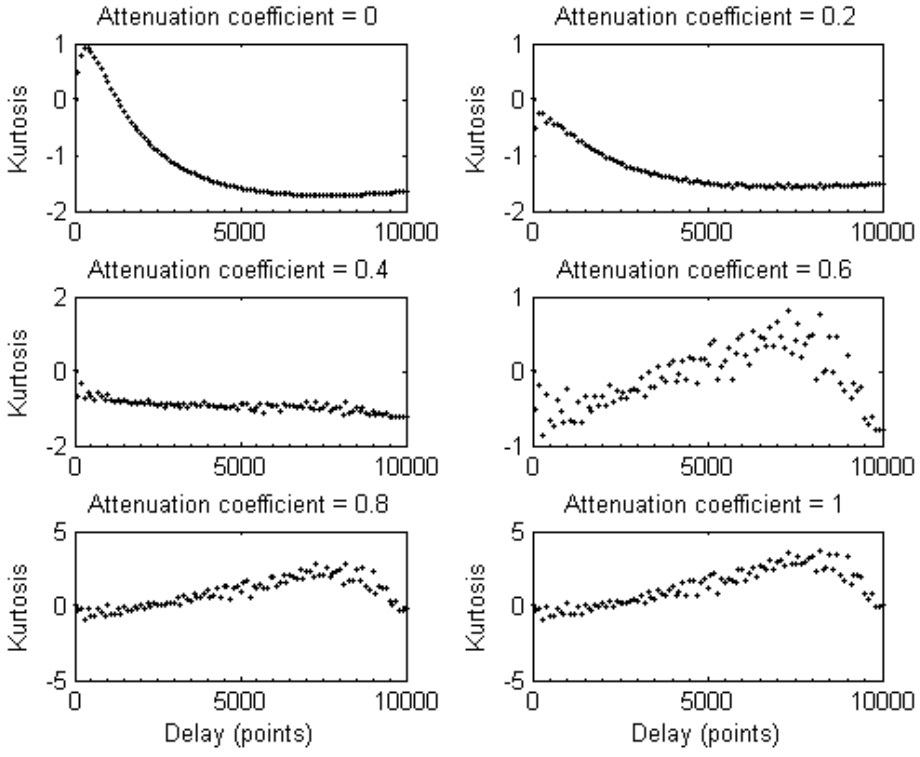

Fig. 6.30: Summary of kurtosis for a signal plus a delayed attenuated copy.

Figs. 6.29 and 6.30 show that there are a range of attenuations and delays for which a signal plus an attenuated and delayed signal will produce an increase in skew and kurtosis. This suggests that it is this feature of the chaotic signal that has caused the increase in skew and kurtosis for the signal that has reflected off the surface, and/or bottom, rather than an interaction with a resonance.

The fact that there is a mechanism other than direct interaction with an acoustic resonance that causes a measurable increase in the values of skew and kurtosis is problematic. This means that chaotic pulses can be used to suggest the presence of a resonant object within the area illuminated by the chaotic pulse, but not rule out some other effect (i.e. multiple reflections).

It may be possible to reduce the influence of surface reflections by:

Increasing the directionality of the pulse: through beamforming, or the use of directional arrays.

Frequency domain analysis: A chaotic signal interacting with a resonance may produce a distinctive frequency response that may allow us to identify a resonance.

Comparing the length of the returned pulse to the original: Multiple reflections will produce a pulse that is significantly longer than the transmitted pulse. It may be possible to differentiate between a surface reflection and a resonant object by the length of the returned pulse

Change the orientation of the set-up: The effect the surface waves have on the signal will be influenced by its orientation with respect to the signal. Changing their respective orientation should change values of skew and kurtosis. Therefore we may be able to differentiate between surface reflection (whose skew and kurtosis will vary with orientation), and a resonant object (whose skew and kurtosis should remain constant).

6.5 Experimental conclusions

These experiments have demonstrated several results. The first is that transmission of chaotic pulses through piezoelectric transducers is feasible, but it has also demonstrated that due to the presence of resonances inherent in the structure of the piezoelectric material, transmission of chaotic pulses will contain some bursting (Fig. 6.7). Appropriate selection of the drive frequency can act to reduce this bursting, and can also preserve the relative amplitudes of the two dominant peaks for a Duffing signal (Fig. 6.8).

These results also show that it is possible to detect an increase in bursting produced when these transmitted chaotic signals interact with an acoustic resonance. This effect has been demonstrated using a simple acoustic resonance provided by a flat plate, and has also been demonstrated using plates with non-linear resonances and a hollow steel sphere, which suggests that this is a general result.

6.6 Discussion

The presence of bursting on the signals transmitted by the transducer acted as a limiting factor on the capability of the detection method. Figs. 6.13 and 6.14 show that when the drive frequency was increased, both the skew and kurtosis of the output signal increased to the point where it became impossible to measure any change in these values due to interaction with resonances. It was also important that the peaks of f_d and $f_d/3$ had approximately the same power level, which also limited the drive frequencies that could be used. (If the drive frequency was either too high or too low, one of the two peaks would suffer a reduction in its power). It may be possible to reduce this effect by using a transducer with a flatter frequency response, or by pre-

correcting the chaotic signal by multiplying it by the inverse form function of the transducer to counteract the transducer's effect. (This was investigated, but the output power from a pre-corrected chaotic signal was too low to provide any measurable results.)

One avenue of further research would be to investigate whether pre-correcting and amplifying the signal applied to a transducer might provide a reduction in busting on the transmitted pulse, and might increase the bandwidth of drive frequencies over which this technique worked.

This research has focused on relatively simple resonances. As it has been demonstrated to be effective it could prove worthwhile to investigate more complex resonant objects such as pipelines, buoys, and naval mines (the main motivation behind this research).

Large-scale trial demonstrated that the technique worked over longer ranges, but also demonstrated that surface/bottom reflections produced similar changes in skew and kurtosis. As outlined previously, it may be possible to reduce these contributions by:

- Increasing the directionality of the pulse.
- Frequency domain analysis.
- Comparing the length of the returned pulse to the original.
- Checking the changes with different water surface conditions

All these methods provide avenues for further research, and should they prove successful, would open the possibility of direct comparison between the current methods used in mine hunting with the use of chaotic pulses.

Chapter 7

Thesis discussion and conclusions

7.1 Overview

The two strands of research presented in this thesis, namely acoustic time reversal and chaotic signals, have both led to significant results. The aim of the present chapter is to summarise the main conclusions of each type of research, already presented (Chapters 4 and 6 respectively), showing their complementarities and outlining some more general conclusions, as well as suggesting areas for further study.

7.2 Conclusions from Time reversal experiments

Several different measurements were taken (wave height, etc). Each of these measurements is discussed in turn, and finally the results as a whole are discussed.

7.2.1 Variations with wave height measurements

Experiments examining the wave heights produced by the wavemaker demonstrated that the simple wavemaker equation first discussed in §4.4 was not valid. The equation was assumed to be that shown in [23], given by:

$$\left(\frac{H}{S}\right)_{piston} = kh \tag{7.1}$$

Where H is the peak-to-peak wave height, S is the stroke length of the wavemaker, h is the height of the water column, and k is the wavenumber of the water wave.

The implication of [23] is that the relationship between wave height and frequency was linear. As this was not the case, a set of measurements characterising

the output wave heights for all wavemaker configurations were taken, and used in the subsequent experiments. These experiments demonstrated that the relationship between the frequency setting and wave height was not linear, as surmised, and that the wavemaker waves were more consistent with a standing wave pattern. This had several repercussions on the rest of the experiments, namely that:

1) The wave heights used in the other time reversal experiments I carried out were not sampled at regular intervals. Although this was desirable, it did not prove to be too important, as a wide range of wave heights were still investigated.
2) The standing wave pattern means that the experiments examining the effect of the angle of the incoming waves with respect to the direction of propagation are not examining pure plane waves. However, there still remained a directional component to the wave pattern, so the results remain of value.

7.2.2 Wave height conclusions

There is a general trend for the measured voltage level (i.e. amplitude) of a time reversed signal to decrease as the height of the surface waves increase, i.e. the voltage level is inversely proportional to the wave height. This is accompanied by an increase in the standard deviation of the voltages of each time reversed signal. This increase in the standard deviation shows that increasing wave height acts to increase the range of voltages that are received at the focus of the time reversed signal. Conversely, it can be said that decreasing the height of the surface waves will in general increase the received voltage of the time reversed signal, *irrespective of the conditions under which the original time reversal took place*.

In terms of the relative performance of the time reversed pulses over a range of wave heights, generally the time reversed signals remained within ~3-4dB of the

signal at its time reversed wave height, demonstrating that these time reversed signals are remarkably stable, even with surface waves ~ 5 times the wavelength of the pulse. According to [19], where a 3.5 kHz signal was used, scaling up these results would correspond to peak-to-peak wave heights of ~2m (i.e. Sea State 4, moderate, on the World Meteorological Organization scale).

7.2.3 Wave angle conclusions

The results of the wave angle experiments are in general agreement with the stroke length experiments, in that they show an inverse relationship between received voltage levels and wave heights. However, this inverse relationship appears to break down at wave angles approaching 90 degrees. Figs. 4.40-4.42 show that some of the time reversed signals *increase* in voltage level as the wave heights increase.

7.2.4 Overall conclusion of time reversal experiments

Even with significant surface wave heights (~5 times the wavelength of the pulse) the signal loss is not too high (~-3-4dB) (cf. Figures 4.20-23). This shows the remarkable robustness of the time reversal process in shallow-water waveguides with surface waves.

7.3 Conclusions of chaotic signal experiments

The chaotic signal experiments demonstrated several important results.

First, they have demonstrated the feasibility of transmitting chaotic pulses through piezoelectric transducers, which to the best of our knowledge had not been accomplished before.

Second, they have also demonstrated that due to the presence of resonances inherent in the structure of the piezoelectric material, transmission of chaotic pulses will contain some bursting (Fig. 6.7). Appropriate selection of the drive frequency can act to reduce this bursting, and can also preserve the relative amplitudes of the two dominant peaks for a Duffing signal (Fig. 6.8).

Third, these results also show that it is possible to detect an increase in bursting produced when these transmitted chaotic signals interact with an acoustic resonance.

Finally, several different resonant targets all demonstrated this behaviour, which suggests that these are general results. A more systematic study using a wide variety of targets is desirable, but time constraints prevented us from doing this during this thesis.

7.4 Overall conclusions

The experiments performed within this thesis have demonstrated the effectiveness of two separate, but complimentary areas of research. Both areas show much initial promise, and it remains a possibility that these two techniques could be used together (time reversal for focusing and chaotic signals for detection). This is discussed in Section 7.7.

7.5 Discussion of time reversal experiments.

7.5.1 Time reversal experimental apparatus.

The experimental set-up of the apparatus used a combination of 'off-the-shelf' components and a bespoke computer program to control the experiment. This introduced a time delay into the experimental technique, as signals were written to the arbitrary waveform generator. There was an approximately 3-5 minute delay between the transmission of the 3-cycle sine wave pulse, and the re-transmission of the time reversed samples captured by the TRM. This limited to steady state measurements at each selected wave height. Given the nature of the waves produced by the wavemaker in the water tank (standing waves), this should not be a significant problem.

7.5.2 Wave height measurements.

Due to the non-linear relationship between wave amplitudes and speed setting of the wavemaker, the sampling of wave heights for these experiments is also not linear, with more data points at lower amplitudes (especially >5mm) than at higher amplitudes. Therefore the behaviour of time reversed signals at low wave heights has been reasonably well measured, but at higher amplitudes, where the data is sparser, the behaviour is much less clear. This is discussed further in the next section.

7.5.3 Time reversal at different wave heights.

The results have presented several areas for discussion; these are outlined below:

General trend

The results indicate that there is, generally speaking, an inverse relationship between wave height and time reversed signal voltage. This implies that all time reversed signals improve as surface waves are reduced (and reduce as surface waves increase)*, regardless of the amount of surface waves present when the time reversal took place*. This result appears to go against one of the basic ideas of time reversal that changes in the environment after a signal has been time reversed will *reduce* the signal level. This relationship may be caused by an intrinsic property of time reversed pulses where the performance of any time reversed pulse is degraded with wave motion, regardless of the circumstances in which it was time reversed. If this is the case, then it implies there will be little to no advantage in time reversing in specific wave amplitudes, as any pulse time reversed in the same channel should have comparable performance.

Relative performance of time reversed pulses

Another area that has provided some unexpected results is in the relative performances of different signals. We would expect that the best possible signal for any particular wave height would be produced by time reversing a test pulse at that wave height (including no surface waves). What the results have shown is that in some cases, (e.g. Fig. 4.16) pulses time reversed in the tank in the presence of surface waves have a higher signal voltage when the surface waves are removed than a signal time reversed in the tank when no surface waves are present.

One possibility for this disparity could be in the method used for time reversing and then re-transmitting. In the process of writing the time reversed pulses to the arbitrary waveform generator, the pulses were all scaled to the maximum output the arbitrary waveform generator could produce. If a pulse is relatively 'flat', in that the voltage received from the direct transmission and its reflections have approximately the same value, then it will have more energy than a pulse that has a higher peak from the direct transmission and lower scattered voltage levels. This may go some way to explaining the increase in voltage levels for some pulses. (A preliminary examination of several pulses does not demonstrate much difference in the relative levels of the direct transmission and first reflections of several pulses, so it seems unlikely that this is the sole cause for this result).

Another possibility could be that those pulses time reversed with high amplitude surface waves will have a much reduced range of scattered returns, so it is possible that the time reversal process has acted in some way to focus more energy along the direct transmission and bottom scatter (as those should remain relatively constant), meaning that less energy will be lost through attenuation than a signal that is using multiple reflections (which have a longer distance to travel). Although, as with the general trend, this would appear to go against what we understand about time reversed pulses in that we would expect a signal time reversed with no surface waves to be composed of the direct path, the bottom reflection (like those time reversed with surface waves) *plus* multiply scattered rays, this should still produce a higher amplitude. Further experimentation is required to determine the cause of this.

Scarcity of data points at high surface wave amplitudes

Due to the non-linear nature of the relationship between the wavemaker's speed setting and the amplitude of the surface waves produced, most of the samples were taken at low surface wave amplitudes, with only a few at higher amplitudes. This means that much of the trends observed in these results are reliant on very few data points (often just a single point in a dataset), which increases the risk of error. Clearly there is a need for more experimentation to collect more points at surface wave amplitudes, from 15mm peak-to-peak to 70mm peak-to-peak, to determine the true behaviour of time reversed signals.

Possible periodicity of amplitudes

The results for the wavemaker set to a 60mm strokelength (Fig. 4.16) show an unexpected increase in amplitudes across all time reversed pulses at ~33-38mm surface wave peak-to-peak amplitude. This is not replicated in the other results, but given the lack of data points, it remains a possibility that there is a certain amount of periodicity in the relationship between time reversed signals and surface wave amplitude. Further experiments with a closer spacing between sample surface wave amplitudes would show if this periodicity exists as a general result for all signals, or if it is something specific to the set-up for the 60mm stroke length experiment.

Wave angle results

The results for the angle of wave propagation with respect to the direction of direct transmission showed an unexpected result. When the direction of propagation is approximately perpendicular to the direction of surface wave propagation, time reversed signals *increase* with increasing wave amplitudes.

These results appear contrary not only to logical expectations, but also to all the other results. The implication, if these results are true, would be that in some cases time reversed pulses perform better in changing environments. This is opposed to a basic assumption of time reversal, that there is no change in the environment over the time taken to perform the time reversal (the time taken for the test pulse to propagate, be received, time reversed, retransmitted, and re-received at its origin).

As it is inferred from a single occurrence, this is unlikely to be the general trend. Further, closer sampling of surface wave amplitudes is needed. It is possible that these high voltage responses could be peaks in the periodic relationship suggested from the results in Fig. 4.16.

These wave angle experiments did differ from the previous experiments in that as the rig was rotated, the curvature of the bottom of the tank changed with respect to the rig due to the bottom sagging under the weight of the water. It is possible that this change in the curvature of the tank could account for the measured increase in signal voltages as the wave angle approached 90 degrees.

Overall synthesis

The experiments looking at the time reversed pulses have, in addition to demonstrating the general robustness of the time reversal process in the presence of surface waves, produced some unexpected trends. The implication that there are cases

when a time-varying environment will increase the performance of a time reversed pulse, and that the optimum time reversed pulse for a particular environment may not be the time reversal *in that environment* both go counter to expectation. If these results are verified by a more in depth study, then this would mean that our current understanding of the time reversal process is incomplete.

7.6 Discussion of chaotic signals experiments.

The presence of bursting in the signals transmitted acted as a limiting factor on the capability of the detection method. Figs. 6.13 and 6.14 show that when the drive frequency of the Duffing oscillator (f_d) as increased, both the skew and kurtosis of the output signal increased to the point where it became impossible to measure any change in these values due to interaction with resonances.

It was important that the peaks of f_d and $f_d/3$ had approximately the same power level, which also limited the drive frequencies that could be used. (If the drive frequency was either too high or too low, one of the two peaks would suffer a reduction in its power). It may be possible to reduce this effect by using a transducer with a flatter frequency response, or by pre-correcting the chaotic signal by multiplying it by the inverse form function of the transducer to counteract the transducer's effect. (This was investigated, but, without a power amplifier, the output from a pre-corrected chaotic signal was too low to provide any measurable results.)

One avenue of further research would be to investigate whether pre-correcting and amplifying the signal applied to a transducer might provide a reduction in bursting on the transmitted pulse, and might increase the bandwidth of drive frequencies over which this technique worked.

The present research has focused on relatively simple resonances. As it has been demonstrated to be effective, it could prove worthwhile to investigate more complex resonant objects such as pipelines, marine waste, and (the main reason for this research) naval mines such as SLMM (Submarine-Launched Mobile Mines) and modified torpedoes.

The large-scale Waterlip trial demonstrated that the technique worked over longer ranges, but also demonstrated that surface/bottom reflections also produced similar changes in skew and kurtosis. As outlined previously, it may be possible to reduce these contributions by

- Increasing the directionality of the pulse.
- Frequency domain analysis and ad hoc filtering.
- Comparing the length of the returned pulse to the original.
- Checking the changes with varying sea conditions/

All these methods provide avenues for further research, and should they prove successful would open the possibility of direct comparison between the current methods used in mine hunting and the use of chaotic pulses for detection.

7.7 Using time reversal and chaotic signals in unison.

As mentioned previously, these two areas of research are complimentary, and so it is possible to use both techniques simultaneously. Here, we would use the time reversal technique as a method of focusing energy on any scatterers within the region of interest, and use a chaotic pulse rather than a sinusoidal pulse to stimulate these objects.

Focusing on scatterers could be achieved using either iterative time reversal or the DORT method. Use of iterative time reversal would be easier to achieve, but would only focus on the most reflective scatterer within the region of interest. It may

prove possible to identify this object and remove it. The process could then be repeated, now focusing on the next most reflective object. Should the most reflective object prove to be immobile, such as a pipeline, then iterative time reversal will fail to detect any more objects.

The DORT method would allow us to focus on all reflective objects with the region of interest, but would prove more difficult to achieve, requiring more test pulses (all while the transmitter remains stationary), more time to perform, and require more computational power. The advantage of DORT is that, once performed, it would allow us to direct energy at any of the scattering objects within the area, and its solution would provide an estimate of the amount of objects within the region. (cf. section 2.2.5)

Using a chaotic pulse would allow to one [the system] to differentiate non-resonant from resonant objects (the resonant objects being more likely to be a mine or mine-like object). Transmitting a chaotic pulse could be achieved in one of two ways:

1) Transmission of a chaotic test pulse

   This would be the easiest to achieve, as the time reversal process would be the same as for a sinusoidal test pulse. The problem with this method is that the pulse would have to be very short, so the likelihood of producing a measurable increase in bursting in a resonant object would be low

2) Use of linear superposition to create the chaotic pulse.

   We could achieve this by linear superposition of the time reversal of a single sinusoidal pulse. This would prove computationally intensive to perform ‘on the fly’. One potential problem with this technique is there

is some degree of distortion in the time reversed signals potentially reducing its ability to refocus on the target.

7.8 Potential areas of future research

The exploratory and novel work carried out in this thesis has presented us with several avenues of further research, discussed below:

7.8.1 Time reversal experiments

The data shown here contained relatively few samples of time reversal with relatively high surface wave amplitudes. This meant that the performance at these higher wave amplitudes is less well defined. In addition, several data sets (those for the wavemaker set to a 60mm stroke length) hint at there being a certain amount of periodicity in the amplitude of the time reversed signal. Both of these issues could be resolved if we were to repeat/replicate these experiments with a much closer sampling of high amplitude surface waves.

The current results have suggested that in some environments it is not always best to use the signal that has been time reversed in that environment (in a situation with high amplitude surface waves, a signal time reversed with a smaller surface wave may perform better). This may be a genuine result, or a consequence of the re-scaling of the amplitude of the time reversed signals.

Further experimentation could be done to examine this by choosing a different method of rescaling the time reversed pulses. One method could be simply re-transmitting the time reversed pulses at the amplitudes that they were received, however given the loss in signal levels, some form of amplification would be

preferable. Amplifying the amplitudes of all the time reversed signals with the same gain (say a factor of 10) would preserve the relative amplitudes.

The experiments examining the effect of direction of surface waves were performed by rotating the array relative to the wavemaker (and also the tank). As the bottom of the tank was very slightly curved, this meant the environment of the time reversal was also changing as the array was rotated. Therefore we are changing another aspect of the environment in addition to the surface wave properties. The exact effect this change in curvature of the bottom had on these experiments is not known. It would be very useful to repeat these experiments using a tank with a flatter bottom, or using a set-up that allows the wavemaker to be rotated relative to the array rather than the opposite. (This was not possible in my experiments, as it had to be clamped to the side of the tank). This will allow us to validate/invalidate the relationship shown in my experiments.

Finally, all the experiments I performed were done at a single water depth (because of the shallowness of the tank), it would be valuable to perform these experiments at different wave depths to see what effect that might have on the results.

7.8.2 Chaotic signal experiments

One of the findings of the chaotic signal experiments was the importance of a wideband transducer to transmit the chaotic signals. Although the transducer used was fairly wideband (Q~1), it was still found to be sufficiently resonant to produce bursting in any signals transmitted through it. It would improve detection of resonances if the presence of bursting on the transmitted signal could be reduced as much as possible. Transmitting a pre-corrected signal (one which has been multiplied by the inverse form function of the transducer) with a sufficient power could provide

a solution to this. This method may also increase the frequency range over which a chaotic signal may be transmitted using a particular transducer. Experiments examining this could prove to be very useful.

This research showed the first experiments looking at the use of chaotic signals in this way; the resonant objects used were therefore kept simple. Now that a detection method has been designed and implemented, it would prove very useful to repeat these experiments using more complex resonant objects (e.g. cylinders, multi-layered materials) to see if the method remains valid. Given that the desired application for this research was mine hunting, it would prove invaluable to investigate the interaction between chaotic pulses and naval mines.

The large-scale trial using chaotic pulses demonstrated that surface/bottom scattering also produced an increase in skew and kurtosis, thus producing false positives. There are potentially several ways of reducing the influence of surface/bottom scatter.

1) Increasing the directionality of the pulse.

   Using beamforming or directional arrays will reduce the amount of energy being reflected off the surface/bottom, and so reduce their influence.

   Using time reversal as a method of focusing the signal should eliminate the influence of surface/bottom scatter as they are incorporated into the signal.

2) Frequency domain analysis.

   When a resonant object interacts with a chaotic signal, the resonance is excited, and so the frequency spectrum of the transmitted/reflected signal will contain new peak(s) in its spectrum at the object's resonant frequency(s). Reflections from the surface and bottom are not resonant,

and so should not contain any new peaks, allowing us to differentiate between the two.

3) Comparing the length of the returned pulse to the original.

   A signal that has been transmitted through/reflected off a resonant object will have the same signal length as the incident signal. Signals scattered off the surface/bottom produce an increase in skew and kurtosis when two or more signals with different time delays are superimposed. Therefore these signals will have a longer duration than the original signal, and so allow us to differentiate between them and any signals coming from resonant objects.

All these methods provide avenues for further research, and should they prove successful would open the possibility of direct comparison between the current methods used in mine hunting with the use of chaotic pulses

7.8.3 Combining Time reversal techniques with chaotic signals

Given its ability to focus on reflective objects, time reversal would be ideal as a method of focusing a chaotic signal so that it eliminated the influence of surface/bottom scatter. Further experiments could examine the feasibility of producing a time reversed chaotic signal. Many applications can be envisaged beyond the original motivation of this work. Detecting, and, more importantly, identifying buried waste in the seabed has long proved a complex problem (e.g. [37]). The combination of chaotic signals with time reversal would allow distinguishing pristine waste (e.g. fluid-filled drums) from decaying waste containers (leaking their contents, i.e. with different resonances) and harmless objects, speeding up the prioritisation of clean-up or containment operations. Similarly, underwater archaeology is making an

increasing use of underwater acoustic techniques [38], with the similar problem of identifying targets of interest, in often complex environments. Finally, the emerging field of habitat mapping is now moving away from traditional (and often limited) sonar mapping techniques to incorporate innovative acoustic instruments [39]. Coupled with the noise-like characteristics of chaotic signals, the combination of the two techniques presented here can make an environment-friendly study of multifaceted, and often fragile, environments. As acoustic time reversal moves away from the laboratory to the field, it can now be combined with specific approaches like chaotic signals to be applied to a wide variety of fields and challenges.

References

1 M Fink.1992 Time reversal of ultrasonic fields-part 1: Basic principles. IEEE Transactions on ultrasonics, ferroelectrics and frequency control. Vol. 39, NO.5, 555-66

2 Underwater Acoustics: An Introduction, X. Lurton, Springer-Praxis Books 2002

3 H. Medwin and C.S. Clay. Fundamentals of Acoustical Oceanography 1998 Academic Press, London.

4 P M Morse and K U Ingard Theoretical acoustics New York: McGraw-Hill 1968

5 Cassereau D and Fink M. 1992 Time reversal of ultrasonic fields-part 3: Theory of the Closed Time Reversal Cavity. IEEE Transactions on ultrasonics, ferroelectrics and frequency control. Vol. 39, NO.5, 579-92

6 Draeger C, Aime J-C and Fink M. 1999 One channel time reversal in chaotic cavities: Experimental results J. Acoust. Soc. Am. 105 611-7

7 Derode A, Roux P and Fink M. 1995 Robust acoustic time reversal with high order multiple scattering. Phys. Rev. Lett. 4206-9

8 Fink M, Cassereau D, Derode A, Prada C, Roux P, Tanter M, Thomas J-L and Wu F. 2000 Time reversed acoustics Rep. Prog. Phys. 63. 1933-1995

9 Roux P, Roman B, and Fink M, 1997 Time reversal in an ultrasonic waveguide Appl. Phys. Lett. 70 1811-3

10 Wu F, Thomas J-L, and Fink M. Time reversal of ultrasonic fields-part 2: Experimental results IEEE Transactions on ultrasonics, ferroelectrics and frequency control. Vol. 39 No 5, September 1992 567-92

11 Prada C, Maenneville S, Spolainsly D and Fink M 1996 Decomposition of the time reversal operator: Detection and selective focusing on two scatterers J. Acoust. Soc. Am. 99 2067-6

12 Chambers D and Gautesen A 2001 Time reversal for a single spherical scatterer J. Acoust. Soc. Am.109 2616-24

13 P Roux, M Fink 2000 Time reversal in a waveguide: Study of the temporal and spatial focusing J. Acoust. Soc. Am. 107 2418-29

14 Mordant N, Prada C and Fink M 199 Highly resolved detection and selective focusing in a waveguide using the D.O.R.T. method J. Acoust. Soc. Am. 105 2634-42

15 Cunningham K, Hamilton F, Brysev A and Krutyansky L. Time reversed sound beams of finite amplitude 2001 J. Acoust. Soc. Am. 109 2668-74

16 Parvelescu 1995 Matched-signal (PESSS) processing in the ocean J. Acoust. Soc. Am. 98 943-60

17 Parvelescu A and Clay C S 1965 Reproductibility of signal transmission in the ocean Radio Elect. Eng. 29 233

18 Song H, Kuperman W, Hodgkiss W, Akal T and Ferla C 199 Iterative time reversal in the ocean J. Acoust. Soc. Am. 105 3176-84

19 Hodgkiss W, Song H, Kuperman W, Akal T, Ferla C, Jackson D. 1999 A long-range and variable focus phase-conjugation experiment in shallow water J. Acoust. Soc. Am. 105 1597-604

20 Song *H,* Kuperman W and Hodgkiss W 1998 A time reversal mirror with variable range focusing J. Acoust. Soc. Am. 103 3234-40

21 Edelmann G, Akal T, Hodgkiss W, Kim S, Kuperman W and Song H. 2002 An initial demonstration of underwater acoustic communication using time reversal J. Acoust. Soc. Am. Vol.27 No.3 602-9

22 Dungan M and Dowling D 2000 Computational narrowband time-reversing array retrofocusing in a dynamic shallow ocean J. Acoust. Soc. Am. 107 3101-11
23 R Dean, R Dalrymple "Water wave mechanics for engineers and scientists" World Scientific, 1990
24 http://en.wikipedia.org/wiki/Naval_mine Accessed on 30/08/06
25 http://www.royal-navy.mod.uk/server/show/nav.1952 Accessed on 30/08/06.
26 http://www.exwar.org/Htm/ConceptDocs/Navy_USMC/MWP4thEd/appendix_a.htm Accessed on 30/08/06.
27 http://www.royal-navy.mod.uk/server/show/nav.1954 Accessed on 30/08/06.
28 http://www1.eguermin.org/training/nms.asp Accessed on 30/08/06
29 http://www.fas.org/man/dod-101/sys/ship/weaps/mine_sweep.htm Accessed on 30/08/06
30 http://www1.eguermin.org/training/nmh.asp Accessed on 30/08/06
31 A.J. Fenwick, J E Adamson and V F Humphrey. 2004. Conference papers on bursting in target echoes. Internal QinetiQ report. QinetiQ/FST/TR040954
32 J. C. Sprott. 2003. Chaos and time-series analysis. Oxford university press. ISBN 0-19-850840-9
33 Y Tyapkin and B Ursin. J. Geophys. Eng. 2 177-187 doi:10.1088/1742-2132/2/3/001. 2005
34 L.E. Kinsler, A. R Frey, A. B. Coppens and J. V. Sanders.. Fundamentals of acoustics 4th Ed. 2000. John Wiley and Sons. ISBN 0-471-84789-5
35 http://davidmlane.com/hyperstat/A69786.html Accessed on 30/08/06
36 http://davidmlane.com/hyperstat/A53638.html Accessed on 30/08/06
37 Ph. Blondel and A. Caiti (eds.); Buried Waste in the Seabed Acoustic imaging and Biotoxicity (Results from the European SITAR Project) Springer-Praxis, 202pp. ISBN 3-540-28120-7, 2007
38 T. Akal R.D. Ballard, GF Bass (eds.). Proc. First Internal Congress on the Application of Recent Advances in Underwater Detection and Survey Techniques to Underwater Archaeology. May 2004. ISBN 0-970794-2-4
39 A.J. Kenny, I Cato, M Desprez, G Fader, R.T.E. Schuttenhelm, J Side. Overview of seabed-mapping technologies in the context of marine habitat classification. ICES J. Mar. Sci. 60, No 2 (2003) 411-418

Appendix 1:

Number of reflections present in the signal.

The preliminary experiment (section 4.2.1) examining the number of reflections present was taken with a slight difference to the final configuration (section 4.3) and is summarised below:

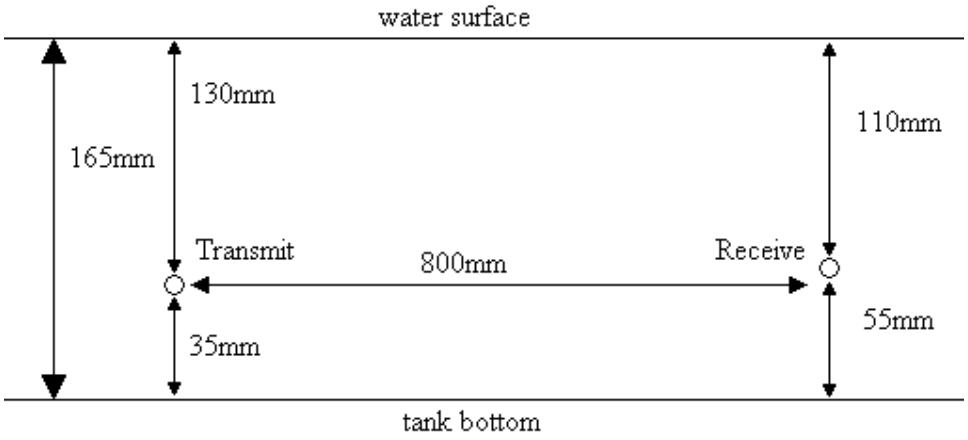

Fig. A.1: Positioning of transducers for preliminary experiment (side view).

When calculating the time taken travelling from the transmitter to receiver, we must know the distance the pulse has travelled. This can be calculated using Pythagoras theorem.

All pulses will travel the same horizontal distance (800mm), the only difference in path length will be due to the vertical distance traversed as the pulse undergoes any reflections off the tank bottom and/or surface.

Note that after the first reflection from either the bottom or surface, the additional distance travelled will be either 110mm (an additional bounce off the bottom) or an additional 220mm (an additional bounce off the top).

These distances are shown in tables A1 and A2. The time taken is calculated using a water sound velocity of 1500 m/s (consistent with the equations of Kinsler and

Frey (2000) assuming a water temperature of 25^{o}C and with our own experimental measurements)

Number of reflections	Horizontal distance (mm)	Vertical distance (mm)	Distance travelled (mm)	Time taken (ms)
0 (Direct path)	800	20	800.25	0.5335
1	800	130	810.4937	0.540329
2	800	350	873.2125	0.582142
3	800	460	922.8218	0.615215
4	800	680	1049.952	0.699968
5	800	790	1124.322	0.749548
6	800	1010	1288.449	0.858966
7	800	1120	1376.372	0.917581
8	800	1340	1560.641	1.040427
9	800	1450	1656.05	1.104033
10	800	1670	1851.729	1.234486

Table A.1. Calculated arrival times for a signal reflecting multiple times, reflecting off the bottom first.

Number of reflections	Horizontal distance (mm)	Vertical distance (mm)	Distance travelled (mm)	Time taken(ms)
0 (Direct path)	800	20	800.25	0.5335
1	800	240	835.2245	0.556816
2	800	350	873.2125	0.582142
3	800	570	982.2932	0.654862
4	800	680	1049.952	0.699968
5	800	900	1204.159	0.802773
6	800	1010	1288.449	0.858966
7	800	1230	1467.276	0.978184
8	800	1340	1560.641	1.040427
9	800	1560	1753.169	1.168779
10	800	1670	1851.729	1.234486

*Table A.2. Calculate*d *arrival times for a signal reflecting multiple times, reflecting off the top first.*

Measurements of arrival times from the walls of the tank indicated that reflections off the walls of the tank arrived at ~1.1 – 1.8ms, which meant that the time window was limited to ~1.0ms. Examining tables A1 and A2, we see that in this time we can have up to a total of 8 (or possibly 9) reflections off the tank bottom and water surface. This means that the time reversed pulse will benefit from the summation of multiple images, and so will have the characteristics of signals in a waveguide, which these experiments are designed to simulate.

Appendix 2:

Individual plots of time reversal experiments.

List of plots:

Tables 1 and 2 outline the different settings used for each individual run of the time reversal experiments. Table B1 covers the variation in stroke length experiments, and Table B2 the variation of wave angle. Note that the wavemaker speed settings are expressed in the form set on the wavemaker. To convert these into Hertz, one uses the formula

$$F = 0.0287 * \text{speed setting (Hz)} \qquad \text{(A.2.1)}$$

The speed setting shown is the speed setting at which the original pulse was time reversed.

	Speed settings (arbitrary units)					
Stroke length (mm)	**0**	**10**	**20**	**30**	**40**	**50**
60	1	2	3 (corrupt*)	4	5	6
80	7	8	9	10	11	
100	12	13	14	15		
120	16	19	17	18		

Table B1: List of runs for stroke length time reversal experiments. Note that runs 17-19 are out of sequence

* The disk that this dataset was stored on was corrupted before the data was analysed, therefore the data could not be recovered to be used in the analysis.

.

	Speed setting (arbitrary units)				
Angle (degrees)	**0**	**10**	**20**	**30**	**40**
10	20	21	22	23	24
20	25	26	27	28	29
30	30	31	32	33	34
40	35	36	37	38	39
50	40	41	42	43	44
60	45	46	47	48	49
70	50	51	52	53	54
80	55	56	57	58	59
90	60	61	62	63	64

Table B2: List of runs for wave angle time reversal experiments.

The points on the graphs represent the average measured amplitudes (V) of the time reversed pulses, and the error bars indicate the standard deviation of the measured voltages.

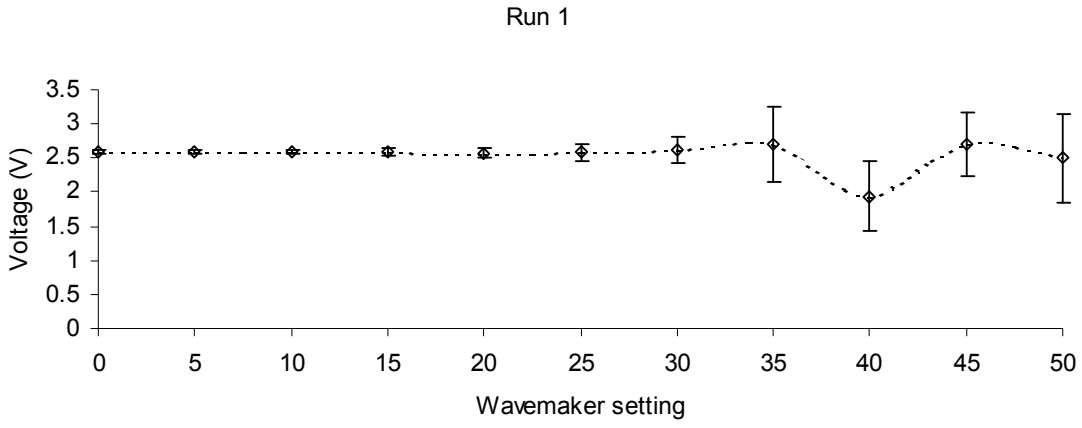

Fig. B.1: Plot of average amplitude of time reversed pulses from run 1

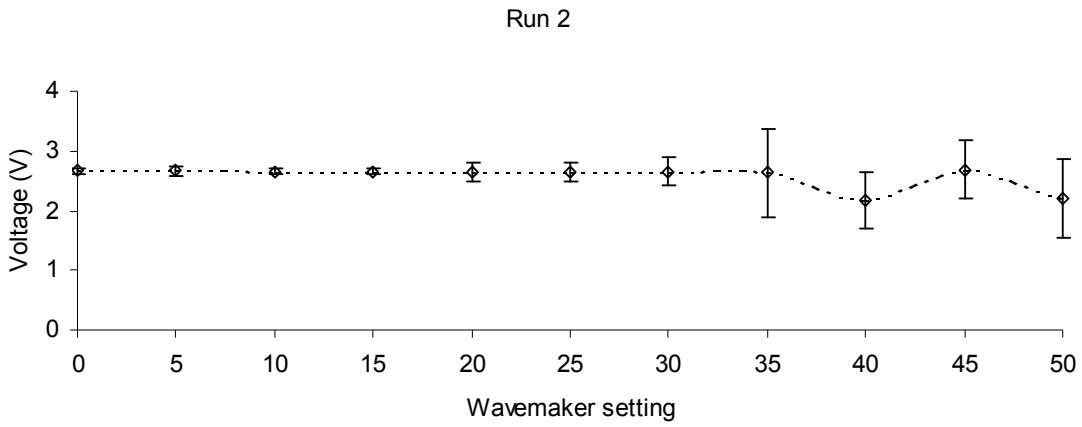

Fig. B.2 Plot of average amplitude of time reversed pulses from run 2

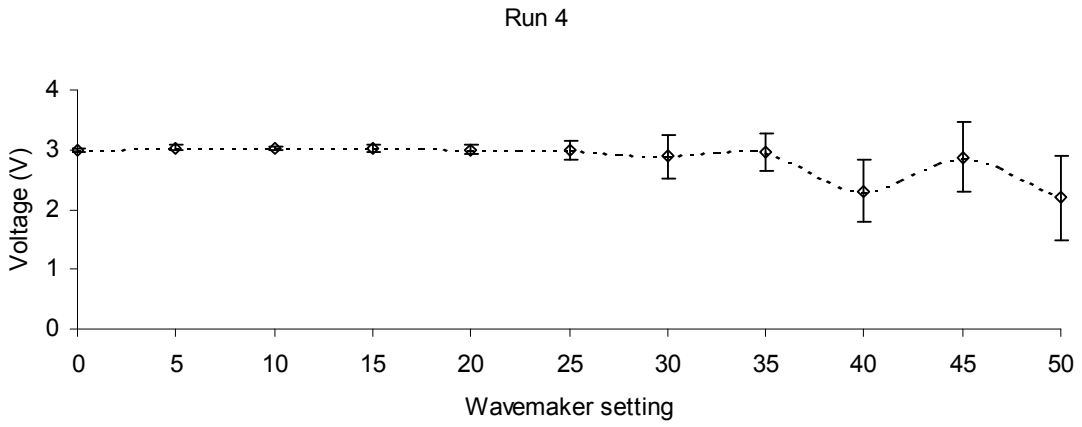

Fig. B.3: Plot of average amplitude of time reversed pulses from run 4

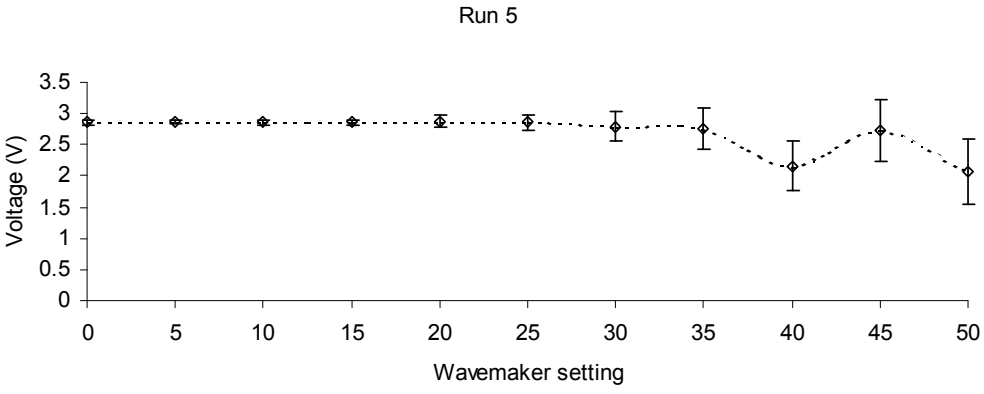

Fig. B.4: Plot of average amplitude of time reversed pulses from run 5.

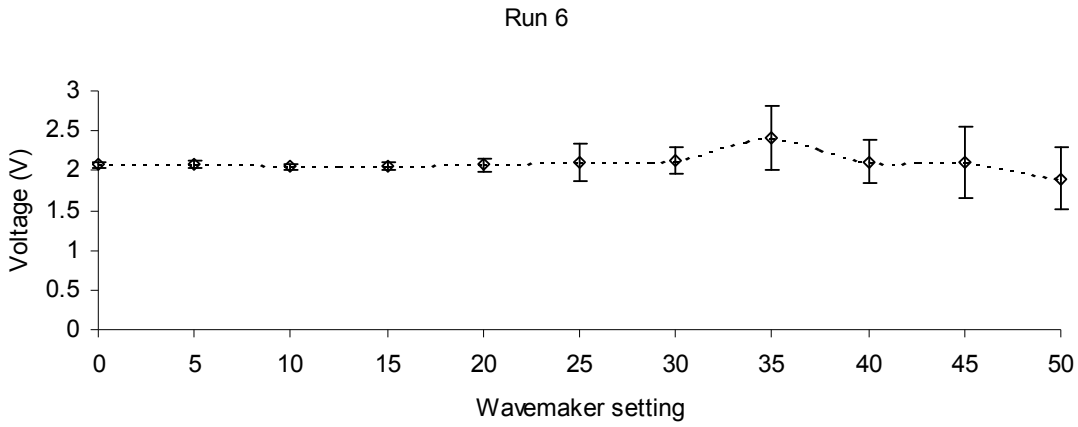

Fig. B.5: Plot of average amplitude of time reversed pulses from run 6.

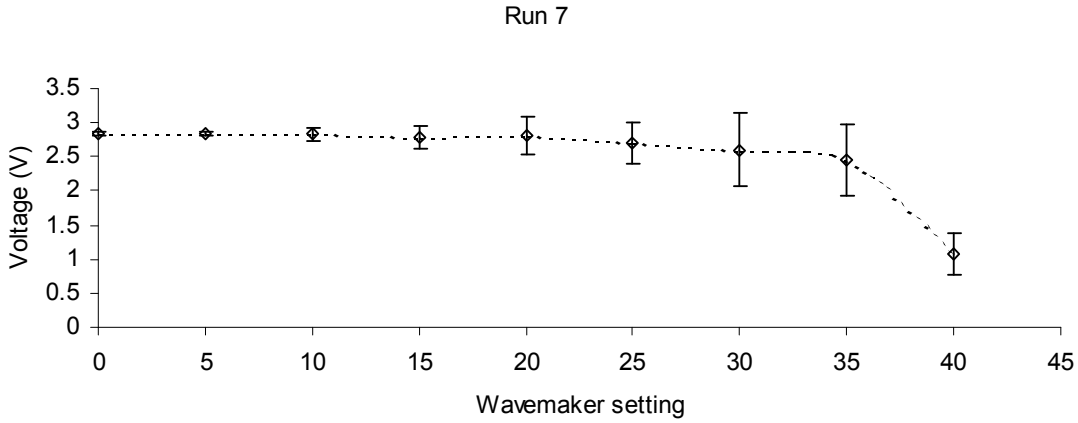

Fig. B.6: Plot of average amplitude of time reversed pulses from run 7

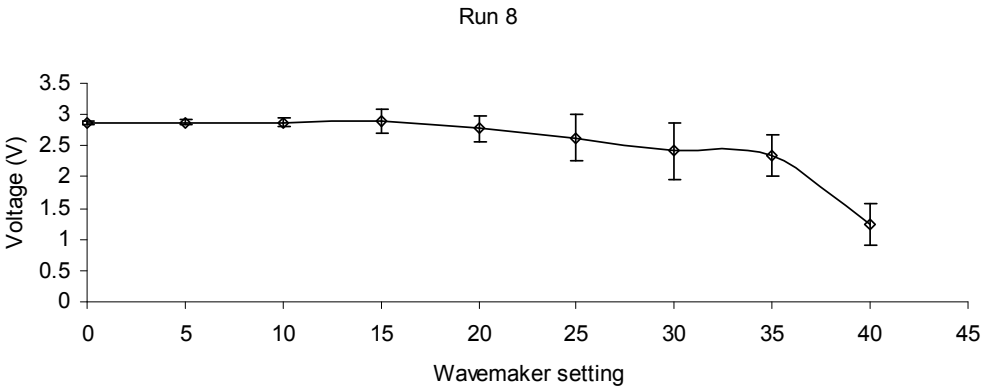

Fig.B.7: Plot of average amplitude of time reversed pulses from run 8.

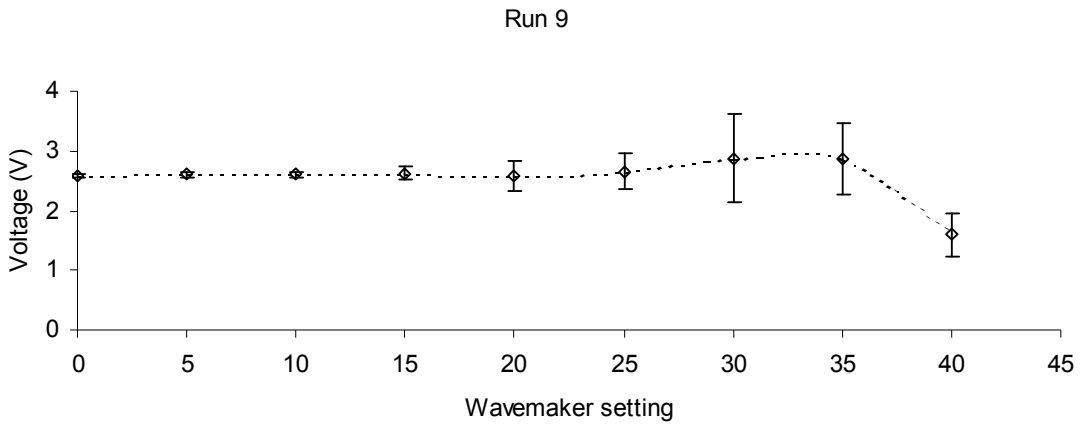

Fig. B.8: Plot of average amplitude of time reversed pulses from run 9.

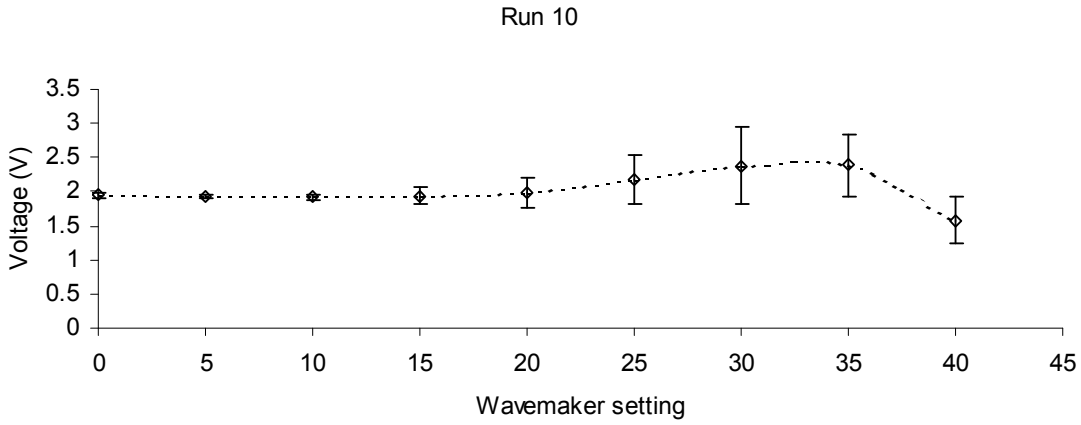

Fig B.9: Plot of average amplitude of time reversed pulses from run 10.

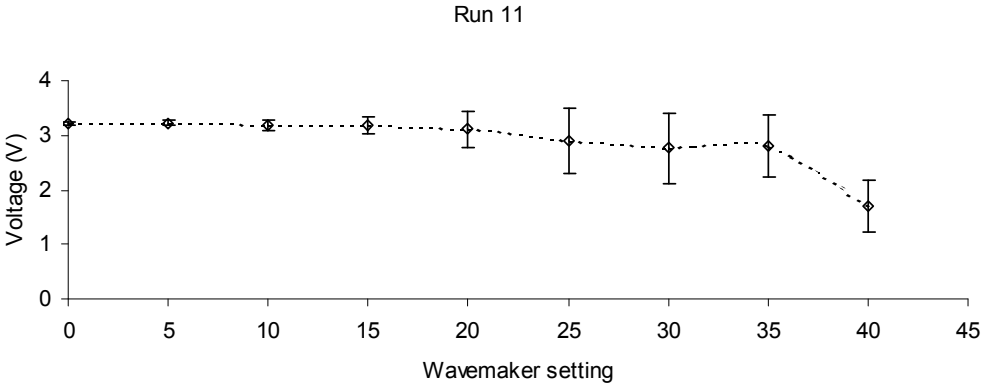

Fig. B.10: Plot of average amplitude of time reversed pulses from run 11.

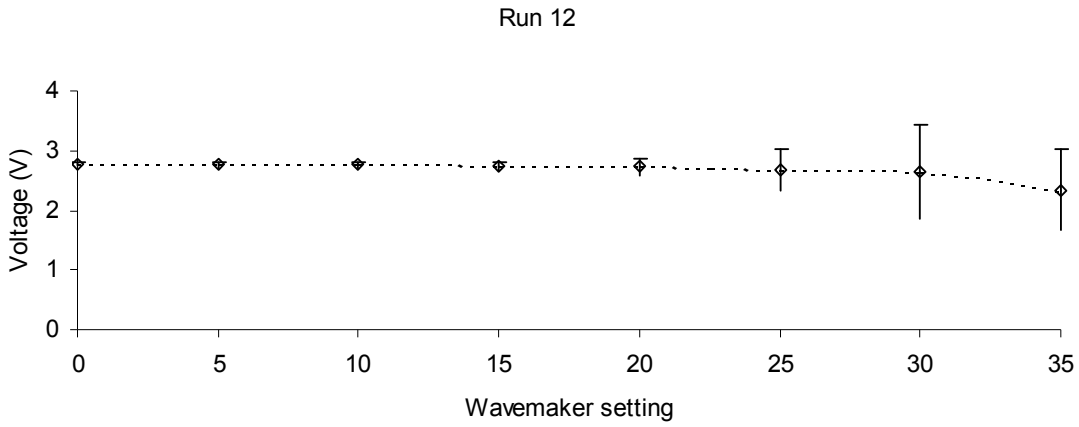

Fig B.11: Plot of average amplitude of time reversed pulses from run 12.

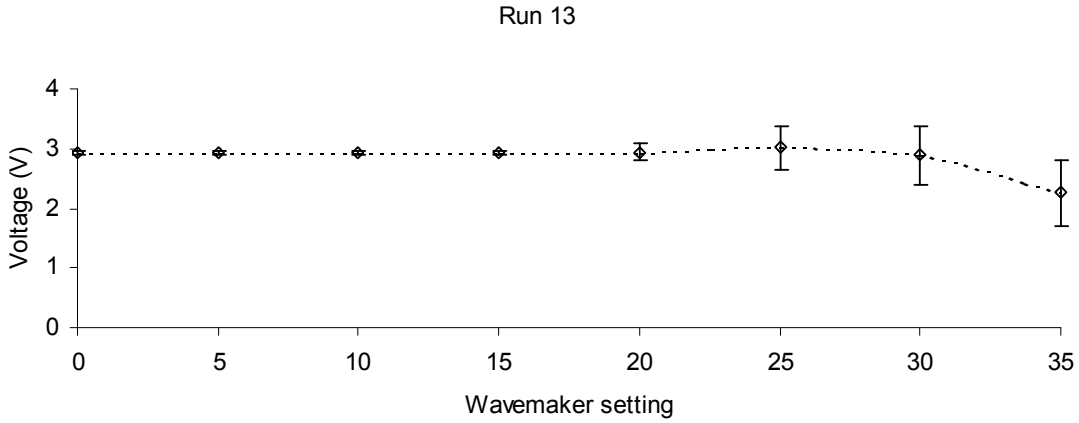

Fig B.12: Plot of average amplitude of time reversed pulses from run 13.

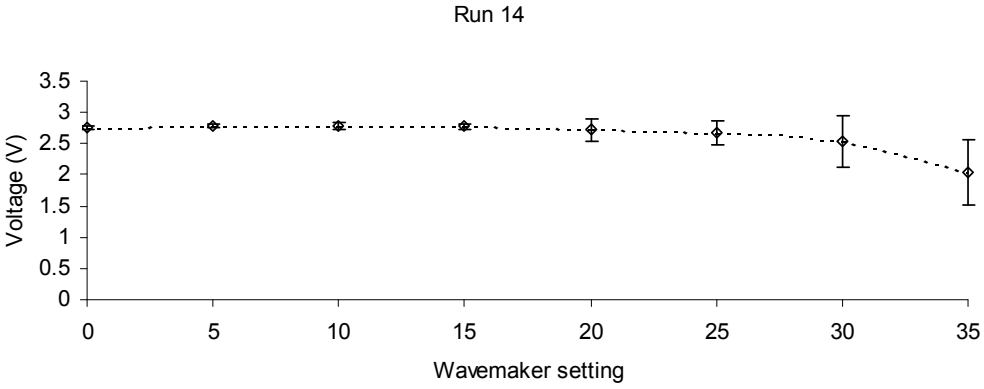

Fig B.13: Plot of average amplitude of time reversed pulses from run 14.

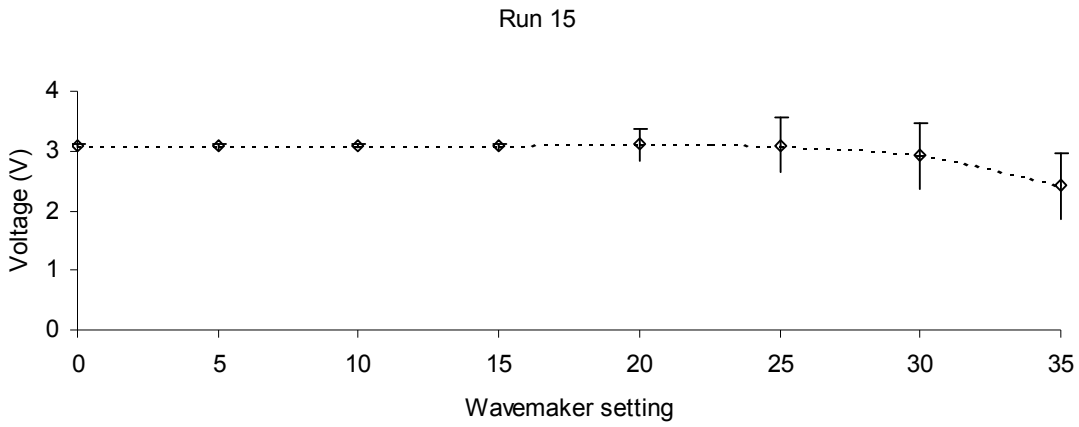

Fig B.14: Plot of average amplitude of time reversed pulses from run 15.

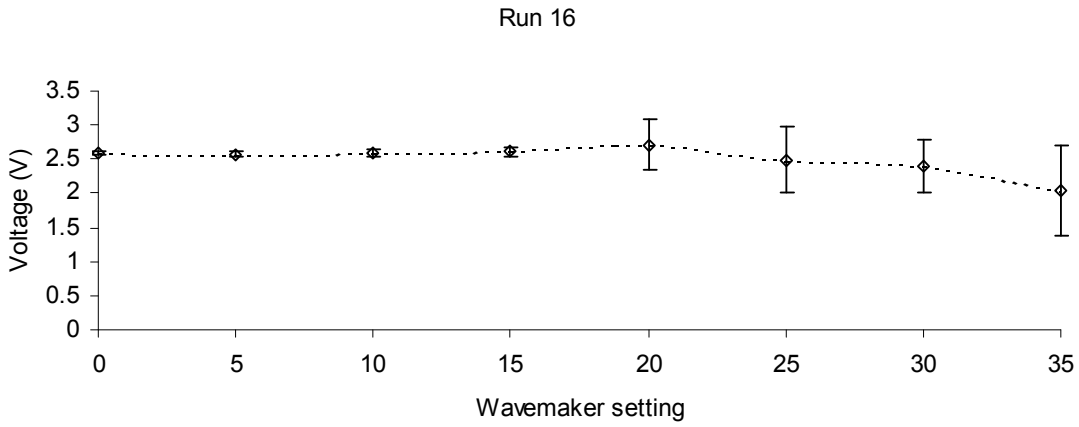

Fig B.15: Plot of average amplitude of time reversed pulses from run 16.

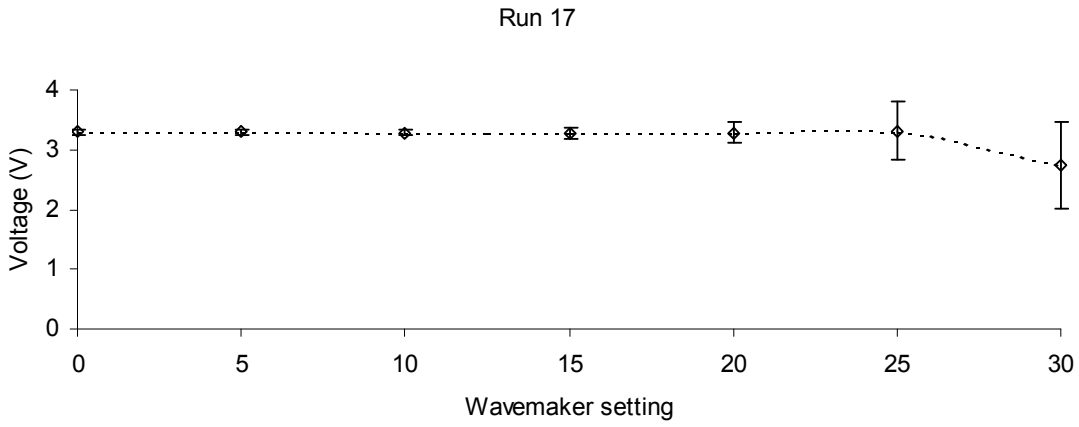

Fig B.16: Plot of average amplitude of time reversed pulses from run 17.

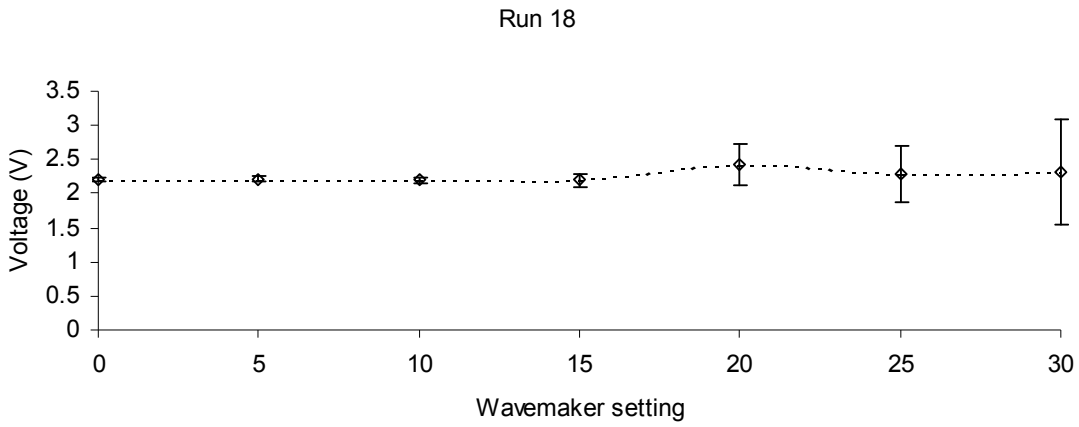

Fig B.17: Plot of average amplitude of time reversed pulses from run 18.

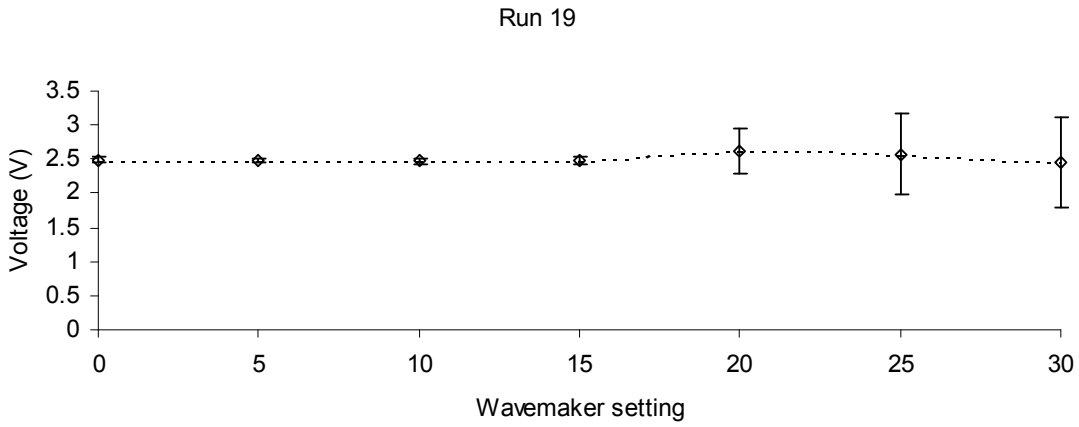

Fig B.18: Plot of average amplitude of time reversed pulses from run 19.

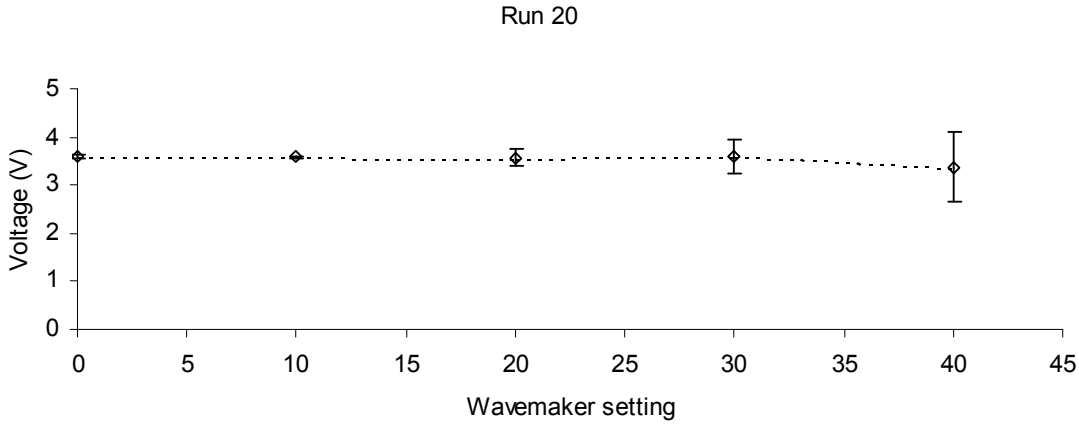

Fig B.19: Plot of average amplitude of time reversed pulses from run 20.

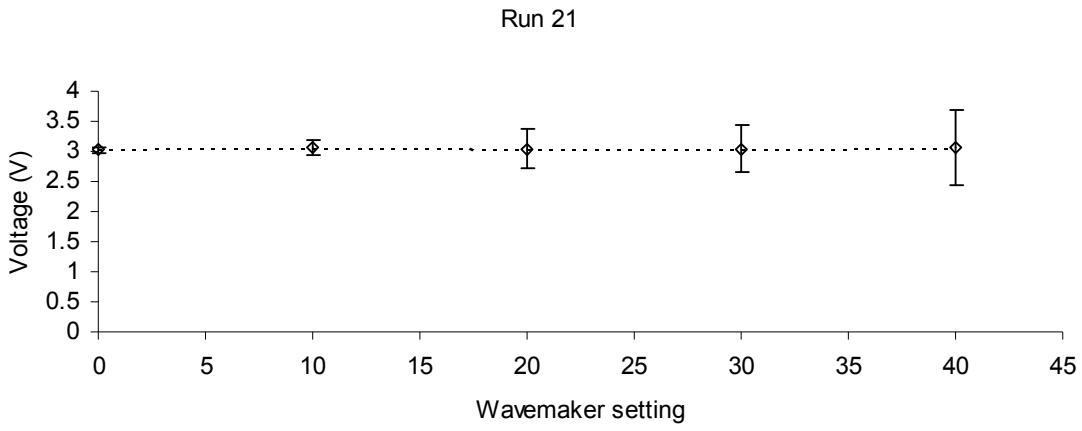

Fig B.20: Plot of average amplitude of time reversed pulses from run 21.

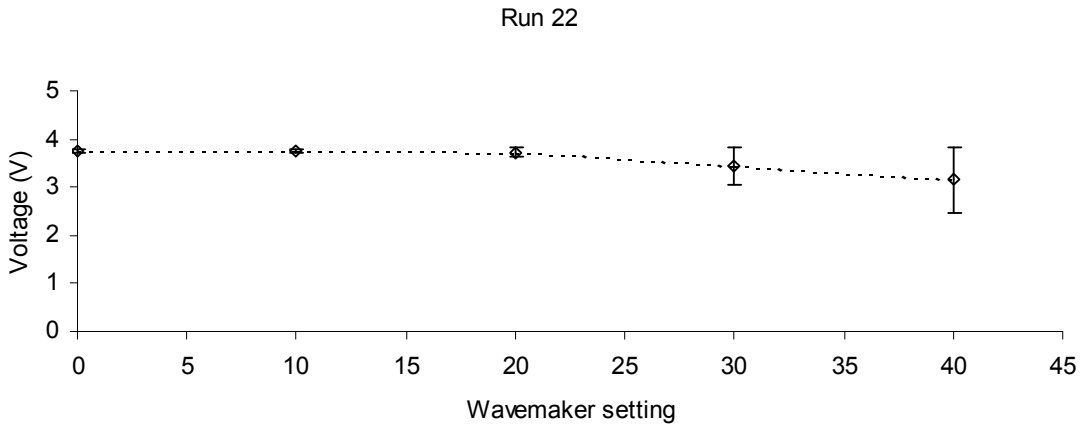

Fig B.21: Plot of average amplitude of time reversed pulses from run 22.

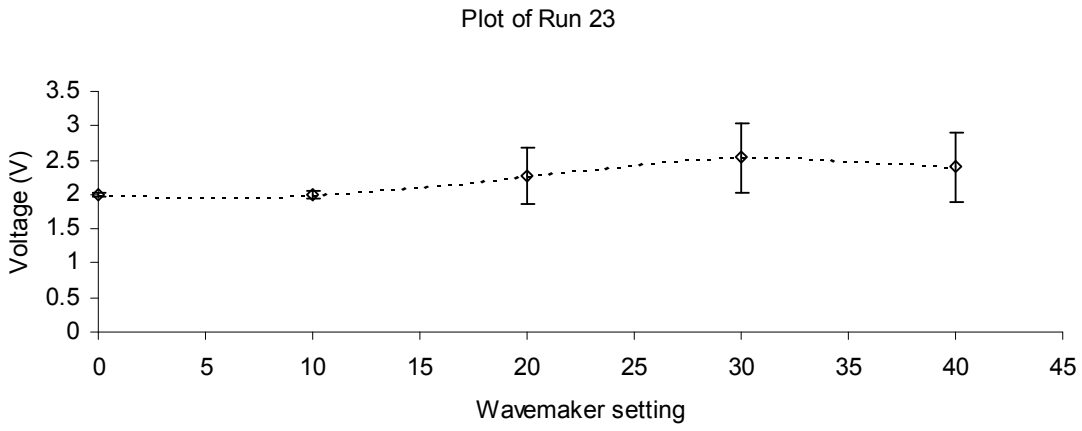

Fig B.22: Plot of average amplitude of time reversed pulses from run 23.

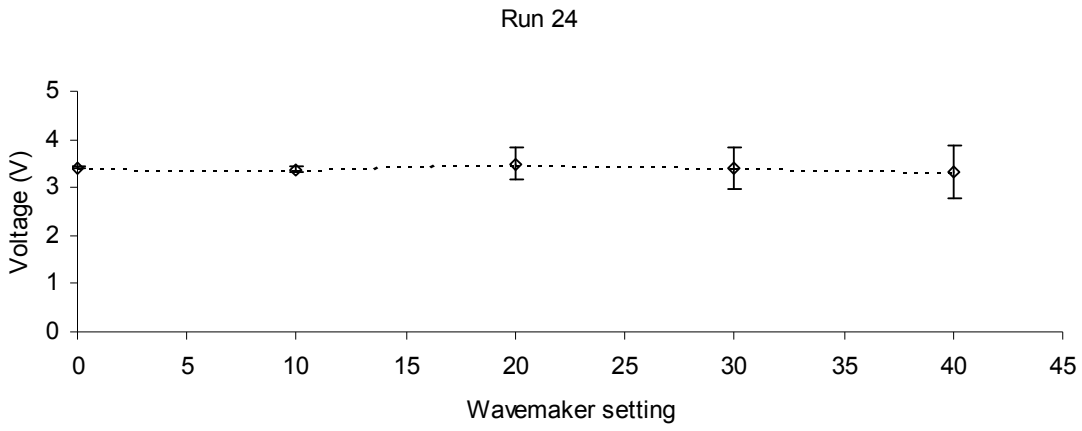

Fig B.23: Plot of average amplitude of time reversed pulses from run 24.

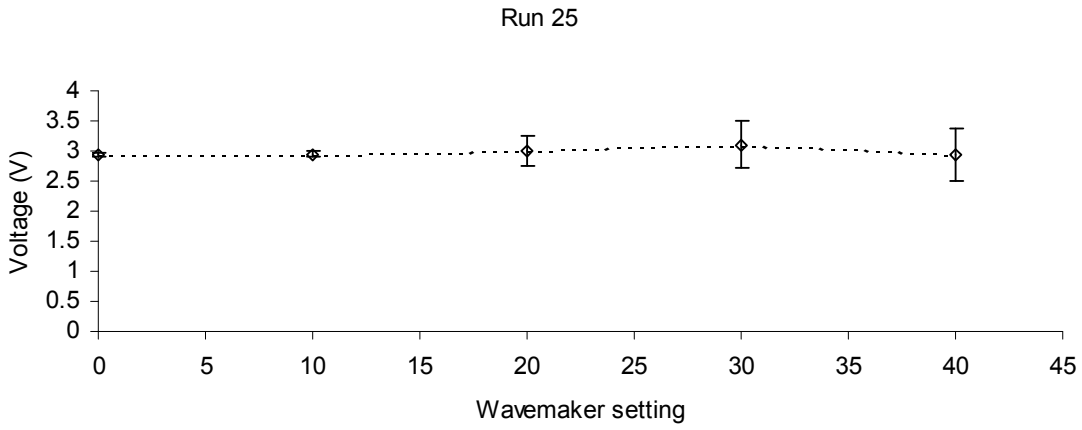

Fig B.24: Plot of average amplitude of time reversed pulses from run 25.

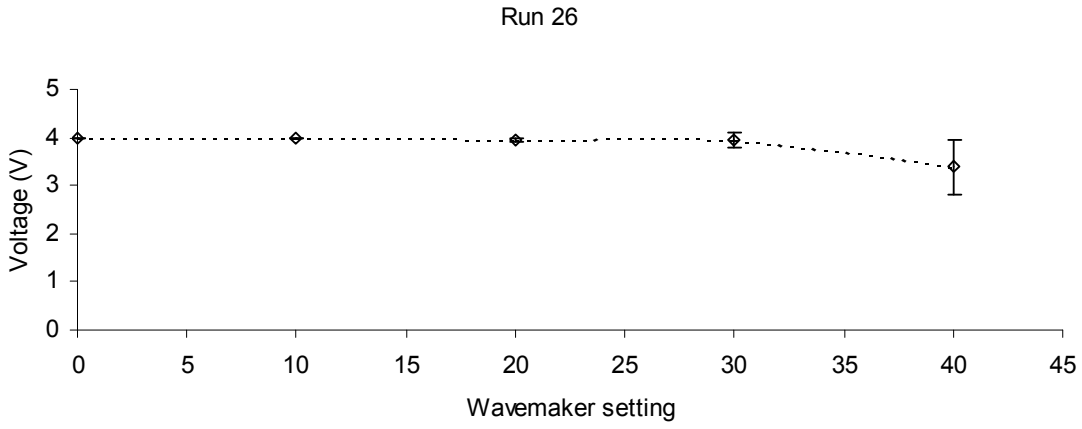

Fig B.25: Plot of average amplitude of time reversed pulses from run 26.

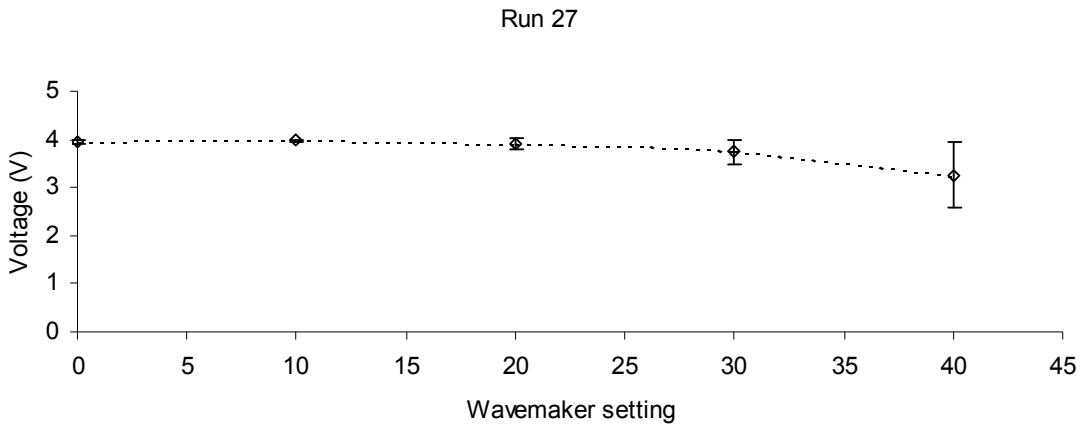

Fig B.26: Plot of average amplitude of time reversed pulses from run 27.

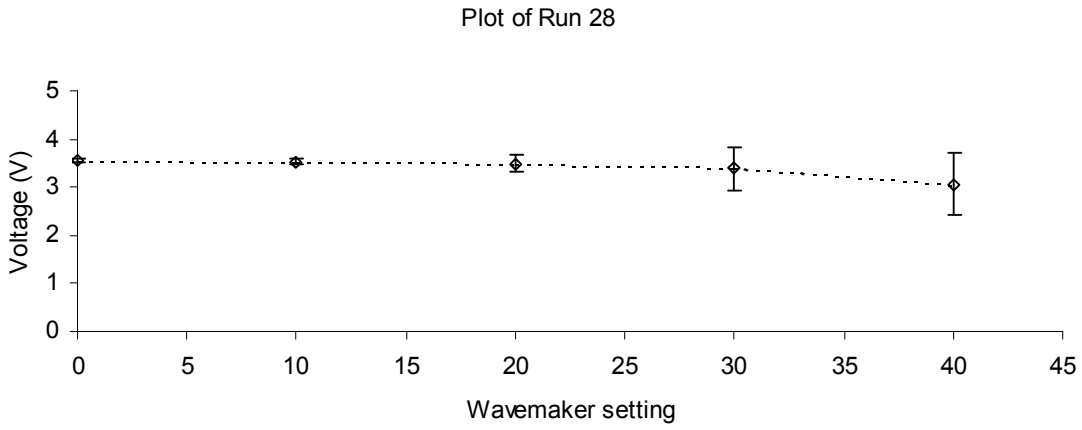

Fig B.27: Plot of average amplitude of time reversed pulses from run 28.

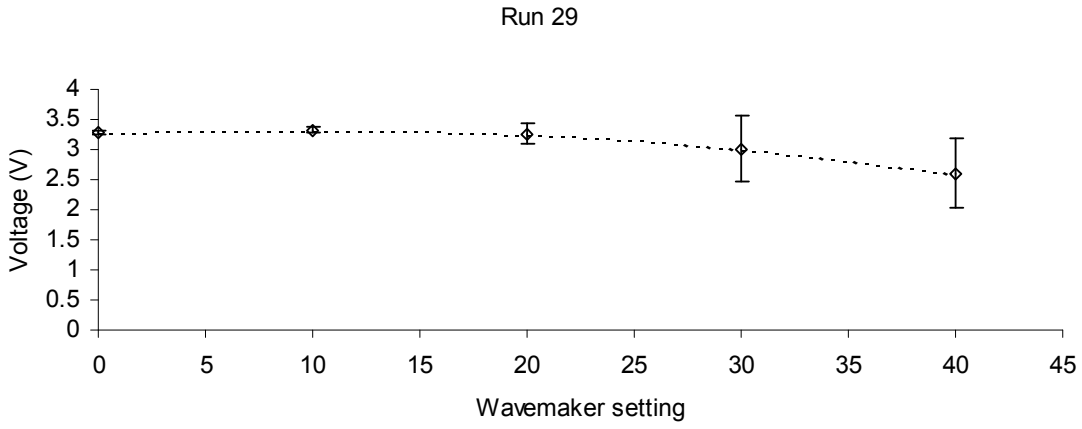

Fig B.28: Plot of average amplitude of time reversed pulses from run 29.

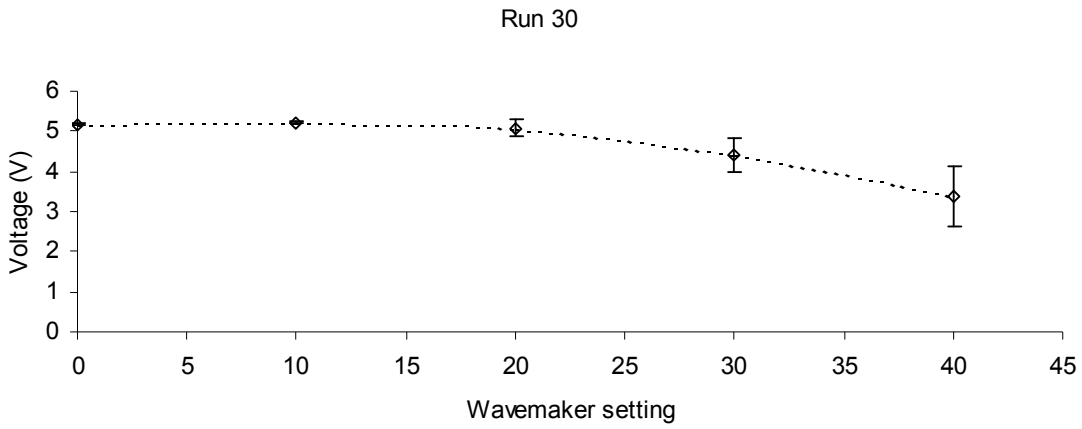

Fig B.29: Plot of average amplitude of time reversed pulses from run 30.

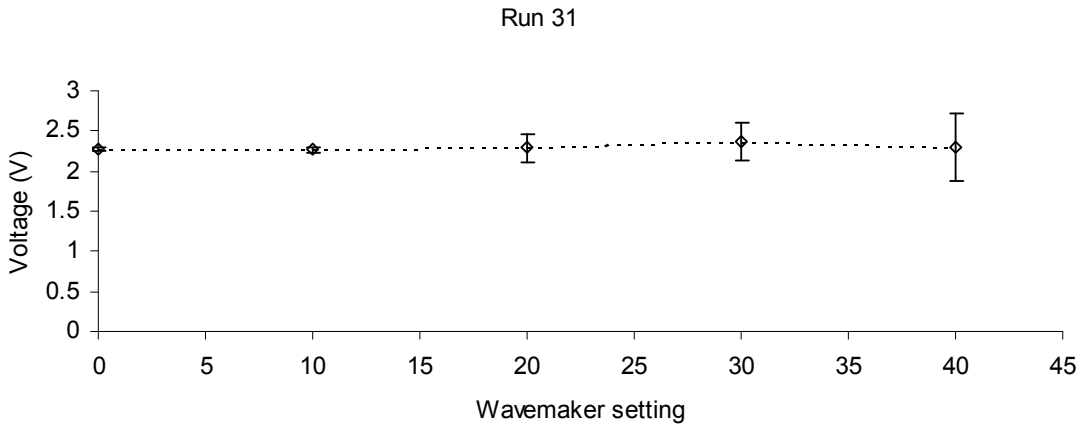

Fig B.30: Plot of average amplitude of time reversed pulses from run 31.

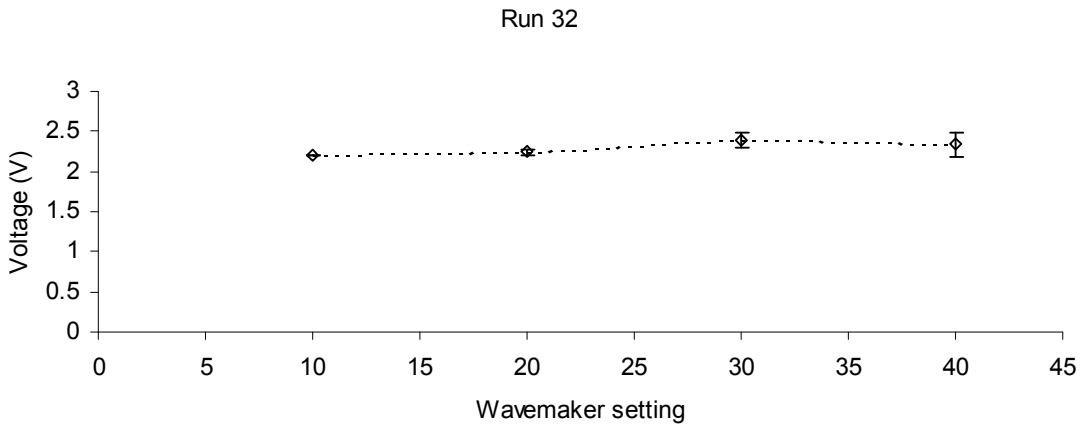

Fig B.31: Plot of average amplitude of time reversed pulses from run 32.

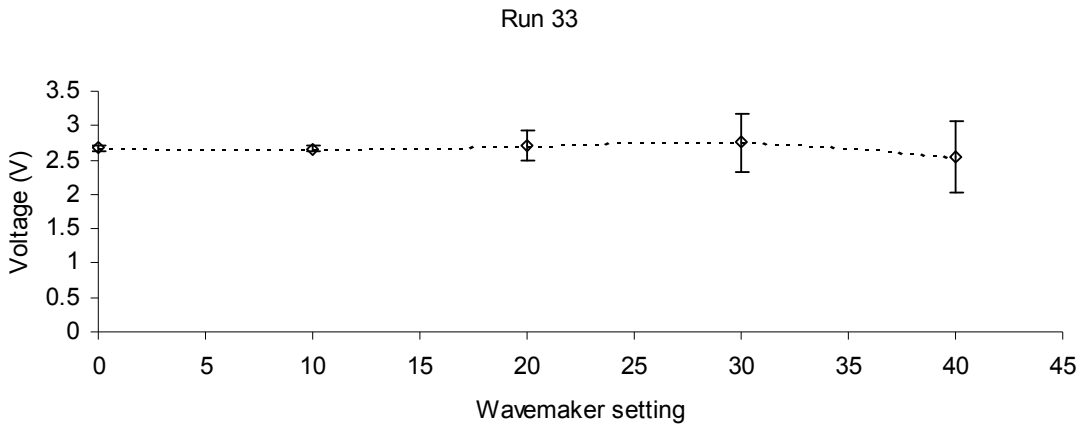

Fig B.32: Plot of average amplitude of time reversed pulses from run 33.

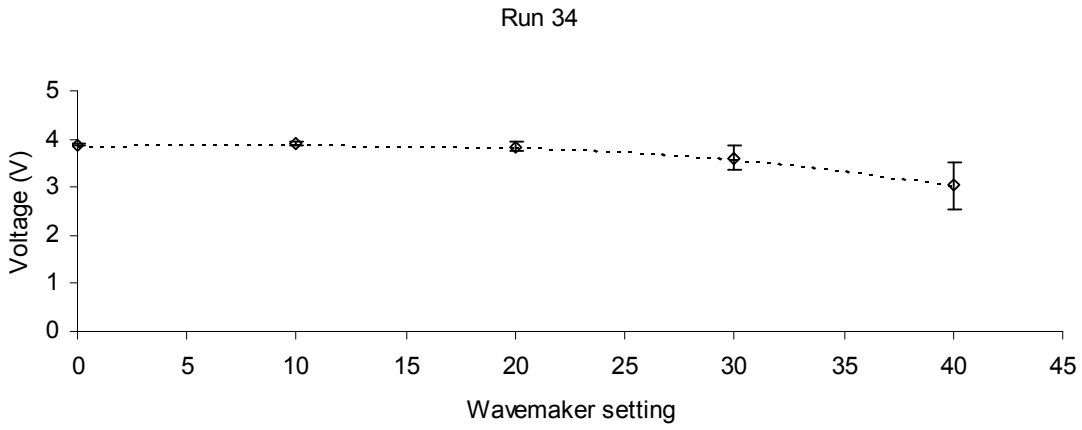

Fig B.33: Plot of average amplitude of time reversed pulses from run 34.

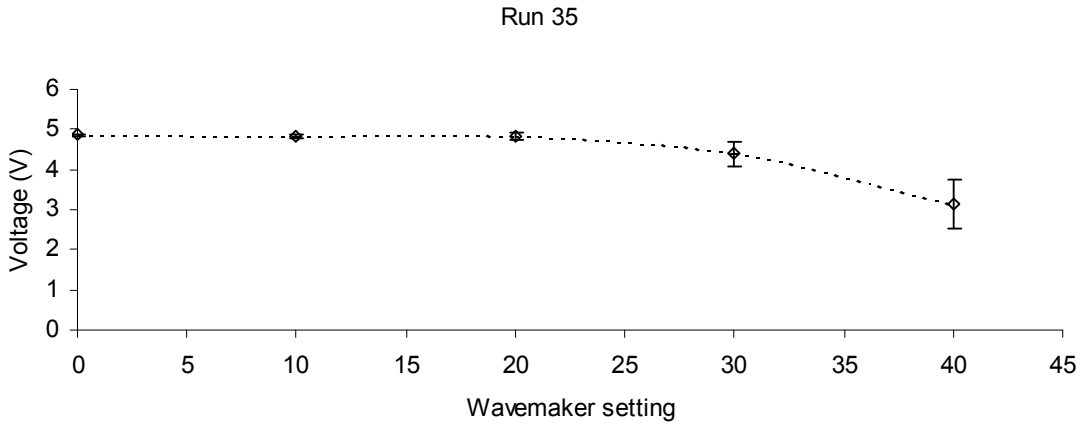

Fig B.34: Plot of average amplitude of time reversed pulses from run 35.

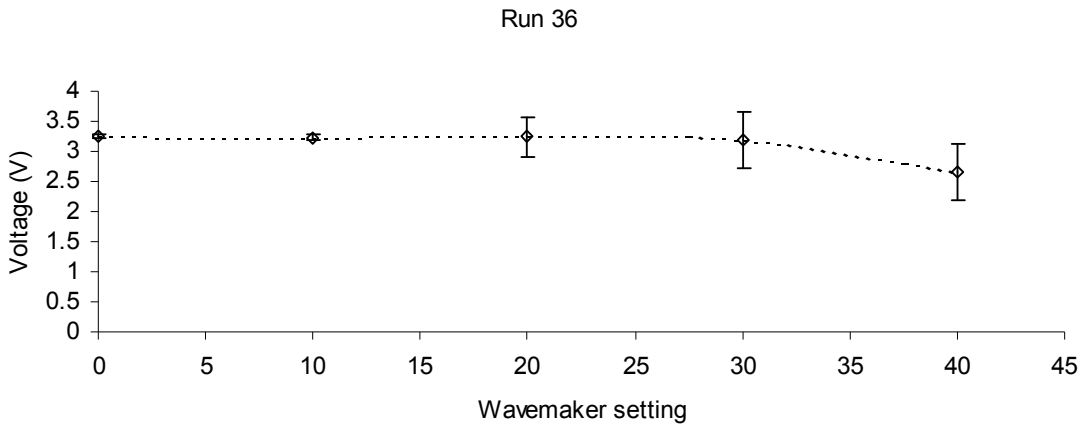

Fig B.35: Plot of average amplitude of time reversed pulses from run 36.

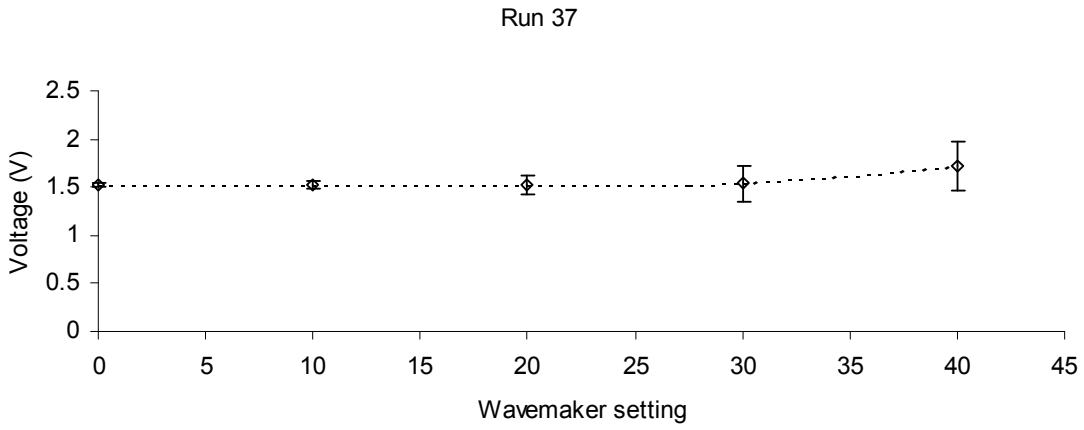

Fig B.36: Plot of average amplitude of time reversed pulses from run 37.

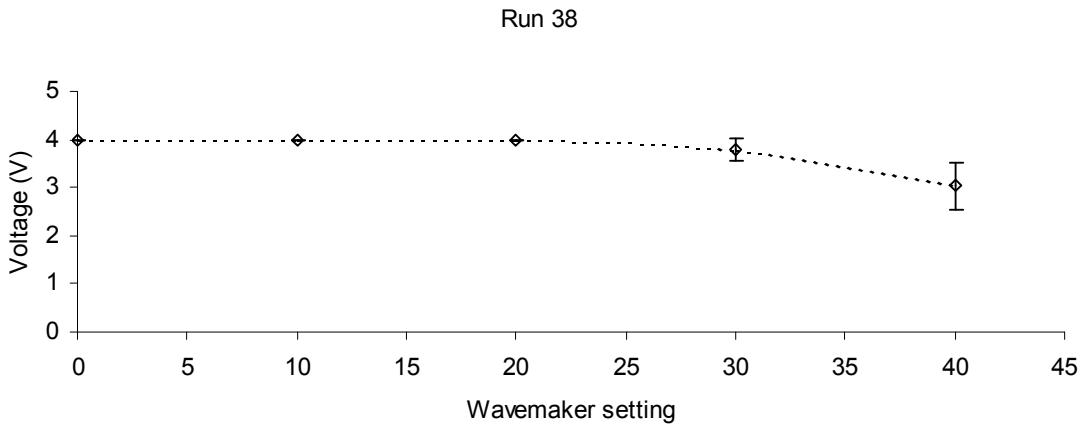

Fig B.37: Plot of average amplitude of time reversed pulses from run 38.

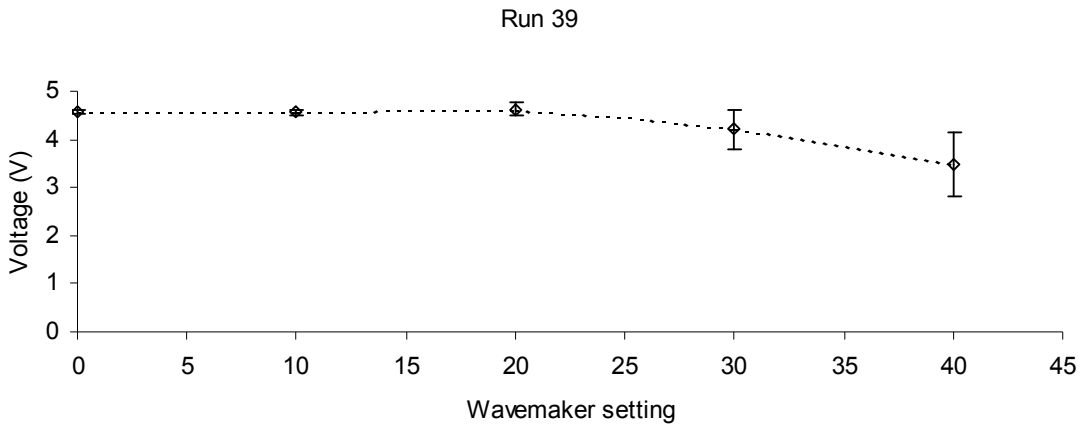

Fig B.38: Plot of average amplitude of time reversed pulses from run 39.

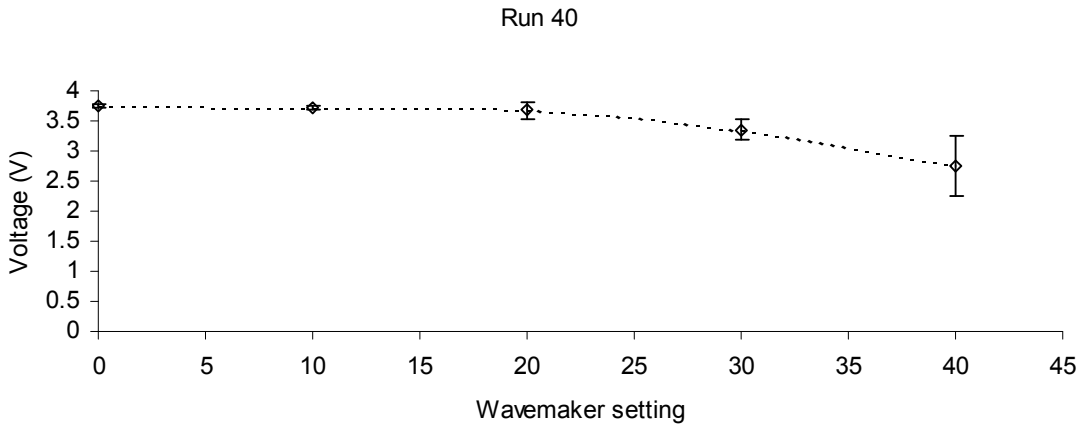

Fig B.39: Plot of average amplitude of time reversed pulses from run 40.

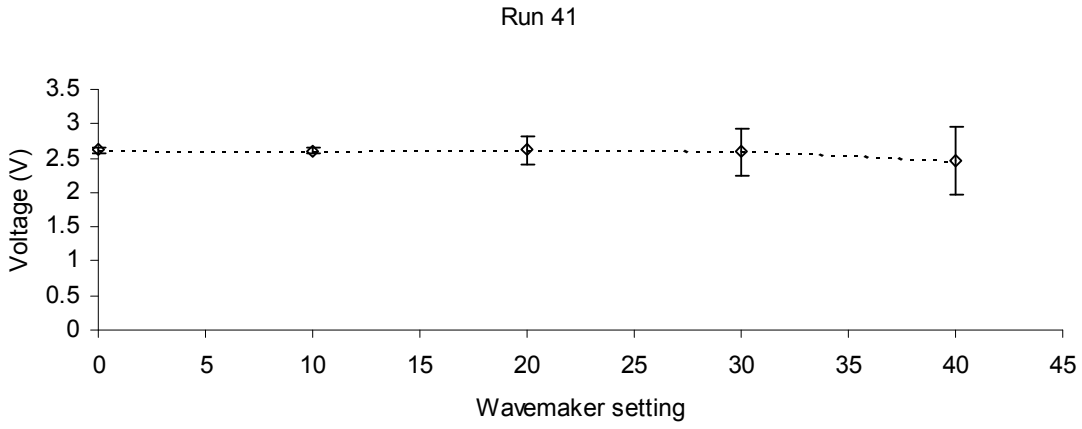

Fig B.40: Plot of average amplitude of time reversed pulses from run 41.

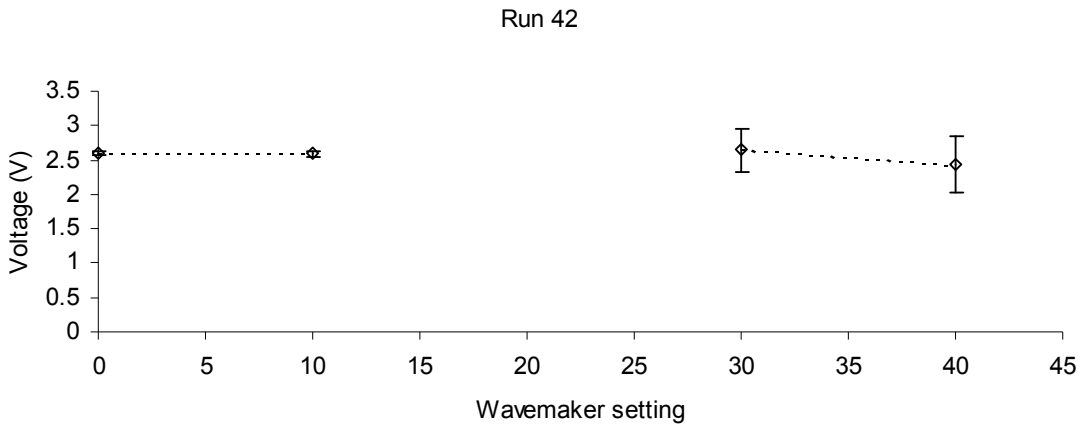

Fig B.41: Plot of average amplitude of time reversed pulses from run 42.(point at setting 20 was not recorded correctly, and so was not included in the analysis)

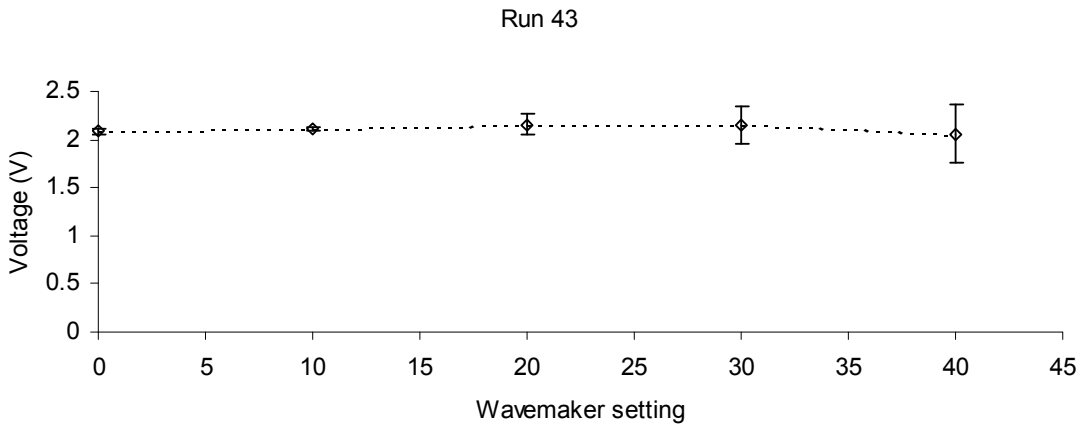

Fig B.42: Plot of average amplitude of time reversed pulses from run 43.

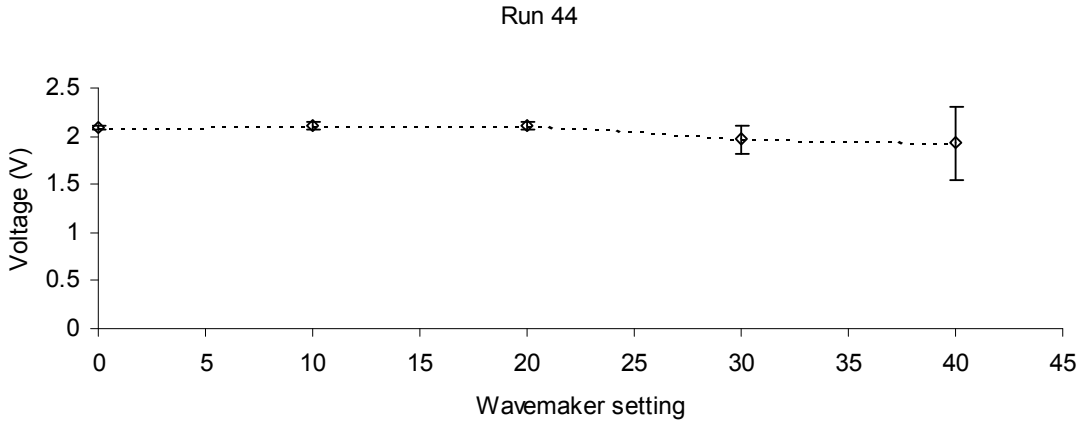

Fig B.43: Plot of average amplitude of time reversed pulses from run 44.

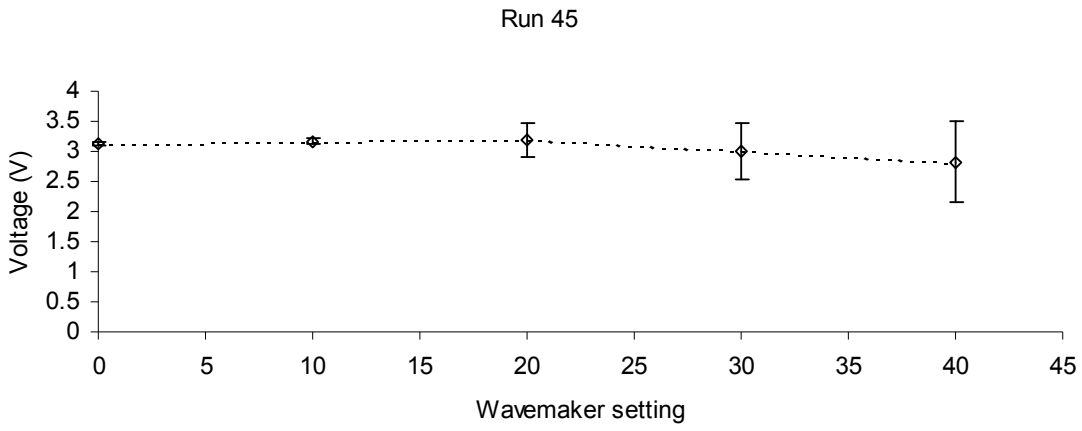

Fig B.44: Plot of average amplitude of time reversed pulses from run 45.

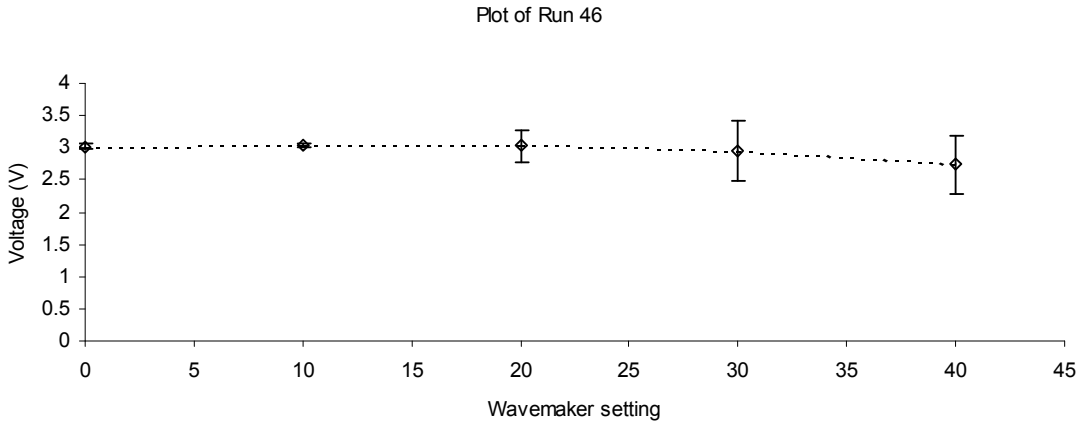

Fig B.45: Plot of average amplitude of time reversed pulses from run 46.

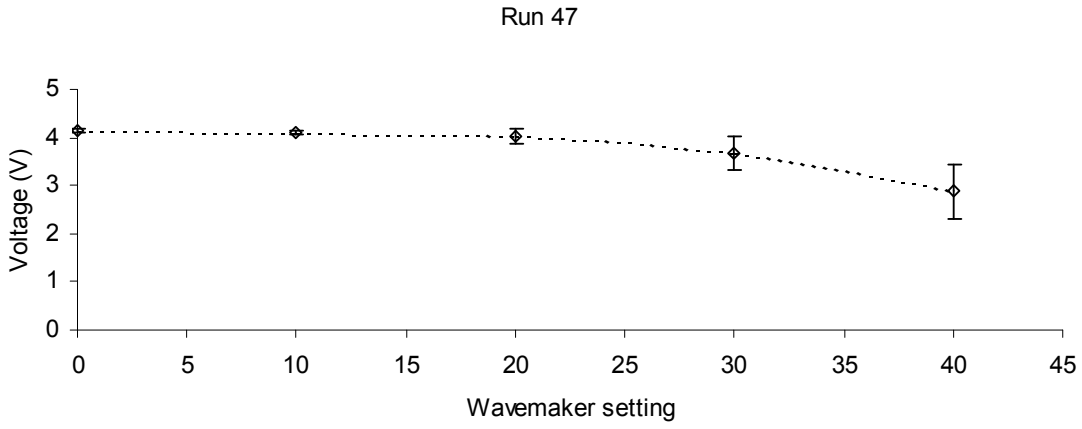

Fig B.46: Plot of average amplitude of time reversed pulses from run 47.

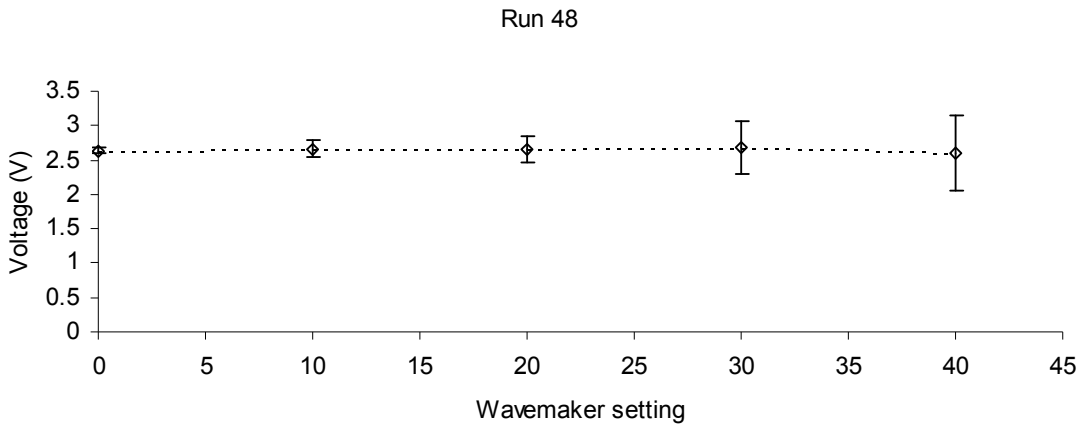

Fig B.47: Plot of average amplitude of time reversed pulses from run 48.

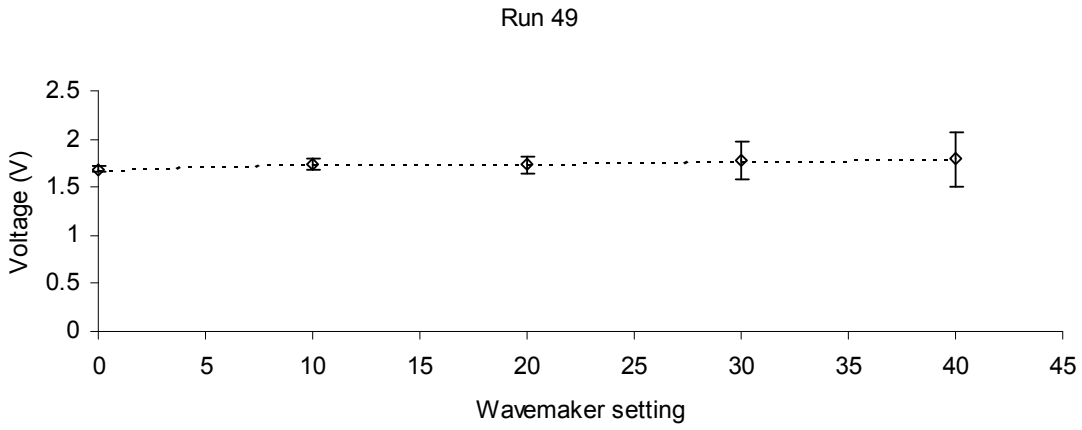

Fig B.48: Plot of average amplitude of time reversed pulses from run 49.

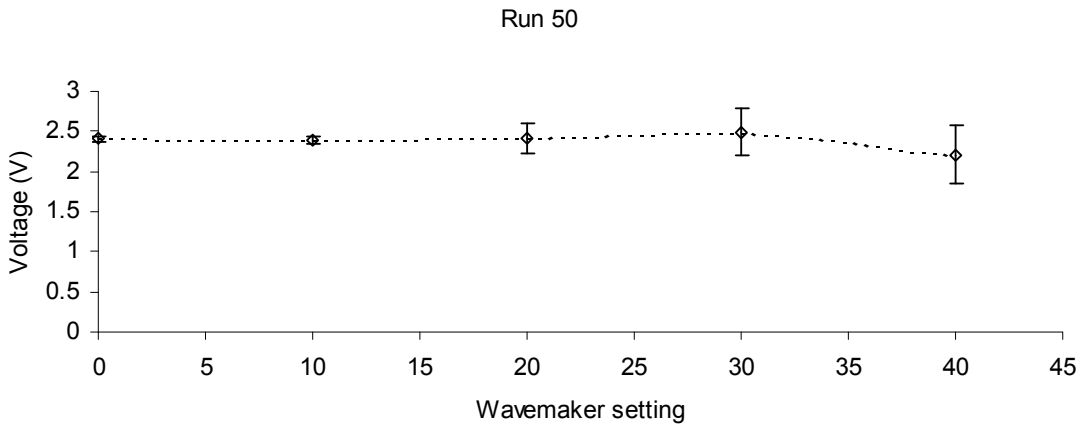

Fig B.49: Plot of average amplitude of time reversed pulses from run 50.

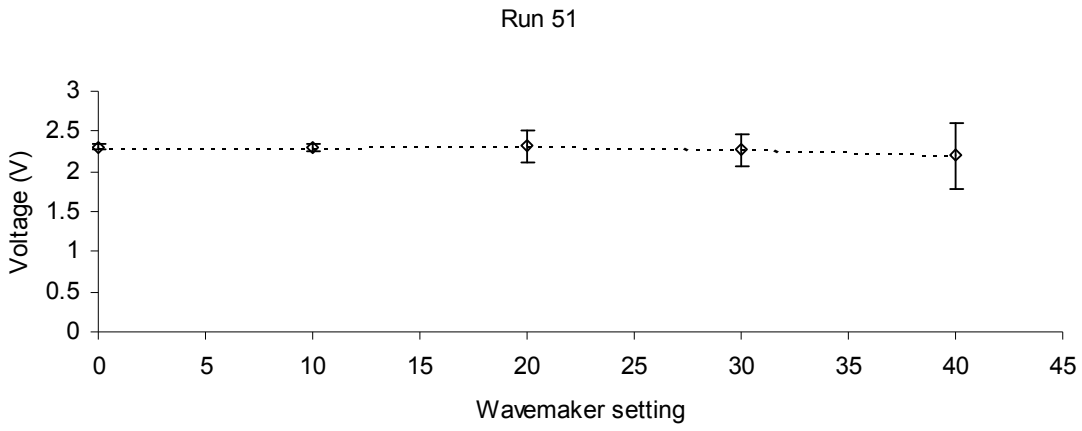

Fig B.50: Plot of average amplitude of time reversed pulses from run 51.

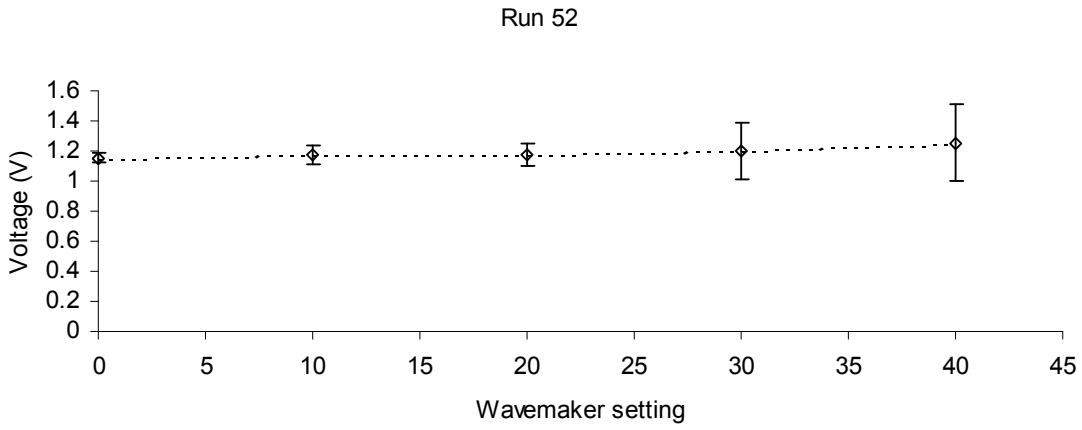

Fig B.51: Plot of average amplitude of time reversed pulses from run 52.

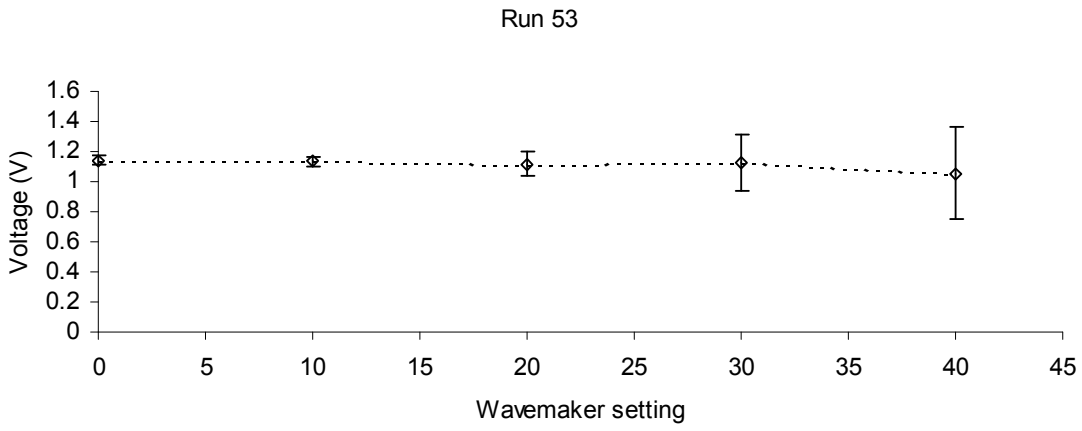

Fig B.52: Plot of average amplitude of time reversed pulses from run 53.

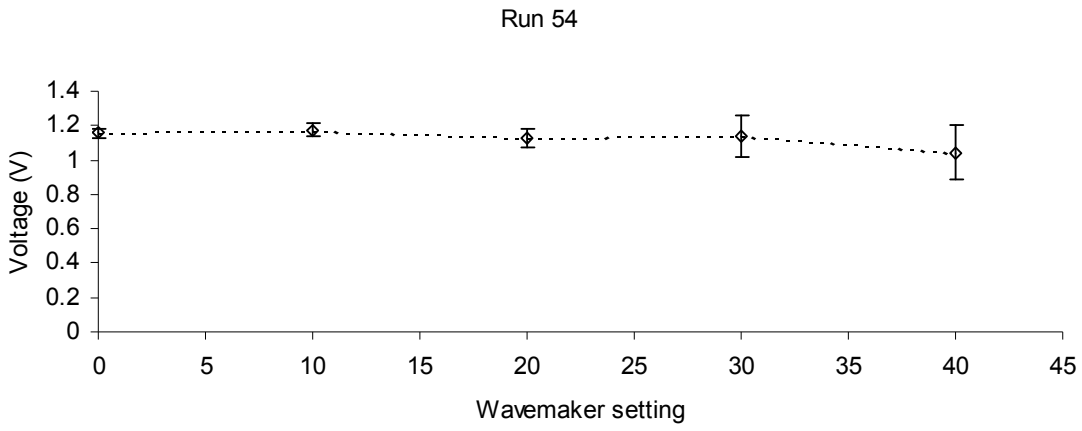

Fig B.53: Plot of average amplitude of time reversed pulses from run 54.

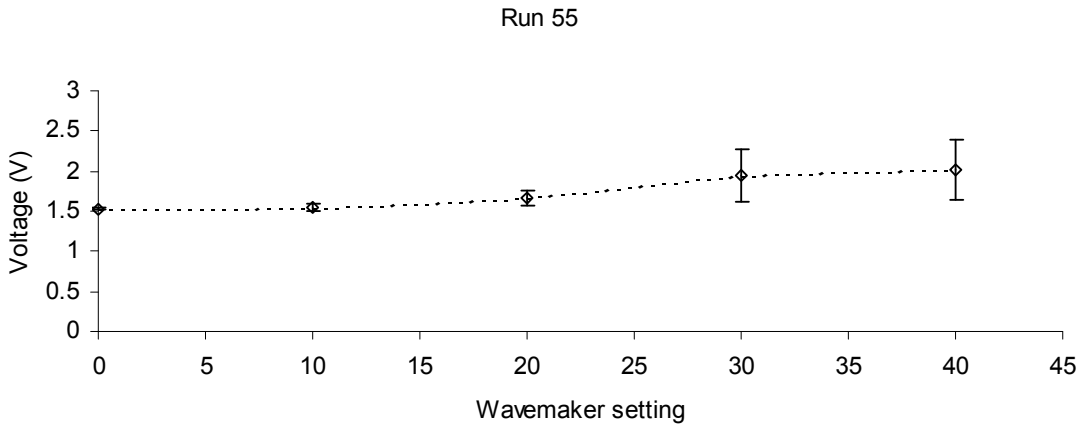

Fig B.54: Plot of average amplitude of time reversed pulses from run 55.

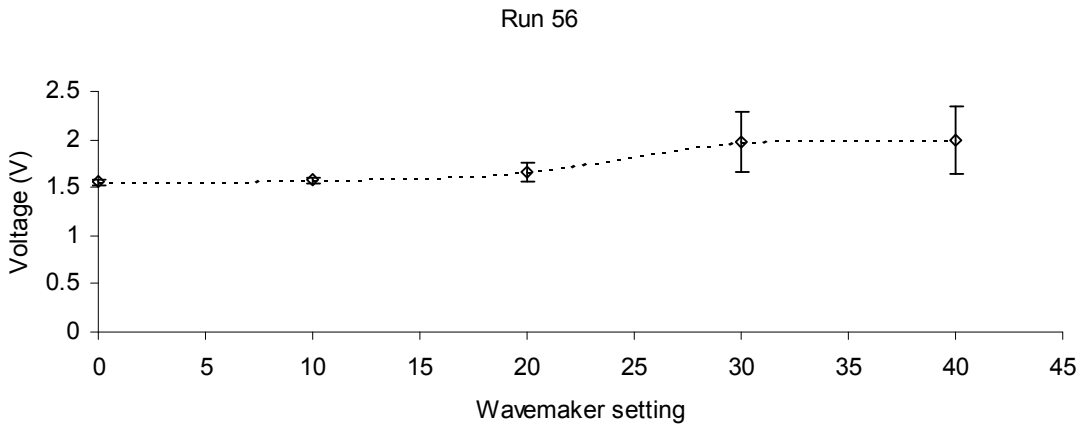

Fig B.55: Plot of average amplitude of time reversed pulses from run 56.

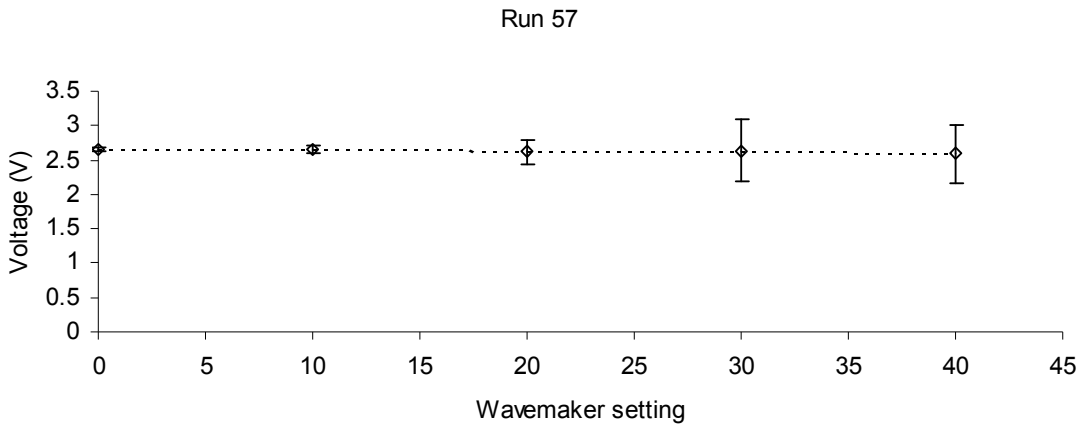

Fig B.56: Plot of average amplitude of time reversed pulses from run 57.

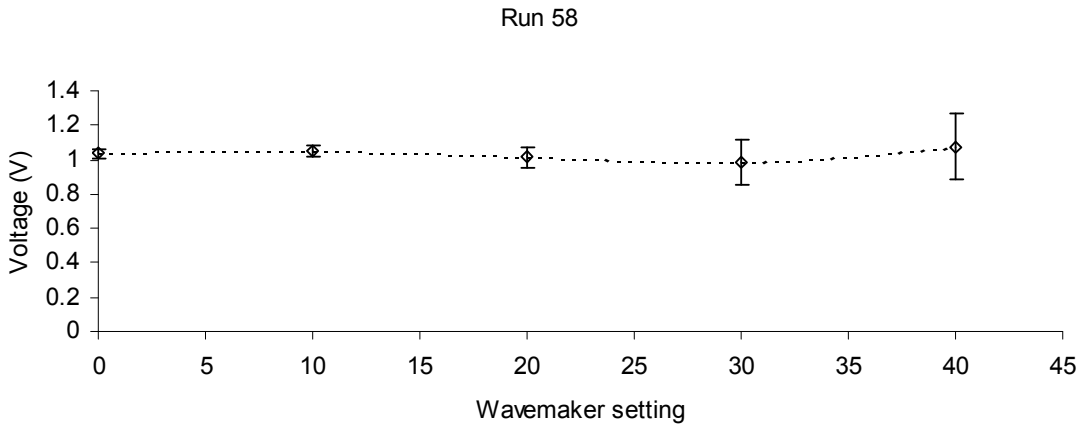

Fig B.57: Plot of average amplitude of time reversed pulses from run 58.

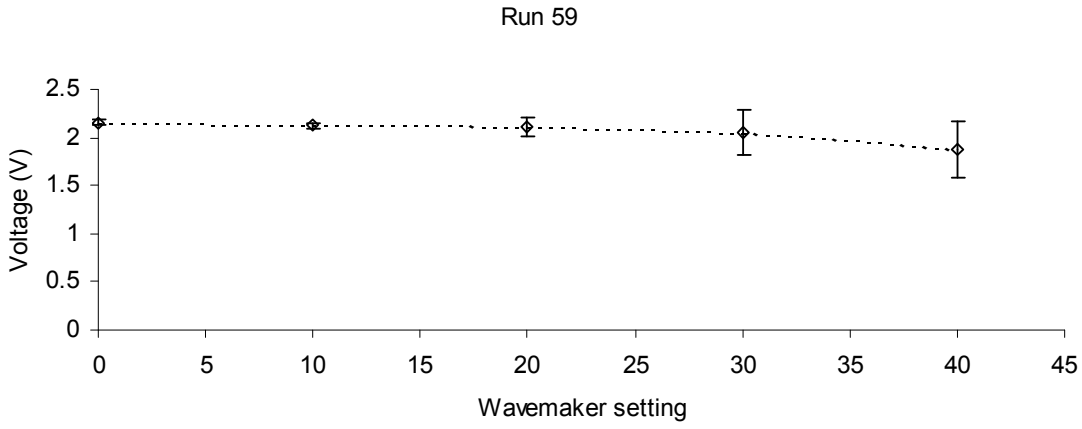

Fig B.58: Plot of average amplitude of time reversed pulses from run 59.

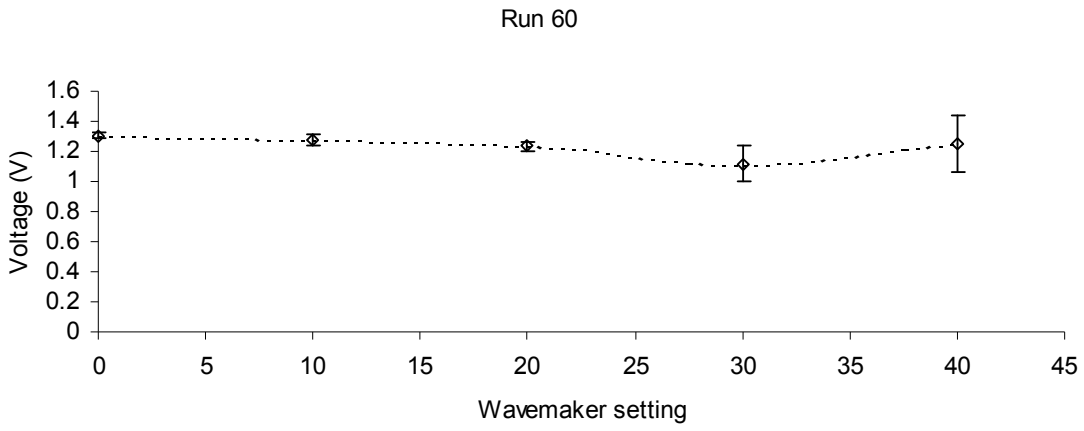

Fig B.59: Plot of average amplitude of time reversed pulses from run 60.

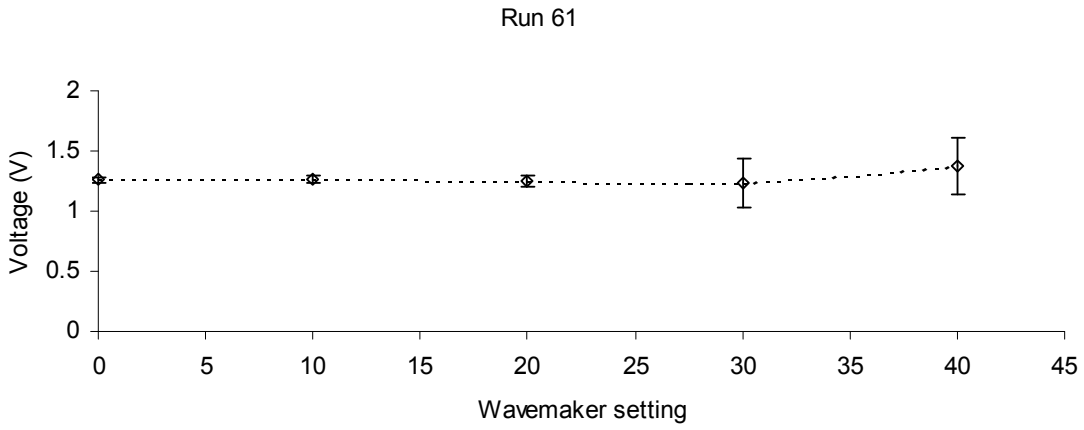

Fig B.60: Plot of average amplitude of time reversed pulses from run 61.

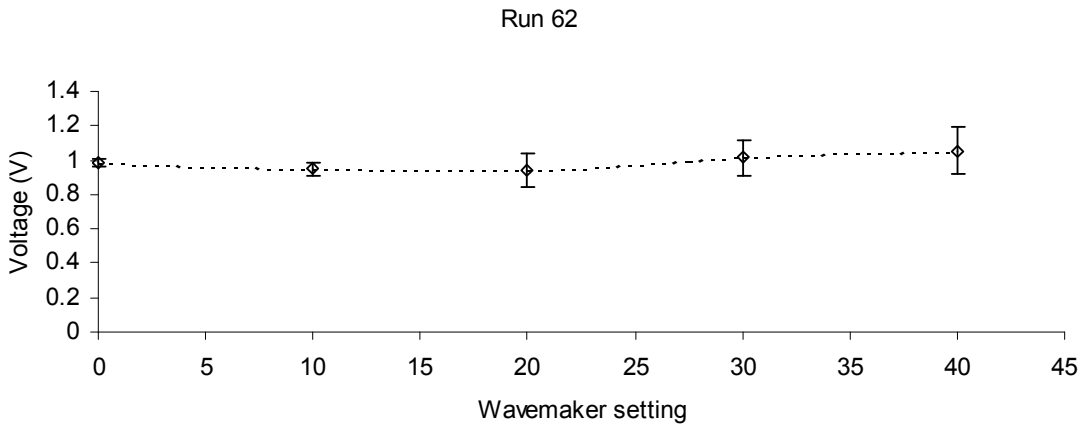

Fig B.61: Plot of average amplitude of time reversed pulses from run 62.

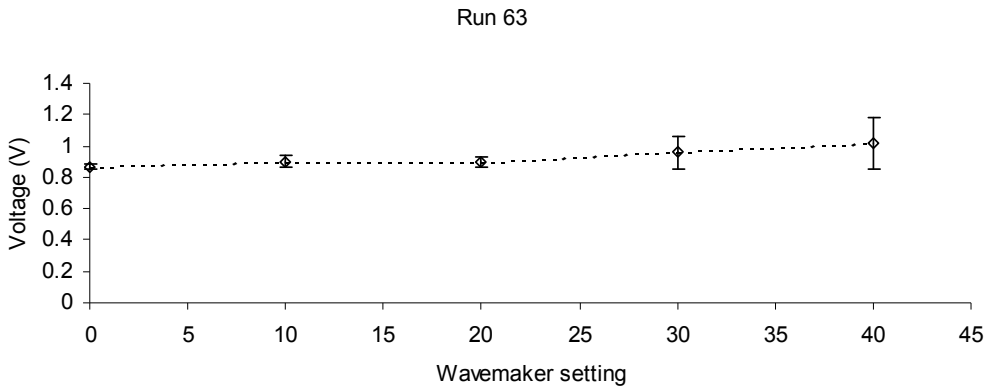

Fig B.62: Plot of average amplitude of time reversed pulses from run 63.

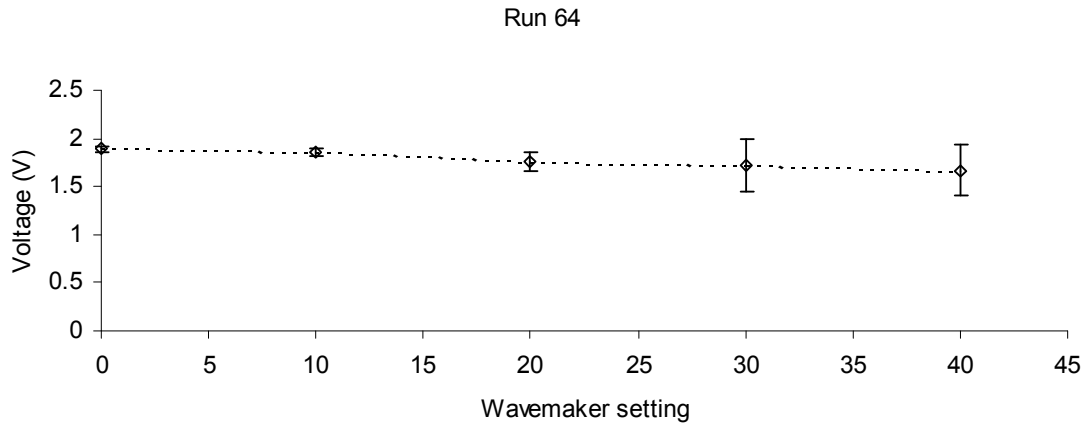

Fig B.63: Plot of average amplitude of time reversed pulses from run 64.